

AD-A154 629

COORDINATED RESEARCH PROGRAM IN PULSED POWER PHYSICS
(U) TEXAS TECH UNIV LUBBOCK DEPT OF ELECTRICAL
ENGINEERING M KRISTIANSEN ET AL. 20 DEC 84

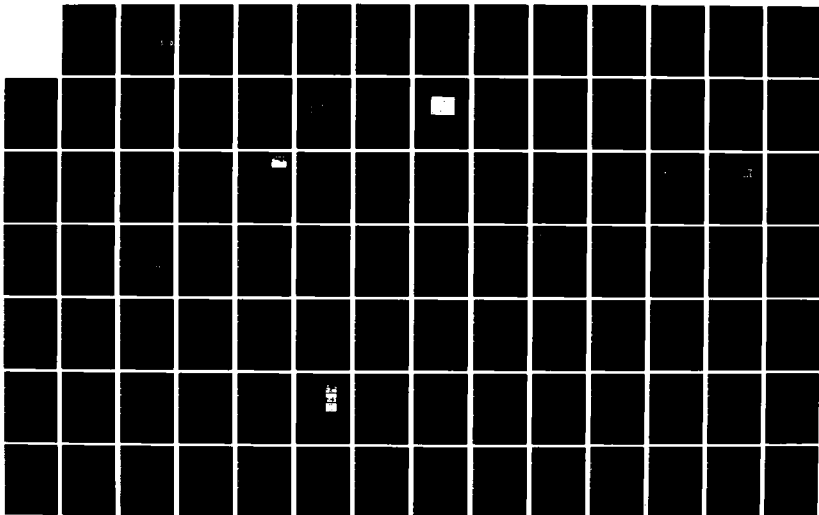
1/3

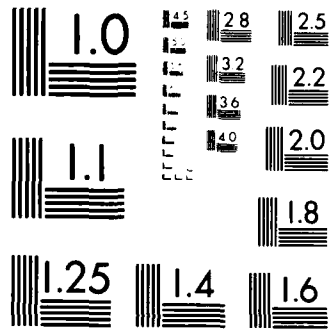
UNCLASSIFIED

AFOSR-TR-85-0457 AFOSR-84-0032

F/G 10/2

NL





MICROCOPY RESOLUTION TEST CHART
NATIONAL BUREAU OF STANDARDS 1963 A

AFOSR-TR-85-0157

ANNUAL REPORT

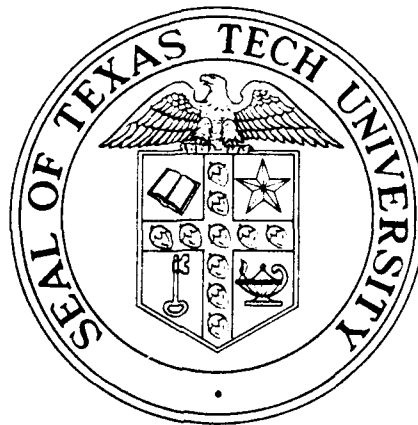
✓

on

COORDINATED RESEARCH PROGRAM in PULSED POWER PHYSICS

December 20, 1984

AD-A154 629



Air Force Office of Scientific Research
Grant No. 84-0032

DTIC
ELECTE
JUN 6 1985
S A D

Approved for public release;
distribution unlimited.

DTIC FILE COPY

PLASMA AND SWITCHING LABORATORY
LASER LABORATORY

Department of Electrical Engineering
TEXAS TECH UNIVERSITY

Lubbock, Texas 79409

REPORT DOCUMENTATION PAGE

1a. REPORT SECURITY CLASSIFICATION Unclassified		1d. RESTRICTIVE MARKINGS	
2a. SECURITY CLASSIFICATION AUTHORITY		3. DISTRIBUTION/AVAILABILITY OF REPORT APPROVED FOR PUBLIC RELEASE; Distribution Unlimited	
2b. DECLASSIFICATION/DOWNGRADING SCHEDULE N/A		5. MONITORING ORGANIZATION REPORT NUMBER(S) AFOSR-TR-85-0457	
4. PERFORMING ORGANIZATION REPORT NUMBER(S)		7a. NAME OF MONITORING ORGANIZATION Air Force Office of Scientific Research	
6a. NAME OF PERFORMING ORGANIZATION Texas Tech University	6b. OFFICE SYMBOL (If applicable) EE	7b. ADDRESS (City, State and ZIP Code) Bldg. 410, Bolling AFB Washington, DC 20332	
8a. NAME OF FUNDING/SPONSORING ORGANIZATION Air Force Office of Scientific Res.		8b. OFFICE SYMBOL (If applicable) NP	9. PROCUREMENT INSTRUMENT IDENTIFICATION NUMBER AFOSR 84-0032
8c. ADDRESS (City, State and ZIP Code) Bldg. 410, Bolling AFB Washington, DC 20332		10. SOURCE OF FUNDING NOS.	
		PROGRAM ELEMENT NO. 61102F	PROJECT NO. 2301
		TASK NO. A7	WORK UNIT NO.
11. TITLE (Include Security Classification) COORDINATED RESEARCH PROGRAM IN PULSED POWER PHYSICS			
12. PERSONAL AUTHOR(S) M. Kristiansen, L. Hatfield, G. Schaefer, K. Schoenbach, H. Krompholz and F. Williams.			
13a. TYPE OF REPORT Annual	13b. TIME COVERED FROM 10/1/83 TO 10/31/84	14. DATE OF REPORT (Yr., Mo., Day) 1984/12/20	15. PAGE COUNT 210
16. SUPPLEMENTARY NOTATION			
17. CCSATI CODES		18. SUBJECT TERMS (Continue on reverse if necessary and identify by block number)	
FIELD	GROUP	SUB. GR.	Pulsed Power, Diffuse Discharges, Opening Switches, Laser Triggering, Surface Discharges, Field Distortion, Streak Photography, X-ray Triggering.
19. ABSTRACT (Continue on reverse if necessary and identify by block number)			
<p>The work on three program elements, related to pulsed power research, is described. The program is a multi-investigator program whose main emphasis is on gaining a better understanding of repetitive opening and closing switch phenomena. The main effort is on diffuse discharge opening switches but considerable progress has also been made on understanding and describing fundamental, transient discharge phenomena. In addition several smaller studies have considered various novel ideas and concepts to determine their potential for further investigations.</p>			
20. DISTRIBUTION/AVAILABILITY OF ABSTRACT UNCLASSIFIED/UNLIMITED <input checked="" type="checkbox"/> SAME AS RPT. DTIC USERS <input type="checkbox"/>		21. ABSTRACT SECURITY CLASSIFICATION Unclassified	
22a. NAME OF RESPONSIBLE INDIVIDUAL Maj. H. Pugh		22b. TELEPHONE NUMBER (Include Area Code) 202/767-4906	22c. OFFICE SYMBOL AFOSR/NP

TABLE OF CONTENTS

Summary of Research Objectives for 1983-84

Introduction

Opening Switches

Transient Processes in the Triggered Electrical
Breakdown of Gases

Exploratory Concepts

Faculty Publications, 1983-84

Interactions, 1983-84

Advanced Degrees Awarded, 1983-84

Seminars, 1983-84

Guests, 1983-84

AIR FORCE OFFICE OF SCIENTIFIC RESEARCH (AFSC)
NOTICE
This is
Approved
Distribution
MATHEW
Chief, Research Division

15



Accession For	
NTIS GR&I	<input checked="" type="checkbox"/>
DTIC TAB	<input type="checkbox"/>
Unannounced	<input type="checkbox"/>
Justification	
By	
Distribution/	
Availability Codes	
Avail and/or	
Dist	Special

AT

SUMMARY OF RESEARCH OBJECTIVES

for

1983-84

OPENING SWITCHES

1. Investigations of repetitive e-beam controlled discharges with respect to gas properties.
2. Investigation of optogalvanic effects with respect to their use as discharge control mechanisms.
3. Studies of concepts for optically assisted, e-beam sustained, diffuse discharge switches.
4. Modeling of diffuse discharges, including control mechanisms.
5. Feasibility studies of novel opening switch concepts.

TRANSIENT PROCESSES IN TRIGGERED ELECTRICAL BREAKDOWNIN GASES

1. A facility for investigating triggering in trigatron devices will be constructed as discussed in the proposal text.
2. Triggering in trigatron devices will be investigated making use of this facility and optical diagnostics.
3. Studies of laser triggering of spark gaps will continue.
4. Numerical models of triggering and breakdown already developed will be improved and applied to the study of trigatron and laser-induced triggering.

EXPLORATORY CONCEPTS

1. The most important parameter dependencies in surface discharge switches will be determined.
2. The feasibility of geometrically enhanced field distortion triggering of spark gaps will be determined.
3. Several novel switch (opening and/or closing) concepts will be investigated for feasibility.

INTRODUCTION

The Coordinated Research Program in Pulsed Power Physics is a multi-investigator Program involving 5 Principal Investigators, 2 Associate Investigators and 10 Graduate Students. Other faculty investigators from Electrical Engineering, Physics and Chemistry, and also interacted and cooperated at various times. The program is jointly sponsored by AFOSR and ARO. Some 12 refereed journal articles and 3 conference proceedings papers were published last year. The three main projects are Opening Switches, Transient Processes in Triggered Electrical Breakdown of Gases, and Exploratory Concepts. The second one of these projects will not be carried on in its present form beyond this contract period since the Principal Investigator is moving to another university.

*Added by other principal investigators
 (1) Opening Switches, (2) Transient Processes in Triggered Electrical Breakdown of Gases, (3) Exploratory Concepts*

Opening Switches

(C. Harjes, G. Hutcheson, L. Thurmond, D. Skaggs, E. Strickland,
G. Schaefer, K.H. Schoenbach, H. Krompholz,
M. Kristiansen, and F. Williams)

I. SUMMARY

The primary objective of this work is to study control processes in externally sustained or controlled diffuse discharges, with respect to their application as opening switches. Concepts for diffuse discharge opening switches have been developed, experimental facilities have been assembled and experiments have been performed to investigate the applicability of these concepts. computer codes have been developed and applied to different systems to allow optimization and scaling.

The different groups of concepts discussed herein are:

- the electron-beam sustained diffuse discharge (Section B)
- the optically controlled diffuse discharge where optical control either means increased conductivity of the discharge by means of laser radiation or optical stimulation of loss processes in self-sustained discharges (Section C)
- exploratory opening switch projects

For the investigation of the electron-beam sustained discharge an apparatus was designed which allows investigations of repetitive opening in the time range of 100 ns at current levels of up to 10 kA.

The work done in the last year includes:

1. Opening Switch investigations in the following gas mixtures:
N₂:N₂O
N₂:SO₂
N₂:CO₂
2. Modification of the computer code to include ion current.

For investigations of optically controlled discharges the following steps were taken to approach a feasible switch system:

1. Design and construction of a new flowing after-glow cell
2. Small scale experiments on optically enhanced attachment
3. Externally sustained discharge experiments with photo-detachment
4. Change of the computer code to calculate attachment rates depending on the electron generation mechanism.

Several other exploratory concepts related to diffuse discharge opening switches have also been examined. Among these are a magnetically controlled switch (collaboration with GTE Laboratories, Inc.) and electrodes for diffuse discharge switches.

II. E-BEAM CONTROLLED OPENING SWITCH SYSTEM

A. Introduction

An electron-beam controlled discharge circuit has been constructed to study the behavior of an e-beam sustained, attachment dominated discharge:

- a) at high discharge current densities,
- b) in gases which are suitable for low loss, fast opening operation,
- c) for rep-rated operation.

The main objective of the investigation is to determine a set of criteria concerning electrical and gas parameters of an e-beam sustained discharge, which will guide the design of the rep-rated electron-beam controlled opening switch.

The switch concept is as follows: An e-beam is used to ionize the gas between two switch electrodes. An inductor can be charged through the then conducting gas. The switch voltage remains below the self breakdown voltage so there is no avalanche ionization. Thus, when the e-beam is turned off, electron attachment and recombination processes in the gas cause the conductivity to decrease and the switch opens.

1. Experimental Arrangement

a) E-Beam Gun/Control System

The e-beam was designed to satisfy the following requirements:

- 1) high repetition rate,
- 2) fast turn on and turn off times,

3) variable beam energy and current density.

The e-beam gun is constructed as a tetrode to achieve the required fast response control of the e-beam. A simple trigger circuit allows the generation of a burst of e-beam pulses with variable pulse duration and pulse separation. The tetrode has a thermionic cathode which allows variation of e-beam current and voltage, independent of each other. The design and performance of the system is described in Ref. 1 (attached as an Appendix).

b) Switch/Diagnostic System

The switch is located in a pressurized stainless steel chamber just above the e-beam chamber, as shown in Fig. 1. The e-beam enters the switch chamber through a 1 mil thick Titanium foil window which separates the two chambers. After entering the switch chamber, the e-beam passes through the lower electrode of the switch which is a 1/2 mil thick aluminum foil and is incident on the stainless steel upper electrode. The e-beam ionizes the gas between the two switch electrodes and generates a diffuse discharge. The two electrodes are connected coaxially to the switch pulser, as shown. This pulser is a 2 Ω PFN that is able to deliver a 25 kV, 12.5 kA, 1 μ s pulse to a matched load. The impedance of the PFN can easily be increased.

E-beam and switch currents are measured by transmission line current transformers [2]. The e-beam and switch voltages are monitored by resistive voltage dividers. Since the switch diagnostics are floating at the switch chamber potential (i.e. the potential of the top plate of the stripline),

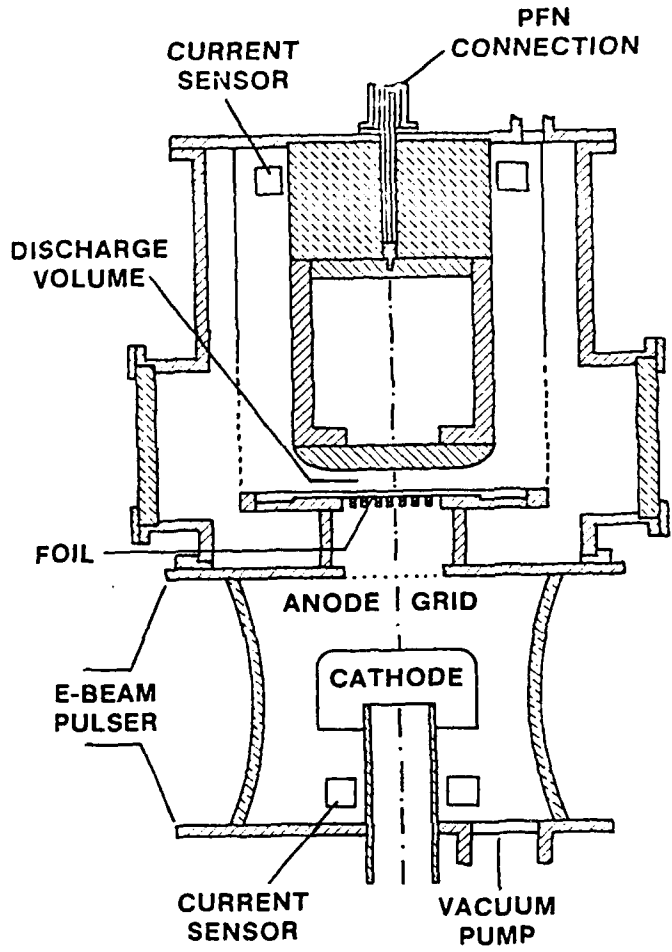


Fig. 1. Cross-Section of E-Beam Tetrode and Switch Chamber.

the signals are recorded in a floating screen room with oscilloscopes which are battery powered.

2. Experimental Results

Diffuse discharge investigations were performed in the gas mixtures $N_2:N_2O$, $N_2:SO_2$, and $N_2:CO_2$. The experimentally obtained current-voltage characteristic for $N_2:N_2O$ agrees with previously obtained theoretical results at high E/N [3]. The discrepancy in theoretical and experimental data at low E/N reflects the uncertainty in basic data for N_2O . With respect to the criteria for optimum switch gases (low losses during conduction (at low E/N), large losses during and after opening (at high E/N)) N_2O in N_2 is superior to the other investigated gases. For opening times of 100 ns, the current gain was in the order of 10. With better utilization of the e-beam energy in our system a gain of 100 can be achieved. Shorter opening times, down to ~ 10 ns, are possible with higher attachment concentrations, however, at the expense of reduced current gain. The published results are discussed in more detail in Ref's. 4, 5, and 6 (attached).

B. Modification of the Computer Code to Include Ion Current

In order to model the behavior of the diffuse discharge during and after turn-off of the e-beam, electron and ion current densities have to be considered. The computer code was therefore modified to include the transport of negative and positive ions and ion-ion recombination. The results showed that the contribution of ion current to the total current even after turn-off of the e-beam, where a strong increase in attachment occurs, does not exceed 10% (see Fig. 2).

The results of our investigations were presented at the GEC 1984 in Boulder, CO [14] (Abstract is attached).

B. Electrodes for Diffuse Discharge Switches

A general problem related to large volume diffuse discharges is the initiation of instabilities leading to current density inhomogeneities and finally to arcs. In most cases these instabilities start in regions with increased electric field intensity close to the electrodes. Cathodes with a lower potential difference across the sheath and positive I-V characteristics should therefore delay or prevent the onset of instabilities. Since hollow cathode discharges (HCD) are known to have these properties electrodes with a larger number of small holes acting as a multiple hollow cathode devices could be used. These holes could in addition be flushed with a gas (preferably a rare gas) which is known to be less sensitive to instabilities.

At the beginning of this project no information was available to determine the time required to initiate such a hollow cathode discharge. Experiments were therefore performed to investigate the delay time and rise time of a hollow cathode discharge in the nanosecond time scale. A paper presenting the results of these experiments is attached as an Appendix [15].

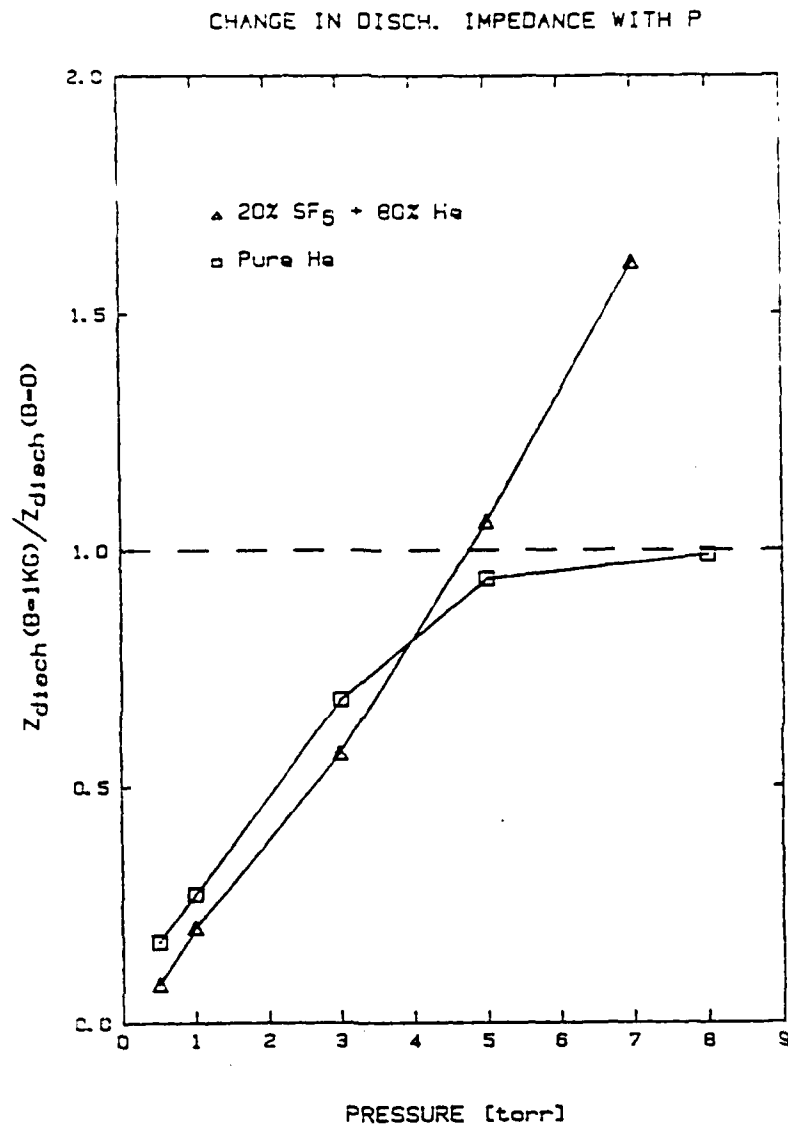


Fig. 6. The ratio of discharge impedance with and without magnetic field for the gases He and He + SF₆ as a function of total pressure.

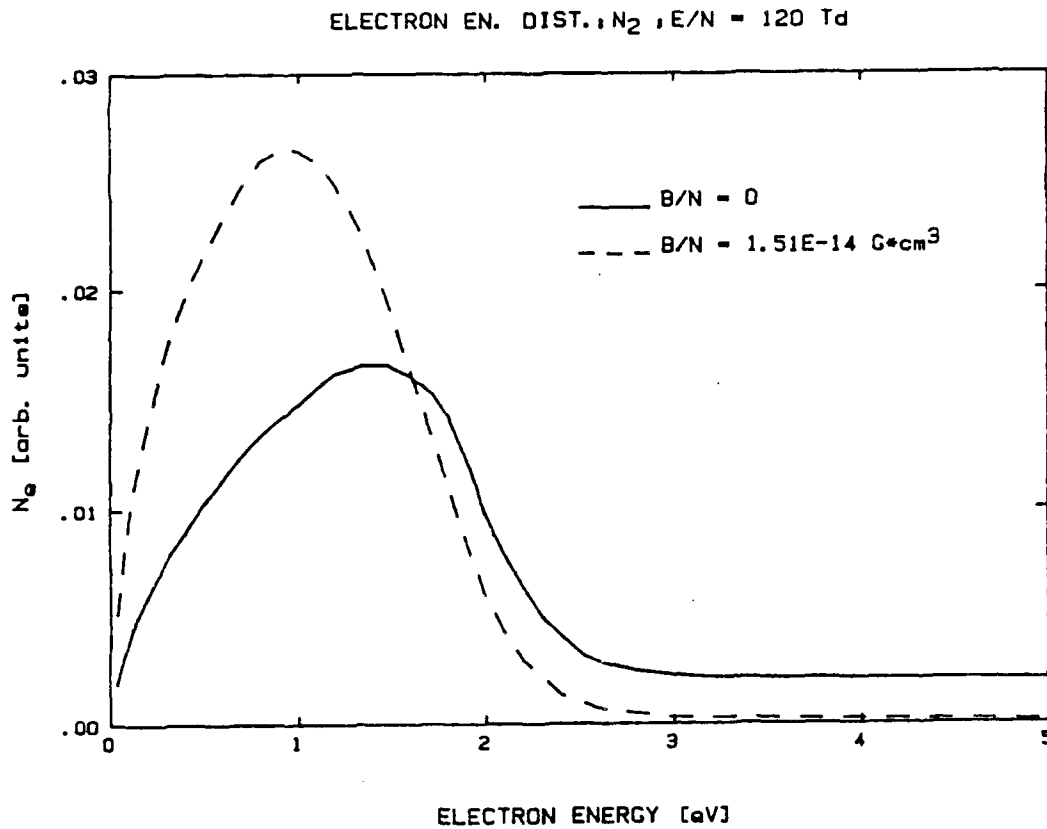


Fig. 5. Electron energy distributions with no magnetic field applied and with $B/N = 1.5 \cdot 10^{-14} \text{ G cm}^3$ (1 kG at $p = 4$ Torr)

low electron energies the attachment losses will thereby be increased. This effect, together with a reduced ionization rate can be utilized in an opening switch.

The effect of a magnetic field on the electron energy distribution in a low pressure gas discharge was studied by means of a Monte Carlo code for gas mixtures containing SF_6 in He or N_2 as buffer gases. Figure 5 shows the shift in the electron energy distribution with increasing magnetic field. At this time we perform calculations with model gases (artificial attachment cross-sections) to find the optimum gas mixture for low pressure discharge switches.

Simultaneously to the modeling of the discharge, experiments have been performed to demonstrate the feasibility of our opening switch concept. The experimental apparatus, constructed at the GTE Laboratories consists of a coaxial discharge system, with a magnetic field coil, which allows application of longitudinal magnetic fields up to several kG. Results of experiments in pure He and a He + SF_6 mixture are shown in Fig. 6. The ratio of discharge resistance with and without magnetic field at various pressures is plotted. Below 6 Torr discharges with either gas mixture have the same characteristic: the applied magnetic field reduces the discharge impedance (closing switch effect). Above 6 Torr there is no change in impedance for pure He. However, in He + SF_6 the impedance is increased in discharges with magnetic fields compared to that without magnetic field (opening switch effect). Further investigations are planned with gas mixtures, which according to our calculations, show better opening switch characteristics.

attachment. (2) Electron beam ionization will mainly produce electrons with energies above the value at which the maximum attachment cross-section occurs and thermalization at low values of E/N will cause the electron to cross the range of strong attachment.

The existing Monte Carlo code has been modified to allow the direct calculation of rate constants for all collision processes considered. Calculations of the attachment rate constant of N_2O in N_2 as a function of E/N are under way. Variable parameters of the calculation are the initial energy of the secondary electrons and the electron density.

IV. Exploratory Opening Switch Projects

Two exploratory concepts have been examined for potential use as opening switches, or for improvement of the efficiency of high pressure diffuse discharge opening switches, respectively. One is a magnetically controlled low pressure switch, the second concept deals with electrodes for high pressure diffuse discharges.

A. Magnetically Controlled Opening Switch

A joint research program between TTU and GTE Laboratories, Inc. was initiated to explore the possibility of controlling the conductivity of low pressure plasmas, containing attachers, by means of externally applied magnetic fields. The concept is based on the change in the electron energy distribution towards lower energies, when external magnetic fields are applied. In a gas containing attachers with attachment cross-sections which peak at

discharge and circuit parameters we used a code with two independent steps. In the first step, all rate constants necessary for the calculation of all rates of the significant processes are calculated, depending on E/N , for a representative gas mixture. These calculations are based on the electron energy distribution functions with E/N as the variable parameter obtained with preceding Monte Carlo calculations. This code has been used to calculate the characteristic and the transient behavior of an electron beam sustained discharge in N_2 with admixtures of an attachment (N_2O). Photodetachment of O^- was discussed as an additional optical control mechanism. The results of these calculations were presented in a paper at the 4th IEEE Pulsed Power Conference [13] and in a paper published in "Lasers and Particle Beams" [3]. As discussed in this paper, discrepancies are observed between attachment rate constants for N_2O calculated with our code from cross-sections and experimentally obtained attachment rate constants. But, rate constants obtained experimentally with different methods also show discrepancies, especially at low values of E/N . Consequently, discrepancies also occur between measurements [6] and calculations [3] of the discharge characteristics.

A project has, therefore, been started to evaluate the influence of the electron generation mechanism on the attachment rate constant depending on E/N . Two main cases are considered: (1) With photoionization the major fraction of the electrons produced will have energies below the value at which the maximum attachment cross-section occurs and thermalization at low values of E/N will not cause the electrons to cross the energy range of strong

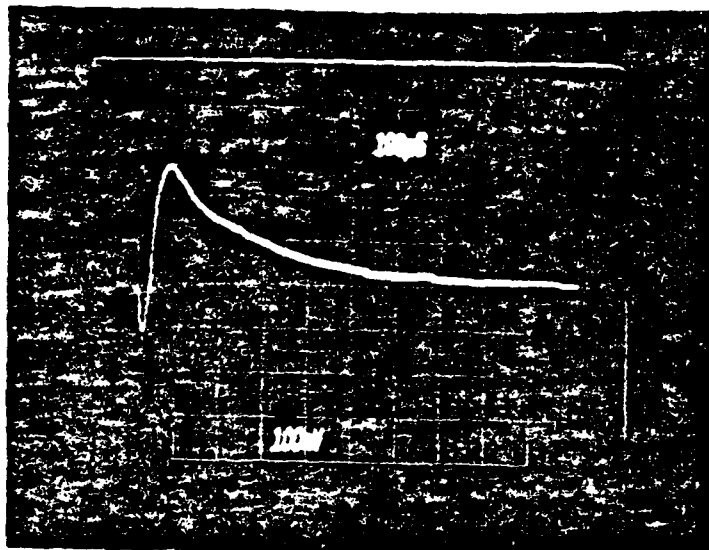


Fig. 4. Optogalvanic Signal of Photoenhanced Attachment in $\text{H}_2\text{C}=\text{CF}_2$.

signal is shown in Fig. 4. For the continuation of these experiments the following improvements are planned: (1) Optimization of the primary discharge to avoid attachment of the initial admixture and (2) an increase of the UV source energy.

D. High Power Discharge System

The design of an optically controlled high power discharge system was described in previous Annual Reports on AFOSR Contract No. F49620-79-0191. Although its' design has not been modified its' mode of operation has been changed to allow operation in the appropriate E/N range. As discussed in the previous chapters photodetachment was considered as a control mechanism, especially for the transition from the open state to the closed state to reduce losses significantly and to allow fast closing [3]. Here photodetachment is used in an externally sustained discharge in an E/N range well below self breakdown. The discharge system, which was originally designed for the operation of pulsed, self sustained discharges with UV-preionization is, therefore, now used to produce externally sustained discharges by using the UV-sources as an external ionization source. The initial experiments were performed in Helium with admixtures of oxygen.

E. Computer Calculations

In previous research periods on AFOSR Contract No. F49620-79-0191 a computer code was developed to evaluate the time-dependent behavior of an externally controlled discharge in a given circuit. In order to allow fast calculations for different

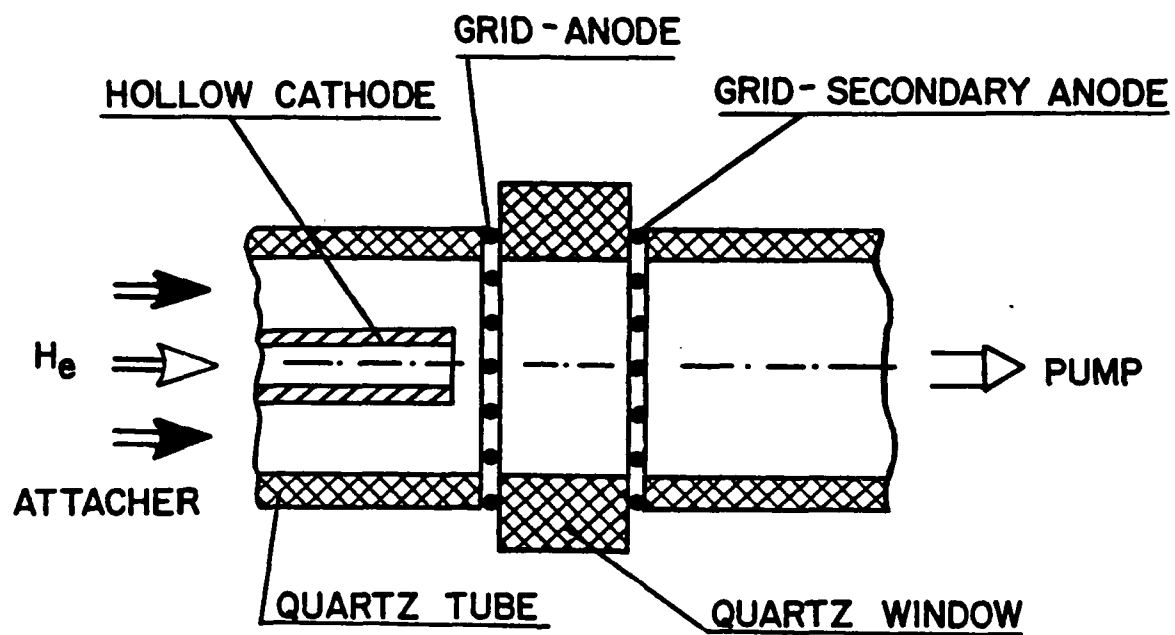


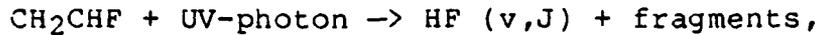
Fig. 3. Flowing Discharge Cell

The next group of processes considered for optical control of diffuse discharges includes processes allowing photo enhanced attachment, as discussed in Section C.2. At this time special emphasis is given to investigations of photodissociation of larger molecules generating fragments with a higher attachment rate (see Section III B). Since the starting products for these processes are attachers themselves but with high attachment rates at high values of E/N the effect of photo enhanced attachment has to be investigated in discharges at low values of E/N . For these experiments a new discharge tube had to be developed.

Figure 3 shows the experimental setup. The flowing discharge tube has similarities with the one used for the flowing afterglow experiments. The major difference is the use of a hollow cathode for the primary discharge with a separate flow through it. This allows operation of the primary discharge between the hollow cathode and grid 1 as the anode in pure helium. In a mixing regime between grid 1 and grid 2 the flowing helium plasma is mixed with the admixtures and between grid 2 and grid 3 a secondary discharge is operated at low E/N and low current. This secondary discharge is an externally sustained discharge since the carrier for this discharge are produced in the primary discharge. The time dependent current of this secondary discharge is measured after applying the optical signal.

With this device experiments have been performed in helium with admixtures of $H_2C=CF_2$ and $H_2C=CCl_2$ using a spark as a UV source. In preliminary experiments an increase of the resistivity in the order of 30% was observed. A typical optogalvanic

tation of lasers with transitions between excited vibrational states. An example is the reaction [10]:



which is used to operate HF lasers on rotational and vibrational transitions. Such processes have in the meanwhile proven to increase the attachment rate by orders of magnitude using the 195 nm radiation of an ArF laser [11]. At Texas Tech University the direct influence of these processes on the conductivity of an externally sustained discharge is being investigated. Since no laser with sufficiently high photon energy is available, UV-spark sources were considered as an appropriate alternative.

C. Small Scale Experiments (in collaboration with Frazer Williams)

Although the basic data available for several processes allow us to estimate the magnitude of certain optogalvanic effects, small scale experiments are necessary to prove the feasibility of these concepts. The reasons are that in a discharge the optogalvanic effect competes with a large number of processes and that a full set of rate constants is not available in most cases. Even if fairly complete sets of cross-sections are available the necessary calculations are difficult and time consuming. In the first study in 1982, in corporation with J. Mosely, University of Oregon, we looked at photodetachment of O^- in the flowing after-glow of a discharge containing O_2 . A paper describing the results of these experiments has been published in IEEE Trans. Plasma Sci. [12]. The investigations on photodetachment are now continued in an externally sustained discharge.

It should be pointed out that all these research areas strongly interact with the work on electron beam controlled diffuse discharges, described in the previous section.

B. Concepts for Optical Control of Diffuse discharge Opening Switches

The aim of this work is to investigate several types of opto-galvanic processes and to estimate the magnitude of the change of the discharge resistivity with regard to their possible application as a control mechanism for diffuse discharge switches. Some of the earlier results are summarized in a paper published in IEEE Trans. Plasma Sci. [7]. An overview was also given in an invited paper at the 4th IEEE Pulsed Power Conference [8], and more recently as an Air Force Pulsed Power Lecture Note [9].

As a result of all previous investigations it was concluded that the generation of electrons should be accomplished by cheaper methods than laser photons such as electron beams while photons could be used to control the electron depletion mechanism. The main emphasis is, therefore, on processes related to the necessity of using attachers to achieve fast opening times. Photodetachment has already been investigated in previous research periods and is now used in an externally sustained discharge (see Section C.4). The emphasis is now on processes of photo enhanced attachment, and here mainly on the generation of vibrationally excited molecules with much higher attachment cross-sections than the same molecule in it's ground state. In the last annual report photodissociation of larger molecules has been suggested which is used for the exci-

III. OPTICALLY CONTROLLED DISCHARGES

A. Introduction

Optical discharge control means to make use of an optogalvanic effect. Here the conductivity of a discharge is changed by irradiation with light. Optogalvanic effects have been mainly applied to processes where the wavelength-specific response of the discharge is used, such as in spectroscopy, sensing of impurities, and frequency stabilization. In these applications a detectable signal is required but its magnitude is of minor importance. For switching applications, however, only those processes can be considered that show a strong influence on the charge carrier balance of the discharge. In the beginning of this project the following four research areas were felt necessary for the solution of this problem:

- a. Concepts for optical control of diffuse discharge opening switches must be developed, based on known effects from optogalvanic experiments.
- b. Small scale optogalvanic experiments must be performed on promising systems where sufficient data are not yet available.
- c. High power discharge system experiments must be carried out to check the scaling laws for the optogalvanic processes and to investigate promising control systems.
- d. Detailed calculations on promising systems must be performed to predict the optimum parameter range for the experiments with respect to the suggested transient behaviors of the discharges.

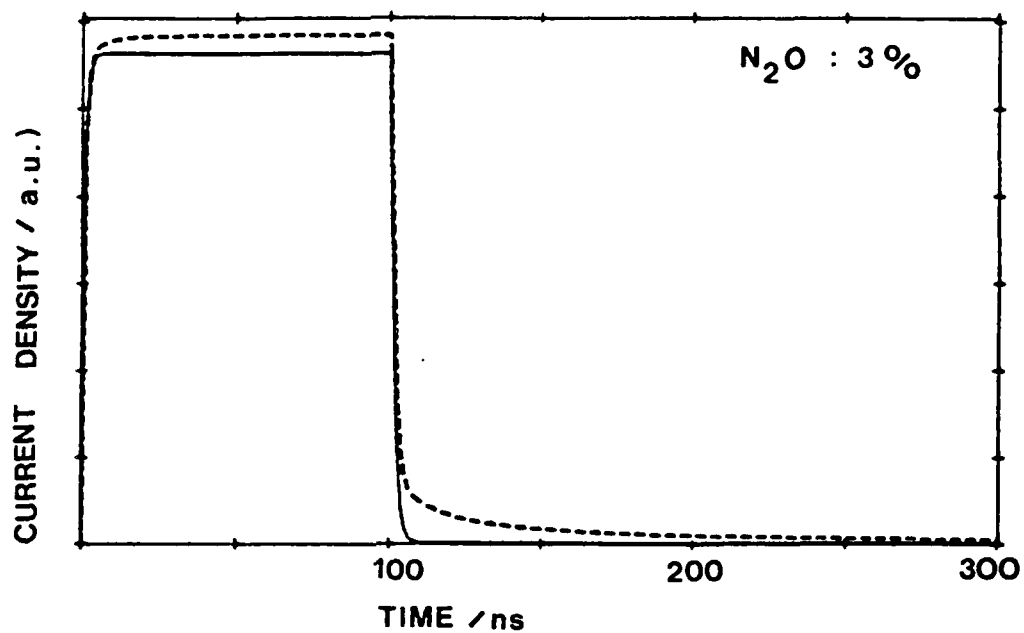


Fig. 2 The time dependence of the current density of an e-beam sustained discharge in 1 atm N₂ with an N₂O fraction of 3%. Dashed line represents calculated results with the ion component included, the solid line represents just the electron current density.

VI. REFERENCES

1. H.C. Harjes, K.H. Schoenbach, G. Schaefer, M. Kristiansen, H. Krompholz, and D. Skaggs, "Electron-Beam Tetrode for Multiple, Submicrosecond Pulse Operation", Rev. Sci. Instrum., 55, 1684 (1984).
2. H. Krompholz, J. Doggett, K.H. Schoenbach, J. Gahl, C. Harjes, G. Schaefer, and M. Kristiansen, "Nanosecond Current Probe for High-Voltage Experiments", Rev. Sci. Instrum., 55, 127 (1984).
3. G. Schaefer, K.H. Schoenbach, H. Krompholz, M. Kristiansen, and A.H. Guenther, "The Use of Attachers in Electron Beam Sustained Discharge Switches - Theoretical Considerations", Lasers and Particle Beams. 2, part 3, 273 (1984).
4. K. Schoenbach, G. Schaefer, M. Kristiansen, H. Krompholz, H. Harjes, and D. Skaggs, "Investigations of E-Beam Controlled Diffuse Discharges" in Gaseous Dielectrics IV, ed. L.G. Christophorou, Pergamon Press, 1984, p. 246.
5. K. Schoenbach, G. Schaefer, M. Kristiansen, H. Krompholz, H.C. Harjes, and D. Skaggs, "An E-Beam Controlled Diffuse Discharge Switch", Conf. Record, 1984 Sixteenth Power Modulator Symposium, Arlington, VA, p 152.
6. K.H. Schoenbach, G. Schaefer, M. Kristiansen, H. Krompholz, H.C. Harjes, and D. Skaggs, "An Electron-Beam Controlled Diffuse Discharge Switch", accepted for publication in J. Appl. Phys.

7. K.H. Schoenbach, G. Schaefer, M. Kristiansen, L.L. Hatfield, and A.H. Guenther, "Concepts for Optical Control of Diffuse Discharge Opening Switches", IEEE Trans. Plasma Sci., PS-10, 246 (1982).
8. G. Schaefer, K.H. Schoenbach, A.H. Guenther, and W.K. Pendleton, "Some Recent Advances in Optically Controlled Discharges", Proc. 4th IEEE Pulsed Power Conf. Albuquerque, NM, June 1983. (Invited Paper).
9. G. Schaefer, "Optically Controlled Diffuse Discharges", Pulsed Power Lecture Series, No. 49, 1983, AFOSR Grant No. 78-3675.
10. E.R. Sirkin and G.C. Pimentel, "HF rotational laser emission through photoelimination from vinyl fluoride and 1;1-difluoroethene", J. Chem. Phys., 75, 604 (1981).
11. M.J. Rossi, H. Helm, and D.C. Lorents, "Photoenhanced Electron Attachment in Vinylchloride and Trifluorethylene", 37th Gaseous Electronics Conference, B-1, Boulder, CO, 1984.
12. G. Schaefer, P.F. Williams, K.H. Schoenbach, and J. Moseley, "Photodetachment as a Control Mechanism for Diffuse Discharge Switches", IEEE Trans. Plasma Sci., PS-11, 263 (1983).
13. G. Schaefer, K.H. Schoenbach, P. Tran, J.-S Wang, and A.H. Guenther, "Computer Calculations of the Time Dependent Behavior of Diffuse Discharge Switches", Proc. 4th IEEE Pulsed Power Conf., Albuquerque, NM, June 1983.
14. J.R. Cooper, K.H. Schoenbach, G. Schaefer, J.M. Proud, and W.W. Byszewski, 37th Annual GEC, Boulder, CO, 1984, Abstract CB-4.

15. G. Schaefer, P. Husoy, K.H. Schoenbach, H. Krompholz, "Pulsed Hollow-Cathode Discharge with Nanosecond Risetime", IEEE Trans. Plasma Sci., accepted for publication in 1984.

Electron-beam tetrode for multiple, submicrosecond pulse operation^{a)}

C. H. Harjes, K. H. Schoenbach, G. Schaefer, M. Kristiansen, H. Krompholz, and D. Skaggs

Department of Electrical Engineering, Texas Tech University, Lubbock, Texas 79409

(Received 9 April 1984; accepted for publication 4 June 1984)

The design and the operation of a 250-kV, 400-A, *e*-beam tetrode is described. A simple trigger circuit allows the generation of a burst of *e*-beam pulses with variable pulse duration and pulse separation.

INTRODUCTION

There is an increasing interest in fast, repetitive opening switches for inductive energy storage systems.¹ An opening switch concept that shows promise for fast, repetitive operations is the electron-beam-controlled diffuse discharge switch.²⁻⁴ It contains a gas mixture which becomes conductive when an ionizing *e*-beam is injected. When the *e*-beam is turned off, electron attachment and recombination processes cause the reduction of the electron density in the gas and the switch opens. For the investigation of *e*-beam-controlled conductivity in switch gases, an *e*-beam tetrode was designed. The operating characteristics are: (a) burst mode operation in the Mpps (Megapulses/second) range; (b) variable pulse duration and pulse separation; (c) turn-on and turn-off times in the range of 10 ns; (d) variation of *e*-beam energy ($E_B < 250$ keV); and (e) variation of *e*-beam current density ($J_B < 4$ A/cm²).

I. ELECTRON-BEAM GUN

A cross section of the tetrode is shown in Fig. 1(a). The cathode is located in an evacuated ($p = 2 \times 10^{-7}$ Torr) Pyrex cylinder, between the two plates of a stripline. The anode consists of a grid of 250- μ m molybdenum wires at a distance of 7 cm to the cathode. The anode grid covers the entrance of a 12.9-cm-long drift tube which is terminated by a 25- μ m titanium foil. The foil is supported by an array of titanium bars. The bottom plate of the stripline is grounded and the *e*-beam voltage is applied to the top plate by a two-stage Marx generator. The generator (Physics International Co. FRP-250) can deliver a maximum voltage of 250 kV with a 10-ns rise time and with an exponential decay time constant of about 2.5 μ s into a 300- Ω load.

A more detailed cross section of the cathode is shown in Fig. 1(b). The electron source is an electrically heated array of 375- μ m-diam thoriated tungsten filaments. A negatively biased spreader plate ($V_s = -500$ V) prevents electron current flow from the filaments back to the grounded cathode base when no plate voltage is applied. At a filament temperature of about 2100 K, the *e*-beam current density is about 4 A/cm² over the 100-cm² cross sectional area of the beam. The current density can be varied independently of the accelerating voltage by adjusting the filament temperature.

The control grid is located 0.4 cm above the filament array. It is formed by an array of 250- μ m-diam molybdenum wires stretched across a 17.5-cm-diam circular hole in the outer shell of the cathode assembly. A negative bias voltage, $V_B = 4$ kV, is applied to the grid to hold the *e*-beam off, even

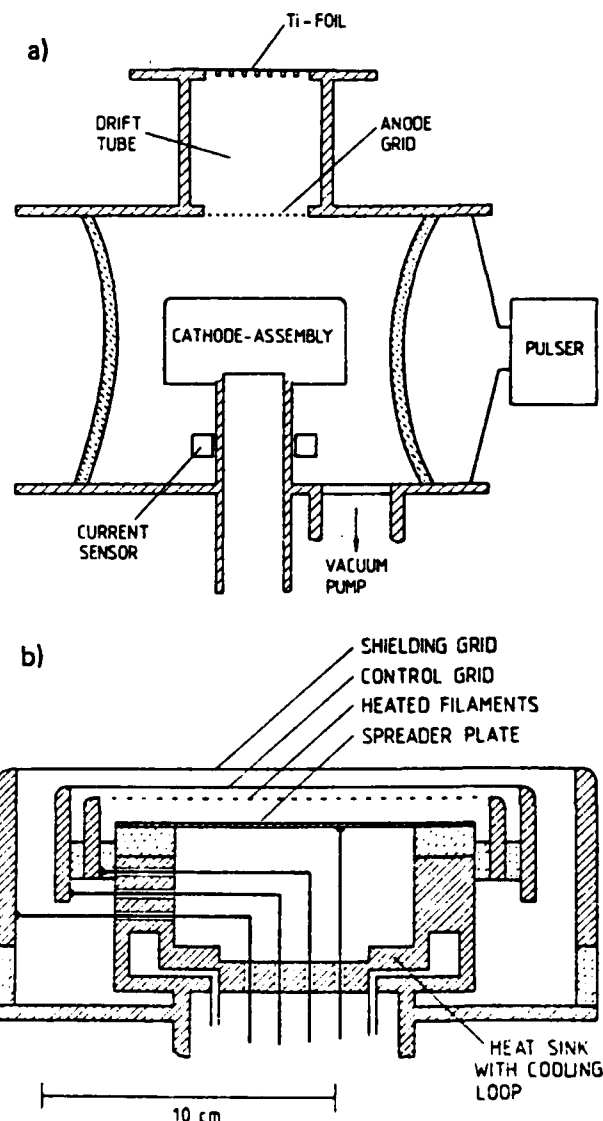


FIG. 1. (a) Cross section of *e*-beam tetrode. (b) Cross section of cathode assembly.

when the accelerating voltage is applied to the plate. The e -beam is turned on by applying a positive voltage pulse of typically $V_2 = +4$ kV to the grid. A second grid, which is biased to $+4$ kV, shields the control system electrostatically. It is positioned 0.6 cm above the control grid. The grids and cathode are connected to external power supplies through high-vacuum electrical feedthroughs located in the aluminum base of the cathode. The base is water cooled and serves as a heat sink for the cathode.

II. CONTROL SYSTEM

The pulser driving the grid is depicted in Fig. 2(a). It consists of two, 75- Ω cables (lengths d_1 and d_2) separated by a triggerable spark gap. Cable 1 is connected to the grid, as shown, and is charged to the negative bias voltage $-V_B$. Cable 2 is charged through a 10-M Ω resistor to the voltage $+V_2$. After triggering the spark, the positive voltage from cable 2 propagates towards the grid, is reflected with the same polarity, travels back to the charging resistor, and is reflected again. The negative bias voltage from cable 1 is reflected at the open end, etc. Hence, the cable pulser with two open ends generates a periodic rectangular grid voltage V_g , with alternating polarity as shown in Fig. 2(b), and the electron beam is repetitively turned on and off.

The primary advantage of this pulser is its simplicity and versatility. The pulse magnitudes are variable by changing the cable charging voltages, and the pulse width and pulse separation can be adjusted by changing the lengths of the cables. However, due to the effect of the capacitive termination in the tetrode and cable dispersion, subsequent pulses are degraded. This degradation limits the useful length of the pulse train to three or four pulses. The output of the grid pulser, when fired into a 100-k Ω dummy load, is shown in Fig. 3. The rise and fall time of the first pulse is about 10 ns

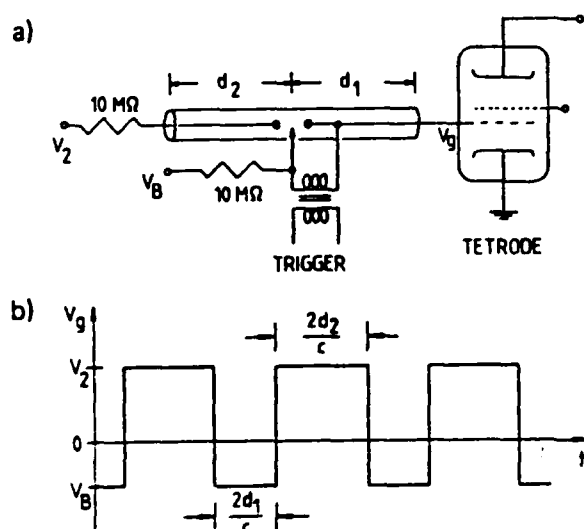


FIG. 2. (a) Schematic diagram of grid pulser. (b) Ideal output signal of the grid pulser.

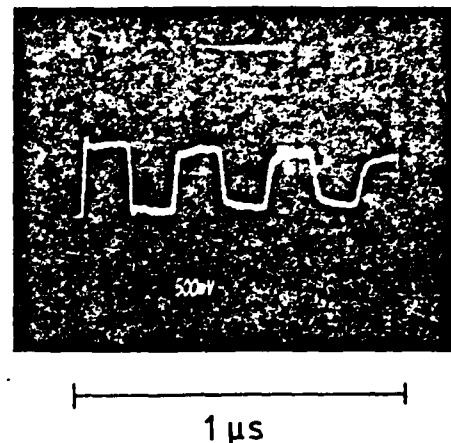


FIG. 3. Grid pulser signal output into 100-k Ω load.

and of the second and third pulses 20 and 30 ns, respectively. The reduction of the pulse amplitude is not important as long as the pulse voltage is above the threshold voltage for e -beam turnon.

III. ELECTRON-BEAM CURRENT MEASUREMENT

Measurements of the electron-beam current at the cathode and at the anode—after passing the titanium foil—were performed with transmission line current transformers.⁵ Figure 4(a) shows current signals, $i_{out}(t)$, recorded at the cathode. The e -beam current pulses shown in Fig. 4(b) are evaluated from these signals by using the relation $i_{out} = 1/(2N)[I(t) - I(t - T)]$, where $I(t)$ is the current to be measured, T denotes the coil transit time, and N is the number of turns.⁵ The decay in amplitude is caused by the exponential plate voltage decay. Because of the reduced transmission of electrons through the foil at lower electron energies, the effective time of operation is limited to approximately 1 μ s for the voltage generator used in this experiment.

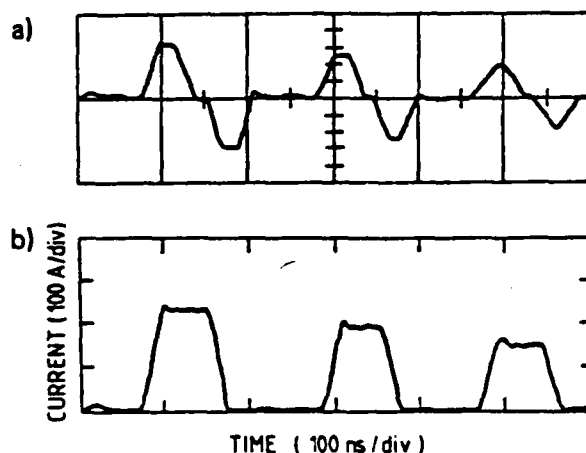


FIG. 4. (a) Current signals obtained with transmission line current transformer at the cathode. (b) Corresponding e -beam pulses.

*Supported by ARO and AFOSR.

¹K. H. Schoenbach, M. Kristiansen, and G. Schaefer, Proc. IEEE 72, 1019 (1984).

²M. R. Hallada, P. Bletzinger, and W. F. Bailey, IEEE Trans. Plasma Sci. PS-10, 218 (1982).

³R. J. Commisso, R. F. Fernsler, V. E. Scherrer, and I. M. Vitkovitsky, IEEE Trans. Plasma Sci. PS-10, 241 (1982).

⁴K. H. Schoenbach, G. Schaefer, M. Kristiansen, L. L. Hatfield, and A. H. Guenther, IEEE Trans. Plasma Sci. PS-10, 246 (1982).

⁵H. Krompholz, J. Doggett, K. H. Schoenbach, J. Gahl, C. Harjes, G. Schaefer, and M. Kristiansen, Rev. Sci. Instrum. 55, 127 (1984).

37th Annual Gaseous Electronics Conference,
Oct. 9-12, 1984, University of Colorado,
Boulder, CO, p. 29.

CB-4 Magnetic Control of Low Pressure Glow Discharges*

J. R. Cooper, K.H. Schoenbach, G. Schaefer, Texas Tech,
J.M. Proud, W.W. Byszewski, GTE Laboratories--The energy
distribution $f(\epsilon)$ of electrons in low pressure gases
under the influence of an electric field is shifted to-
wards lower energy values if a crossed magnetic field
is applied. This change in $f(\epsilon)$ was studied by means of
a Monte Carlo code for gas mixtures containing SF_6 , He,
and N_2 . In gases with a strong increase in the net ion-
ization (ionization minus attachment) coefficient with
field strength this effect should lead to a considerable
reduction of the electron density and thus the conduct-
ivity. The controllability of plasma conductivity by
means of magnetic fields was studied experimentally in
a low pressure glow discharge in SF_6 plus He. A decrease
in conductance of a factor of two was obtained with an
applied magnetic field of 1 kGauss.

*Supported by GTE Laboratories and the Center for Energy
Research at Texas Tech University.

An electron-beam controlled diffuse discharge switch^{a)}

K. H. Schoenbach, G. Schaefer, M. Kristiansen, H. Krompholz, H. C. Harjes, D. Skaggs
Department of Electrical Engineering, Texas Tech University, Lubbock, Texas 79409

(Received 18 September 1984; accepted for publication 30 October 1984)

The performance of externally controlled, high-pressure, diffuse discharges as switching elements in pulse power systems is strongly determined by the recombination and attachment processes in the fill gas. To obtain high control efficiency and fast response of the diffuse discharge switch the discharge must be attachment dominated with the attachment rate coefficient increasing with field strength. An electron-beam controlled diffuse discharge system was constructed to study the behavior of pulsed discharges in the submicrosecond range in gas mixtures containing N_2 as a buffer gas and small additives of electronegative gases. The results of experiments in N_2 plus N_2O were compared with values obtained with a Monte Carlo code and a rate equation calculation.

INTRODUCTION

Inductive energy storage is attractive in pulsed power applications because of its intrinsic high energy density compared to capacitive storage systems. The key technological problem in developing inductive energy discharge systems, especially for repetitive operation (repetition rates greater than one kilopulse per second) is the development of opening switches. Promising candidates for repetitive opening switches are *e*-beam or laser controlled diffuse discharges.¹ The schematic diagram of an electron-beam controlled opening switch as part of an inductive storage system is shown in Fig. 1. The switch chamber is filled with a gas of pressures of 1 atm and above. The gas between the electrodes conducts and allows charging of the inductor, when an ionizing *e*-beam is injected into the gas (usually through one of the electrodes which might be a mesh or a foil). The switch voltage remains below the self-breakdown voltage, so that avalanche ionization is negligible. Thus, the discharge is completely sustained by the *e*-beam. When the *e*-beam is turned off, electron attachment and recombination processes in the gas cause the conductivity to decrease and the switch opens. Consequently the current through the inductor is commutated into the load.

EXPERIMENTAL SETUP

For the investigation of *e*-beam controlled conductivity in a high-pressure diffuse plasma discharge system was constructed with an *e*-beam tetrode as the control element.² A schematic cross-section of the discharge chamber and *e*-beam tetrode is shown in Fig. 2. The *e*-beam cathode is located in an evacuated Pyrex cylinder between the two plates of a stripline. The anode consists of a grid of molybdenum wires at a distance of 7 cm from the cathode. The anode grid covers the entrance of a 13-cm-long drift tube which is terminated by a 25- μ m titanium foil. The foil is supported by an array of titanium bars. The *e*-beam voltage is applied to the anode by a two-stage Marx generator. The generator (Physics International Co. FRP-250) can deliver a maximum voltage of 250 kV with a 10 ns rise time and with an exponential decay time constant of about 2.5 μ s into a 300- Ω load.

The electron source is an electrically heated array of 375- μ m-diameter thoriated tungsten filaments. At a filament temperature of about 2100 K, the *e*-beam current density is about 4 A/cm² over the 100 cm² cross-sectional area of the beam. The current density can be varied independently of the accelerating voltage by adjusting the filament temperature. The control grid, which is located 0.4 cm above the filament array, is negatively biased to hold the *e*-beam off, even when the accelerating voltage is applied to the plate. The *e*-beam is turned on by applying a positive voltage pulse of typically $V = +4$ kV to the grid. The control grid is driven by a pulser which provides a train of pulses with variable amplitude, pulse duration and pulse separation.² A second grid, 0.6 cm above the control grid, shields the control system electrostatically.

Measurements of the electron beam current at the cathode and at the anode—after passing through the titanium foil—were performed with transmission line current transformers.³ Figure 3 shows the *e*-beam current pulses, evaluated from current transformer signals. The decay in amplitude is caused by the exponential plate voltage decay. Because of the reduced transmission of electrons through the foil at lower electron energies the effective time of operation is limited

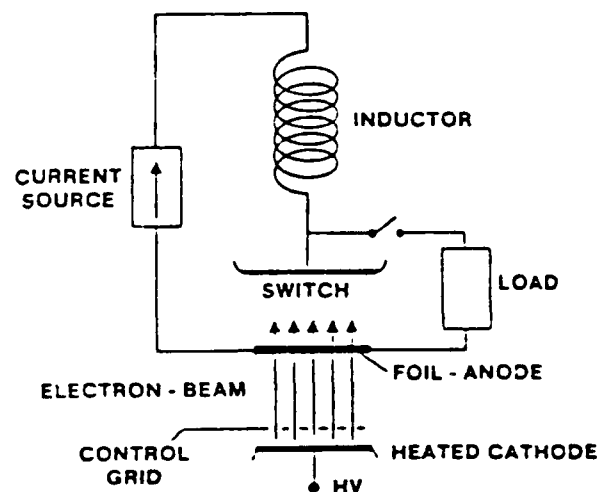


FIG. 1. Schematic of an *e*-beam controlled diffuse discharge opening switch.

^{a)} Supported by Air Force Office of Scientific Research and Army Research Office.

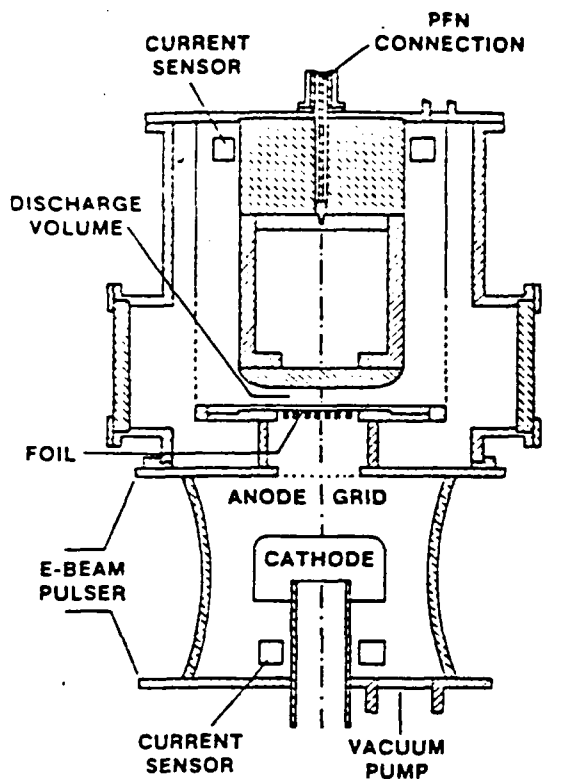


FIG. 2. Cross section of e-beam tetrode and switch chamber.

to approximately $1 \mu\text{s}$ with the voltage generator used in this experiment.

After passing through the titanium foil and a $12.5 \mu\text{m}$ aluminum foil, which serves as an electrode in the diffuse discharge switch, the e-beam generates diffuse plasma between the electrodes in the stainless steel discharge chamber. The current through the plasma is provided by a $2-\Omega$ pulse-forming network (PFN), which delivers a flat top current pulse of $1 \mu\text{s}$ duration and an amplitude of up to 12.5 kA .

SWITCH-GAS PROPERTIES

The switch opening time, after e-beam turn-off, is determined by the electron loss processes in the diffuse discharge: recombination and attachment. In order to achieve opening times of less than a microsecond at initial electron densities $< 10^{14} \text{ cm}^{-3}$, the dominant loss process must be attachment, which means that the switch gas mixture must contain an electronegative gas. On the other hand, additives of attachers increase the power losses during conduction. Both

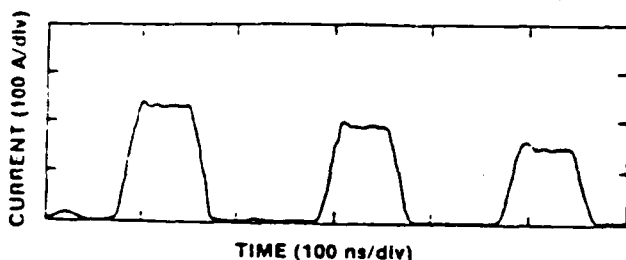


FIG. 3. e-beam current pulses measured at the cathode.

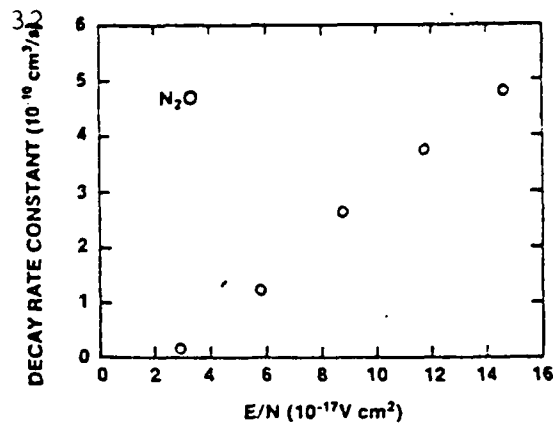


FIG. 4. Decay rate constants of the electron conduction current by adding N_2O in 350 Torr of N_2 at various E/N (see Ref. 7).

low forward voltage drop and fast opening can only be obtained by choosing gases or gas mixtures which satisfy the following conditions^{1,4,5}:

- (1) For low values of the reduced field strength E/N (conduction phase) the gas mixture should have a high drift velocity v_d and low attachment rate coefficient k_a .
- (2) For high E/N values (opening phase) the gas mixture should have lower drift velocities and high attachment rate coefficients.

(3) To avoid the onset of the attachment instability during conduction, the switch should be operated at E/N values where the attachment rate coefficient has a minimum or a negative slope.

Along with these considerations, several gas mixtures have been proposed for diffuse discharge opening switches.⁴ For our theoretical investigations N_2 was chosen as a buffer gas with N_2O as the added attacher. The N_2 was used since a complete set of cross sections is available⁶ and the plasma chemistry in a mixture of N_2 and N_2O appears to be relatively simple. Furthermore, N_2O in an N_2 buffer gas exhibits an E/N dependent electron decay rate which increases by more than a factor of 20 in the E/N range from 3 to 15 Td, as shown in Fig. 4. It should be noted that N_2 has an electron drift velocity which increases with E/N and therefore is not the optimum buffer gas in diffuse discharge opening switches. However, for gas mixtures which show a strong attachment rate increase, the drift velocity condition at high E/N is generally of minor importance.

DISCHARGE ANALYSIS

To calculate the current-voltage characteristics of a diffuse plasma sustained by an electron beam, as well as to evaluate the time dependent impedance of an externally controlled discharge in a given circuit, a computer model has been developed that enables fast calculations for a variety of conditions.⁵ It does not, however, provide for spatial analysis of the discharge. The code uses two independent programs. In a first computation, all rate constants of the significant processes are calculated as a function of E/N for a representative gas mixture. These calculations use the E/N dependent electron energy distribution functions that have been previously compiled using a separate Monte Carlo

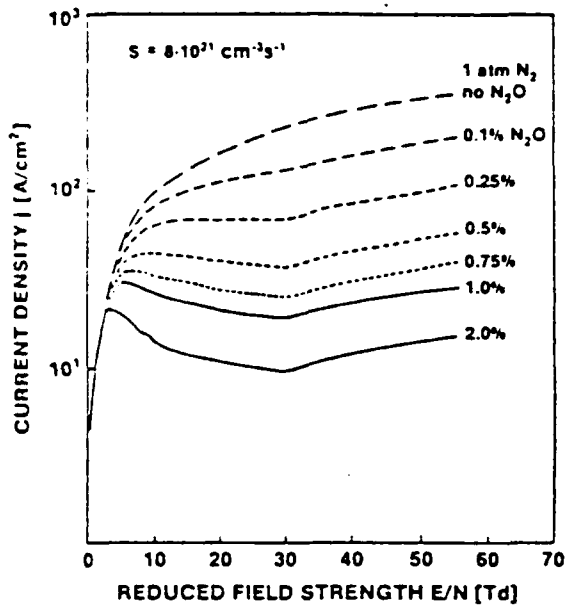


FIG. 5. Calculated steady-state j vs E/N characteristics for an e -beam sustained discharge in N_2 with admixtures of N_2O . The electron generation rate is $8 \times 10^{21} \text{ cm}^{-3} \text{ s}^{-1}$. The parameter is the N_2O fraction in percent (see Ref. 5).

code. In a second step, a system of circuit equations and rate equations has been solved, where we used the previously calculated E/N dependence of the rate constants, assuming that they do not change significantly for small variations of the gas mixture.

The transient behavior of the discharge as part of a discharge circuit is discussed in Ref. 5. The calculation of the steady-state behavior of the diffuse does not require information about the circuit. Calculations of the steady-state discharge characteristics were performed with the relative attachment concentration in the buffer gas as the parameter. Figure 5 shows the current density j versus reduced field strength E/N characteristics for different N_2O concentrations in an N_2 buffer gas. The total pressure is 1 atm. At small E/N , below 4 Td, the electron loss is due to recombination only. At about 4 Td the attachment rate coefficient rises steeply. This means that, for reasonably high attachment concentrations in the buffer gas, the losses increase drastically, causing a negative slope in the current-voltage characteristics. At 30 Td, where the attachment rate coefficient is assumed to level off, recombination becomes more important again, as demonstrated by the change in the slope j vs E/N , at this value.

EXPERIMENTAL RESULTS

Diffuse discharge experiments were performed in N_2O , SO_2 , and CO_2 with N_2 as the buffer gas. The e -beam tetrode was for these experiments mostly used in the single pulse mode. The source term, the number of electrons produced per cm^3 and per second, was in the range of $10^{20} \text{ cm}^{-3} \text{ s}^{-1}$ to $10^{21} \text{ cm}^{-3} \text{ s}^{-1}$. The voltage applied at the PFN was varied between 2 and 20 kV. The switch electrode gap was kept constant at 3.5 cm.

Figure 6 shows the influence of attachment concentration (N_2O) on the switch current. For high N_2O concentrations

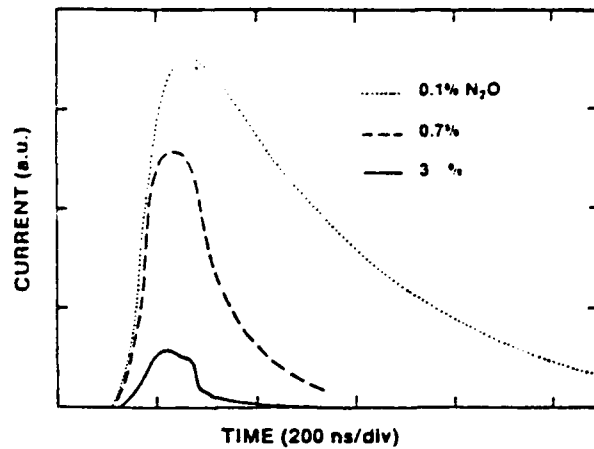


FIG. 6. Time dependence of switch current with N_2O concentration as the variable parameter.

(3%) the switch current pulse replicates the e -beam current pulse, except for the tail. The tail may be caused by the current carried by positive and negative ions. The current gain (switch current/electron beam current) is about 2 for this high attachment concentration. For concentrations of 0.7%, the fall time ($1/e$ -time) increases to approximately 100 ns. For 0.1% it is on the order of 500 ns. The gain increases to values of 9 and 12 for 0.7% and 0.1% N_2O , respectively.

Figure 7 shows the j vs E/N characteristics of the e -beam sustained discharge under steady-state condition in 1 atm N_2 with 0.7% N_2O . The curve represents the calculated values, circles the experimental results. The experimental values at higher E/N correspond well to the theoretical curve. However, the measured discharge characteristics do not exhibit the predicted current maximum at E/N values of approximately 4 Td. These results seem to indicate that attachment is dominant even at $E/N < 4$ Td, where, according to the measured values of the decay rate (see Fig. 4), attachment should be negligible. This assumption is confirmed by results of recently performed attachment rate coefficient measurements⁵ and by Monte Carlo calculations of the attachment rate coefficient⁹ based on experimentally obtained

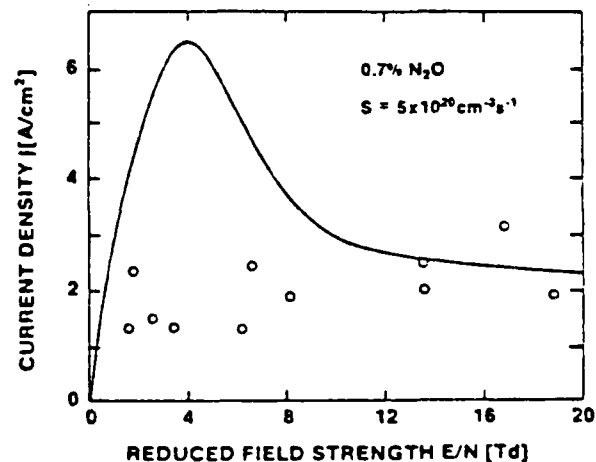


FIG. 7. Current density j vs reduced strength E/N for a discharge in N_2 with 0.7% N_2O (calculated curve and experimental data points).

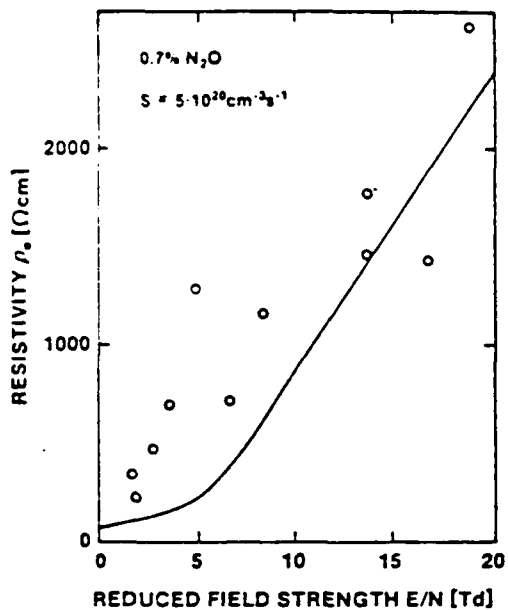


FIG. 8. Discharge resistivity ρ_0 as a function of reduced field strength E/N for a discharge in $N_2:N_2O$ (calculated curve and experimental data points).

attachment cross-sections.¹⁰ The loss of initially high energy secondary electrons by attachment as they lose energy by inelastic collisions could also, at least partially, account for the absence of the current density maximum in the experimental values at low E/N . Monte Carlo calculations are under way to gain a quantitative understanding of this effect.

Even with the attachment onset at $E/N < 4$ Td, that means with an attachment dominated discharge during conduction, the $N_2O:N_2$ mixture seems to work fairly well as an opening switch gas. It satisfies the requirement of having low resistance at low E/N and high resistance at large E/N , as seen on Fig. 8, where the results of current-voltage measurements (Fig. 7) are plotted in a resistivity versus reduced field strength diagram. It shows an increase in resistivity of almost two orders of magnitude in an E/N range of 3 to 20 Td.

$N_2:SO_2$

Another gas which has the required E/N dependence of the attachment rate coefficient is SO_2 (Ref. 11). The SO_2 has a lower attachment rate and an onset of attachment at higher values of E/N , compared to N_2O . In order to get opening times similar to those in the 0.7% $N_2O:N_2$ mixture, the concentration of SO_2 in N_2 as the buffer gas had to be increased to 20%. The total gas pressure was reduced to 250 Torr, to cover a wider range of E/N with the given switch voltage.

Figure 9 shows the resistivity versus E/N of an $SO_2:N_2$, e-beam sustained discharge with $S = 3 \times 10^{20} \text{ cm}^{-3} \text{ s}^{-1}$. The resistivity rises above an E/N of 50 Td, indicating an increase in attachment at this value. This rise is in agreement with measured attachment characteristics in pure SO_2 .¹¹ An increased discharge impedance is also observed at low reduced field strength, as indicated by two high resistivity values shown in Fig. 9, below an E/N of 10 Td. This increase might be caused by strong three-body attachment processes at near thermal electron energies^{12,13} and SO_2^- formation via the radiative stabilization process.¹³ Both the increased dis-

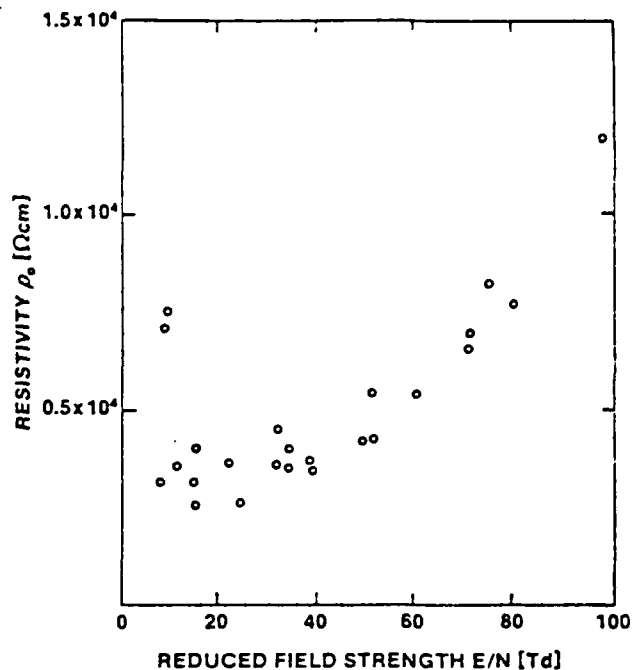


FIG. 9. Discharge resistivity ρ_0 as a function of reduced field strength E/N for a discharge in $N_2:SO_2$ (250 Torr).

charge impedance at low E/N and the relatively high overall resistivity make the $SO_2:N_2$ mixture not a good gas mixture for switching. The $N_2O:N_2$ mixture, under the same conditions (gas pressure, e-beam source term, and opening time), has a much lower resistivity at low E/N , which means that the Joule losses during conduction can be kept lower for this gas mixture.

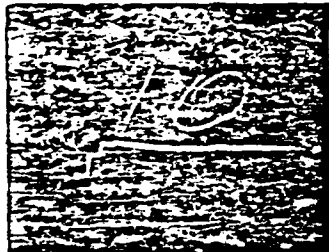
$N_2:CO_2$

Like N_2O and SO_2 , CO_2 has an increasing attachment rate coefficient with E/N . The disadvantage of CO_2 for use as an opening switch gas is its relatively low ionization energy. The field strength range where the attachment coefficient η exceeds the ionization coefficient α reaches only up to approximately 60 Td.¹¹ This value determines the hold-off field strength in this gas. For $E/N > 60$ Td the current rises again, which means that the switch closes further instead of opens after e-beam turn-off.

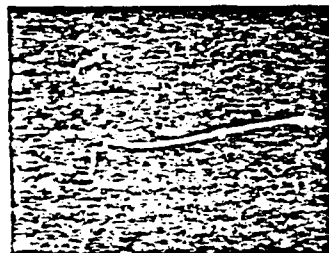
This effect was demonstrated by operating the diffuse discharge at different values of E/N about the crossing point of the attachment and ionization curves (Fig. 10). The discontinuities in the switch current curves represent the stepwise increase in electron concentration in the switch gas due to three successive, ionizing, e-beam pulses. The applied field E/N is given by the upper values at each picture. E/N drops to the lower value at the maximum of the switch current after approximately $1 \mu\text{s}$. In the range of E/N below 60 Td the net ionization coefficient ($\alpha - \eta$) is negative; thus electron attachment losses outweigh the ionization gain. The switch current decreases after e-beam turn-off (Fig. 10, top); i.e., this means the switch opens. However, because of the small attachment coefficient of CO_2 compared to SO_2 and N_2O , the switch opening time (even for the high concentration of 20% in N_2 as buffer gas) is much longer than for the



32 - 39 Td



54 - 58 Td



75-78 Td

5 μ s

$p = 200$ TORR, 20% CO_2 , 80% N_2

FIG. 10 Time dependence of switch current in a discharge in $\text{N}_2\text{:CO}_2$ with reduced field strength E/N as the variable parameter.

other gases. In the E/N range above 60 Td, $(\alpha - \eta)$ is positive; consequently ionization dominates over attachment, and the switch current increases (Fig. 10 bottom) until the field strength in the switch gas drops to a value where the net ionization is 0. Operation in an E/N range close to this value is demonstrated in Fig. 10, center. After turn-off of the e-

beam, the current stays constant because the ionization and attachment processes balance each other.

SUMMARY

Diffuse discharge investigations were performed in the gas mixtures $\text{N}_2\text{:N}_2\text{O}$, $\text{N}_2\text{:SO}_2$, and $\text{N}_2\text{:CO}_2$. The experimentally obtained current-voltage characteristic for $\text{N}_2\text{:N}_2\text{O}$ agrees with previously obtained theoretical results at high E/N . The discrepancy in theoretical and experimental data at low E/N reflects the uncertainty in basic data for N_2O . With respect to the criteria for optimum switch gases [low losses during conduction (at low E/N), large losses during and after opening (at high E/N)], N_2O in N_2 is superior to the other investigated gases. For opening times of ~ 100 ns, the current gain was in the order of 10. With better utilization of the e-beam energy in our system, a gain of 100 can be achieved. Shorter opening times, down to ~ 10 ns, are possible with higher attachment concentrations, however, at the expense of reduced current gain.

¹K. H. Schoenbach, G. Schaefer, M. Kristiansen, L. L. Hatfield, and A. H. Guenther, IEEE Trans. Plasma Sci., PS-10, 246 (1982).

²C. H. Harjes, K. H. Schoenbach, G. Schaefer, M. Kristiansen, H. Krompholz, and D. Skaggs, Rev. Sci. Instrum. ~~55, 1664 (1984)~~ **55**, 1664 (1984).

³H. Krompholz, J. Doggett, K. H. Schoenbach, J. Gahl, C. Harjes, G. Schaefer, and M. Kristiansen, Rev. Sci. Instrum. **55**, 127 (1984).

⁴L. L. Christophorou, S. R. Hunter, J. A. Carter, and R. A. Mathis, Appl. Phys. Lett. **41**, 147 (1982).

⁵G. Schaefer, K. H. Schoenbach, H. Krompholz, M. Kristiansen, and A. H. Guenther, Lasers Part. Beams ~~to be published~~ **2**, 273 (1984).

⁶A. V. Phelps (private communication).

⁷L. C. Lee, C. C. Chang, K. Y. Tang, D. L. Huestis, and D. C. Lorents, Second Annual Report on Coord. Res. Progr. in Pulsed Power Physics, Department of Electrical Engineering, Texas Tech University, Lubbock, TX (1981).

⁸L. C. Lee and F. Li, J. Appl. Phys. **56**, 3169 (1984).

⁹G. Schaefer, K. H. Schoenbach, and J.-S. Wang (unpublished).

¹⁰P. J. Chantry, J. Chem. Phys. **51**, 3369 (1969).

¹¹J. W. Gallagher, E. C. Beaty, J. Dutton, and L. C. Pitchford, J. Chem. Phys. Ref. Data **12**, 109 (1983).

¹²V. K. Lakdawala and J. L. Moruzzi, J. Phys. D **14**, 2015 (1981).

¹³J. Rademacher, L. G. Christophorou, and R. P. Blaunstein, J. Chem. Soc. Faraday Trans. **2** **71**, 1212 (1975).

A Review of Opening Switch Technology for Inductive Energy Storage

KARL H. SCHOENBACH, SENIOR MEMBER, IEEE, M. KRISTIANSEN, FELLOW, IEEE, AND GERHARD SCHAEFER, SENIOR MEMBER, IEEE

A review of the state of the art in opening switches is presented. The general operating principles and present and potential future operating parameters for several switch categories are discussed. Among the switch categories described are: mechanical, solid state, vacuum arc, crossed field, fuse, explosive, plasma gun, superconducting, thermal, MHD instability, diffuse discharge, plasma erosion switches, and reflex triodes.

1. INTRODUCTION

Energy storage for pulsed power devices commonly implies capacitive storage for which the state of the art is relatively well developed. The components of capacitor banks, including capacitors and switches, are commercially available and relatively inexpensive. However, in terms of energy density, capacitor banks are inefficient compared to inductive storage systems. In Fig. 1 the energy density in commercially available capacitors is compared with that in an inductive storage system, a coil [1]. The ratio of capacitive to inductive energy density is 25 for an assumed coil current of $I = 5$ kA. In other words, it takes approximately 300 capacitors of the type shown in Fig. 1 to replace the coil with respect to its energy content. By stressing the technology of coil design, the difference in energy storage density becomes even larger (by a factor of ~ 10). One should note that these comparisons do not account for power supplies, cooling systems, etc., but the differences are still intriguing, although great strides are currently being made in improving the energy storage density of capacitors.

The interest in inductive energy storage systems and the appreciation of the difficult opening switch problems are evidenced by two recent Army Research Office sponsored workshops on Repetitive Opening Switches [2] and Diffuse Discharge Opening Switches [3] in Tamaron, CO, USA, in 1981 and 1982, respectively. There has also been several other recent national and international workshops devoted to the same general problem, as well as special discussion sessions at international conferences. The basic considera-

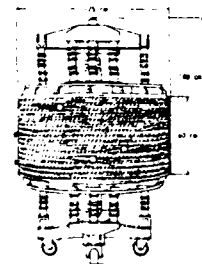
Manuscript received December 16, 1983; revised May 10, 1984. This research was sponsored jointly by the Air Force Office of Scientific Research and the Army Research Office under Contract AFOSR-84-0032. The U.S. Government is authorized to reproduce and distribute reprints for Governmental purposes notwithstanding any copyright notation thereon. The submission of this paper was encouraged after review of an advance proposal.

The authors are with Plasma and Switching Laboratory, Department of Electrical Engineering, Texas Tech University, Lubbock, TX 79409, USA.



PULSE DISCHARGE CAPACITORS*	
CAPACITANCE	: $C = 2.8 \mu\text{F}$
VOLTAGE	: $V = 50 \text{ kV}$
ENERGY	: $W = 3.5 \text{ kJ}$
VOLUME	: $V = 6.3 \times 10^4 \text{ cm}^3$
ENERGY DENSITY	: $W' = 5.5 \times 10^{-2} \text{ J/cm}^3$

*Maxwell Laboratories, Inc.



INDUCTIVE STORAGE COIL [1]	
INDUCTANCE	: $L = 80 \text{ mH}$
CURRENT	: $I = 5 \text{ kA}$
ENERGY	: $W = 1 \text{ MJ}$
VOLUME	: $V = 74 \times 10^4 \text{ cm}^3$
ENERGY DENSITY	: $W' = 1.35 \text{ J/cm}^3$

Fig. 1. Capacitive and inductive energy storage systems.

tions and the fundamental factors involved in inductive energy storage are discussed in several places, including [4].

There are two major obstacles to the practical use of inductive storage in pulsed-power devices. They become obvious when the basic capacitive and inductive energy discharge circuits are compared. In the capacitive energy discharge circuit¹ (Fig. 2(a)) the capacitor C is charged

¹Other charging networks are also possible, but this does not change the basic argument.

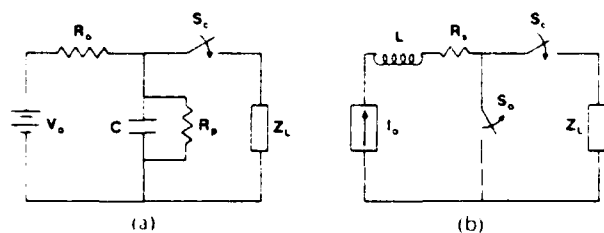


Fig. 2. (a) Capacitive energy discharge circuit. (b) Inductive energy discharge circuit.

through a resistor R_s to the voltage V_0 . The time constant for self-discharge of the capacitor is $\tau_c = R_p C$, where R_p is the leakage resistance. For low inductance, high-voltage capacitors τ_c may be in the order of tens of minutes [5]. For such capacitors, the charging currents can be kept at fairly low values.

The capacitor is discharged into the load Z_L by means of the closing switch S_c , which is often a spark gap. The discharge current is usually large compared to the charging current and a capacitive discharge circuit can, therefore, be considered as a current amplifier.

In an inductive energy storage circuit (Fig. 2(b)), the inductor L is "charged" to a current I_0 . The time constant for self-discharge is $\tau_L = L/R_s$, where R_s is the series resistance of the current source, switch S_0 , and inductor. For inductive energy storage systems, τ_L can be in the order of seconds [1]. This means that inductors have to be charged in relatively short times.² Therefore, high-power, primary power sources are needed.

The energy stored in the inductor is transferred to the load by means of an opening switch S_0 , an element which breaks the current I in the charging circuit. By means of a closing switch S_c , the current path is then connected to the load. Simultaneously, due to the decrease of current, a high voltage of magnitude $L(di/dt)$ is induced across the opening switch and load. Inductive discharge circuits can, therefore, be considered as voltage amplifiers. The two major technical problems in inductive energy storage systems are the charging circuit and—even more severe—the opening switch design.

II. OPENING SWITCH CHARACTERIZATION AND REQUIREMENTS

The various types of opening switches can be divided into two general classes depending upon their operation: direct interruption or counterpulse interruption. In the direct interruption class, the impedance of the opening switch is rapidly increased to cause the current to transfer to a lower impedance load. In the counterpulse class, the switch current is counterpulsed, that means an artificial current zero is created by injecting an equal but opposite current through the switch. This allows the switch to return to its off state, without having, at least temporarily, to hold off the inductive voltage. The counterpulse technique can be used with almost any type of switch, however, it works best with switches that recover rapidly.

Fig. 3 shows a counterpulse circuit with current and voltage diagrams. Up to the time t_1 the total inductive discharge current I_0 flows through the closed switch S_0 . Switches S_1 and S_2 are open. At t_1 , switch S_0 is closed and

² It is, of course, necessary to charge capacitors in very short times for the purposes related to the dielectric medium use [1].

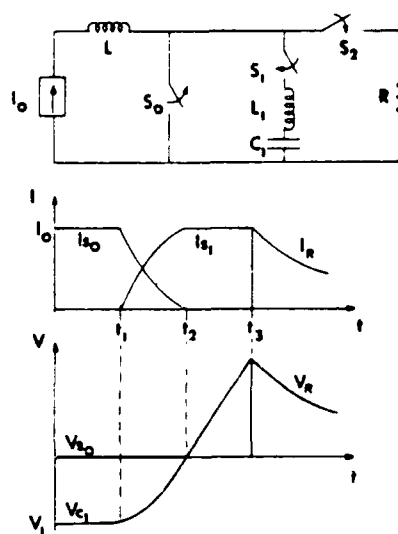


Fig. 3. Basic counterpulse circuit with current and voltage diagrams.

the capacitor which was charged up to V_1 is discharged through the inductor L_1 and switches S_1 and S_0 . The direction of the current is chosen so that the current through S_0 is reduced. The frequency of the discharge current, which determines the speed of counterpulsing, is given as

$$\omega = \frac{1}{\sqrt{L_1 C_1}} \quad (1)$$

At t_2 , when the current is zero in switch S_0 and I_0 in S_1 , switch S_0 is opened. After opening of S_0 , C_1 is charged again but now with opposite polarity. The voltage rise across C_1 is

$$\frac{dV}{dt} \approx \frac{I_0}{C_1} = \text{constant} \quad (2)$$

if $L \gg L_1$, which means constant current I_0 . At t_3 , switch S_2 is closed and the stored energy is transferred to the load, which in this example is a resistor R .

Another way to characterize opening switches is by a generalized impedance $Z(t)$, which increases in time [6]. The opening mechanism may be resistive, inductive, or capacitive. It is resistive if the impedance rise is caused primarily by increased dissipation in the switch. Fuses are examples of this type of opening switch. The switch has an inductive characteristic if $Z(t)$ is increasing due to the rise of self-inductance. Examples are flux compressors. Examples for switches where the opening is based on a decreasing capacitance of the switch are rare. The principal exception is the space-charge-dominated sheath of a glow discharge, where the spacings are very small and relative motions may be at high speed [6]. Whereas capacitive and inductive opening is in principle reversible, resistive opening always changes the switch medium irreversibly.

Independent of their characteristics, opening switches should satisfy the following qualitative conditions:

- long conduction times
- large currents (low losses) during conduction
- fast rise of impedance during opening
- high impedance after opening
- high stand-off voltage
- fast recovery (high repetition frequency).

Presently, it is not possible to satisfy all these conditions

submicrosecond, multiple pulse operation. The 250-kV, 100-cm² electron-beam gun is designed as a tetrode with a thermionic cathode. Current densities up to 4 A/cm² can be obtained and varied independently of the beam energy. The first switch experiments have been performed in N₂-N₂O gas mixtures. Discharge current fall times of approximately 10 ns were measured in an N₂-N₂O mixture, containing 3 percent N₂O.

B. Optically (Laser) Controlled Diffuse Discharge

The use of a laser to sustain or control a diffuse, high pressure discharge has not been considered previously for opening switches. The main reason is that direct ionization as in the case of electron-beam sustained discharges is possible only in some alkali-metal vapors using UV lasers. However, it is possible to use a combination of collisional and photo processes to ionize commonly used gases even with visible laser radiation. Laser control has the advantage that resonance processes can be used to ionize the gas. This may be important for high-repetition-rate opening switches, where excessive heating of the filling gas has to be avoided.

Concepts for using lasers for generating electrons in discharges are shown in Fig. 29. The opening process, after turning off the laser, in each case is determined by attach-

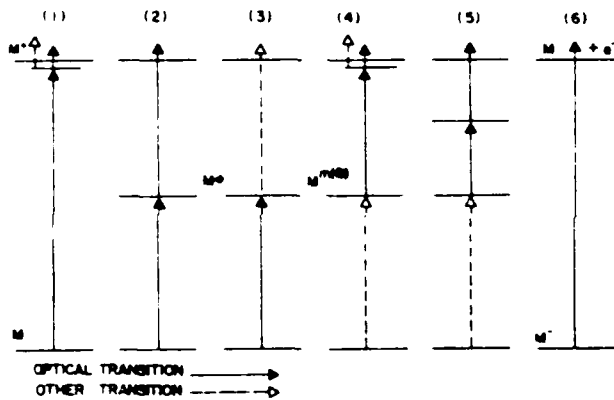


Fig. 29. Optically controlled electron generation [101].

ing processes of an added attachers. A more detailed discussion of these processes can be found in [102], [103]. The processes shown in Fig. 29 are: 1) direct photoionization; 2) resonant two-step photoionization; 3) photoexcitation and subsequent collisional ionization as in laser resonance pumping; 4) photoionization from an intermediate state in one step; or 5) a resonant two-step process; and 6) photodetachment. For the processes 1), 4) and 6) no narrow-bandwidth light sources are required. Spark UV sources for direct photoionization, for example, have successfully been used to operate optically sustained discharges for TE lasers.

To produce electrons with lasers will, in general, be an expensive method due to the cost of laser photons. An exception may be photodetachment b). The photon energy required for detachment of the negative ion is in most cases much smaller than the energy required for ionization of the neutral species. Since attachers have to be used to achieve fast opening, laser photodetachment may be a suitable process to overcome attachment in a specific switch phase in electron-beam sustained discharges [104], [105].

A second possibility for using lasers to control a diffuse discharge as an opening switch is to reduce the electron density by stimulating loss processes in the plasma during the opening phase of the switch [103]. It is, for instance, possible to get higher attachment cross sections by vibrationally exciting certain electronegative gases. The mechanism for dissociative attachment can be understood by considering the potential energy diagram of attaching diatomic molecules (Fig. 30). The potential energy curve of a neutral diatomic molecule, AB, is crossed at an energy E_0^*

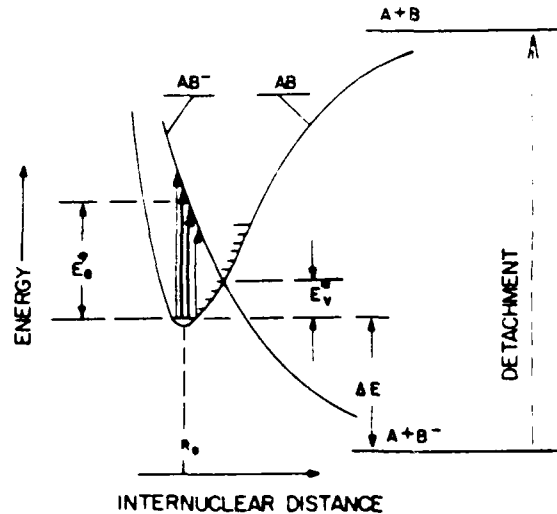


Fig. 30. Resonance dissociative electron attachment [101].

above the ground state by a repulsive potential energy curve of the negative ion AB^- . The cross section for dissociative attachment is larger and its maximum is shifted towards smaller electron energies the nearer the energy of the vibrationally excited state of the molecules is to the energy of curve crossing. A way to increase the generation rate for negative ions is, therefore, the selective excitation of vibrational states (in most cases $v > 1$) of the molecule AB near the curve crossing point. Using this method, an increase in attachment rate of several orders of magnitude can be obtained. For HCl molecules calculations have been performed [106], based on measurements of attachment rates as a function of temperature [107], which show an increase of the maximum value of the cross section from 10^{-17} cm² for the $v = 0$ vibrational level, to 10^{-15} cm² for $v = 2$ (Fig. 31).

Using attachment processes to enhance the resistance of a diffuse discharge switch during opening, opening times on the order of 100 ns should be possible. On the other hand opening switches, where the opening effect is based on attachment, are lossy, because a continuous energy supply is necessary to keep the electron density at a certain level. Improvements in their efficiency can be attained if gas mixtures are used with attachers for which the attachment rate increases and the electron mobility decreases with increasing reduced field strength E/N [102], [103], [108]. This effect is independent of the generation mechanism for the electrons. It can be used in electron-beam-controlled as well as in laser-controlled switches. A concept to externally enhance losses which can only be realized by means of lasers, however, is that of enhancement of the

the externally sustained discharge in pure argon are shown in Fig. 26(a) for various electron-beam currents. After turn-off of the electron beam, the current decreases due to the recombination processes in the diffuse plasma. Time constants, or "opening times," are 10 to 20 μ s. Fig. 26(b) again shows current traces of the externally sustained discharge for two different electron-beam currents, but now the gas composition is slightly different: 0.02 torr SF₆, an electronegative gas, has been added to the argon. Due to attachment processes, the opening time is reduced by approximately one order of magnitude. However, this desirable effect—important for opening switches—has a side effect which limits the application of attachers in diffuse discharge switches. The faster the reduction of electron density due to attachment processes, the shorter the opening time, but the higher is the electron-beam or laser power necessary to keep the electron density and hence the conductivity of the plasma constant. In Bletzinger's experiment [93], with the electron-beam power kept constant, the switch current dropped from 14 to 7.5 A after adding 0.02 percent SF₆ to the argon.

Using a simple balance equation, the power necessary to sustain a discharge in a diffuse switch, is determined by

$$P = V n_e E_{ion} \frac{1}{\tau_{op}} \quad (9)$$

where V is the volume of the discharge, n_e the electron density, E_{ion} the mean ionization energy, and τ_{op} is the time necessary to replace all electrons lost due to recombination and attachment processes. The time τ_{op} can be considered as the opening time for diffuse discharge switches. For an attachment dominated discharge $\tau_{op} = (k_A N_A)^{-1}$, where N_A is the concentration of the attacher and k_A is the attachment rate coefficient.

To overcome the conflict between short opening time and large energy consumption, the attachment rate coefficient should be kept small during charging, to avoid large energy consumption. It should, however, have large values when the switch is to be opened to provide for short opening times. Due to the fact that the reduced field strength E/N in the diffuse discharge is small during charging and starts growing after the ionization source is turned off, the required time dependence can be converted into a field strength dependence for the attachment rate coefficient. k_A should be small for low values of E/N and have a maximum at higher E/N . The electron mobility should behave in just the opposite way. It should be high for low values of E/N and low for high values of E/N . Whereas, the considerations about electron drift velocity or mobility, respectively, were presented already in 1976 by Hunter [94], the importance of attachment rate dependence on E/N was emphasized at first by the plasma research group at Texas Tech University in 1981 [95]–[97]. It was confirmed by computer calculations [96] performed for a diffuse discharge opening switch containing attachers with different E/N characteristics of k_A . The desired behavior of electron mobility and attachment rate versus E/N is shown in Fig. 27.

The use of this inherent attachment feedback effect requires an externally sustained diffuse discharge. There are two concepts for the externally controlled generation of electrons in a diffuse discharge:

- the electron-beam sustained discharge
- the optically (laser) sustained discharge

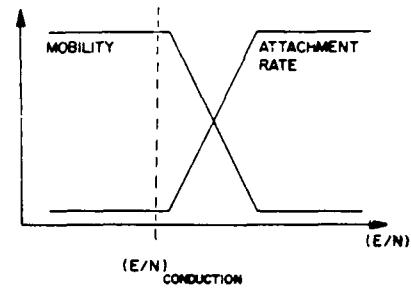


Fig. 27. Ideal E/N characteristic of electron mobility, μ_e , and attachment rate coefficient, k_A , in a diffuse discharge opening switch.

A. Electron-Beam Sustained Diffuse Discharge

The feasibility of using an electron beam to control the conductivity of the gas volume between two charged electrodes (see Fig. 28) was first demonstrated by Hunter [94] and Kovaltchuk and Mesyats [98]. In these experiments, large electron-beam current densities of up to 5 A/cm² were used. The current gain (switch current/electron-beam

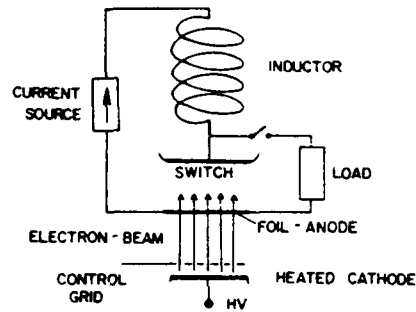


Fig. 28. Schematic of an electron-beam-controlled diffuse discharge switch in an inductive energy storage circuit.

current) was small. Also their electron-beam guns, derived from laser experiments, were cold-cathode types requiring the full electron-beam voltage to be switched and therefore resulting in even lower power gain. On the other hand, they achieved very fast rise times and could afford to work with added attaching gases which resulted in fast opening times of less than 1 μ s. Hunter recognized the importance of having a gas with a high electron drift velocity and therefore chose methane, which has a drift velocity peaking at more than $v_d = 10^7$ cm/s at about $E/N = 3$ Td (1 Td = 10^{17} V · cm⁻²).

Systematic measurements of current-voltage characteristics of electron sustained discharges in methane and argon (+ attachers) have been performed by Bletzinger [93], [99]. He concentrated on the high current gain regime (at low values of the electron-beam current density) and found in this regime a strong influence of cathode sheath effects on the conductivity of the discharge plasma.

The temporal behavior of gas resistivity as a function of electron-beam current was investigated at NRL [100] in a high electron-beam current density device. Measurements were performed for N₂ and Ar mixed with attaching gases (O₂, CO₂, CH₄, and SF₆). Discharge current fall times of approximately 100 ns were obtained, limited by the electron-beam fall time.

For the investigation of electron-beam controlled diffuse discharges a system was constructed [10] which allows

With one of their switches, they transferred a peak power of 25 MW (2.5 kA, 10 kV) from a 50-kJ inductive storage system. The maximum current is 8 kA/unit and $\Delta R \sim 20\text{--}50 \Omega$ at $T = 20 \text{ K}$. A particularly important feature of these switches is their potential modularity and at least two of the switches have been successfully operated in parallel. Successful parallel operation [85] of s.c. switches was also demonstrated at Los Alamos National Laboratory (LANL). Two switches which reached 6 and 7 kA individually were operated in parallel at 13 kA.

At LANL the s.c. switch work was pursued for several years in connection with the Magnetic Fusion Confinement Program. The work was discontinued in favor of counter-pulsed vacuum interrupters. Some of their experimental results with a switch using a 70–30 Cu–Ni matrix with a 1:3:1 matrix to s.c. ratio were [86]

$$I_{c \text{ max}} = 10.8 \text{ kA}$$

$$V_{\text{max}} = 25.0 \text{ kV}$$

$$\Delta R = 3.44 \Omega$$

XI. THERMALLY DRIVEN OPENING SWITCHES

Thermally driven opening switches are the result of attempts to achieve the speed and economy of fuse opening switches but with the added advantage of repetitive operation [86]–[90]. The strategy is simple: let the wire heat almost to, but not beyond, its melting point so that its resistance increases several-fold and hence decreases the current. The wire can thus partially interrupt (decrease considerably) the current without melting or exploding and hence can be reused. For some applications, partial interruption is sufficient. Basic design information for thermally driven opening switches is given in [87]. Reports on applications are given in [87]–[90]. At this point, both low carbon steel [89]–[91] and tungsten [87], [90], [91] have been investigated. For low carbon steel, cooled initially to -193°C and allowed to heat to $+800^\circ\text{C}$, the resistance changes by a factor of 70 [89], [90].

The maximum reported voltage standoff is 20 kV [89], [90]. Electric fields of about 1.7 kV/cm were held off in the work described in [87]. Neither of these figures is likely to represent a real limit. However, the voltage standoff should be lower for thermally driven opening switches than for fuses because thermally driven opening switches do not vaporize. The maximum peak current reported so far is 200 kA [89], [90]. Higher currents can be realized successfully by paralleling elements since the $V\text{--}I$ characteristics for thermally

ally driven opening switches have the proper characteristics for stability ($dv/di > 0$).

The pulse repetition rate is determined by how fast the wire can be cooled. After an initial cooling period of 15 min, before the first shot, repeated cooldowns are possible at the rate of about 1 shot per minute [89], [90] when the initial temperature is -193°C . The best reported rise time is 6–8 μs , although this figure depends on the current density in the wire. No quantitative data are available on the lifetime of such a switch.

The main attractive feature of thermally driven opening switches is the promise of repetitive operation. At present, a major unknown is how well the wires will hold up under recycling.

XII. DIFFUSE DISCHARGE OPENING SWITCHES

A concept which seems to be particularly attractive for repetitive opening switches is the diffuse discharge opening switch. A diffuse discharge is defined as an extended volume, nonequilibrium discharge. If self-sustained, the current–voltage characteristics may be negative, constant, or positive, depending on the reduced field, E/N , and the gas. If externally sustained, e.g., by an electron beam, the ideal diffuse glow discharge has a positive current–voltage characteristic. After sufficient voltage has been applied to establish the electrode sheath conditions the slope of this characteristic depends on the external ionization source. The discharge is in a nonequilibrium state in that the electron temperature $>$ vibrational temperature $>$ gas temperature [92].

There are two ways to use a diffuse discharge as an opening switch

- by turning off the ionization source in an externally sustained discharge,
- by controlled reduction of the conductivity in a self-sustained or externally sustained discharge.

Whereas a controlled conductivity reduction seems to be possible only by using a laser, concept a) can be realized with either a laser or an electron beam as the ionization source. In such a switch, reduction of current carriers or carrier mobility after turn-off of the external source is determined by recombination and attachment processes, respectively.

Fig. 26 shows experimental results [93] with a low-power electron beam as the ionization source. Current traces of

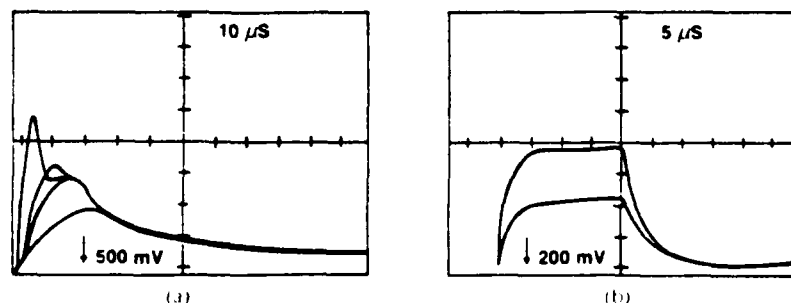


Fig. 26. Current decay in gas mixtures without (a) and with (b) additives [93]. (a) Measured switch current in atmospheric pressure argon (10 $\mu\text{s}/\text{div}$ horizontal, 5 A/div vertical) with electron beam current of 20, 40, 80, 100 mA. (b) Measured switch current in atmospheric pressure argon with 0.02 Torr of SF_6 added (5 $\mu\text{s}/\text{div}$ horizontal, 2 A/div vertical) with electron beam current of 20, 30 mA [93].

perpendicular to J , where J is the current density. These differences are related to the shielding effect of the conductor. For foil conductors it has been found [74] that the best (fastest) quench occurs with B perpendicular to J and tangential to the foil surface, as shown by B_z in Fig. 24. The thermal quench can be induced by heating all or part of the switch with an external heating filament.

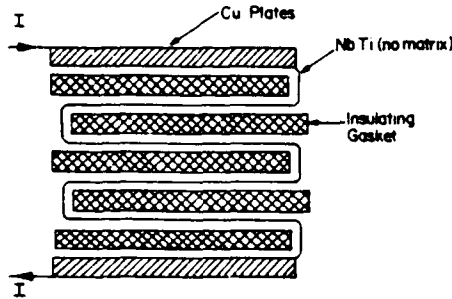


Fig. 24. Superconducting opening switch [80].

The thermal quench is the slowest [75] one with a Δt_{\min} of approximately 1 ms. The B -field quench has about 200 times faster dR/dt but involves generally bulkier and more complicated equipment. The simplest quench method for $\Delta t \leq 10 \mu s$ appears to be the current induced one. The quench proceeds from several points along the wire which then goes normal. Opening times as short as 200 ns can be obtained with 200- μm -diameter wires [76]. One should note that the switching condition must be maintained long enough to deliver enough energy (or extract it from the storage circuit) to raise the temperature of the switch and all associated material above the critical temperature [77].

When the switch is triggered, it is important that the entire switch goes normal so that a sufficient ΔR will reduce the current enough to avoid switch burnout. If the superconductor is stabilized sufficiently (Cu matrix), then this is difficult. The switch is therefore either partly stabilized [78], [79] (e.g., with 70 percent Cu, 30 percent Ni matrix) or not stabilized [80] at all. The power density in the switch (MW/cm^3) is generally limited by the allowable temperature rise of the enclosing epoxy [81] (~ 100 K). Typical values are 1–2 MW/cm^3 .

The repetition rate of the switch depends on how fast it recovers its superconducting stage, which again depends upon the design details, total mass (matrix + s.c. + epoxy), cooling channels, etc. It is difficult to see how this kind of a switch can be operated at high repetition rates and the losses (refrigeration power) would then probably be excessive. References [77] and [82] describe various design considerations and tradeoffs. From these studies, and maybe also intuitively, it is clear that one wants to maximize the switch current density and the resistivities of the matrix and the superconductor in the normal state. One also wants the smallest possible ratio of matrix to superconductor volume.

The switch must be designed with a low-inductance winding (bifilar) arrangement to allow fast switching (low Δt) and with sufficient conductor length to give sufficiently large ΔR . Too large a loop length in the switch coil can cause voltage breakdown problems between adjacent conductors. However, when the switch quenches, high-voltage

spikes are observed as a result of the high $L(di/dt)$ (even though L is made as small as possible). Also, when accidental quenches occur, high-voltage spikes occur along the switch where the quench occurs [79]. These spikes can be 10 times higher than the voltage which is seen with a normal (triggered) quench. The insulation must, therefore, be designed accordingly.

Some considerations of switch losses and energy transfer times, which are also functions of the external circuit parameters, are discussed in [83]. For fast switching, one must also keep the conductor dimensions small so as to limit magnetic and thermal diffusion times. The switching times of superconducting wires of various dimensions versus the switching di/dt have been measured [84].

At the Kernforschungszentrum Karlsruhe in Germany, several s.c. switches and inductive energy storage systems have been investigated [81], [83]. The largest storage system was 220 kJ but the switch in this case was designed to handle 1 MJ. Some of the experimental results included switching times (Δt) of 20 μs , peak voltages of 47 kV, and dR/dt of $22 \times 10^{11} \Omega/s$. The switch recovery time was about 3 min, set by the epoxy encapsulation. The switch jitter, using current triggering, was $\sim 5 \mu s$.

At the D. V. Efremov Scientific Research Institute of Electrophysical Apparatus in Leningrad, USSR (ESRIEA) the research has been concentrated on building small, compact, modular s.c. switches [80] using NbTi foils with no matrix material. The s.c. switch is constructed as a bifilar pack of a 20- μm -thick strip of the s.c. foil, as shown in Fig. 25.

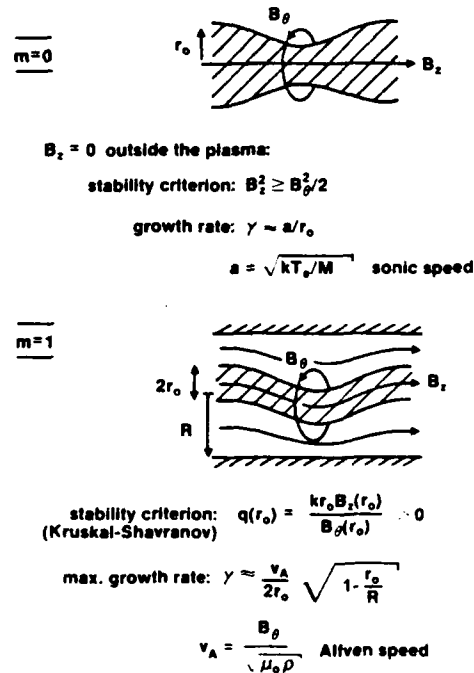


Fig. 25. Pinch instabilities with axial magnetic field [“sharp” pinch (infinite conductivity)] [69]

Insulating fiberglass gaskets impregnated with epoxy resin (at 40-atm pressure) are placed between the layers. The switch dimensions are typically 4 cm \times 5 cm \times 15 cm. Several switches have been constructed and tested for currents in the 2.5–8-kA range.

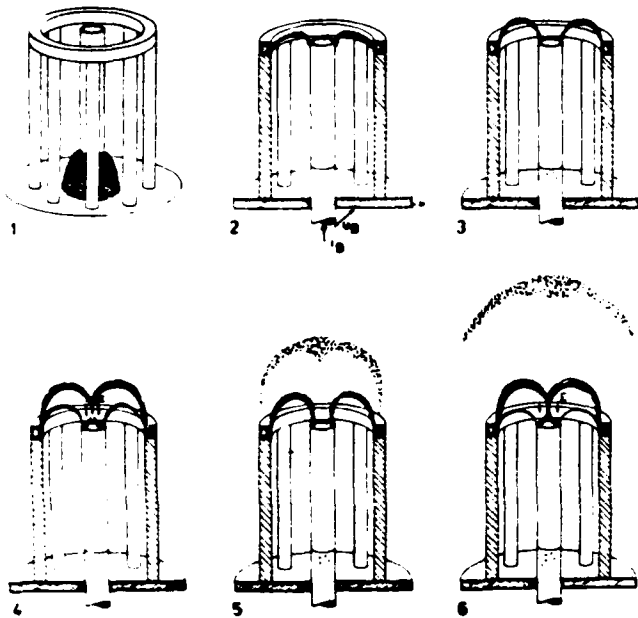


Fig. 21 Repetitive operation of a dense plasma focus [72]. 1—Formation of plasma layer along insulator 2—Plasma layer reaches end of coaxial gun. 3—Radial collapse of plasma layer 4—Focus event and formation of second plasma layer at the end of the gun 5—Radial collapse of second plasma layer 6—Focus event and formation of third plasma layer at the end of the gun.

individual events. The voltage and power pulses, respectively, occur randomly, as shown in Fig. 22 [72]. The maximum voltage peak of 25 kV was obtained at a current of 90 kA, which resulted in a characteristic ohmic resistance of 0.3Ω , a value close to the one measured on several other

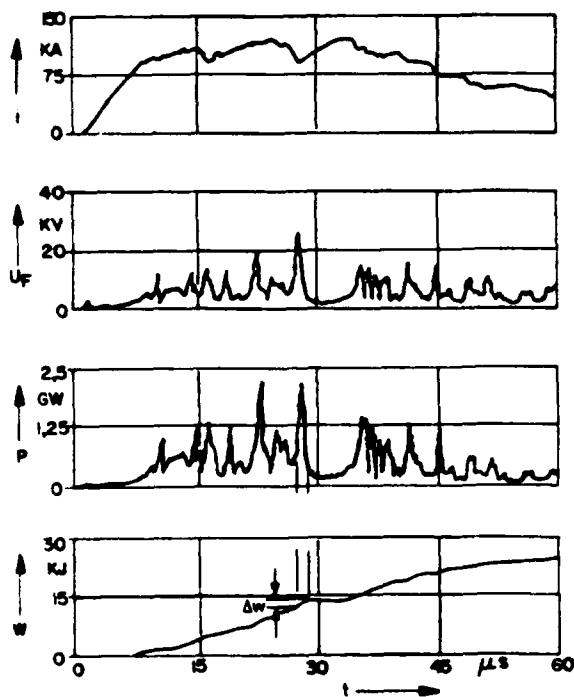


Fig. 22 Current i , voltage u_f , power P , and energy W versus time during a repetitive operation of a plasma focus (Gas: deuterium, $p = 1$ mbar) [72].

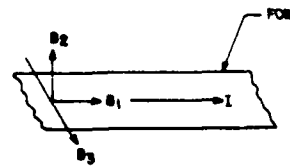


Fig. 23. Possible B -field orientations for s.c. switch quenching [74].

focus devices [7]. Higher reproducibility and a controllable repetition rate may possibly be achieved by means of cylindrical gas puff injection at the end of the coaxial line [69].

The deformation of a current-carrying plasma column due to MHD instabilities (Fig. 23) [69] also leads to an increase in inductance and hence in plasma impedance. Whereas the opening effect of the $m = 0$ (sausage) instability is rather weak [69], the $m = 1$ instability seems to be promising for an opening switch [67]. An increase of plasma resistance (that means an opening effect), at least for a short time, is expected. Theoretical and experimental observations of plasma-wall interactions in fusion devices and in conventional circuit breakers may help to understand the cooling processes in this type of opening switches.

Other MHD-type opening switches have also been investigated. A particularly promising approach [73] uses a coaxial plasma gun, where a coaxial discharge is initiated by the explosion of a foil or wire array. The plasma is accelerated down the gun, storing energy from a slow store (e.g., a homopolar generator or capacitor bank) in the gun inductance. This energy is then delivered rapidly to a load as the plasma blows off the end of the coaxial gun and completes the current path to the load. The basic idea is similar to the inductive pulse sharpening circuits, employing exploding wire fuses, used on some large capacitor banks (e.g., the SHIVA experiment at the Air Force Weapons Laboratory).

X. SUPERCONDUCTING OPENING SWITCHES³

Superconducting (s.c.) opening switches are generally used in connection with superconductive inductive energy storage. They represent an attempt to exploit the low-temperature environment already present in the superconductive energy storage system in providing a conceptually simple means of repetitive switching. The switch is caused to change from the s.c. to the normal state in some characteristic switching time Δt . The main problem with s.c. switches is the additional refrigeration required to remove the heat dissipated into the low-temperature fluid when the switch goes normal.

This transition can be induced by three distinctly different trigger (quench) methods: current, B -field, and thermal quench. The current from the source through the switch can be increased to cause self-quench or the current can be induced by one of several means from a separate, external trigger source. An external magnetic field can be applied to cause B -field quenching. The magnetic field can be applied, with different results, parallel or transverse to the current. With foil conductors, there is also a difference with B perpendicular or parallel to the foil surface while B is

³Most of the material in this section and in Section XI is from a chapter written by one of the authors (MK) in a Naval Surface Weapons Center Report NP 30/78, Sept. 1978.

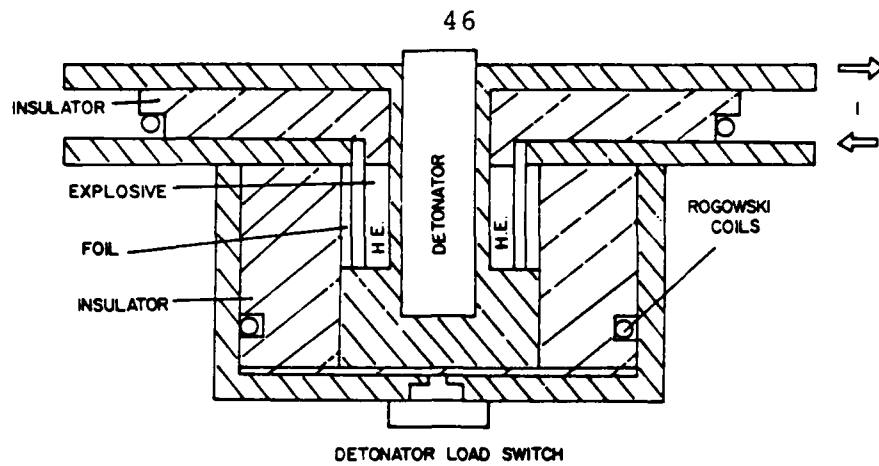


Fig. 19. Schematic diagram of cylindrical plasma switch used for high-current tests [66].

the order of $1 \mu\text{s}$ but at somewhat lower currents and voltage gradients than reported by Pavlovskii *et al.*

IX PLASMA GUNS, DENSE PLASMA FOCUS, AND MHD SWITCHES

Plasma guns, and especially the dense plasma focus (DPF), have been suggested as opening switches because of their rapid change in inductance due to linear plasma acceleration and, in the case of a DPF, due to additional fast radial compression of the current-carrying plasma. A plasma gun is shown as part of an inductive discharge circuit in Fig. 20

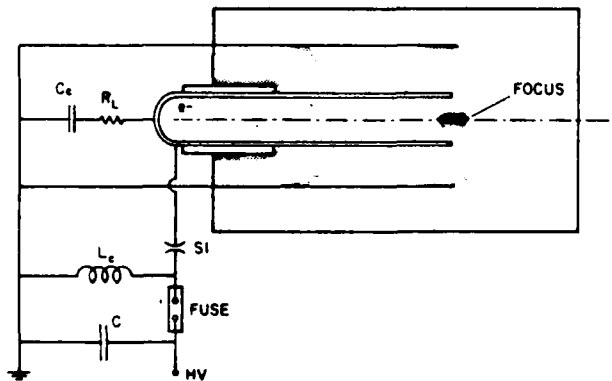


Fig. 20. Dense plasma focus switch arrangement [67].

[67] The inductor L_c is charged by a capacitor bank C . The current is interrupted by means of a fuse. Simultaneously, the switch S is closed and the current is fed into a plasma gun, which serves as intermediate inductive storage and an opening switch as well. The gun is a coaxial device with a length several times its diameter and a coaxial separation of several centimeters. The electrodes are separated at the rear end by a cylindrical insulating sleeve. The system is operated at gas pressures of a few torrs.

When a voltage is applied across the electrodes, a discharge is formed along the insulator surface. Due to magnetic forces, this current sheet is lifted and driven down the line with a speed approaching the value

$$v_s = \left(\frac{\mu}{2\rho} \right) \frac{I}{2\pi r} \quad (b)$$

where I is the sheet current, r_0 is the radius of the inner conductor, and ρ_0 the density of the filler gas [68]. Related to the motion of the current-carrying plasma layer is an increase in impedance up to the value

$$\frac{dL}{dt} = L'v_0 \quad (7)$$

where L' is the inductance per unit length and v_0 the velocity of the plasma layer. That means a plasma gun, or in general any electric rail gun, can be considered as an opening switch. In case of the coaxial plasma gun for values of $L' = 1-5 \text{ nH/cm}$ and $v_0 = 5-10 \times 10^8 \text{ cm/s}$ impedances of up to $10^{-2} \Omega$ can be obtained.

In case of the DPF, which can be considered as a modified plasma gun, the more important opening effect occurs after the plasma layer passes the end of the coaxial line. The self-magnetic field of the plasma current drives the plasma layer towards the axis (plasma focus) which causes a rapid increase in inductance. The impedance in this phase is approximately that of a collapsing cylinder with radius r and length l

$$\frac{dL}{dt} = -\frac{\mu_0 l}{2\pi r} \frac{dr}{dt} \quad (8)$$

The speed dr/dt and consequently the impedance dL/dt can be optimized by proper choice of the electrode shape [69]. The maximum possible impedance however seems to be determined by resistive changes due to microinstabilities, such as the two-stream instability [70], rather than by inductive changes. Values of 0.35Ω were measured for different plasma focus devices, independent of current [71]. Upon opening, part of the magnetic energy stored in the plasma gun is released into the load R_L through a coupling capacitor C_c .

In inductively driven devices, this opening effect occurs repetitively (Fig. 21) [72]. After the ignition of the process at the bottom of the gun and the first collapse of the plasma layer on the axis, a reignition in the close vicinity of the discharge occurs, and the current is transferred back to a region apart from the axis. In this sequence, a new radial collapse of the plasma occurs, resulting in a second focus event. The complete process is repeated several times.

If these events can be made reproducible and repeatable the inductively driven plasma focus could be used as a repetitive opening switch, operating in the burst mode. However, thus far it has not been possible to control the

bridgewire detonators [59] to realize jitter times of about $10 \mu\text{s}$. Such precise triggering permits series and parallel operation of single-switch modules to achieve operation at higher voltages and currents. The major disadvantage of explosive opening switches is that repetitive operation, in the usual sense, is not possible. They offer [60] the possibility of precise timing and permit the delay before explosion to be controlled independently of the current flowing through the switch (with a minimum delay of $\sim 40 \mu\text{s}$).

The basic operation of the exploding switch shown in Fig. 17 and described in [59] consists of the following steps.

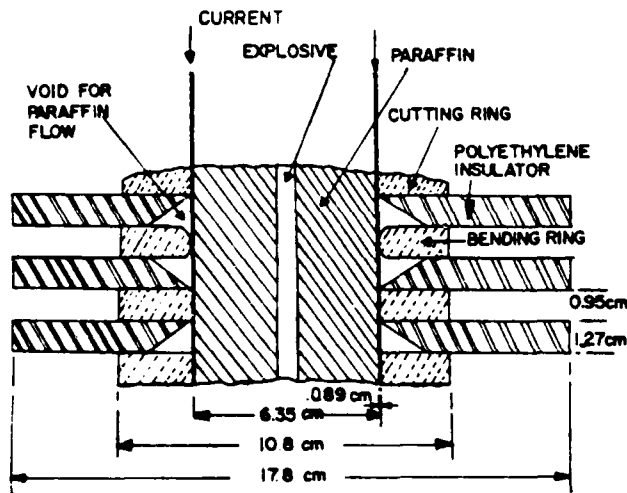


Fig. 17. Schematic cross section of the explosively actuated switch [59].

Initially, current is conducted by an Al cylinder for any period, limited only by the thermal capacity of the switch parts. The cylinder is loaded with paraffin and exploded by one or more detonators, leading to a radially outward pressure on the cylinder. Confining cutting rings, alternated with nonconducting rings, allow the cylinder to rupture in controlled areas. The rupturing decreases the current as a result of arc formation in each gap. The arc voltage, typically 25 to 10 kV/gap, can be used to commutate the current into the succeeding switch stage. Removal of the current from the exploding switch leads to rapid cooling of the arc plasma with a consequent increase in the ability of the switch to withstand high voltage without conduction or restrike. Performance values [56] of 600 kV and 400 kA have been achieved in the United States.

In the USSR a similar arrangement has been used [62] to interrupt 100 kA in 50–60 μs and holding off 50 kV. A two-stage series switch was tested to 70 kV (limited by the power supply but should test out at $> 100 \text{ kV}$) and opened in 7–10 μs . The switch losses were $\sim 100 \text{ kJ}$ in the first stage and 35–30 kJ in the second stage. It is felt [63] that a converging explosive shock type breaker may improve these results. There will then be problems with increased explosive mass but the possibility is being studied.

A novel exploding switch concept where the explosive and the conductor is the same element has been reported [63]. This is achieved by mixing 10 percent explosive and 90 percent copper powder (50–50 percent by volume) in a powder metallurgical process. The copper is in the form of

$100\text{-}\mu\text{m}$ "pellets." The mixture is pressed (sintered) at 5000 kg/cm^2 and annealed in hydrogen. The product can be heated up to 300°C for short times and is "safe against impacts." Preliminary results exceeded best results with the "conventional" explosive switch arrangement. The arrangement is shown schematically in Fig. 18. The resistivity of the

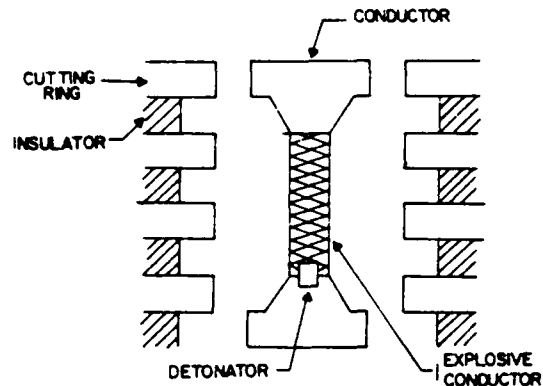


Fig. 18. "New" explosive switch [63], explosive conductor made of 90 percent Cu and 10 percent explosive (50–50 vol %) in a metallurgical process, $\rho = 20 \mu\Omega \cdot \text{cm}$, preliminary results 25 kA, 25 kV in $\Delta t = 8\text{--}10 \mu\text{s}$.

explosive conductor was initially about $100 \mu\Omega \cdot \text{cm}$. The explosive must, of course, be set off by a detonator.

Further developments [62] of this material using a "wetting agent" to "reduce pellet friction" (molybdenum dichloride?) resulted in a higher packing factor and reduced the resistivity to $\sim 20 \mu\Omega \cdot \text{cm}$. With a 2-cm-diameter, 2-cm-long conductor-explosive element, it was possible to interrupt 25 kA in 8–10 μs , holding off 25 kV. Some of the main operational problems are with the end contacts where "waffled" copper disc surfaces are used in compression to achieve good electric contacts. The dielectric strength of the switch recovers at a rate of $3 \times 10^9 \text{ V/s}$ and the detonation velocity is $\sim 5 \text{ km/s}$ with a mass flow velocity of 2–3 km/s. The investigations are in their infancy and it is difficult to predict what the ultimate results may be, but the concept is of sufficient novelty and merit to warrant further studies.

A somewhat different type of a chemically exploding switch has been described by Kassel [64] in a review of Soviet Pulsed-Power R & D. In these cases, the explosive cartridge is placed at a right angle to the arc discharge. The explosively generated shock wave and the explosion debris then extinguish the arc (somewhat similar operation to an airblast breaker). The interrupted currents were fairly low (0.5–2.5 kA) but the interruption times Δt were quite short (2.1–39 μs).

Pavlovskii *et al* [65] reported an experiment where 7 MA of current was directed to a 30-nH load with a current rise time of 0.5 μs and a voltage gradient of 25 kV/cm. Experiments have been carried out in the United States [66] to duplicate these results. The basic switch arrangement is shown in Fig. 19. The plasma switching element is located coaxially around a cylinder of high explosive material. The plasma is initiated with a thin aluminum foil and then compressed by the cylindrical shock wave from the explosive. Results, so far, have demonstrated opening times on

conduction time of 0.1 ms the cross section of the fuse has to be $\sim 0.25 \text{ mm}^2$.

The current density, on the other hand, also determines the maximum obtainable electric field strength across the fuse. This relation is demonstrated in Fig. 15 [52], where the electric field strength is plotted versus delay time, which in

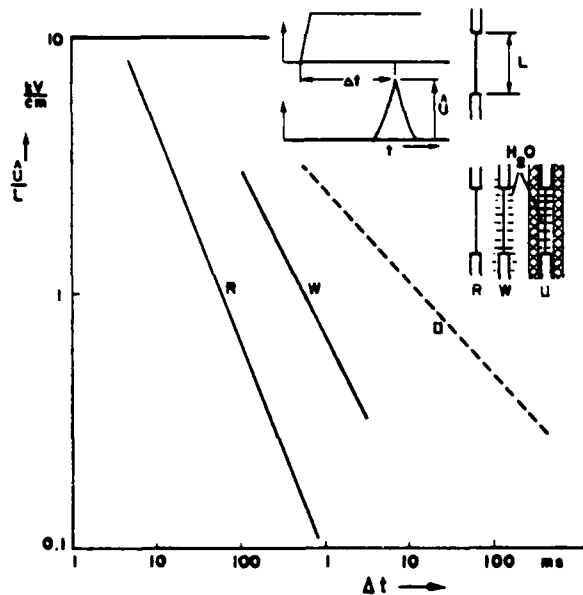


Fig. 15. Peak voltage per length of Cu wires versus time to explosion, Δt Parameter, surrounding medium [52].

turn depends on the current density. The parameter is the surrounding dielectric. Using the above example, where Δt was 0.1 ms, the value of voltage/length for a 0.25-mm^2 cross-section copper wire in atmospheric pressure air is 0.6 kV/cm. To generate a voltage of $V = 6 \text{ kV}$ or to get a resistance of $V/I = 0.6 \Omega$, the length of the fuse has to be $l = 10 \text{ cm}$.

For reasons discussed here, it is obvious that for a fuse operated in vacuum the inductively generated field is much lower than for a fuse in atmospheric air, since the confining function of the surrounding medium is missing [53], [54].

The resistance of the gas channel in vacuum is also reduced through thermionic emission of electrons and ions and subsequent ionization of the gas [41].

The realization of fast opening times under conditions of long charging times for the inductor has been demonstrated using a three-stage opening switch with parallel fuses with different conductor cross sections [55]. In this application, the fuse recovery of all but the last stage is crucial for successful operation [56], [57]. In a different approach, the combination of commercially available circuit breakers for long charging times and a fuse for fast opening has been operated successfully [52], [58].

Experiments which demonstrate the feasibility of fuse opening switches in high-power inductive discharge systems were recently performed by Reinovsky *et al.* [32]. A 1.9-MJ capacitor bank was discharged into an inductor. An electrically exploding foil was used to open the circuit and to transfer the energy to the load, which was an imploding foil. The fuse package is shown in Fig. 16. It is integrated into the transmission line which connects bank and load. The fuse, a 0.001-inch Al foil, is 70 cm long and 44 cm wide. The volume of the fuse package also serves as an inductive store with an inductance of $\sim 10 \text{ nH}$. This system demonstrates clearly the simplicity and compactness of inductive discharge systems. It has been operated with an electrolytic load of $12\text{-m}\Omega$ resistance and 5.8-nH inductance. With the system operating at 1.9 MJ stored energy, approximately 16 MA were interrupted, generating a 300-kV voltage across the load. About 7.5 MA were transferred to the load with a 10–90-percent rise time of 190 ns (opening time).

VIII. EXPLOSIVE OPENING SWITCHES

Explosive opening switches have been developed as a more rapidly opening alternative to mechanical breakers [59]. Opening times of less than $20 \mu\text{s}$ have been achieved in comparison to about $1000 \mu\text{s}$ or more for typical mechanical breakers. The short opening time, of course, reduces the effects of switch dissipation. In typical explosive opening switches, the current is interrupted by using an explosive to sever a conductor by blowing it apart or by forcing it against "cutting rings."

The explosion can be initiated with standard exploding

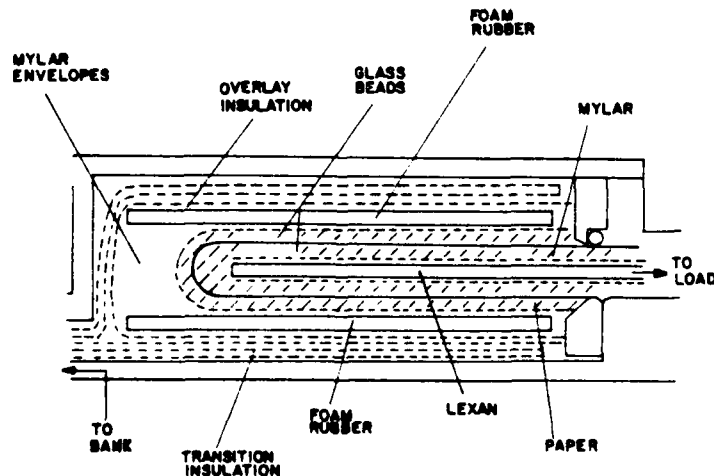


Fig. 16. Fuse construction [32].

the wire is bridged by an arc the voltage drops, which means that the resistance of the fuse is decreasing.

Embedding the wire in a liquid dielectric with low compressibility [40] delays the expansion of evaporated material and suppresses inhomogeneities, which lead to early arcing in the vapor, and the onset of peripheral discharges can hence be delayed, or even prevented. The effect of a liquid dielectric on the development of the fuse explosion is shown in Fig. 12 [1]. The dielectric was water in a completely closed, approximately 1-cm-diameter tube. The de-

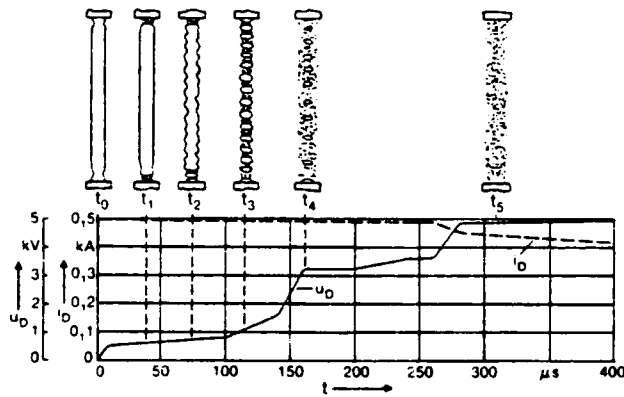


Fig. 12. Time development of the electrically induced explosion of a Cu wire in a water-filled tube with current and voltage traces after 1-ms current flow duration (Cu wire: $\phi = 0.25$ mm, $l = 6$ cm) [1].

velopment of the wire explosion in this system is similar to that of a fuse in air (Fig. 11), except for the fact that the formation of constrictions is much more regular and the voltage generated is higher by a factor of 5 to 6. A quite different behavior occurs after this. The voltage does not drop as in the case of air as the dielectric, but increases by another factor of two. This effect is due to the suppressed expansion of the completely vaporized metal [41], demonstrated by streak camera pictures which show a smaller increase in the diameter of the vapor column [40].

The results are summarized in Fig. 13 [42]. In the upper diagram, the current flow through wires is plotted versus time. The lower diagram shows the voltage drop across exploding wires in different surrounding media. There are large differences in peak voltage/length and in maximum resistivity of the wire, depending on whether the fuse is surrounded by air or water in an open or closed system. In order to generate high voltages along a fuse, it is important to use dielectrics with low compressibility in systems which prevent the expansion of the evaporated metal.

Beside atmospheric pressure air and liquids, high-pressure gases [43] and solid dielectrics, cast or as compressed dust, have also been used [44]–[46] to slow down the radial expansion and to stabilize the explosion, but the experimental results predicting the most suitable material are contradictory. In other experiments it was demonstrated that a strong oxidizer (H_2O_2 in water), especially in combination with wires of Al, which has a relatively high chemical activity, increased the maximum voltage [47].

The efficiency of a fuse as a switching element for transferring energy from the storage to the load is strongly influenced by the wire material. Since the cross section of

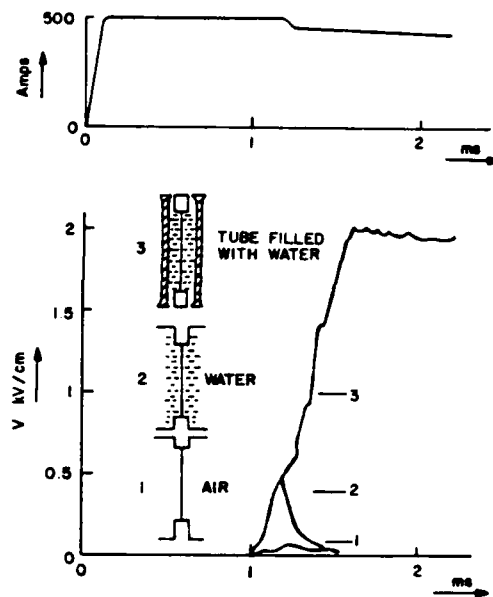


Fig. 13. Peak voltage per length, V^* , and current of slowly exploding wires in different surrounding media [42].

the wire can be reduced with increasing conductivity, and the energy loss is proportional to the product of wire volume and specific heat required to reach vaporization (approximately the specific sublimation heat), a good switch efficiency requires materials with high conductivity and low sublimation heat, such as gold, silver, copper, and aluminum [30], [48]–[50].

The maximum generated voltage is not only dependent on the length of the wire, the wire material, and the surrounding dielectric but also on the current density I in the fuse [46]. Another important parameter, the delay time Δt , or the time until the fuse explodes, is also related to the current density [30], [51]. According to the experimental results, as shown in Fig. 14, the conduction time Δt is

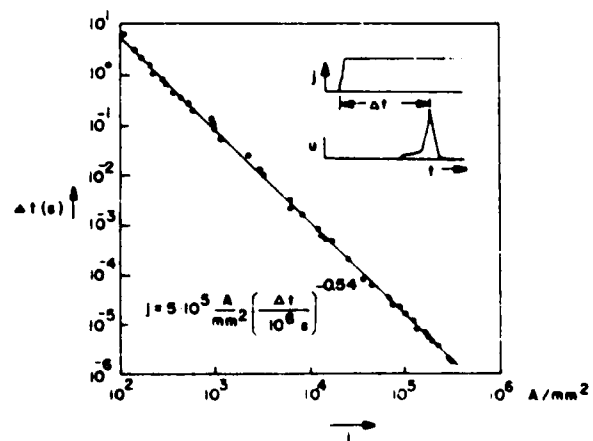


Fig. 14. Time to explosion Δt of Cu wires versus current density [51].

inversely proportional to $I^{0.54}$ and the coefficient only depends on the fuse material. For example, for a current $I = 10$ kA flowing through a Cu fuse and for a desired

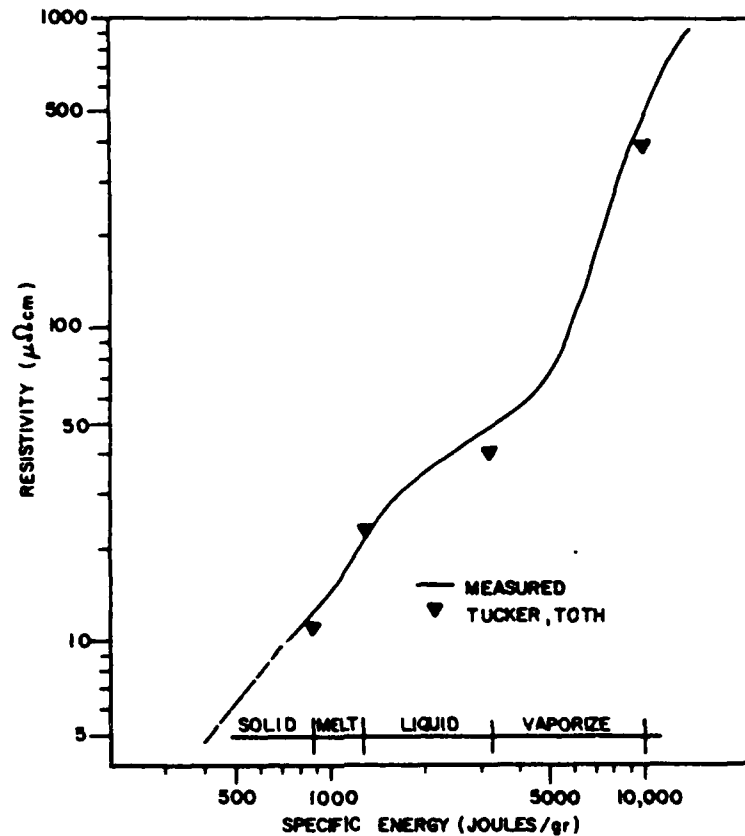


Fig. 10. Aluminum fuse resistivity as a function of specific energy [32].

energy. Also shown are other measured values [33] which were shown to be in excellent agreement with calculated values.

There are several mechanisms reversing the increase of resistivity. When the vapor channel expands, the gas density decreases and an arc may occur. This effect strongly depends on the wire material, the material embedding the wire, and the current density and duration. Another mechanism which prevents the generation of high voltages is breakdown along the fuse surface which is initiated by thermal emission before evaporation occurs. Tungsten and other metals with high boiling point, therefore, do not explode if operated in atmospheric pressure gases. The voltage at which surface arcs occur can also be influenced by the embedding material and the current distribution in these arcs is determined by the self-magnetic field [34]. If foils are used, edge effects, such as the initiation of corona discharges and subsequent microscopic explosions, can initiate the surface discharge [35]. Investigations of explosion phenomena which cause early ignitions of gas discharges in electrically exploded wires were performed by Jäger [36]. MHD instabilities ($m = 0$ and $m = 1$ instabilities) and early breaking of the wire cause an inhomogeneous density of evaporated metal and therefore irregular arcing [37]. The MHD instabilities of the $m = 0$ type were suppressed by means of a longitudinal magnetic field [36], [37].

To explain the fast opening of exploding wires it has been suggested that the decrease of conductivity occurs throughout the wire volume [38], [39]. The time development of electrically exploded Cu wires were investigated by means of optical and electrical diagnostic techniques [1].

For a wire in air the different stages in the development of the explosion and the current and voltage traces are shown in Fig. 11. The time zero corresponds to a state where the fuse is already molten ($T \sim 1000 \mu s$). Constrictions have

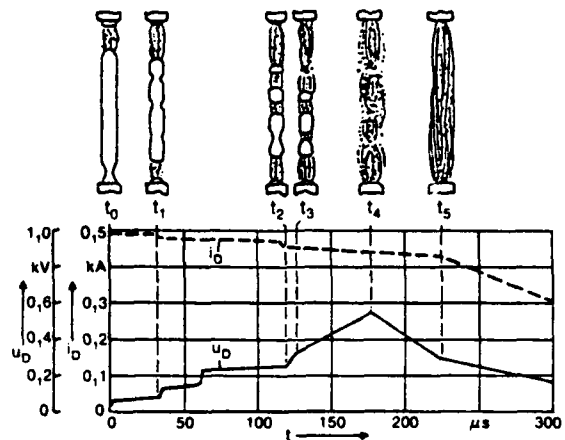


Fig. 11. Time development of the electrically induced explosion of a Cu wire in 1-atm air with current and voltage traces after 1-ms current flow duration (Cu wire: $\phi = 0.25$ mm, $l = 6$ cm) [1].

developed at the wire connections, leading to formation of arcs at $t = 30 \mu s + T$. During the following 100 μs the wire is breaking along the entire length and successive arcs are formed at the breaking positions. After the entire length of

current considerably. Hall currents in such an axial system are flowing in the azimuthal direction along closed paths and hence do not influence the radial current extinction mechanism. Vacuum arcs are sustained through the ejection of electrode material from hot cathode spots. As the current drops due to magnetic interaction the number of spots diminishes and finally, at a certain current level, the remaining spot vanishes. Hence by magnetic reduction of the current below the "chopping current" for a time longer than the time for the spot to vanish, the arc will be extinguished completely.

Metal plasma arc switches can be used in series to interrupt high voltages and, because of the positive current-voltage characteristics, used in parallel for high currents. The status (1976-1981) of metal plasma arc switches is, according to Gilmour [22], [23]:

current interrupted:	10 kA
load voltage interrupted:	25 kV
T_{on} :	0.1 μ s
T_{off} :	2 μ s
$T_{conduction}$:	10 μ s-dc
repetition rate:	10 kpps
life:	10^7 - 10^8 C.

It should, however, be noted that these values are *not* achieved all at the same time or in the same device and it has proven most difficult to get any of the researchers in this field to commit themselves to a self-consistent set of values (i.e., one device performance, stressing all parameters).

A second approach to the extinction of a vacuum arc by a magnetic field is described by Kimblin and Voshall [24]. Whereas in axial systems, which were considered so far, the azimuthal Hall field is shorted out, in case of a transverse geometry the Hall field

$$E_H = \frac{I_x B_z}{n_x e} \quad (4)$$

can reach values of 10^2 V/cm [25]. The Hall force acting on the ions leads to a separation of the plasma from the anode and hence to an arc extinction. A recent paper [26] reviews and compares different versions of the metal plasma arc switch

VI. CROSSED-FIELD TUBES (XFT)

Crossed-field tubes [17], [18] (XFT) operate in low-pressure regimes, to the left of the Paschen curve minimum but below the vacuum breakdown curve (Fig. 9). In this pd (pressure \times spacing) range magnetic fields applied perpendicular to the electric field between the electrodes enhance the conductivity, contrary to the effect in metal plasma arc switches. The reason for this phenomenon is that in this pd range, without magnetic fields, electrons are crossing the gap without causing ionization in the gas. With an applied transverse-magnetic field, electrons, due to their spiral motion, experience an increased path length and create a self-sustained discharge.

The operating principle of XFT's as closing and opening switches is based on these considerations. The pd product is maintained at such a low value that in the absence of a magnetic field, a gas discharge cannot form. By applying a magnetic field perpendicular to the electric field between

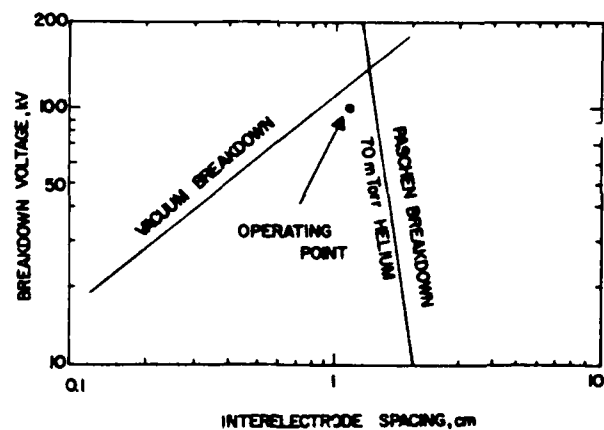


Fig. 9. Crossed-field tube operation parameters [27].

the electrodes, electrons that normally would be captured by the electrodes without causing ionization now spiral in the magnetic field and may create a self-sustained discharge. The magnetic field necessary to cause ionization is

$$B \geq \frac{1}{d} \sqrt{\frac{2mV}{e}} \quad (5)$$

where m and e are the electronic mass and charge, d is the interelectrode spacing, and V is the applied voltage. This condition expresses that the height of the cycloidal path of the electrons emitted from the cathode is smaller than the electrode gap d . At $V = 600$ kV and $d = 1$ cm the field required for ignition is 0.083 T.

During the conduction phase, the discharge voltage is relatively independent of current density and is in the range of 300 to 500 V. Current densities of up to 10 A/cm² can be conducted. When the magnetic field is removed, ionization ceases and the current is interrupted. The plasma decay time or switch opening time, depends on parameters such as pressure, ionic species, current density prior to interruption, and the external circuit and is generally on the order of several microseconds.

Investigations were performed at Hughes Research Laboratories with a coaxial tube [28]. The cathode surface area was 500 cm² with an interelectrode gap spacing of 1.15 cm. The discharge gas was He at pressures around 100 mtorr. The tubes, operated as high-power, on-off switches, achieved single-pulse operation at 40 kV and 3.2 kA. Pulse trains of 25- μ s-wide pulses, about 10 in number, were generated by pulsing the controlling magnetic field at 120 pps. The interruption voltage was 50 kV and the current was 1.3 kA.

VII. FUSES

The most familiar opening switches are fuses [29], [30]. They are relatively cheap and easily fabricated. The interruption process can be very fast ($t \sim 50$ ns) [31] and the conduction time can be determined by fuse material, dimension, and the surrounding media. Wires and foils embedded in gaseous, liquid, and solid media or in vacuum have been used. The opening mechanism of fuses is melting, boiling, and vaporization of a metallic conductor caused by joule heating and the subsequent creation of a highly resistive channel of dense vapor [30]. In Fig. 10 [32] the resistivity of an Al foil is plotted versus specific internal

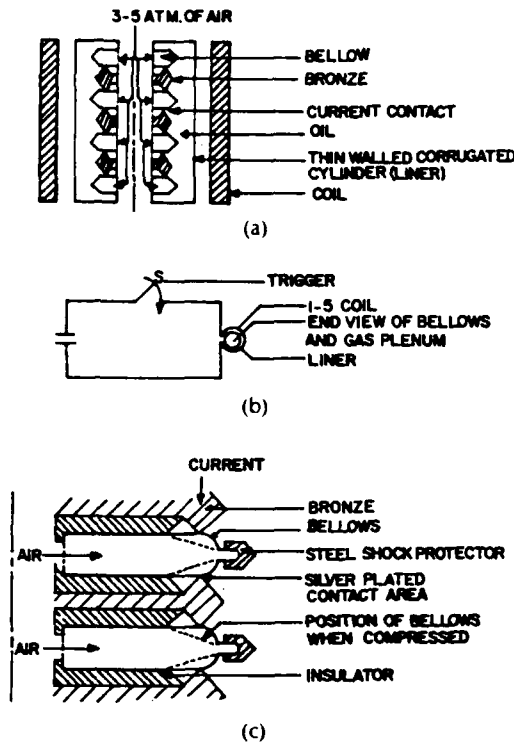


Fig. 7. "Bellows" opening switch. (a) Basic arrangement of bellows switch. (b) Electronic diagram of bellows control circuit. (c) Details of switch arrangement.

A system of three bellows in series has been tested and found to interrupt more than 50 kA to 40 kV in approximately $50 \pm 5 \mu\text{s}$. The switch appears to be scalable in current and voltage by changing the bellows diameter and the number of bellows (N). The design effort was for a switch with more than 1000 operations before major repair.

IV. SOLID-STATE SWITCHES

The counterpulsing (artificial commutation) technique can obviously be also used with solid-state switches, such as thyristors, in much the same way as described for mechanical vacuum interrupters in the previous section [14]. Although this can result in higher repetition rates, the voltages and currents per switch unit are, in general, less than for the mechanical switches. It is beyond the scope of this paper to discuss the various aspects of series-paralleling semiconductor switches for high-power operation but some of the tradeoffs are summarized in [15].

Different types of candidate solid-state switches are discussed in [16]. These switches include photoconductive switches where the conduction process is initiated and turned off by a photon source (e.g., laser) as well as various gate-controlled devices. The Hall-effect switch [17] is also discussed. The operation of Hall-active elements as resistive circuit interrupters depends upon applying a strong magnetic field perpendicular to the current flow in the element. Interruption capabilities, for a single element device, of 1.8 kV at 28.6 kA is suggested for a radial flow geometry in a Corbino disc arrangement. Opening switches based on conductivity changes during phase transitions have also been studied [18]. Particularly successful examples of this type of switch are the fuses and the superconducting switches which will be described in separate sections of this paper. Materials which experience several orders of magnitude

resistivity changes over fairly narrow temperature ranges and at moderate temperatures ($\sim 125^\circ\text{C}$) include BaTiO_3 and carbon filled polymers [19]. The search for candidate materials for this type of opening switch is in its infancy and it is difficult to predict how successful such a switch may be.

V. METAL PLASMA ARC SWITCHES

The metal plasma arc switch is, like the vacuum circuit breaker, a switch which operates in the arc mode. However, opening is not based on counterpulsing but on magnetic field interruption. The cathode is a relatively small electrode placed on the axis and the anode is an annulus surrounding the cathode. A coaxial magnetic field can be applied to the device in such a way that the field lines are essentially perpendicular to the paths of the electrons from the cathode to the anode.

The metal plasma arc is a discharge burning in electrode material which is vaporized and ionized in the arc spots of the cathode. It can be ignited by bringing the igniter electrode into contact with the cathode and then withdrawing it. It can also be ignited by applying a high-voltage pulse to a trigger electrode [9]. Another technique is laser-triggering of the vacuum arc [20]. The electrode material is vaporized and ejected into the gap causing breakdown of the switch. A technique reported to be very successful employs a titanium hydride igniter [21]. A small current pulse is passed through the igniter causing the release of a small amount of hydrogen. The hydrogen is then ionized and forms an arc. A similar technique was developed at the State University of New York at Buffalo [22]. Here a current pulse is used to vaporize a portion of a conductive film on the surface of an insulator (Fig. 8) [23]. The film is regenerated by deposition of material from the metal plasma.

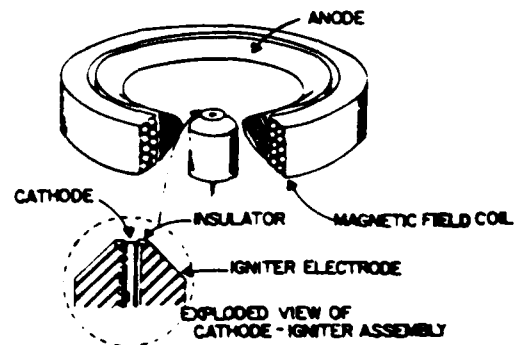


Fig. 8. Metal plasma arc switch triggered by the surface flashover mechanism [23].

For current interruption to occur in such an axial system, a magnetic field is applied with field lines perpendicular to the electron paths. Due to Larmor motion the effective mobility of the electrons is reduced, causing a reduction of conductivity from σ_0 to σ_1 . The conductivity ratio is

$$\frac{\sigma_1}{\sigma_0} = \frac{1}{1 + (\omega_l/\nu_c)^2} = \frac{1}{1 + kB^2} \quad (3)$$

where ω_l is the Larmor frequency, ν_c is the collision frequency, B the magnetic induction, and k is a constant which depends on electron energy and electron density. The current through the arc is proportional to the conductivity if the electric field in the gap is kept constant. Moderate magnetic fields of some 0.01 to 0.1 T can reduce the

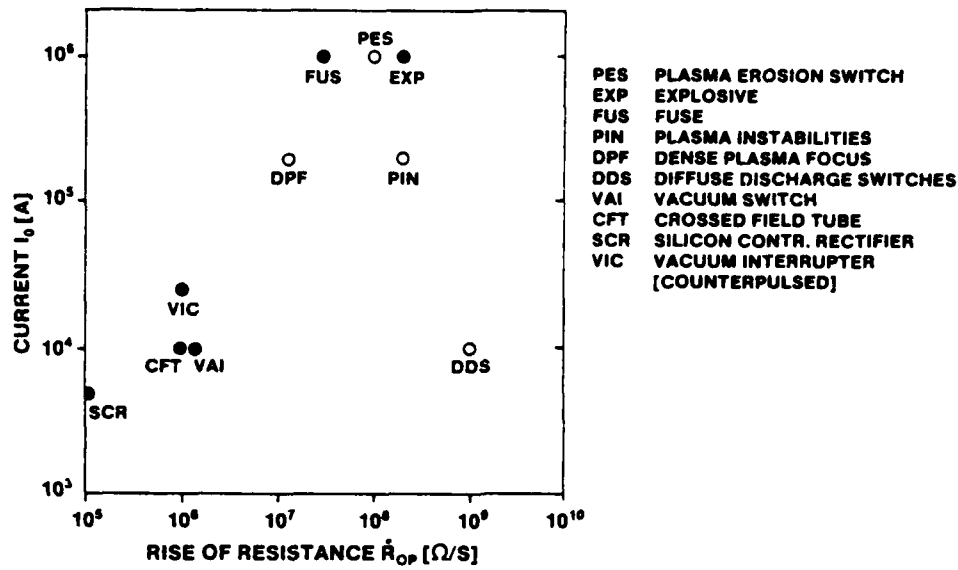


Fig. 5. Current, I_0 , versus rise of resistance, R_{op} , for high power opening switches.

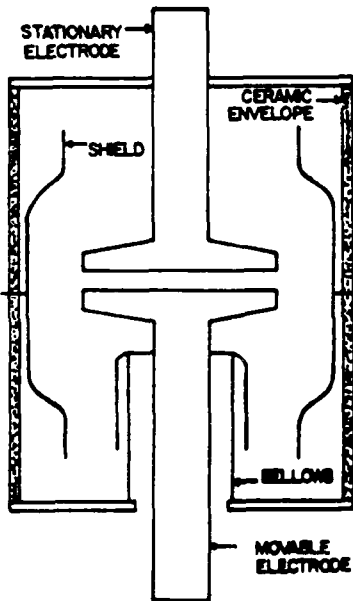


Fig. 6. Standard vacuum interrupter [9]

The switch is closed when the electrodes are in contact. The contact resistance of $10\text{--}35\ \mu\Omega$ gives very low conduction losses. To interrupt the current the contacts are opened. However, in most circuit breakers, the mechanical motion does not cause opening of the circuit by itself. During the separation of the contacts an arc is formed which has to be extinguished by the assistance of an externally produced current zero using a "counterpulse" technique. The electrode gap recovers only if the current zero is held long enough to allow plasma deionization. For vacuum arcs—arcs which operate in partially ionized electrode metal vapor—this is on the order of 3 to $15\ \mu\text{s}$.

For repetitive operation, the standard vacuum interrupter is limited to about 50 pps repetition rate because the electrodes must be moved mechanically for each opening and closing operation. To achieve higher repetition rates, a triggered vacuum interrupter is used [9]. The triggered vacuum interrupter is operated like a standard one during the coil charging period and the first output pulse. After the

mechanical opening, however, it is closed again electrically instead of mechanically by triggering the arc rather than closing the contacts. The arc drop is $25\text{--}40\ \text{V}$, large compared to the voltage drop in closed metal-metal contacts but still less than the conduction drop in most other opening switches. With this method currents of $8.6\ \text{kA}$ have been interrupted at peak voltages of $8.6\ \text{kV}$ in a burst mode at $5\ \text{kpps}$, using the counterpulse technique [8].

Several fast ($10\text{'s}\ \mu\text{s}$) mechanical switches have been described in the literature. Circuit breakers for the utility industry work in the millisecond range and take advantage of the natural zero crossing of the alternating current to extinguish the arc (a similar effect as in counterpulsing). For dc transmission lines, the technology is less developed but there have been several studies and concepts proposed and some of these are described in [10]. Much of the very fast ($10\text{'s}\ \mu\text{s}$) mechanical opening switch work has been carried out in the Soviet Union [11]. A particularly interesting switch is the "bellows type" [12], [13] shown in Fig. 7.

The basic idea is that the current in the external coil will try to compress the thin-walled (0.6-mm) corrugated liner. Because of the oil inside the liner, it will only move about $1\ \text{mm}$ and compress all the bellows which form the electric switch (current flows from one bellows to the next through the contact circles). Each of the bellows contact circles will compress approximately $1\ \text{mm}$ and oil will be forced between the contacts at high velocity. This provides for very rapid switching action since no mechanical motion is more than $1\ \text{mm}$ and the arc is subdivided into $2N$ gaps where N is the number of bellows. At the same time, oil is being forced between the contact gaps at very high velocity.

The "stay-open" time of the bellows, which are filled by $3\text{--}5\ \text{atm}$ of air to provide good contact pressure, is limited by the diffusion time of the magnetic field through the liner to $\tau_{open} < 1\ \text{ms}$. To keep the switch open longer, some latching mechanism must be provided. The switch was, however, also tested by using gas (probably SF_6) instead of oil and providing a sudden high overpressure on the outside of the bellows. In this case, the opening time was approximately $1\ \text{ms}$ but the switch remained open as long as the overpressure was maintained. In principle, the same effect can be provided by mechanically induced pressure in oil.

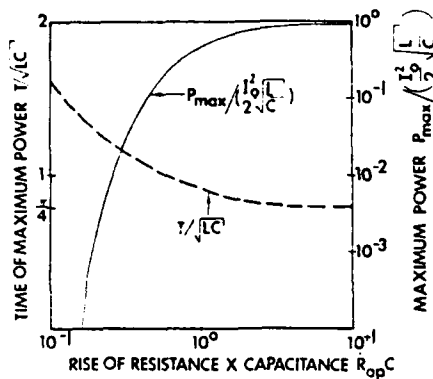


Fig. 4. Normalized maximum power, P_{\max} , and normalized time to reach the power maximum, T , versus rise of resistance, \dot{R}_{op} , times capacitance, C , for a capacitive load.

simultaneously with one opening switch. Hence, the selection of an opening switch requires the matching of the opening switch characteristics to the application of the system under consideration. Modeling of an inductive discharge system in order to find the best opening switch requires a thorough knowledge of the switch characteristics and, because of the coupling of switch and system parameters, generally an elaborate numerical calculation. However, it is possible to establish rules of thumb for the selection of an opening switch for a certain inductive discharge system by using some crude assumptions about the switch characteristics. The inductive discharge circuit considered earlier (Fig. 2(b)) consists of a primary current source which charges the inductor L . After establishing a current I_0 , the switch S_0 is opened and switch S_c is closed, thereby transferring energy stored in L to the load Z_L . The opening switch impedance is assumed to be purely resistive and to increase linearly in time during opening

$$R_{op} = \dot{R}_{op} t, \quad \text{with } \dot{R}_{op} = \text{constant.}$$

The series resistances of the current source and inductor are assumed to be zero.

Circuit calculations were performed for resistive, inductive, and capacitive loads. Results are shown in Table 1 and Fig. 4. The maximum power transferred from the inductor to the load P_{\max} , and the time of maximum power transfer T , are expressed in terms of the inductance L ; the load parameters R_L , L_L and C_L ; the current I_0 ; and the rise of the opening switch resistance \dot{R}_{op} . Analytic expressions for P_{\max} and T are given in case of resistive and inductive loads. For

a capacitive load, P_{\max} and T were calculated numerically. They are plotted in Fig. 4 versus $\dot{R}_{op} C$. Assume, for instance, a circuit with $L = 10^{-4}$ H "charged" to $I_0 = 10^4$ A and a load resistance of $R_L = 10 \Omega$. If the maximum power is needed to be $P_{\max} = 100$ MW, then \dot{R}_{op} must exceed $10^7 \Omega/s$, the switch has to stand a voltage of $V_{\max} = 700$ kV, and the necessary opening switch resistance is $R_{op} = 100 \Omega$ at $T = 1 \mu s$. Although these calculations cannot replace a thorough circuit analysis, they help to identify the demands made on the opening switch.

According to these calculations, two parameters seem to be of particular importance, the current through the opening switch I_0 (the ability of the opening switch to carry large currents), and the rise of opening switch resistance \dot{R}_{op} . The greater these values, the more efficient is the transfer of energy to the load in a high-power inductive discharge circuit. During an Army Research Office Workshop on "Repetitive Opening Switches" [2] efforts were made to compare and summarize capabilities of various opening switches. From these data, values for the rise of resistance \dot{R}_{op} were derived for the various switch concepts and are plotted in Fig. 5 versus maximum current through the switch. The larger the product of I_0 and \dot{R}_{op} the higher is the power that can be switched from inductor to load. That means, high-power switches are located in the right upper part of the diagram. However, the most powerful switches—fuses and explosives—are typical single-shot devices. For many applications, repetitive switches with repetition rates in the kilopulses per second (kpps) range are required [7]. So far only switches in the power range of < 75 MW meet this requirement in a short burst mode [8]. Experiments are under way to test the feasibility of novel opening switch concepts like the Dense Plasma Focus and Diffuse Discharge Opening Switches (discussed later in this paper), which may be applicable in high-power, repetitive systems.

Hence, this paper describes two different fields of opening switch technology. In the first part "conventional" opening switches (filled dots in Fig. 5) are discussed. The second part deals with novel opening switch concepts (open dots in Fig. 5).

III. MECHANICAL CIRCUIT BREAKERS—COUNTERPULSING

A mechanical opening switch consists of two separate contacts in an insulating medium which may be liquid, gas, or vacuum. A standard switch design is shown in Fig. 6 [9].

Table 1 Maximum Power P_{\max} and Time to Reach the Power Maximum T for Resistive and Inductive Load in an Inductive Energy Discharge Circuit. For Capacitive Load the Analytic Expression for the Power in the Load P is Given. Solutions for P_{\max} and T are Evaluated Numerically (Fig. 3)

Resistive Load: R_L	
$P_{\max} = I_0^2 R_L \frac{\alpha^2}{(1+\alpha)^2} \exp \left[-\frac{2}{\alpha} + \frac{2}{\alpha^2} \ln(1+\alpha) \right]$	$\alpha^2 = \frac{\dot{R}_{op} L}{R_L}, \quad T = \left(\frac{L}{\dot{R}_{op}} \right)^{1/2}$
Inductive Load L_L	
$P_{\max} = 0.33 I_0^2 \left(\frac{L}{L+L_L} \right)^{1/2} (\dot{R}_{op} L_L)^{1/2}$	$T = 1.46 \left[\frac{L L_L}{\dot{R}_{op} (L+L_L)} \right]^{1/2}$
Capacitive Load: C_L	
$P = \left(\frac{L}{C_L} \right)^{1/2} I_0^2 \frac{5^{1-2s}}{(2s-1)} (\omega t)^{-2s+1} J_s(\omega t) [J_s(\omega t) - \omega t J_{s+1}(\omega t)]$	
$s = \frac{1}{2} \left(1 + \frac{1}{C_L \dot{R}_{op}} \right), \quad \omega = (L C_L)^{-1/2}, \quad J_s \hat{=} \text{Bessel function of order } s$	

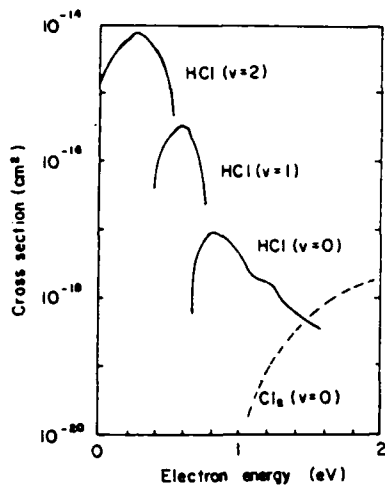


Fig. 31. Dissociative attachment cross sections for vibrationally excited HCl molecules [106].

attachment rate by vibrational excitation of attachers. Processes considered for producing highly excited vibrational states are IR photoexcitation, transitions from electronically excited state, collisional or radiative, and photodissociation of larger molecules producing vibrationally excited fragments [109]. The efficiency of opening switches based on these mechanisms should be high, because the laser energy is used only during the opening phase, and not to sustain the discharge.

XIII. THE PLASMA EROSION SWITCH

The plasma erosion switch operates on a very short time scale of 10 to 100 ns, both with regard to conduction and opening times. It is successfully used for suppression of

prepulses and steepening of the pulse rise time in high-power generators [110]–[112]. Recently, pulse compression experiments in a vacuum inductive storage system were also performed with plasma erosion switches used as opening switches [113].

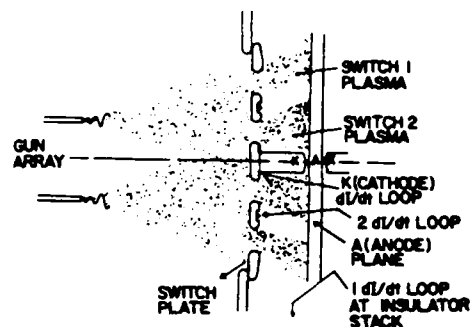


Fig. 32. Schematic of the plasma erosion switch (apparatus used in the Proto I experiment) [110].

Fig. 32 shows the schematic of a plasma erosion switch [110]. Plasma is injected into the switch region between anode A and cathode K. Holes in the cathode allow plasma from a plasma-gun array to flow in columns through the switch plate C to the anode plate. In this experiment, the injected plasma has densities in the range of $5 \times 10^{12} \text{ cm}^{-3}$ to $5 \times 10^{13} \text{ cm}^{-3}$ [105], [106] and moves with velocities of typically $7.5 \times 10^6 \text{ cm/s}$ [114]. Switch areas are in the order of 100 cm^2 [113] to 1000 cm^2 [112].

The present understanding of the switch dynamics is illustrated in Fig. 33(b) which shows the time history of the

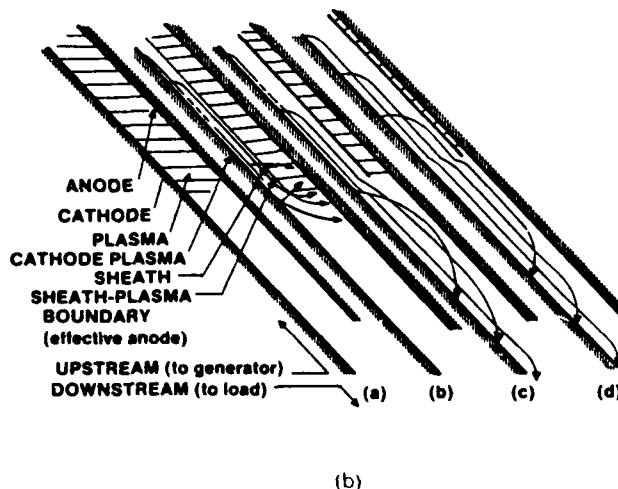
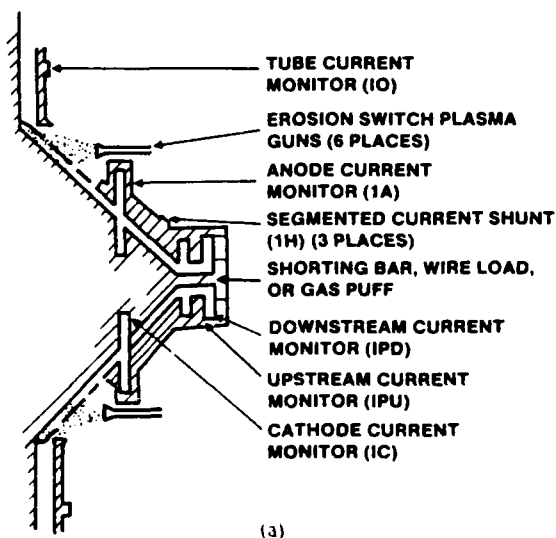


Fig. 33. (a) Diagram of the vacuum feed region of PITHON, identifying the current monitors used in the experiment and the location of the erosion switch [112]. (b) Illustration of the phases of switch opening [112]. (a) Denotes the early time shorted phase in which the sheath thickness is insignificant and the impedance of the switch is essentially zero. (b) Denotes the behavior of the switch as a parapotential diode. Ions are accelerated essentially straight to the cathode, extracted from the plasma by sheath expansion. The electron trajectories are bent by the magnetic field of the generator current. (c) Denotes the onset of magnetic cutoff of the electron flow between the electrodes. Ion current and sheath expansion continue. (d) Denotes the continued expansion of the sheath leading to full erosion of the plasma.

erosion switch in the PITHON experiment (Fig. 33(a)) [112], and is as follows: As a finite voltage appears across the injected plasma, a sheath forms near the cathode. In this sheath, the electrons are swept out, and a planar diode-like gap with the cathode as a surface on one side and the edge of the plasma on the other side is formed. The cathode becomes a space-charge-limited electron emitter with plasma-induced field emission [115]. Ions supplied by the injected plasma reduce the negative space charge and provide for a current enhancement of 1.86 over the Child-Langmuir current for stationary sheaths. The ion current density j_i for one-dimensional current flow [116] is

$$j_i = 1.86 \cdot \frac{4\epsilon_0}{9} \left(\frac{2e}{m_i} \right)^{1/2} \frac{V^{3/2}}{d^2} \quad (10)$$

and the electron current density j_e is

$$j_e = \left(\frac{m_i}{m_e} \right)^{1/2} j_i \quad (11)$$

where m_e and m_i are the electron and ion masses, respectively, ϵ_0 the permittivity of free space, e the electron charge, V the voltage across the sheath, and d the sheath thickness.

As the current increases, the ion flux from the plasma-gun into the gap is not sufficient to maintain bipolar flux across the plasma interface. An additional flux of ions is provided by "eroding" the plasma, thereby increasing the sheath. This effect causes the effective resistance of the switch to increase and, with a series inductance in the switch circuit, generates an increased voltage across the sheath.

With further increase in current, the trajectories of the electrons in the switch region are bent by the self-magnetic field. The switch opens when the electron flow across the gap exceeds the critical current value I_c [117] for the onset of magnetic insulation

$$I_c = I_a g \beta \gamma \quad (12)$$

with

$$I_a = \frac{m_0 c^2}{e} 2\pi\epsilon_0 c \approx 8500 \text{ A} \quad (13)$$

$$\beta = \frac{v}{c} \quad (14)$$

$$\gamma = (1 - \beta^2)^{-1/2} = 1 + \frac{eV}{m_0 c^2} \quad (15)$$

with v being the electron velocity, c the speed of light, m_0 the rest mass of an electron, and g a geometry factor. After magnetic cutoff of the electron flow, the ion current still continues, since cutoff of ion flux requires a magnetic field larger than that for electrons by a factor $(m_i/m_e)^{1/2}$. However, the ion current density is so low that the expansion of the sheath continues, leading to full erosion of the plasma (Fig. 32(b)).

These three stages of the switch, a) conduction, b) bipolar diode with increasing sheath thickness, and c) magnetic insulation are demonstrated in the impedance history (Fig. 34) of a short circuit shot in the PITHON system [112], which operates with an imploding plasma load. The figure shows that the impedance rises to values of several 10's ohms in less than 50 ns. The maximum switch current was ~ 1 MA and the maximum voltage across the switch 1.8 MV. Even lower opening times were achieved in pulse

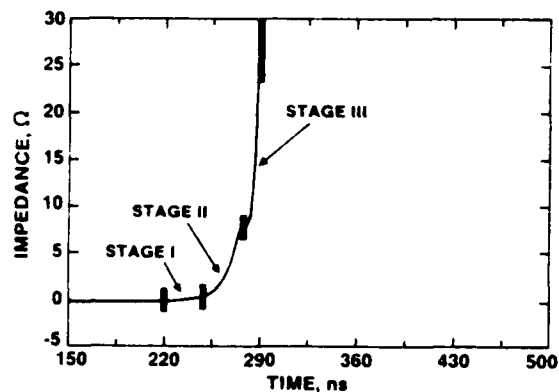


Fig. 34. Impedance history for a short-circuit shot, showing three stages [112].

compression experiments in a vacuum inductive storage system with an electron-beam diode load, performed at NRL [113]. After a conduction time of ~ 50 ns the switch opened in an interval of ~ 10 ns. The switch current was in the excess of 200 kA and a voltage in excess of 1 MV was generated. The power compression ratio was 4, compared to measurements without the switch.

XIV REFLEX TRIODE SWITCH

Another novel opening switch for short pulse vacuum inductive energy storage systems is the Reflex Triode [118]. The basic experimental arrangement is shown in Fig. 35. The operation of this arrangement as a switch is explained [118] as follows:

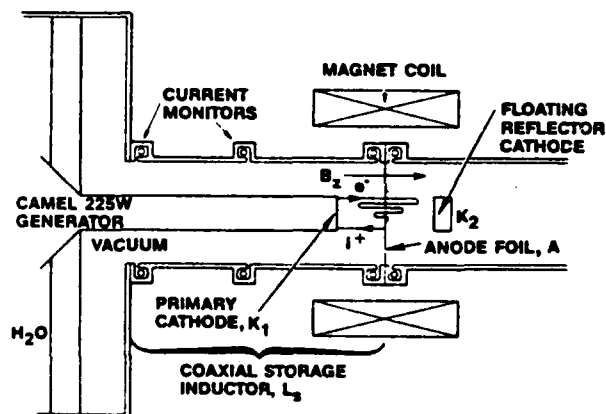


Fig. 35. Reflex switch experimental setup [118].

The switch is based on reflex triode physics. It consists of a primary cathode, K_1 , a thin anode, A , and a secondary cathode, K_2 , which is electrically floating and serves to reflect electrons back through the anode toward K_1 , which in turn repels them back through the anode toward K_2 , etc. The reflexing electron scatter in the anode and deposit some of their energy in it on each pass. An axial magnetic field is used to minimize radial loss of electrons. Positive ions are accelerated from the anode to the cathode, K_1 .

The combination of multiply reflected electrons and counterstreaming positive ions flowing between cathode, K_1 , and anode, A , results in several unique properties. One

of the most important of these is that the total current in the reflex mode can be orders of magnitude greater than the Langmuir-Child (L-C) current appropriate for an ordinary vacuum diode of the same dimensions. Thus, the "impedance" of the reflex mode can be far lower than the impedance of the A-K₁ gap in the absence of reflexing. The reflex triode can function as a "closed" switch if we first establish the reflex mode and then as an "opening" switch if we bring about an abrupt termination of electron reflexing. This forces a fast transition from the low-impedance reflex mode ("closed" switch) to the much higher impedance Langmuir bipolar mode ("open" switch). Reflexing is terminated, in our technique, by allowing the floating electrode, K₂, to undergo a short-circuit to the anode at the desired time. When the negative potential of K₂ collapses to anode potential, electrons no longer reflect from K₂ and instead deposit in it after one pass through A-K₁. Once reflexing is terminated, the transition of A-K₁ to the Langmuir bipolar mode is governed by ion and neutral atom dynamics in A-K₁.

An impedance transition of 0.8 to 15.3 Ω has been achieved, i.e., a factor of 19, with a peak, open switch, accelerating voltage of 1.8 MV.

XV. SUMMARY

The area of opening switch research and development for inductive energy storage is clearly a very complex and interdisciplinary one, involving electrical and mechanical engineering, physics, chemistry, etc. Most "successful" opening switches are presently single shot in nature (e.g., fuses). Due to the high energy storage density inherent in inductive storage systems, the potential payoff in developing repetitive, or at least reusable, opening switches is very high and new ideas are met with considerable interest.

Besides the categories and switch types described in this review, there are undoubtedly many other, different schemes or modifications of the ones discussed here. It is felt, however, that the switch types discussed in this paper include most of the best known or investigated ones.

REFERENCES

- [1] U. Schwarz, "Über die Erzeugung von Hochspannungsimpulsen mit Drahtexplosionen aus induktiven Energiespeichern," Ph.D. dissertation TU Braunschweig, p. 44, 1977.
- [2] M. Kristiansen and K. Schoenbach, Eds., *Proc. Army Research Office Workshop on Repetitive Opening Switches* (Tamarron, CO, Jan. 23-30, 1981), DTIC AD-A110770.
- [3] M. Kristiansen and K. Schoenbach, Eds., *Proc. of Army Research Office Workshop on Diffuse Discharge Opening Switches* (Tamarron, CO, Jan. 13-15, 1982), DTIC AD-A115483.
- [4] M. Kristiansen, "Fundamentals of inductive energy storage," in *Proc. Army Research Office Workshop on Repetitive Opening Switches* (Tamarron, CO, 1981), DTIC AD-A110770, p. 233.
- [5] W. I. Sargeant, *Energy Storage Capacitors* (Air Force Pulsed Power Lecture Series, Texas Tech University, Lubbock, TX), Lecture No. 10, 1981 (Coord. M. Kristiansen and A. H. Günther).
- [6] R. I. Harvey and A. J. Palmer, "Opening switch technology," in *Proc. Army Research Office Workshop on Repetitive Opening Switches* (Tamarron, CO, 1981), DTIC AD-A110770, p. 20.
- [7] M. F. Rose and A. K. Hyder, Jr., "Opening switches—Scenarios for their use," in *Proc. Army Research Office Workshop on Diffuse Discharge Opening Switches* (Tamarron, CO, 1982), DTIC AD-A115883, p. 18.
- [8] E. M. Honig, "Generation of a 75-MW 5 kHz pulse train from an inductive energy store," *IEEE Trans. Plasma Sci.*, vol. PS-12, p. 24, 1984.
- [9] E. M. Honig, "Vacuum interrupters and thyatrons as opening switches," in *Proc. Army Research Office Workshop on Repetitive Opening Switches* (Tamarron, CO, 1981), DTIC AD-A110770, p. 233.
- [10] J. P. Bowles, A. B. Turner, and R. L. Vaughan, "System studies for HVDC circuit breakers," Electric Power Research Institute Rep. EPRI EL-1260, Project 326-1, Dec. 1979.
- [11] *Proc. 2nd All-Union Conf. on Engineering Problems of Thermonuclear Reactors* (Leningrad, USSR, June 23-25, 1981).
- [12] B. A. Larionov and N. A. Mikhavlov, "High speed breaker of repeated action with electrodynamic drive," in *Proc. 2nd All-Union Conf. on Engineering Problems of Thermonuclear Reactors* (Leningrad, USSR, June 23-25, 1981), vol. III, pp. 96-102.
- [13] B. Larionov, personal communication to M. Kristiansen, June 1981.
- [14] M. M. Parsons, "A comparison between an SCR and a vacuum interrupter system for repetitive opening," in *Proc. Army Research Office on Repetitive Opening Switches* (Tamarron, CO, 1981), DTIC AD-A110770, p. 246.
- [15] J. P. O'Loughlin, "Applications related issues," in *Proc. Army Research Office Workshop on Solid State Switches for Pulsed Power* (Tamarron, CO, Jan. 12-14, 1983), DTIC AD-A132687, p. 272.
- [16] M. Weiner, "Solid state opening switches," in *Proc. Army Research Office Workshop on Solid State Switches for Pulsed Power* (Tamarron, CO, Jan. 12-14, 1983), DTIC AD-A132687, p. 189.
- [17] P. J. Turchi, "Magnetoplasma dynamic and Hall effect switching for repetitive interruption of inductive circuits," in *Proc. Army Research Office Workshop on Repetitive Opening Switches* (Tamarron, CO, 1981), DTIC AD-A220770, p. 149.
- [18] I. M. Vitkovitsky, "State transition switches," in *Proc. Army Research Office Workshop on Solid State Switches for Pulsed Power* (Tamarron, CO, Jan. 12-14, 1983), DTIC AD-A132687, p. 258.
- [19] R. D. Ford and I. M. Vitkovitsky, "Non-linear resistivity materials for pulsed power application," in *Proc. 4th IEEE Pulsed Power Conf.* (Albuquerque, NM, June 1983), pp. 118-121 (IEEE Catalog No. 83CH1908-3).
- [20] A. S. Gilmour, Jr. and R. J. Clark, Jr., "Studies on a laser-triggered, high voltage, high vacuum switch tube," in *Proc. 3rd Int. Symp. on Discharges and Electrical Insulation in Vacuum* (Paris, France, 1968), p. 367.
- [21] J. M. Lafferty, "Triggered vacuum gaps," *Proc. IEEE*, vol. 54, p. 23, 1966.
- [22] A. S. Gilmour, Jr., "Vacuum arc switching," in *Proc. Army Research Office Workshop on Repetitive Opening Switches* (Tamarron, CO, 1981), DTIC AD-A110770, p. 164.
- [23] ———, "The present status and projected capabilities of vacuum arc opening switches," in *Proc. 1st IEEE Int. Pulsed Power Conf.* (Lubbock, TX, 1976), paper ICI-1.
- [24] C. W. Kimblin and R. E. Voshall, "Interruption ability of vacuum interrupters subjected to axial magnetic fields," *Proc. Inst. Elec. Eng.*, vol. 119, p. 1754, 1972.
- [25] C. W. Kimblin, "Development of a current limiter using vacuum arc current commutation," Final Rep. EPRI EL-393, Westinghouse Electric Corp., 1977.
- [26] D. R. Dettman, R. Dollinger, and J. Sargeant, "Pulsed power characterizations of metal plasma arc switches (MPAS)," in *Proc. 4th IEEE Pulsed Power Conf.* (Albuquerque, NM, June 1983), pp. 762-765 (IEEE Catalog 83CH1908-3).
- [27] M. A. Lutz and G. A. Hoffman, "The Gamitron—A high power crossed-field switch tube for HVDC interruption," *IEEE Trans. Plasma Sci.*, vol. PS-2, p. 11, 1974.
- [28] R. I. Harvey and M. A. Lutz, "High power on-off switching with crossed field tubes," *IEEE Trans. Plasma Sci.*, vol. PS-4, p. 210, 1976.
- [29] H. C. Early and F. J. Martin, "Methods of producing a fast current rise from energy storage capacitors," *Rev. Sci. In-*

- strum., vol. 36, p. 1000, 1965
- [30] Ch. Maisonnier, J. G. Linhart, and C. Courlan, "Rapid transfer of magnetic energy by means of exploding foils," *Rev. Sci. Instrum.*, vol. 37, p. 1380, 1966
- [31] Yu. A. Kotov, N. G. Kolganov, and B. M. Koval'chuk, "A fast contact breaker based on electrically exploded wires," translated from *Pribovy i Tekhnika Eksperimenta*, no. 6, p. 107, 1974
- [32] R. E. Reinovsky, D. L. Smith, W. L. Baker, J. H. Degnan, R. P. Henderson, R. J. Kohn, D. A. Kloc, and N. F. Rodenick, "Inductive store pulse compression system for driving high-speed plasma implosions," *IEEE Trans. Plasma Sci.*, vol. PS-10, p. 73, 1982
- [33] T. J. Tucker and R. P. Toth, "A computer code for predicting the behavior of electrical circuits containing exploding wire elements," Sandia Nat. Lab., Rep. 75-0041, 1975
- [34] V. A. Burtsev, V. A. Dubyanskii, N. P. Egorov, M. P. Kasatkina, A. B. Produvnov, and I. V. Shestakov, "Electrical explosion of a cylindrical foil in air. Current distribution in the high-current shunting discharge," *Sov. Tech. Phys. Lett.*, vol. 4, p. 264, 1978
- [35] V. A. Burtsev, V. N. Litunovskii, and V. F. Prokopenko, "Electrical explosion of foils. I," *Sov. Phys.—Tech. Phys.*, vol. 22, p. 950, 1977
- [36] H. Jäger, "Zur Entstehung primärer Gasentladungszonen bei elektrischen Drahtexplosionen," *Z. Naturforsch.*, vol. 27a, p. 1586, 1972
- [37] ———, "Probleme zur Erzeugung extrem dichter Plasmen mittels elektrischer Drahtexplosionen," *Deutsche Luft und Raumfahrt—Mittellungen*, vol. 74, p. 20, 1974
- [38] A. P. Baikov, L. S. Gerasimov, and A. M. Iskol'dskii, "Electrical conductivity of an aluminum foil in an electrical explosion," *Sov. Phys.—Tech. Phys.*, vol. 20, p. 29, 1975
- [39] E. V. Krivitskii and V. P. Litvinenko, "Exploding wire mechanism," *Sov. Phys.—Tech. Phys.*, vol. 21, p. 1218, 1976
- [40] U. Seydel, R. Schoefer, and H. Jäger, "Temperatur und Druck explodierender Drähte beim Verdampfungsbeginn," *Z. Naturforsch.*, vol. 30a, p. 1166, 1975
- [41] I. M. Vitkovitsky, "Fuses and repetitive current interruption," in *Proc. Army Research Office Workshop on Repetitive Opening Switches* (Tamaron, CO, 1981), DTIC AD-A220770, p. 269
- [42] J. Salge, U. Braunsberger, and U. Schwarz, "Circuit breaker for ohmic-heating systems," in *Proc. 8th Symp. on Engineering Problems of Fusion Research* (San Diego, CA, 1975), p. 643
- [43] G. P. Grazunov, V. P. Kantsedal, and R. V. Mitin, "Use of electric explosion of wires in a high-pressure gas to break a current circuit," translated from *Zhurnal Prikladnoi Mekhaniki i Tekhnicheskoi Fiziki*, no. 6, p. 102, 1976
- [44] V. A. Burtsev, V. N. Litunovskii, and V. F. Prokopenko, "Electrical explosion of foils II," *Sov. Phys.—Tech. Phys.*, vol. 22, p. 957, 1977
- [45] L. V. Dubovoi, I. M. Roife, E. V. Seredenko, and B. A. Strekol'nikov, "A powerful foil breaker for a current of 0.5 MA which actuates in 5 μ sec," translated from *Pribovy i Tekhnika Eksperimenta*, no. 2, p. 107, 1974
- [46] E. A. Azizov, N. A. Akhmerov, and V. A. Yagnov, "Influence of a dielectric medium on the characteristics of a high-speed explosive circuit breaker," *Sov. Tech. Phys. Lett.*, vol. 2, p. 121, 1976
- [47] D. Conte, M. Friedman, and M. Urv, "A method for enhancing exploding aluminum foil fuses for inductive storage switching," in *Proc. 1st IEEE Int. Pulsed Power Conf.* (Lubbock, TX, 1976), paper 11D7
- [48] G. Sargent James and H. Kowitz, "High power pulse steepening by means of exploding wires," *Rev. Sci. Instrum.*, vol. 30, p. 1032, 1959
- [49] J. N. DiMarco and L. C. Burkhardt, "Characteristics of a magnetic energy storage system using exploding foils," *J. Appl. Phys.*, vol. 41, p. 3894, 1970
- [50] Yu. A. Kotov, N. G. Kolganov, V. S. Sedoi, B. M. Koval'chuk, and G. A. Mesvats, "Nanosecond pulse generators with inductive storage," in *Proc. 1st IEEE Int. Pulsed Power Conf.* (Lubbock, TX, 1976), paper 1A
- [51] U. Braunsberger, J. Salge, and U. Schwarz, "Circuit breaker for power amplification in poloidal field circuits," in *Proc. 8th Symp. on Fusion Technology* (Nordwijkerhout, The Netherlands, 1974), p. 399
- [52] J. Salge, U. Braunsberger, and U. Schwarz, "Circuit breaking by exploding wires in magnetic energy storage systems," in *Proc. Int. Conf. on Energy Storage, Compression and Switching* (Torino, Italy, 1974), p. 477
- [53] I. Holmstroem, S. K. Haendel, and B. Stenerhag, "Undegassed and degassed exploding tungsten wires in vacuum," *J. Appl. Phys.*, vol. 39, p. 2998, 1968
- [54] I. M. Vitkovitsky and V. E. Scherrer, "Recovery characteristic of exploding wire fuses in air and vacuum," *J. Appl. Phys.*, vol. 52, p. 3012, 1981
- [55] D. Conte, R. D. Ford, W. H. Lupton, and I. M. Vitkovitsky, "Trident—A megavolt pulse generator using inductive energy storage," in *Proc. 2nd IEEE Int. Pulsed Power Conf.* (Lubbock, TX, 1979), p. 276 (IEEE Catalog 79-90330)
- [56] I. M. Vitkovitsky and V. E. Scherrer, "Recovery characteristic of exploding wire fuses in air and vacuum," *J. Appl. Phys.*, vol. 52, p. 3012, 1981
- [57] R. D. Ford and I. M. Vitkovitsky, "High recovery voltage switch for interruption of large currents," *Rev. Sci. Instrum.*, vol. 53, p. 1098, 1982
- [58] R. C. Walker & H. C. Early, "Half-megampere magnetic-energy-storage pulse generator," *Rev. Sci. Instrum.*, vol. 29, p. 1020, 1958
- [59] R. D. Ford and I. M. Vitkovitsky, "Explosively actuated 100 kA opening switch for high voltage applications," NRL Memo Rep. 3561, July 1977
- [60] D. Conte, R. D. Ford, W. H. Lupton, and I. M. Vitkovitsky, "Two stage opening switch techniques for generation of high inductive voltage," in *Proc. 7th Symp. on Engineering Problems of Fusion Research* (Knoxville, TN, 1977), p. 1066
- [61] I. M. Vitkovitsky, D. Conte, R. D. Ford, and W. H. Lupton, "Current interruption in inductive storage system using inertial current source," in *Energy Storage, Compression and Switching*, vol. II, V. Nardi, H. Selin, and W. H. Bostick, Eds. New York: Plenum, 1983
- [62] B. A. Larianov, Efremov Scientific Research Institute for Electrophysical Apparatus, USSR. Personal communication to M. Kristiansen, 1981
- [63] B. A. Larianov et al., "Some methods of increasing the response of fast breakers," in *Proc. All-Union Conf. on Engineering Problems of Fusion Reactors* (Leningrad, USSR, July 28–30, 1977)
- [64] S. Kassel, "Soviet pulsed-power R & D," Report R-2212-ARPA, Chapter X. Rand Co., Santa Monica, CA (Preliminary Report), 1978
- [65] A. I. Pavlovskii, R. Z. Lyudaev, A. S. Kravchenko, V. A. Vasyukov, L. N. Pljashkevich, A. M. Shuvalov, A. S. Russkov, Y. Ye. Gurin, B. A. Boyko, and V. A. Zolotov, "Formation and transmission of magnetic cumulation generators electromagnetic energy pulses," in *Megagauss Physics and Technology*, P. J. Turchi, Ed. New York: Plenum, 1980, p. 595
- [66] B. N. Turman and T. J. Tucker, "Experiments with an explosively opened plasma switch," in *Proc. U.S. Army Research Office Workshop on Repetitive Opening Switches* (Tamaron, CO, 1981), DTIC AD-A110770, p. 284
- [67] K. H. Schoenbach, G. Schaefer, H. C. Harjes, G. Leiker, and M. Kristiansen, "Opening switches," in *Proc. 3rd IEEE Int. Pulsed Power Conf.* (Albuquerque, NM, 1981), p. 74 (IEEE Catalog 81CH1662-b)
- [68] G. Herziger, H. Krompholz, W. Schneider, and K. Schoenbach, "A steady-state fluid model for the coaxial plasma gun," *Phys. Lett.*, vol. 71A, p. 54, 1979
- [69] K. H. Schoenbach, M. Kristiansen, E. E. Kunhardt, L. L. Hatfield, and A. H. Guenther, "Exploratory concepts of opening switches," in *Proc. Army Research Office Workshop on Repetitive Opening Switches* (Tamaron, CO, 1981), DTIC AD-A110770, p. 66
- [70] K. Schoenbach, H. Krompholz, L. Michel, and G. Herziger, "Microinstabilities in the plasma focus," *Phys. Lett.*, vol. 62A,

- A. Bernard *et al.* presented at the 5th Int. Conf. on Plasma Physics and Controlled Nuclear Fusion Research, Bonn, Germany, FRG, 1976, paper IAEA-CN-35/E18-4.
- [73] E. Singer, "Problems of repetitive opening switches demonstrated on repetitive operation of a dense plasma focus," in *Proc. Army Research Office Workshop on Repetitive Opening Switches* (Tamarron, CO, 1981), DTIC AD-A110770, p. 64.
- [74] S. Suter, E. F. Davis, P. J. Turchi, G. Bird, C. Bover, D. Conte, R. Crawford, L. DeRaad, G. Fisher, A. Litter, W. Tsai, and T. Wilcox, "High current coaxial plasma gun discharges through structured foils," in *Proc. 4th IEEE Pulsed Power Conf.* (Albuquerque, NM, June 1983), pp. 346-349 (IEEE Catalog 83CH1147-3).
- [75] M. D. Muchalek, "Foreign travel trip report," Apr. 14-Aug. 4, 1977, USSR and Denmark, CTR Division, LASL.
- [76] K. Grawatsch *et al.*, "Investigations for the development of superconducting power switches," in *Proc. Applied Superconductivity Conf.* (Oakbrook, IL, Oct. 1-2, 1974).
- [77] H. L. Laquer *et al.*, in *Proc. 6th Intersoc. Energy Conversion Eng. Conf.* (Boston, MA, Aug. 3-5, 1971), p. 1089.
- [78] H. L. Laquer *et al.*, "Design options and trade-offs in superconducting magnetic energy storage with irreversible switching," LASL Rep. LA-5314-MS, June 1973.
- [79] J. D. G. Lindsay *et al.*, "Development of a superconducting switch for magnetic energy storage system," in *Proc. Applied Superconductivity Conf.* (Oakbrook, IL, Oct. 1-2, 1974).
- [80] A. Ulbricht *et al.*, "The study of high voltage problems in a superconducting power pulse generator," in *Proc. 6th Int. Cryogenic Engineering Conf.* (Grenoble, France, May, 1976), p. 50.
- [81] V. A. Glukhikh *et al.*, "Results of investigation of high specific breaking power superconducting switches," in *Proc. 7th Symp. on the Engineering Problems of Fusion Research* (Knoxville, TN, Oct. 25-28, 1977), p. 912. Also, in *Proc. 1th All-Union Conf. on Engineering Problems of Fusion Reactors* (Leningrad, USSR, July 28-30, 1977).
- [82] A. Ulbricht, Kernforschungszentrum Karlsruhe, FRG, personal communication to M. Kristiansen.
- [83] R. R. Hake, "Single-shot pulsed fields from inductive energy stores," LANL Rep. LA-4617-MS, Aug. 1970.
- [84] P. Komarek and A. Ulbricht, "Investigations of superconducting energy storage systems concerning fusion technology," Kernforschungszentrum Karlsruhe, FRG, Interner Bericht 75-81-MAG, Apr. 1975.
- [85] H. Laquer *et al.*, "Superconductive energy storage and switching experiments," in *Proc. XIII Int. Congr. on Refrigeration, vol. 1*, Washington, DC, 1971.
- [86] J. D. Lindsay and D. J. Blevins, "10 kA low resistance superconducting switch," in *Proc. 6th Symp. on Engineering Problems of Fusion Research* (San Diego, CA, Nov. 18-21, 1975), pp. 669-672 (IEEE Publ. 75CH1097-5-NPS).
- [87] D. J. Blevins and J. D. Lindsay, "Design and performance of two 10 kA superconducting switches" [LA-UR-75-865], presented at the 1975 IEEE Int. Conf. on Plasma Science, Ann Arbor, MI, May 14-16, 1975.
- [88] D. Y. Cheng, "Application of a variable resistance to arrest oscillations in a pulsed capacitor discharge circuit," *Rev. Sci. Instrum.*, vol. 40, pp. 1153-1157, 1969.
- [89] M. N. Bystrov, B. A. Larianov, V. P. Silin, F. M. Spevakova, and A. M. Stolov, "Pulsed power sources based on transformer inductive energy storage devices with non-linear elements," no. 2 in the series *Inductive Energy Storage Devices and Switching Apparatus for Thermonuclear Installation* (Report of a Joint USSR-USA Seminar, USSR Atomic Energy State Committee, Leningrad, NIIIEFA, 1974, translated by W. J. Grimes, P.O. Box 55, Hingham, MA, 02043, May 1975).
- [90] M. N. Bystrov, L. V. Dubovoy, Ye. A. Larianov, I. A. Monoszon, I. M. Rovfe, A. M. Stolov, Ye. V. Seredenko, V. P. Silin, B. A. Stokol'nikov, and L. A. Sarochin, "Thermal non-linear resistances in energy output systems for inductive storage devices," no. 5 in the series *Inductive Energy Storage Devices and Switching Apparatus for Thermonuclear Installation* (Report of a Joint USSR-USA Seminar, USSR Atomic Energy State Committee, Leningrad, NIIIEFA, 1974, translated by W. J. Grimes, P.O. Box 55, Hingham, MA, 02043, May 1975).
- [91] M. N. Bystrov, V. A. Krvlov, B. A. Larianov, V. P. Silin, and A. M. Stolov, "Impulse power source for feeding the 'pinch with liner' installation," Rep. II, Joint Soviet-American Seminar on Pulsed Fusion Reactors, September 23-27, 1975, ESRII, Leningrad, USSR.
- [92] A. S. Gilmour and J. D. Marshall, "Liquid nitrogen cooled wires as switchable high-power direct current limiting elements," in *Proc. 1st IEEE Int. Pulsed Power Conf.* (76CH1147-8 Reg 5), paper IC-3 (Lubbock, TX, Nov. 9-11, 1976).
- [93] A. Garscadden, "Arcs vs diffuse discharges," in *Proc. Army Research Office Workshop on Diffuse Discharge Opening Switches* (Tamarron, CO, 1982), DTIC AD-A115883, p. 91.
- [94] P. Bletzinger, "Electron beam switching experiments in the high current gain regime," in *Proc. 3rd IEEE Int. Pulsed Power Conf.* (Albuquerque, NM, 1981), p. 81 (IEEE Catalog 81CH1662-6).
- [95] R. O. Hunter, "Electron beam controlled switching," in *Proc. 1st IEEE Int. Pulsed Power Conf.* (Lubbock, TX, 1976), paper IC8 (IEEE Catalog 76CH1147-8 Reg 5).
- [96] K. H. Schoenbach, M. Kristiansen, E. E. Kunhardt, L. L. Hatfield, and A. H. Guenther, "Exploratory concepts of opening switches," in *Proc. Army Research Office Workshop on Repetitive Opening Switches* (Tamarron, CO, 1981), DTIC AD-A110770, p. 65.
- [97] K. H. Schoenbach, G. Schaefer, E. E. Kunhardt, M. Kristiansen, L. L. Hatfield, and A. H. Guenther, "An optically controlled diffuse discharge switch," in *Proc. 3rd IEEE Int. Pulsed Power Conf.* (Albuquerque, NM, 1981), p. 142 (IEEE Catalog 81CH1662-6).
- [98] K. H. Schoenbach, G. Schaefer, M. Kristiansen, L. L. Hatfield, and A. H. Guenther, "Diffuse discharge opening switches," in *Proc. NATO Advanced Study Institute on Electrical Breakdown and Discharges in Gases* (Les Arcs, France, 1981), E. E. Kunhardt and L. H. Luessen, Eds. New York: Plenum, 1983, p. 415.
- [99] B. M. Koval'chuk and G. A. Mesyats, "Current breaker with space discharge controlled by electron beam," in *Proc. 1st IEEE Int. Pulsed Power Conf.* (Lubbock, TX, 1976), paper IC7 (IEEE Catalog 76CH1147-8 Reg. 5).
- [100] P. Bletzinger, "E-beam experiments: Interpretations and extrapolations," in *Proc. Army Research Office Workshop on Diffuse Discharge Opening Switches* (Tamarron, CO, 1982), DTIC AD-A115883, p. 112.
- [101] V. E. Scherrer, R. J. Commisso, R. F. Fernsler, L. Miles, and E. M. Vitkovitsky, "The control of breakdown and recovery in gases by pulsed electron beams," in *Proc. 3rd Int. Symp. on Gaseous Dielectrics* (Knoxville, TN, 1982), p. 34.
- [102] H. Harjes, K. Schoenbach, G. Schaefer, H. Kromplolz, M. Kristiansen, G. Leiker, and L. L. Hatfield, "E-beam triode for multiple submicrosecond pulse operation," in *Proc. 4th IEEE Pulsed Power Conf.* (Albuquerque, NM, 1983) (IEEE Catalog 83CH1908-3).
- [103] K. H. Schoenbach, G. Schaefer, M. Kristiansen, L. L. Hatfield, and A. H. Guenther, "Optical control of diffuse discharge opening switches," in *Proc. Army Research Office Workshop on Diffuse Discharge Opening Switches* (Tamarron, CO, 1982), DTIC AD-A115883, p. 134.
- [104] ———, "Concepts for optical control of diffuse discharge opening switches," *IEEE Trans. Plasma Sci.*, vol. PS-10, p. 246, 1982.
- [105] G. Schaefer, P. F. Williams, K. H. Schoenbach, and J. Mosolev, "Photodetachment as a control mechanism for diffuse discharge switches," *IEEE Trans. Plasma Sci.*, vol. PS-11, pp. 263-265, 1983.
- [106] G. Schaefer, K. H. Schoenbach, H. Kromplolz, M. Kristiansen, and A. H. Guenther, "The use of attachers in electron beam sustained discharge switches—Theoretical considerations," accepted for publication in *Lasers and Particle Beams*.
- [107] W. L. Morgan and M. J. Pound, "Kinetics of e-beam excited

- XeCl⁺ in *Abstracts of 33rd Gaseous Electronics Conf* (Norman OK (1980) abstract FB-3)
- [107] M. Allan and S. F. Wong, "Dissociative attachment from vibrationally and rotationally excited HCl and HF," *J. Chem. Phys.*, vol. 74, p. 1587, 1981.
- [108] E. L. Christophorou, S. R. Hunter, J. G. Carter, and R. A. Mathis, "Cases for possible use in diffuse discharge switches," *Appl. Phys. Lett.*, vol. 41, p. 47, 1982.
- [109] G. Schaeter, K. H. Schoenbach, A. H. Guenther, and W. K. Pendleton, "Recent advances in optically controlled discharges," in *Proc. 4th IEEE Int. Pulsed Power Conf* (Albuquerque, NM, 1983) (IEEE Catalog #3CH1908-3).
- [110] C. W. Mendel, Jr. and S. A. Goldstein, "A fast opening switch for use in REB diode experiments," *J. Appl. Phys.*, vol. 48, p. 1004, 1977.
- [111] R. Stringfield, R. Schneider, R. D. Genuario, I. Roth, K. Childers, C. Stallings, and D. Dakin, "Plasma erosion switches with imploding plasma loads on a multiterawatt pulsed power generator," *J. Appl. Phys.*, vol. 52, p. 1278, 1981.
- [112] R. Stringfield, P. Sincerny, S. Wong, C. James, T. Peters, and C. Gilman, "Continuing studies of plasma erosion switches for power conditioning on multiterawatt pulsed power accelerators," *IEEE Trans. Plasma Sci.*, vol. PS-11, p. 200, 1983.
- [113] R. H. Meger, R. J. Comisso, G. Cooperstein, and S. A. Goldstein, "Vacuum inductive store/pulse compression experiments on a high power accelerator using plasma opening switches," NRL Memo Rep 5037, Mar. 1983.
- [114] J. M. Neri, R. J. Comisso, and R. A. Meger, "Plasma source development for plasma opening switches," *Bull. Amer. Phys. Soc.*, vol. 27, p. 1054, 1982.
- [115] R. K. Parker, R. E. Anderson, and C. V. Duncan, "Plasma-induced field emission and the characteristics of high-current relativistic electron flow," *J. Appl. Phys.*, vol. 45, p. 2463, 1974.
- [116] P. A. Miller, "Electron beam generation in plasma filled diodes," *Phys. Rev. Lett.*, vol. 35, p. 940, 1975.
- [117] J. M. Creedon, "Magnetic cutoff in high current diodes," *J. Appl. Phys.*, vol. 48, p. 1970, 1977.
- [118] B. Ecker, J. Creedon, L. Demeter, S. Glidden, and G. Proulx, "The reflex switch: A high-current, fast-opening vacuum switch," in *Proc. 4th IEEE Pulsed Power Conf* (Albuquerque, NM, June 1983), pp. 354-360 (IEEE Catalog #3CH1908-3).

INVESTIGATIONS OF E-BEAM CONTROLLED
DIFFUSE DISCHARGES*

K. Schoenbach, G. Schaefer, M. Kristiansen,
H. Krompholz, H. Harjes, and D. Skaggs

Department of Electrical Engineering
Texas Tech University
Lubbock, Texas 79409

ABSTRACT

Externally controlled diffuse discharges have attracted considerable interest as submicrosecond opening switches for inductive energy storage systems. Their performance is strongly determined by the basic fill gas parameters and their dependence on the reduced field strength E/N . An electron-beam controlled diffuse discharge system was constructed to study the behavior of pulsed discharges in various gas mixtures under repetitive operation. Experiments were performed with 1 atm N_2 and small additives of N_2O as fill gas in the switch. The experimental results are compared with numerical values, obtained from a code which allows modeling of the discharge voltage-current characteristics and its transient behavior in a discharge circuit.

*Work supported by AFOSR and ARO.

KEYWORDS

Opening switch; high pressure diffuse discharge; e-beam control; gas properties.

INTRODUCTION

Inductive energy storage is attractive in pulsed power applications because of its intrinsic high energy density. The key technological problem in developing inductive energy discharge systems, especially for repetitive operation (repetition rate $> 10^3/s$) is the opening switch [Kristiansen and Schoenbach 1981]. For repetitive, fast operation, when opening times of microseconds and less are required, high pressure diffuse discharges seem to be prime candidates for opening switches. Their moderate energy density offers the possibility of external control of the conductivity by means of e-beams and/or lasers [Schoenbach and others, 1982a,b].

The schematic diagram of an e-beam controlled opening switch as part of an inductive storage system is shown in Fig. 1. The switch chamber is filled with a gas at pressures of 1 atm and above. The gas between the electrodes conducts and allows charging of the inductor, when an ionizing e-beam is injected (usually through one of the electrodes which might be a mesh or a foil). The switch voltage remains below the self breakdown voltage, so that there is no

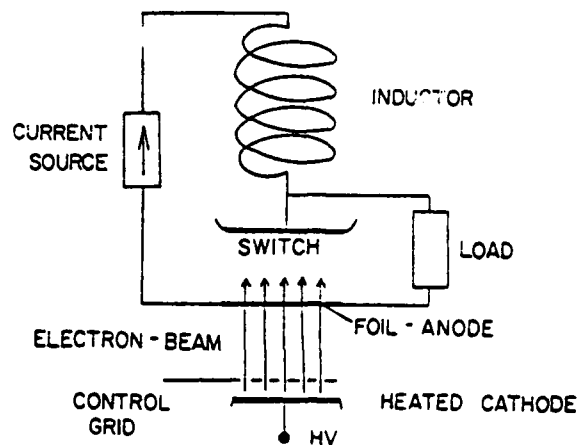


Fig. 1. Schematic of an e-beam controlled diffuse discharge switch in an inductive energy storage circuit.

avalanche ionization. Thus, the discharge is completely sustained by the e-beam. When the e-beam is turned off, electron attachment and recombination processes in the gas cause the conductivity to decrease and the switch opens. Consequently the current through the inductor is commutated into the load.

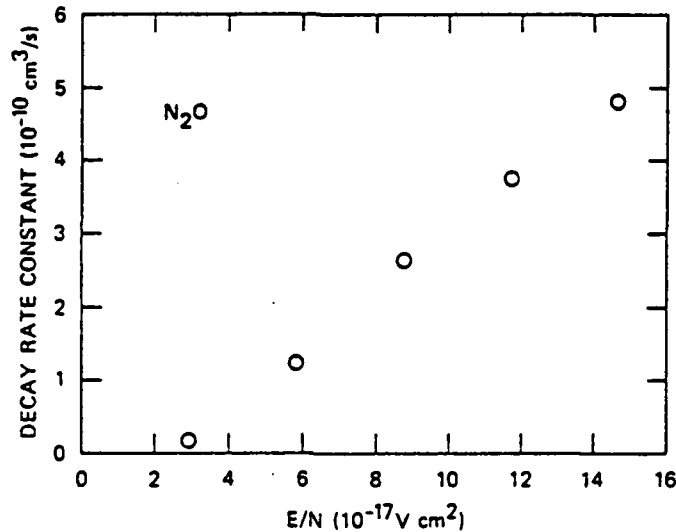
GAS PROPERTIES

The switch performance is strongly determined by the type of gas fill. In order to achieve fast opening of the switch attachers are to be used at a partial pressure which makes the switch attachment dominant during the opening phase. On the other hand additives of attachers increase the power losses during conduction. Both low forward voltage drop and fast opening can only be obtained by choosing gases or gas mixtures which satisfy the following conditions [Schoenbach and others, 1982a,b] [Christophorou and others, 1982] [Schaefer and others, 1984]:

- a) for low values of the reduced field strength E/N in the switch (conduction phase) the gas mixture should have a high drift velocity v_d and a low attachment rate coefficient k_A ,
- b) for high E/N values (opening phase) the gas mixture should have lower drift velocities and high attachment rate coefficients, and
- c) to avoid the onset of the attachment instability [Douglas-Hamilton and Mani, 1974] during conduction, the switch should be operated at E/N values where the attachment rate coefficient is a weak function of E/N or has a minimum .

Along these considerations, several gas mixtures have been proposed for the use in diffuse discharge opening switches [Christophorou and others, 1982]. For the theoretical and experimental investigations described in this paper, N_2 was chosen as a buffer gas with N_2O as added attacher. N_2 was used since a complete set of cross sections was available [Phelps, 1983], and the plasma chemistry in a mixture of N_2 and N_2O appears to be relatively simple. Furthermore N_2O in an N_2

buffer gas exhibits an E/N dependent electron decay rate, which increases by more than a factor of 20 in the E/N range from 3 Td to 15 Td [Lee and others, 1981] as shown in Fig. 2. It should be noted, however, that N₂ has an electron drift velocity which increases with E/N and therefore is not the optimum buffer gas in diffuse discharge switches.



JA-330533-58

Fig. 2. The decay rate constants of the electron conduction current by adding N₂O in 350 torr of N₂ at various E/N [Lee and others, 1981]

DISCHARGE ANALYSIS

To evaluate the time dependent impedance of an externally controlled discharge in a given circuit, as well as to optimize the properties of the gas mixture together with circuit parameters, a computer model has been developed that enables fast calculations for a variety of conditions. It does not, however, provide for spatial analysis of the discharge. The code uses two independent programs. In a first computation all rate constants of significant processes are calculated as a function of E/N for a representative gas mixture. These calculations use the E/N-dependent electron energy distribution functions that have been previously compiled using a separate Monte Carlo code. In a second step a system of circuit equations and rate equations using the E/N dependent rate constants are solved. It is assumed that the E/N dependence of the rate constants does not change significantly for small variations of the gas mixture. Additionally the electron energy relaxation is considered to be faster than any significant change in E/N, thus allowing time dependent solutions.

Steady State Characteristics of the Discharge

The calculation of the steady state characteristics of the diffuse discharge does not require information on the circuit. Calculations were performed with the relative attachment concentration in the buffer gas as parameter. Figure 3

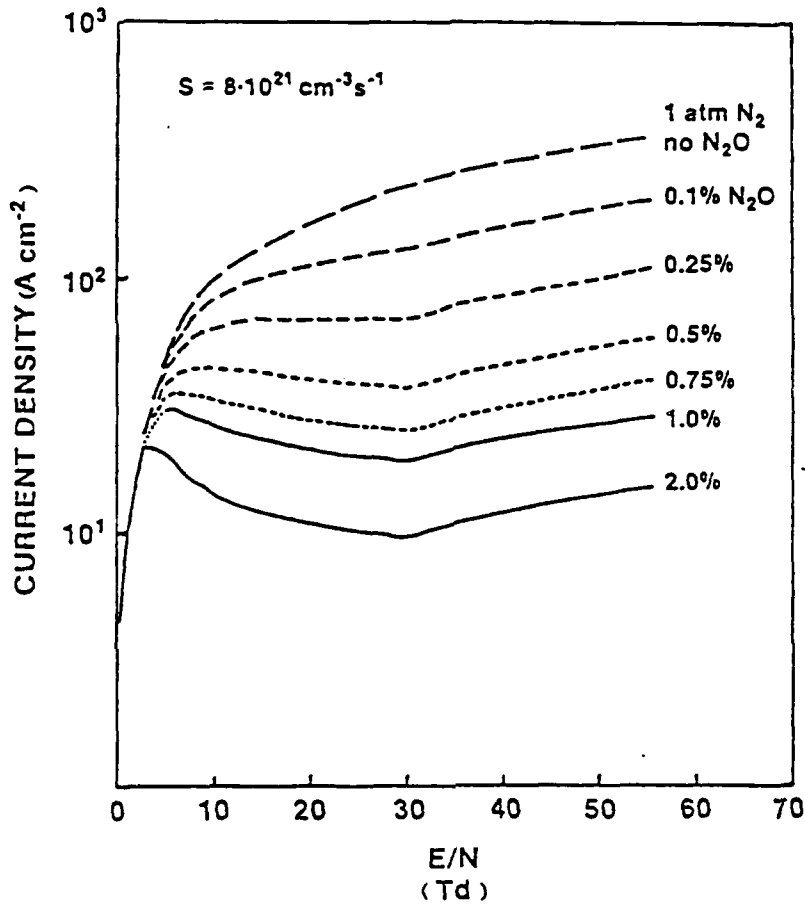


Fig. 3. Calculated steady state E/N - j characteristics for an e-beam sustained discharge in N_2 with admixtures of N_2O . The electron generation rate is $8 \times 10^{21} \text{ cm}^{-3} \text{ s}^{-1}$. Parameter is the N_2O fraction in %.

shows the steady state characteristics for different N_2O concentrations in a N_2 buffer gas. The total pressure is 1 atm and the e-beam electron generation rate is $8 \times 10^{21} \text{ cm}^{-3} \text{ s}^{-1}$. As expected, the steady state characteristics are not affected by the attachers in an E/N -range of 0 - 4 Td, while in the range of approximately 5 - 30 Td high attachers concentrations cause the current density to decrease if the field strength increases, a property which is desirable for opening switch operation. The threshold value of E/N at which the slope of the current density changes is determined by when attachment becomes the major loss mechanism. Thus the maximum of the current density shifts to higher E/N values when the attachers concentration decreases. It should be noted that attachers with a constant attachment rate coefficient result in steady state characteristics where the current density increases monotonically with E/N .

Transient Discharge Behaviour

As discussed before, it should be possible to operate an e-beam sustained, low loss discharge which is not strongly affected by an attachment, provided the attachment rate constant has a clear threshold at a certain value of E/N , below which the attachment is not efficient. How fast such a steady state operation is approached when the e-beam is turned on and how fast the discharge opens if the e-beam is turned off, will depend strongly on the circuit as well. For fast operation (timescale $\sim 10^{-6}$ s), the inductive energy storage system has to be considered as a transmission line with a high value of L' and a low value of C' , i.e., a line with high impedance.

An experimental set-up as shown in Fig. 4 was assumed for the calculation of the transient behavior of the discharge. Parameters were switch area $A = 100 \text{ cm}^2$, gap distance $d = 1 \text{ cm}$, pressure $p(\text{N}_2) = 1 \text{ atm}$, applied voltage $V_0 = 50 \text{ kV}$, electron generation rate $S = 8 \cdot 10^{21} \text{ cm}^{-3} \text{ s}^{-1}$ for the time $0 < t < 100 \text{ ns}$. The values of the pressure p , voltage V_0 , and discharge length d correspond to a maximum value of $E/N = 185 \text{ Td}$. In an initial set of calculations, the total system impedance was kept constant at $Z_t = 20 \Omega$, where $Z_t = Z + R_E$.

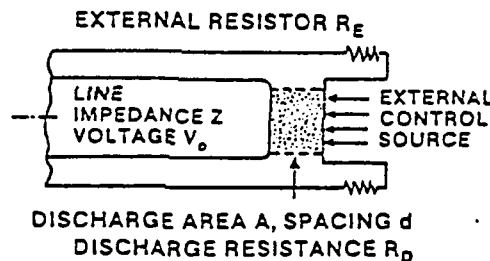


Fig. 4. Schematic setup for an e-beam sustained discharge switch.

Figure 5 shows the time dependent reduced field strength E/N , current density j , and power loss per volume in the discharge. The curves for 0.1%, 0.5%, and 0.75% of N_2O approach the same steady state value for E/N and j in the conducting phase, demonstrating that under these conditions the discharge is not strongly influenced by attachment. Furthermore, after termination of the e-beam, the discharge properties change very slowly until an E/N -value is approached where attachment becomes effective. By contrast, for the case of 1% N_2O , the attachment is strong enough to prevent the discharge from ever reaching a low E/N -state and the steady state is therefore always attachment dominated. Thus, when the e-beam is turned off, the values for E/N and j change quite abruptly.

Experimental Results

Diffuse discharge experiments were performed in N_2 at atmospheric pressure with a small amount of N_2O admixed. An e-beam tetrode which serves as ionization source for the switch gas provides a burst of electron pulses. The pulse duration and pulse separation can be varied from a hundred nanoseconds to one microsecond. The fall time of the single electron pulse is approximately 20 ns. By using a thermionic cathode which provides for an electron current density of up to 4 A/cm^2 over an area of 100 cm^2 it is possible to vary e-beam current and e-beam energy independent of each other [Harjes and others, 1983].

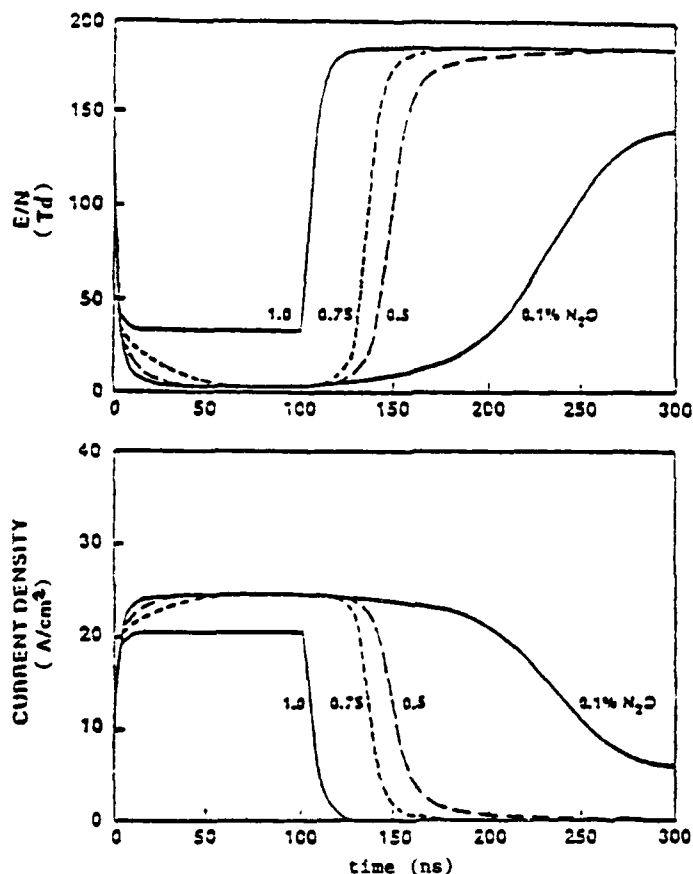


Fig. 5. Time dependence of E/N (top), and current density (bottom) in an e-beam sustained discharge in 1 atm N_2 with admixtures of N_2O . The e-beam is on for $0 \leq t \leq 100$ ns. Parameter is the N_2O fraction in %.

Figure 6 shows the normalized switch current for different concentrations of the attachor N_2O . The source term was $S = 5 \times 10^{20} \text{ cm}^{-3} \text{ s}^{-1}$, the applied voltage $V_0 = 10 \text{ kV}$ and $Z_c = 20 \Omega$. For high concentrations of N_2O (3%) the switch current pulse represents in shape the e-beam current pulse except for the tail. This tail may be caused by the current carried by positive and negative ions. The current gain (switch current/electron beam current) is about 2 for this high attachment concentration. For lower concentrations, (0.7%) the fall time ($1/e$ -time) increases to approximately 100 ns. For 0.1% it is in the order of 500 ns. The gain is increasing to values of 9 and 12 at 0.7% and 0.1% N_2O , respectively. A comparison of these pulse shapes with the calculated ones in Fig. 5 shows that there is no delay between the end of the e-beam pulse and the onset of the decay in current density. This indicates that attachment is dominant even at low E/N , where according to the measured values of the decay rate (see Fig. 2) attachment should be negligible.

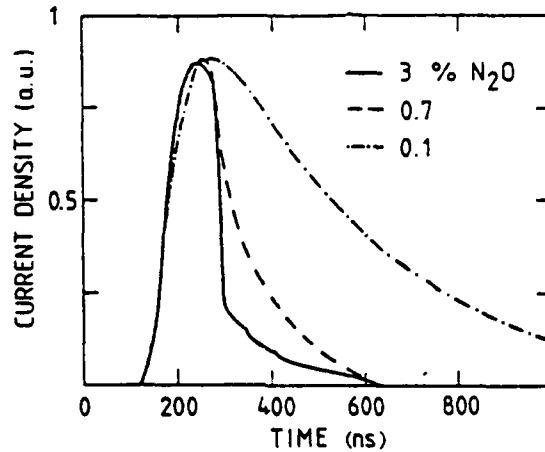


Fig. 6. Time dependence of switch current with N_2O concentration as variable parameter.

Measurements of the steady state current density - field strength characteristic of the e-beam sustained diffuse discharge with N_2 as buffer gas and 0.7% N_2O confirm this conclusion. Figure 7 shows the calculated j - E/N curve and measured values. The measured discharge characteristic does not show the predicted maximum at E/N values of approximately 4 Td. The saturation of the measured current at higher values of E/N however indicates that the attachment rate in the entire E/N range increases with increasing reduced field strength. To achieve the desired switch characteristics as discussed in the section "Gas Properties", attachments with attachment cross sections peaking at higher energies should be considered.

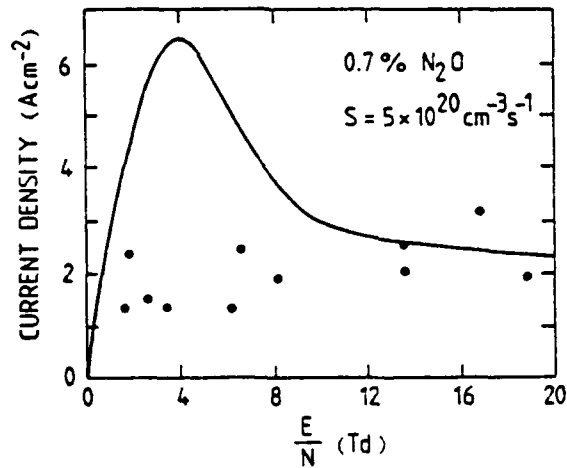


Fig. 7. Current density versus reduced field strength (Calculated curve and experimental data points).

REFERENCES

- Christophorou, L. G., S.R. Hunter, J.G. Carter, and R.A. Mathis (1982). "Gases for Possible Use in Diffuse-Discharge Switches", Appl. Phys. Lett. 41, 147.
- Douglas-Hamilton, D.H., and S.A. Mani (1974). "Attachment Instability in an Externally Ionized Discharge", J. Appl. Phys. 45, 4406.
- Harjes, H., K. Schoenbach, G. Schaefer, H. Krompholz, and M. Kristiansen (1983). "E-Beam Triode for Multiple Submicrosecond Pulse Operation", Proc. IV Pulsed Power Conf., Albuquerque, NM.
- Kristiansen, M., and K. Schoenbach (1981). "Workshop Summary", in Proceedings ARC Workshop on Repetitive Opening Switches, Tamarron, CO, 6.
- Lee, L.C., C.C. Chiang, K.Y. Tang, D.L. Huestis, and D.C. Lorents (1981). "Gaseous Electronic Kinetics for e-Beam Excitation of Cl₂, NO, and N₂O in N₂", Second Annual Report on AFOSR Sponsored Coordinated Research Program in Pulsed Power Physics, Department of Electrical Engineering, Texas Tech University, Lubbock, TX, 189.
- Phelps, A.V. (1983). JILA, Boulder, CO, private communication.
- Schaefer, G., K.H. Schoenbach, H. Krompholz, M. Kristiansen, and A.H. Guenther (1984). "The Use of Attachers in Electron Beam Sustained Discharge Switches - Theoretical Considerations", Lasers and Particle Beams. Submitted.
- Schoenbach, K.H., G. Schaefer, M. Kristiansen, L.L. Hatfield, and A.H. Guenther (1982a). "Optical Control of Diffuse Discharge Opening Switches", Proc. ARC Workshop on Diffuse Discharge Opening Switches, Tamarron, CO, 134.
- Schoenbach, K.H., G. Schaefer, M. Kristiansen, L.L. Hatfield, and A.H. Guenther (1982b). "Concepts for Optical Control of Diffuse Discharge Opening Switches", IEEE Trans. Plasma Science, PS-10, 246.

Use of attachers in electron beam sustained discharge switches

With this as a background, this paper presents calculations to analyze the specific properties of an e-beam controlled discharge switch if an attacher with the suggested properties is present in the dielectric gas. The consequences of attacher properties on the steady state characteristics and the transient behavior in a specific circuit will be discussed. Photodetachment will also be considered as an additional opening switch control mechanism (Schaefer *et al.* 1983).

2. Circuit implications in an inductive energy storage system

Fast, repetitive transfer of power from an inductive energy storage device to a load (e.g. a switch opening time of less than 100 ns) requires detailed consideration of the circuit elements (inductors, connectors) as transmission lines, i.e. effects due to finite transit times and reflections are not negligible. At high frequencies, the distributed capacitance, C' , of the energy storage device in concert with the high distributed inductance, L' , implies a high characteristic impedance $(L'/C')^{1/2}$ of the order of several $k\Omega$ and transit times, $(LC)^{1/2}$, of several 100 ns for a typical system (Kristiansen 1981). Matching of this impedance to the opening switch in parallel with the load is generally not possible, since for most applications the impedance of the load will be quite small compared to the generator impedance. Hence, power transfer from the generator to a low impedance load will be limited due to this mismatch in impedances.

By comparison with a lumped parameter description of the circuit, the reflections arising in the transmission line introduce an additional modulation of the power transfer with a time constant of twice the transit time of the inductive energy storage device, influencing both the load and switch behavior. Additionally, inductive storage devices can be considered as helical slow wave structures at high frequencies. The dispersion inherent in slow wave structures (Watkins 1958) presents further limitations on the efficiency of power transfer to the load for frequencies above 1 MHz.

A detailed consideration of transmission line effects in fast repetitive power transfer from inductive energy storage devices will be published in a separate paper (Krompholz *et al.* 1984). For this paper, the crucial aspect is that for short switching times an inductive energy storage system has to be treated as a line with a relatively high impedance.

3. Discharge analysis

To evaluate the time dependent impedance of an externally controlled discharge in a given circuit, as well as to optimize the properties of the gas mixture together with circuit parameters, a computer model has been developed that enables fast calculations for a variety of conditions. The code does not, however, provide for spatial analysis, but it does allow one to evaluate the influence of general gas properties and of the circuit on the discharge, although not affording information about the sheaths and discharge instabilities.

The code uses two independent programs. In a first computation all rate constants of significant processes are calculated as a function of E/N for a representative gas mixture. These calculations use the E/N -dependent electron energy distribution functions that have been compiled previously using a separate Monte Carlo code. In a second step a system of circuit equations and rate equations using the E/N dependent rate constants are solved. It is assumed that the E/N dependence of the rate constants does not change significantly for small variations of the gas mixture. Additionally the electron energy relaxation is considered to be faster than any significant change in E/N , thus allowing time dependent solutions.

G. Schaefer *et al.*

Recently several papers (Fernsler *et al.* 1980; Commisso *et al.* 1982; Commisso *et al.* 1983; Bletzinger 1981; Hallada *et al.* 1982; Bletzinger 1983; Kline 1982; Dzimianski & Kline 1980; Lowry *et al.* 1983; Schoenbach *et al.* 1982; Harjes *et al.* 1983; Schaefer *et al.* 1983) have appeared concerning e-beam controlled discharges. They specifically relate to switching applications, emphasizing different aspects of modes of operation, such as the influence of the gas mixture (Fernsler *et al.* 1980; Commisso *et al.* 1982), the cathode sheath (Hallada *et al.* 1982; Bletzinger 1983), the low e-beam current density and high current gain regime (Kline 1982; Dzimianski & Kline 1980; Lowry *et al.* 1983), as well as related optical control mechanisms (Schoenbach *et al.* 1982; Schaefer *et al.* 1983).

The use of admixtures of attachers can be employed to achieve fast opening of the switch but attachment will also increase the losses (Fernsler *et al.* 1980; Commisso *et al.* 1982; Bletzinger 1981). It has been proposed that these switch losses can still be kept low, if the gas mixture has the following properties, allowing both low forward voltage drop and fast opening (Kristiansen & Schoenbach 1981; 1982):

- a) at low values of E/N , i.e. during the conduction phase, the gas mixture should have a high drift velocity and a low attachment rate.
- b) at high values of E/N , i.e. during the opening phase, the gas mixture should have a low drift velocity and a high attachment rate.

Since attachers with a rate constant, k_{attach} , which increases with increasing E/N in a given E/N range are known to cause attachment instabilities if the discharge is operated in that E/N range (Douglas-Hamilton & Mani 1974; Long 1979), a third property is also desirable:

- c) the attachment rate should have a minimum at, or above the value of E/N at which the discharge is operated in the conduction phase, or the attacher should have an onset threshold above this value of E/N , below which attachment is not effective.

With these considerations, several gas mixtures have been proposed for the use in diffuse discharge opening switches (Christophorou *et al.* 1982). It seems that these gas properties will allow a low-loss, stable, steady state operation at low values of E/N and a sufficiently high hold off voltage, to assure the attainment of a zero current density if an external controlling e-beam is turned off. Any complete switching cycle, opening and closing, will, however, go through a lossy state and only the analysis of the time dependent behavior, including the losses during the switch transition period will allow one to determine the feasibility of this concept (Schaefer *et al.* 1983) and the optimum operating conditions.

There are two principal reasons to strive for a high dj/dt in the opening switch transition. (1) the efficient power extraction from the inductive energy storage system and (2) low energy loss in the switch (the later reason also applies to the closing transition).

The main concern in achieving fast transitions in the discharge is the electron balance and hence the desirable properties of the attacher as described above in the gas properties a) and b), and the E/N dependence of the electron drift velocity. This paper concentrates on the consequences of the aforementioned attachment properties.

The current density range will also affect the properties of the discharge to some degree. It was shown (Kovalchuk *et al.* 1976a; Hallada *et al.* 1982; Kline 1982), that high current gains can only be achieved if the current density is kept low. On the other hand, device requirements may force one to operate at a high current density, if extremely high total currents are required.

The use of attachers in electron-beam sustained discharge switches—theoretical considerations

**By G. SCHAEFER, K. H. SCHOENBACH,
H. KROMPHOLZ, M. KRISTIENSEN**

Texas Tech University, Lubbock, TX 79409

AND

A. H. GUENTHER

AFWL, Kirtland AFB, Albuquerque, NM 87117

(Received 4 January 1984)

Electron-beam sustained discharges can be used in opening and closing switch applications for producing bursts of energy in pulsed power systems. The incorporation of admixtures of attachers with low attachment rate at low values of E/N and high attachment rate at high values of E/N in the gaseous switch dielectric has been proposed to achieve low forward voltage drop in the conduction phase as well as rapid opening when the sustaining e-beam is terminated. This paper presents model calculations on the characteristics and transient behavior of an electron-beam sustained discharge in the high current density regime in N_2 . The influence of an attacher (N_2O), with the property described above, and of the circuit parameters on the discharge is investigated as an illustrative example. The advantage of using such an attacher is demonstrated for the steady state conduction phases and for the opening phase, while the closing process is obstructed by the attacher. Additional possible control mechanisms, such as photodetachment to aid the closing process are discussed.

1. Introduction

Inductive energy storage is attractive in pulsed power applications because of its intrinsic high energy density. The effective use of inductive storage, however, requires a rapid opening switch. Externally controlled diffuse discharges seem to offer the opportunity for fast as well as repetitive opening switching (Kristiansen & Schoenbach 1981; 1982). Diffuse discharges are advantageous for switching because of their low inductance (Kovalchuk *et al.* 1970), small electrode erosion and heating rates and moderate energy density which offer the possibility of external control of the opening and closing processes by means of e-beams and/or lasers of reasonable powers.

The general feasibility of this concept has been demonstrated in earlier papers (Kovalchuk *et al.* 1970; 1976a; 1976b; Hunter 1976), and can be anticipated from numerous papers related to laser discharges. The practical knowledge of diffuse discharges has been greatly improved through the development of gas discharge lasers. However, the operating conditions, which the discharge must fulfill, are different for switching applications. Other discharge properties and mechanisms of importance in the discharge have to be considered and their collective influence on the coupling between discharge and circuit must be optimized in a different way.

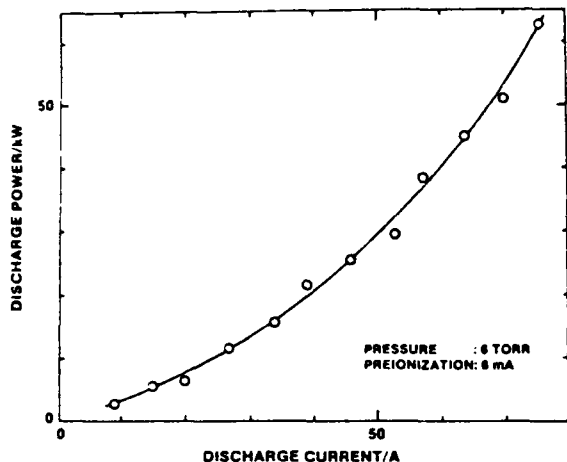


Fig. 10. Discharge power versus discharge current for the pulsed hollow cathode discharge.

for applications in large area diffuse discharges, was not investigated in detail.

2) At charging voltages above 13 kV, frequent arcing occurred across the gap between the electrodes. In this case the oscilloscope traces showed an initial reflection just as for the HCD (see Fig. 3) and then a transition to an unmeasurable small impedance (arcing). Arcing never occurred after the hollow cathode discharge was initiated. At charging voltages of approximately 10 kV, arcing never occurred, even if no preionization was used, resulting in a total reflection of the pulse (open end). Considering a maximum allowed charging voltage for operation without arcing, the maximum current is only limited by the line impedance Z_0 . For a 10- Ω line which, according to our impedance measurements, would be matched to the given HCD in the high-current regime and, for a charging voltage of 10 kV, one would expect arc-free operation at currents of up to 500 A.

Further information on the initiation mechanism of a fast-pulsed HCD can be obtained by recording the time-dependent spatial emission of radiation from the HCD. The existing device

will allow side-on and end-on observations (see Fig. 1). A streak camera analysis is planned.

IV. SUMMARY

In conclusion, we report the successful operation of a pulsed high-power density hollow cathode discharge. The delay time between applied voltage and initiation of the discharge strongly depends on a preionization source (dc discharge). Delay times of 3 ns and discharge risetimes of 2 ns were obtained at a jitter of 1 ns or less. The short initiation time combined with low jitter will allow synchronized operation of parallel hollow cathode discharges. In the given device, the maximum power density was in the range of 200 kW \cdot cm⁻³. With an impedance matched line (approximately 10 Ω for the given HCD), power densities up to 10³ kW \cdot cm⁻³ should be expected. These features indicate that such a device may be useful for the fast production of high energy levels with short decay times as required in discharges for pulsed UV gas lasers. The feasibility of using multiple hollow cathodes for the production of diffuse discharges will depend on the scaling behavior when smaller diameter hollow cathodes are used.

REFERENCES

- [1] D. H. Douglas-Hamilton and S. A. Mani, "Attachment instability in an externally ionized discharge," *J. Appl. Phys.*, vol. 45, pp. 4406-4415, Oct. 1974.
- [2] R. A. Haas, "Stability of excimer laser discharges," in *Applied Atomic Collision Physics*, vol. 3, *Gas Lasers*. New York: Academic, 1982, pp. 423-452.
- [3] W. H. Long, Jr., "Discharge stability in e-beam-sustained rare-gas halide lasers," *J. Appl. Phys.*, vol. 50, pp. 168-172, Jan. 1979.
- [4] J. W. Gewartowski and H. A. Watson, *Principles of Electron Tubes*. Princeton, NJ: Van Nostrand, 1965, p. 56.
- [5] L. Csillag, M. Janossy, K. Rozsa, and T. Salamon, "Near infrared CW laser oscillation in CuII," *Phys. Lett. A*, vol. 50, pp. 13-14, 1974.
- [6] R. W. Falcone and K. D. Pedrotti, "Pulsed hollow-cathode discharge for extreme-ultraviolet lasers and radiation sources," *Opt. Lett.*, vol. 7, pp. 74-76, Feb. 1982.
- [7] H. J. Eichler, H. J. Koch, J. Salk, and G. Schaefer, "Performance of CuII lasers with cylindrical hollow cathodes," *IEEE J. Quantum Electron.*, vol. QE-15, pp. 908-912, Sept. 1979.

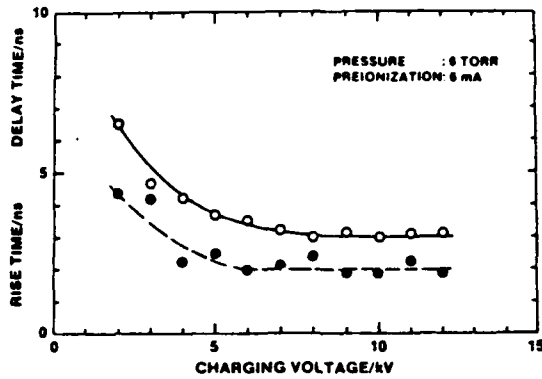


Fig. 6. Delay time (o) and risetime (●) for the initiation of the pulsed hollow cathode discharge in helium versus charging voltage.

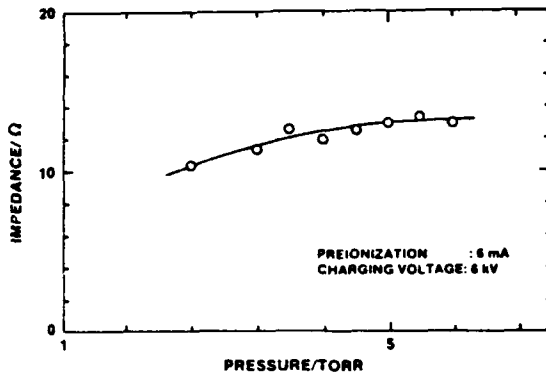


Fig. 7. Impedance of the pulsed hollow cathode discharge versus He-pressure.

lay time for a pressure of 6 torr and a preionization current of 6 mA. At low charging voltages the delay time strongly decreases with increasing charging voltage but approaches a constant value of approximately 3 ns. From Figs. 4-6 it can be concluded that the minimum delay time which can be obtained with this device is approximately 3 ns.

Figs. 4-6 also show the dependance of the risetime on the same operation parameters. The general behavior of the risetime is similar to that of the delay time although much less pronounced. The minimum risetime was $T_R = 2$ ns. This makes the total initiation time for the pulsed HCD (delay time plus risetime) $T_D + T_R = 5$ ns nearly independent of the operation parameters, if the pulsed HCD is operated in the following range:

$$\left. \begin{array}{l} T_D \text{ 3-ns delay} \\ \text{and} \\ T_R \text{ 2-ns risetime} \end{array} \right\} \text{ if } \left\{ \begin{array}{l} I_{PI} \geq 6 \text{ mA (preionization current)} \\ p \geq 5 \text{ torr (He pressure)} \\ V_c \geq 6 \text{ kV (charging voltage)} \end{array} \right.$$

In this operation range the jitter of the total initiation time was in the order of 1 ns. It should be noted that the uncertainty of the time measurement is in the order of ± 0.5 ns.

For the evaluation of the impedance of the discharge only the flat part of the measured voltage pulse was used (see Fig. 3). The voltage peak directly after the initiation of the pulsed HCD is due to the capacitance between cathode and anode and, therefore, not taken into consideration. Once the discharge is initiated, its impedance does not depend on the preionization current. The influence of the pressure on the pulsed HCD (Fig. 7)

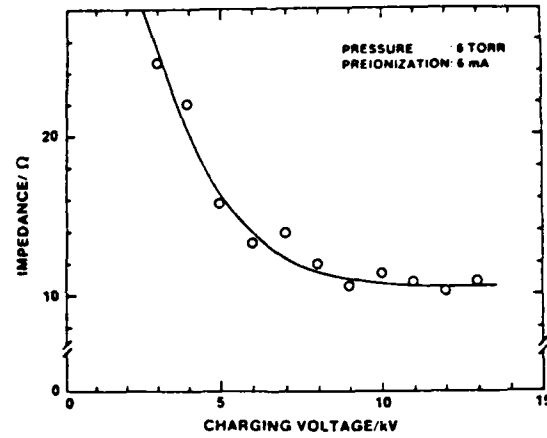


Fig. 8. Impedance of the pulsed hollow cathode discharge in helium versus charging voltage.

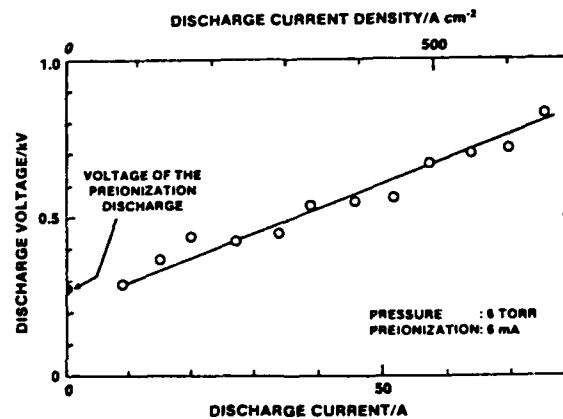


Fig. 9. Discharge voltage versus discharge current and current density, respectively, for the pulsed hollow cathode discharge.

seems not to be significant, while there is a strong dependance of the impedance on the charging voltage for values below 5 kV. For large values (8 kV and above) the impedance tends to approach a nearly constant value. The dependance of the impedance on the operation parameters is of special importance in designing matched systems for high efficiency.

The data used in Fig. 8 also allow the evaluation of the discharge characteristic (Fig. 9) and the power dissipated in the discharge (Fig. 10). The characteristic presented in Fig. 9 indicates a nearly constant dynamic impedance with voltages in the range of 300-800 V and with currents in the range of 10-65 A. This results in a maximum current density at the entrance of the hollow cathode of $560 \text{ A} \cdot \text{cm}^{-2}$. The maximum power dissipated in the discharge was 52 kW. From the side-on observation of the light emitted from the discharge it can be concluded that the penetration depth of the pulsed discharge into the cathode is approximately 20 mm. Thus with the inner cathode radius of 3.86 mm, the maximum power density becomes approximately $220 \text{ kW} \cdot \text{cm}^{-3}$.

The limitations of the current regime in the experiments presented are determined by two properties of the experimental setup limiting the charging voltage.

1) The spark gap design did not allow triggering below 2 kV; therefore the characteristic of the discharge in the low current density range of $10\text{-}100 \text{ A} \cdot \text{cm}^{-2}$, which may be of interest

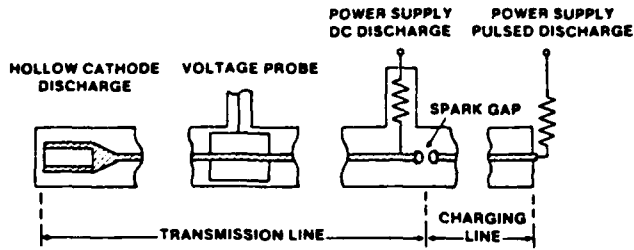


Fig. 2. Experimental setup.

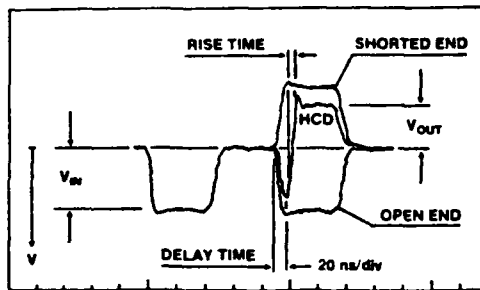


Fig. 3. Three typical oscillograms measured with the voltage probe, for an open end, for a shorted end, and for a hollow cathode discharge.

line is terminated by the HCD. An additional power supply in series with a large resistor is connected to the transmission line and allows the HCD to operate at a low dc level providing for preionization of the pulsed discharge. A capacitive voltage divider is located in the center of the transmission line. Since the length of the transmission cable l_t is more than twice the length of the charging cable ($l_t < 2 \cdot l_c$), the voltage probe will record the incoming pulse and the reflected pulse from the HCD without overlapping. This setup allows measurement of the time dependence of voltage, current, and impedance.

Typical oscillograms of the voltage measured with the voltage probe are shown in Fig. 3. For clarification of the evaluation method three voltage traces are superimposed: one for a typical hollow cathode discharge, one for an open end (infinite impedance) and one for a shorted end (zero impedance). The system with the hollow cathode acts for a time as an high-impedance system. Then the impedance drops to some value which is considered to be the impedance of the pulsed hollow cathode discharge Z_{HCD} :

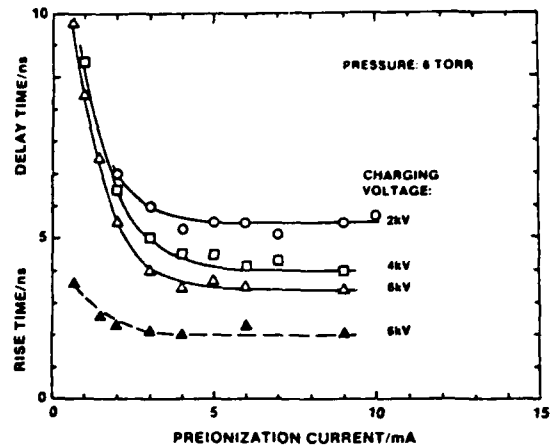
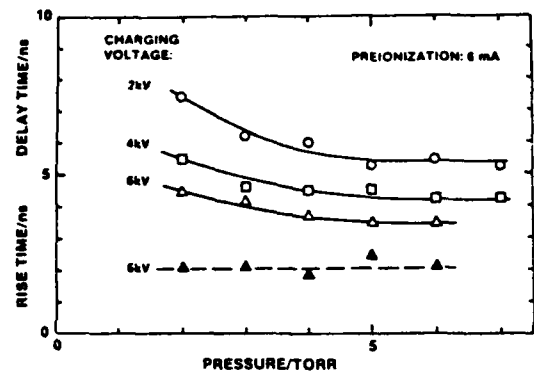
$$Z_{HCD} = Z_0 \frac{1 + V_{out}/V_{in}}{1 - V_{out}/V_{in}}$$

The time interval between the voltage increase of the reflected pulse and the onset of the decay of the reflected voltage is considered the *delay time* for the initiation of the pulsed hollow cathode discharge. The time interval in which the reflected voltage changes from its maximum to its minimum (90 percent-10 percent) is considered the *risetime* of the hollow cathode discharge (see Fig. 3).

III. RESULTS

The operation parameters of the pulsed hollow cathode system were varied in the following ranges allowing for stable arc-free operation:

gas: He with pressures: $1 \text{ torr} < p < 6 \text{ torr}$

Fig. 4. Delay time (\circ , \square , \triangle) and risetime (\blacktriangle) for the initiation of the pulsed hollow cathode discharge in helium versus dc-preionization current with the charging voltage as variable parameter.Fig. 5. Delay time (\circ , \square , \triangle) and risetime (\blacktriangle) for the initiation of the pulsed hollow cathode discharge versus He-pressure with the charging voltage as variable parameter.

charging voltage: $2 \text{ kV} \leq V_0 \leq 13 \text{ kV}$
preionization current: $0 \text{ mA} \leq I_{PI} \leq 10 \text{ mA}$.

With the stainless steel anode, operation at pressures above approximately 8 torr and charging voltages above approximately 13 kV caused small arcs to bridge the gap between cathode and anode, but without damaging the system. With the aluminum anode the stable operation regime was further reduced. In addition, arcing caused permanent damage requiring repolishing of the electrodes.

The first important result was that without preionization the system acted like an open end, indicating that the delay time was at least longer than the pulse length of 50 ns. The dependence of the delay time on the preionization current with the charging voltage as a variable parameter is plotted in Fig. 4. The pressure is constant at 6 torr. At low preionization currents (below 3 mA) the delay time strongly decreases with increasing preionization current but approaches a nearly constant value above approximately 6 mA. The dependence of the delay time on the pressure with the charging voltage as the variable parameter at a preionization current of 6 mA is plotted in Fig. 5, indicating that the pressure does not significantly effect the delay time, especially for the higher values of the charging voltage. At pressures ≥ 5 torr the delay time seems to be constant. Fig. 6 shows the charging voltage dependence of the de-

Pulsed Hollow Cathode Discharge with Nanosecond Risetime

GERHARD SCHAEFER, SENIOR MEMBER, IEEE, PER O. HUSOY, KARL H. SCHOENBACH, SENIOR MEMBER, IEEE,
AND HERMANN KROMPHOLE, SENIOR MEMBER, IEEE

Abstract—This paper reports the operation of a cylindrical hollow cathode discharge with current risetimes of a few nanoseconds at current densities at the entrance of the cathode in the range of $50\text{--}560\text{ A}\cdot\text{cm}^{-2}$ and at voltages of 280–850 V. Time-dependent measurements of the impedance of the discharge are presented. They allow for the evaluation of discharge quantities such as risetime, delay time, discharge voltage, and current, depending on the operation parameters as applied voltage, pressure, and preionization. The power density in the active region of the hollow cathode exceeded $200\text{ kW}\cdot\text{cm}^{-3}$.

I. INTRODUCTION

THE ENERGY LOADING of discharges for TEA lasers and Diffuse Discharge Switches is mainly limited due to instabilities caused by the use of admixtures of attachers [1]–[3]. In most cases, streamer development and subsequent arcing starts at the electrodes, preferably at the cathode [1]. Reduction of the electric field intensity in the cathode region could delay or even prevent the onset of instabilities. Hollow cathode discharges (HCD) are known to operate at lower potential differences than plane electrodes [4]. Therefore TEA laser electrodes with a large number of small holes may allow operation of discharges with a lower cathode fall voltage. Hollow cathode discharge operation, however, is restricted to a certain range of pD ($1\text{ torr cm} < pD < 10\text{ torr cm}$, for rare gases), where p is the gas pressure and D the diameter of the hollow cathode [4]. This range is shifted to smaller values of pD if molecular gases are used. For atmospheric pressure the holes should have diameters of the order of a few microns depending on the filling gas. In addition, such an electrode structure may allow one to flush the hollow cathodes from the back side with a very slight flow of an atomic gas (preferably a rare gas) and, subsequently further reduce the potential difference across the cathode fall.

At this time an important application of dc hollow cathode discharges is its use as the active medium of a gas laser [5]. In a recent paper it was also demonstrated that pulsed hollow cathode discharges allow one to produce high densities of excited states with energies of several tens of electronvolts above the ground state [6]. The efficient use of the excitation of

Manuscript received April 18, 1984. This work was supported by the Center for Energy Research, Texas Tech University, Lubbock, TX, and by AFOSR.

G. Schaefer, K. H. Schoenbach, and H. Kromphole are with the Department of Electrical Engineering, Texas Tech University, Lubbock, TX 79409.

P. O. Husoy was with the Department of Electrical Engineering, Texas Tech University, Lubbock, TX 79409. He is now with the Technical University of Norway, Trondheim, Norway.

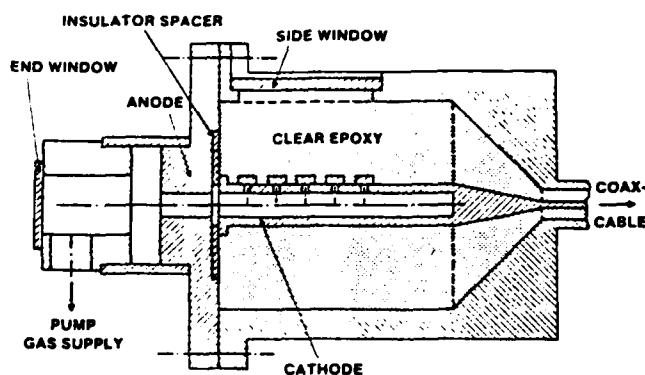


Fig. 1. Design of hollow cathode.

high-lying levels to produce a population inversion for a laser is, in general, supported by a fast risetime of the excitation process.

The feasibility of these HCD applications strongly depends on the risetime that can be achieved with hollow cathode discharges. It is known that in the steady-state operation the hollow cathode makes more efficient use of the UV light emitted from the negative glow and collisions of ions and excited particles (in rare gases preferably metastables) with the cathode surface. The build-up mechanism of the HCD and the dynamic of the densities of these species in the hollow cathode, however, has not yet been investigated. The aim of this work, therefore, was to investigate the initiation characteristics of the hollow cathode discharge and to operate a hollow cathode with fast risetime and at high current densities.

II. EXPERIMENTAL PROCEDURE

The design of the hollow cathode discharge device is shown in Fig. 1. Similar designs have been used for dc discharges [7]. The cathode is a 3.86-mm inner diameter stainless steel tube. Anodes were made of aluminum and stainless steel. The spacer between cathode and anode is a $10\text{-}\mu\text{m}$ thick mylar foil. End-on and side-on windows allow optical diagnostics of the hollow cathode discharge. Except for the discharge itself the HCD device is totally matched to the impedance of the cable $Z_0 = 75\ \Omega$ (Belden 8870). The dielectric in the cathode regime is a clear epoxy.

The experimental setup is shown in Fig. 2. A charging cable with the length l_c is charged by a power supply and discharged by a spark gap into a transmission cable. The voltage is adjusted through pressure controlled self breakdown. The transmission

ns, the current gain was in the order of 10. With better utilization of the e-beam energy in our system a gain of 100, can be achieved. Shorter opening times, down to ~ 10 ns, are possible with higher attach concentrations, however, at the expense of reduced current gain.

References

- [1] K. H. Schoenbach, G. Schaefer, M. Kristiansen, L. L. Hatfield, and A. H. Guenther, "Concepts for Optical Control of Diffuse Discharge Opening Switches", IEEE Trans. Plasma Science, PS-10, 246 (1982).
- [2] C. H. Harjes, K. H. Schoenbach, G. Schaefer, M. Kristiansen, H. Krompholz, and D. Skaggs, "An Electron Beam Tetrode for Multiple, Submicrosecond Pulse Operation", to appear in Rev. Sci. Instrum.
- [3] H. Krompholz, J. Doggett, K. H. Schoenbach, J. Gahl, C. Harjes, G. Schaefer, and M. Kristiansen, "Nanosecond Current Probe for High-Voltage Experiments", Rev. Sci. Instrum. 55, 127 (1984).
- [4] L. L. Christophourou, S. R. Hunter, J. A. Carter, and R. A. Mathis, "Cases for Possible Use in Diffuse Discharge Switches", Appl. Phys. Lett. 41, 147 (1982).
- [5] G. Schaefer, K. H. Schoenbach, H. Krompholz, M. Kristiansen, and A. H. Guenther, "The Use of Attachers in Electron Beam Sustained Discharge Switches - Theoretical Considerations", to appear in Lasers and Particle Beams.
- [6] A. V. Phelps, private communication.
- [7] L. C. Lee, C. C. Chiang, K.Y. Tang, D. L. Huestis, and D. C. Lorents, "Gaseous Electronic Kinetics for E-Beam Excitation of Cl₂, NO and N₂O in N₂", Second Annual Report on Coord. Res. Progr. in Pulsed Power Physics, Department of Electrical Engineering, Texas Tech University, Lubbock, TX (1981).
- [8] L.C. Lee and F. Ki, "Shortening of Electron Conduction Pulses by Electron Attachers O₂, N₂O and CF₄", to be published.
- [9] G. Schaefer, K. H. Schoenbach, and J.-S. Wang, to be published.
- [10] P. J. Chantry, "Temperature Dependence of Dissociative Attachment in N₂O", J. Chem. Phys., 51, 3369 (1969).
- [11] J. W. Gallagher, E. C. Beaty, J. Dutton, and L. C. Pitchford, "A Compilation of Electron Swarm Data in Electro-Negative Gases," JILA Information Center Report No. 22, University of Colorado, Boulder, CO. (1982).

$p = 200 \text{ Torr}, 20\% \text{ CO}_2 \text{ } 80\% \text{ N}_2$

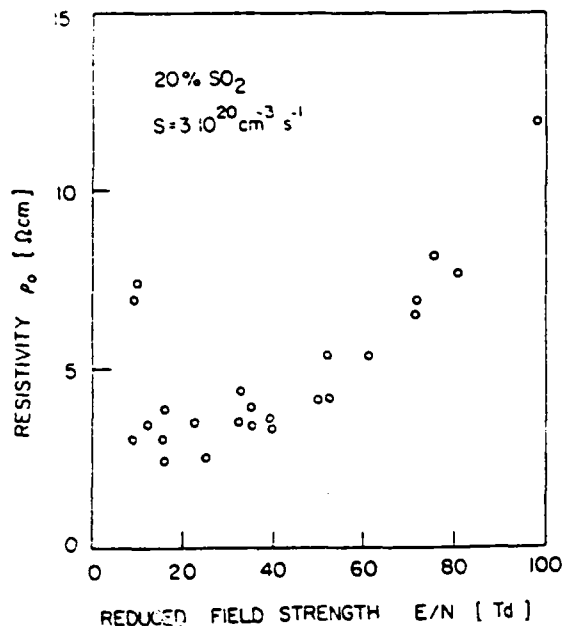


Fig. 11 Discharge Resistivity ρ_0 as a Function of Reduced Field Strength E/N for a Discharge in $\text{N}_2:\text{SO}_2$ (250 Torr).

$\text{N}_2:\text{CO}_2$

Like N_2O and SO_2 , CO_2 has an increasing attachment rate coefficient with E/N . The disadvantage of CO_2 for use as an opening switch gas is its relatively low ionization energy. The field strength range where the attachment coefficient, η , exceeds the ionization coefficient, α , reaches only up to approximately 60 Td [11]. This value determines the hold off field strength in this gas. For $E/N > 60$ Td the current rises again, which means that the switch closes instead of opens after e-beam turn off.

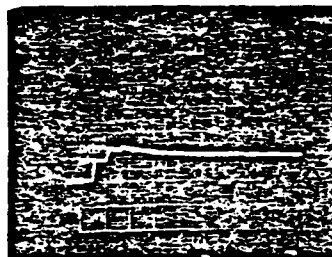
This effect was demonstrated by operating the diffuse discharge at different values of E/N about the crossing point of the attachment and ionization curves (Fig. 12). Depending on the values of $\eta(E/N)$ and $\alpha(E/N)$, the development of the discharge after e-beam turn off is going either towards a closing switch (Fig. 12c) or toward an opening switch (Fig. 12a) behavior. Because of the small attachment coefficient of CO_2 compared to SO_2 and N_2O the switch opening time, even for the high concentration of 20% in N_2 as buffer gas, is much longer than for the other gases.

SWITCH CURRENT VS TIME

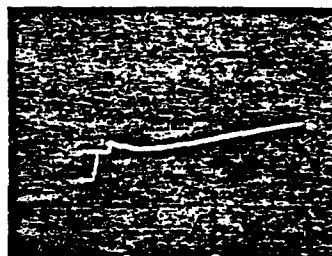
E/N RANGE



32 - 39 Td



54 - 58 Td



75 - 78 Td

5 μs

Fig. 12 Time Dependence of Switch Current in a Discharge in $\text{N}_2:\text{CO}_2$ with Reduced Field Strength E/N as a Variable Parameter.

Summary

An e-beam tetrode was designed for the investigations of e-beam controlled conductivities in switch gases. The operating characteristics are:

- burst mode operation in the Mpps (Mega pulses/per second) range,
- variable pulse duration and pulse separation,
- turn on and turn off times in the range of 10 ns,
- variation of e-beam energy ($E_B \leq 250 \text{ keV}$),
- variation of e-beam current density ($J_B \leq 4 \text{ A/cm}^2$).

Diffuse discharge investigations were performed in the gas mixtures $\text{N}_2:\text{N}_2\text{O}$, $\text{N}_2:\text{SO}_2$, and $\text{N}_2:\text{CO}_2$. The experimentally obtained current-voltage characteristic for $\text{N}_2:\text{N}_2\text{O}$ agrees with previously obtained theoretical results at high E/N . The discrepancy in theoretical and experimental data at low E/N reflects the uncertainty in basic data for N_2O . With respect to the criterion for optimum switch gases - low losses during conduction (at low E/N), large losses during and after opening (at high E/N) - N_2O in N_2 is superior to the other investigated gases. For opening times of 100

0.7%, the fall time ($1/e$ -time) increases to approximately 100 ns. For 0.1% it is in the order of 500 ns. The gain increases to values of 9 and 12 for 0.7% and 0.1% N_2O , respectively.

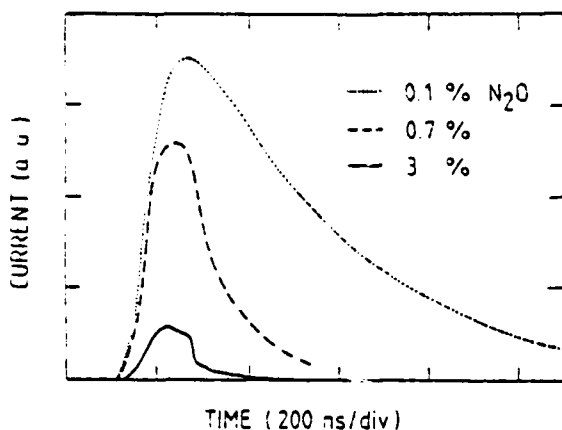


Fig. 8 Time Dependence of Switch Current with N_2O Concentration as Variable Parameter.

Figure 9 shows the j vs E/N characteristics of the e-beam sustained discharge in 1 atm N_2 with 0.7% N_2O . The curve represents the calculated values, dots are experimental results. The experimental values at higher E/N correspond well to the theoretical curve. However, the measured discharge characteristics do not exhibit the predicted current maximum at E/N -values of approximately 4 Td. These results indicate that attachment is dominant even at $E/N < 4$ Td, where, according to the measured values of the decay rate (see Fig. 6), attachment should be negligible. This assumption is confirmed by results of recently performed attachment rate coefficient measurements [8] and by Monte-Carlo calculations of the attachment rate coefficient [9] based on experimentally obtained attachment cross-sections [10].

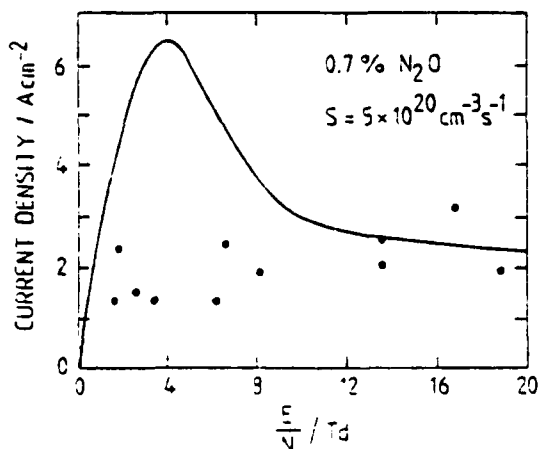


Fig. 9 Current Density j versus Reduced Field Strength E/N (Calculated Curve and Experimental Data Points).

Even with the attachment onset of $E/N < 4$ Td, that means with an attachment dominated discharge during conduction, the $N_2O:N_2$ mixture seems to work fairly well as opening switch gas. It satisfies the requirement of having low resistance at low E/N and high resistance at large E/N , as seen on Fig. 10, where the results of current-voltage measurements (Fig. 9) are plotted in a resistivity versus reduced field strength diagram. It shows an increase in resistivity of almost two order of magnitude in an E/N -range of 4 to 20 Td.

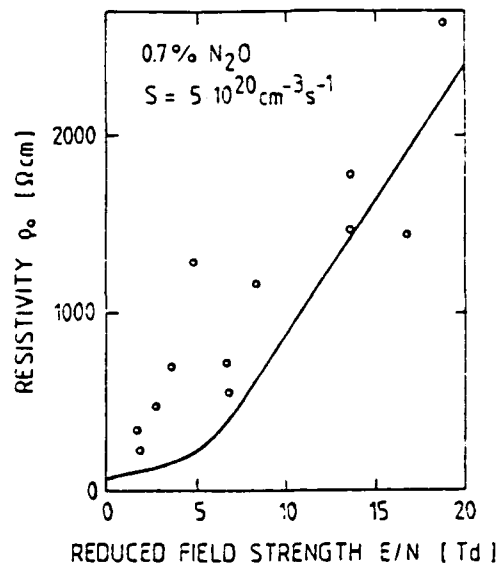


Fig. 10 Discharge Resistivity ρ_0 as a Function of Reduced Field Strength E/N for a Discharge in $N_2:N_2O$ (1 Atm).

$N_2:SO_2$

Another gas which has the required E/N dependence of the attachment rate coefficient is SO_2 [11]. SO_2 has a lower attachment rate and an onset of attachment at higher values of E/N , compared to N_2O . In order to get opening-times similar to those in the 0.7% $N_2O:N_2$ mixture, the concentration of SO_2 in N_2 as buffer gas had to be increased to 20%. The total gas pressure was reduced to 250 Torr, to cover a wider range of E/N with the given switch voltage. Fig. 11 shows the resistivity versus E/N of an $SO_2:N_2$ e-beam sustained discharge with $S = 3 \cdot 10^{20} \text{ cm}^{-3} \text{ s}^{-1}$. The resistivity rises above an E/N of 50 Td, indicating an increase in attachment at this value. This rise is in agreement with measured attachment characteristics in pure SO_2 [11]. Taking into account the different gas pressures and different e-beam currents in the $N_2O:N_2$ and $SO_2:N_2$ experiments, the N_2O mixture seems to be preferable to the mixture with SO_2 as the attachers. $N_2O:N_2$ has lower resistivity at low E/N for the same opening time, that means the Joule losses during conduction can be kept lower for this gas mixture.

Along these considerations, several gas mixtures have been proposed for diffuse discharge opening switches [4]. For our theoretical investigations N_2 was chosen as a buffer gas with N_2O as added attacher. N_2 was used since a complete set of cross section is available [6] and the plasma chemistry in a mixture of N_2 and N_2O appears to be relatively simple. Furthermore, N_2O in an N_2 buffer gas exhibits an E/N dependent electron decay rate, which increases by more than a factor of 20 in the E/N range from 3 Td to 15 Td, (Fig 6) [7]. It should be noted that N_2 has an electron drift velocity, which increases with E/N and therefore is not the optimum buffer gas in diffuse discharge opening switches. For gas mixtures, however, which show a strong attachment rate increase the drift velocity condition at high E/N is generally of minor importance.

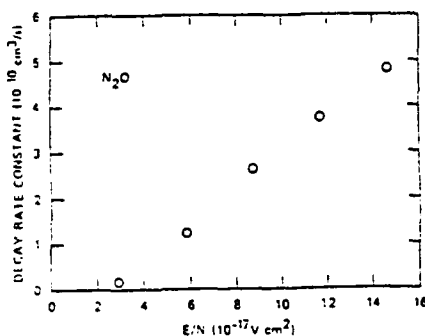


Fig. 6 Decay Rate Constants of the Electron Conduction Current by Adding N_2O in 350 Torr of N_2 at various E/N [7].

Discharge Analysis

To calculate the current-voltage characteristics of a diffuse plasma sustained by an electron beam, as well as to evaluate the time dependent impedance of an externally controlled discharge in a given circuit, a computer model has been developed that enables fast calculations for a variety of conditions [5]. It does not, however, provide for spatial analysis of the discharge. The code uses two independent programs. In a first computation, all rate constants of significant processes are calculated as a function of E/N for a representative gas mixture. These calculations use the E/N dependent electron energy distribution functions that have been previously compiled using a separate Monte Carlo code. In a second step a system of circuit equations and rate equations has been solved, where we used the previously calculated E/N dependence of the rate constants, assuming that they do not change significantly for small variations of the gas mixture.

The calculation of the current-voltage characteristics of the diffuse discharge does not require information about the circuit. Calculations were performed with the relative attacher concentration in the buffer gas as parameter². Figure 7 shows the current density (j) - reduced field strength (E/N) characteristics for different N_2O concentrations in an N_2 buffer gas. The total pressure is 1 atm. At

small E/N, below 4 Td, the electron loss is due to recombination only. At about 4 Td the attachment rate coefficient rises steeply. This means that for reasonably high attacher concentrations in the buffer gas the losses increase drastically, causing a negative slope in the current-voltage characteristics. At 30 Td where the attachment rate coefficient is assumed to level off, recombination becomes more important again, as demonstrated by the change in the slope j vs (E/N) - at this value.

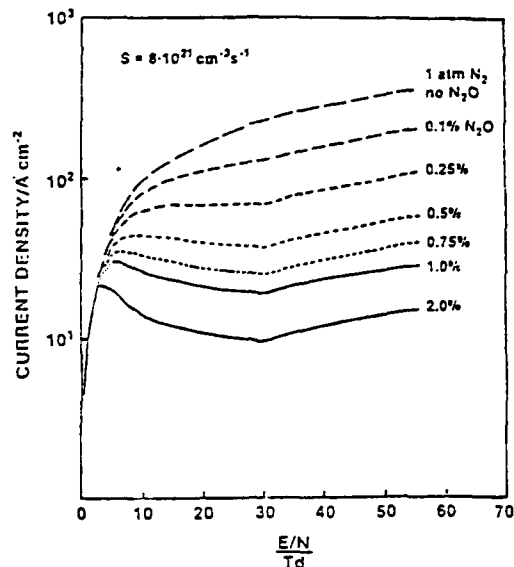


Fig. 7 Calculated Steady State j - E/N Characteristics for an e-Beam Sustained Discharge in N_2 with Admixtures of N_2O . The Electron Generation Rate is $8 \cdot 10^{21} \text{ cm}^{-3} \text{ s}^{-1}$. Parameter is the N_2O Fraction in % [5].

Experimental Results

Diffuse discharge experiments were performed in N_2O , SO_2 and CO_2 with N_2 as buffer gas. The e-beam tetrode was for these experiments mostly used in the single pulse mode. The source term, the number of electrons produced per cm^3 and s, was in the range of $10^{20} \text{ cm}^{-3} \text{ s}^{-1}$ to $10^{21} \text{ cm}^{-3} \text{ s}^{-1}$. The voltage applied at the PFN was varied between 2 kV and 20 kV. The switch electrode gap was kept constant at 3.5 cm.

$N_2:N_2O$

Figure 8 shows the influence of attacher concentration (N_2O) on the switch current. For high N_2O concentrations (3%) the switch current pulse represents the e-beam current pulse except for the tail. The tail may be caused by the current carried by positive and negative ions. The current gain (switch current/electron beam current) is about 2 for this high attachment concentration. For concentrations of

*The transient behavior of the discharge as part of a discharge circuit is discussed in Reference [5].

cross-sectional area of the beam. The current density can be varied independently of the accelerating voltage by adjusting the filament temperature. The control grid which is located 0.4 cm above the filament array is negatively biased ($V_3 = -4$ kV), to hold the e-beam off, even when the accelerating voltage is applied to the plate. The e-beam is turned on by applying a positive voltage pulse of typically $V_2 = +4$ kV to the grid. A second grid, 0.6 cm above the control grid, shields the control system electrostatically.

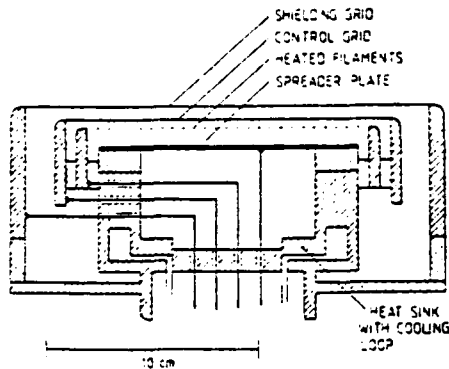


Fig. 3 Cross-Section of Cathode Assembly.

The pulser driving the grid is depicted in Fig. 4. It consists of two, 75 Ω cables (lengths d_1 and d_2) separated by a triggerable spark gap. Cable 1 is connected to the grid, as shown, and is charged to the negative bias voltage V_3 . Cable 2 is charged through a 10 M Ω resistor to the voltage V_2 . After triggering the spark, the positive voltage from cable 2 propagates towards the grid, is reflected with the same polarity, travels back to the charging resistor, and is reflected again. The negative bias voltage from cable 1 is reflected at the open end, etc. Hence, the cable pulser with two open ends generates a periodic rectangular grid voltage, and the electron beam is repetitively turned on and off. The primary advantage of this pulser is its simplicity and

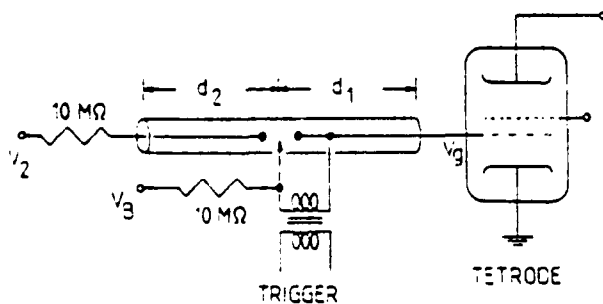


Fig. 4 Schematic Diagram of Grid Pulser.

versatility. The pulse magnitudes are variable by changing the cable charging voltages and the pulse width and pulse separation can be adjusted by changing the lengths of the cables. However, due to the effect of the capacitive termination in the tetrode and due to cable dispersion, subsequent pulses are degraded. This degradation limits the useful length of the pulse train to 3 or 4 pulses.

Measurements of the electron beam current at the cathode and at the anode - after passing the titanium foil - were performed with transmission line current transformers [3]. Fig. 5 shows the e-beam current pulses, evaluated from current transformer signals. The decay in amplitude is caused by the exponential plate voltage decay. Because of the reduced transmission of electrons through the foil at lower electron energies the effective time of operation is limited to approximately 1 μ s with the voltage generator used in this experiment.

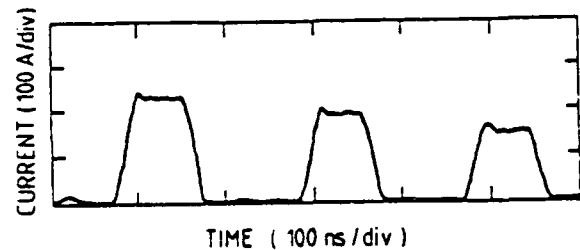


Fig. 5 e-Beam Current Pulses Measured at the Cathode.

After passing the titanium foil and a 12.5 μ m aluminum foil which serves as electrode in the diffuse discharge switch the e-beam generates a diffuse plasma between the electrodes in the stainless steel discharge chamber. The current through the plasma is provided by a 2 Ω pulse forming network, which delivers a flat top current pulse of 1 μ s duration and an amplitude of up to 12.5 kA.

Switch-Gas Properties

The switch opening time, after e-beam turn off, is determined by the electron loss processes in the diffuse discharge: recombination and attachment. In order to achieve opening times of less than a microsecond, the dominant loss process must be attachment, that means the switch gas mixture must contain an electronegative gas. On the other hand additives of attachers increase the power losses during conduction. Both low forward voltage drop and fast opening can only be obtained by choosing gases or gas mixtures which satisfy the following conditions [1,4,5]:

- for low values of the reduced field strength E/N (conduction phase) the gas mixture should have a high drift velocity, v_d , and low attachment rate coefficient, k_a .
- for high E/N values (opening phase) the gas mixture should have lower drift velocities and high attachment rate coefficients.
- to avoid the onset of the attachment instability during conduction the switch should be operated at E/N values where the attachment rate coefficient has a minimum or a negative slope.

K.H. Schoenbach, G. Schaefer, M. Kristiansen, H. Krompholz
H.C. Harjes, and D. Skaggs
Department of Electrical Engineering
Texas Tech University
Lubbock, Texas

Introduction

Inductive energy storage is attractive in pulsed power applications because of its intrinsic high energy density compared to capacitive storage systems. The key technological problem in developing inductive energy discharge systems, especially for repetitive operation (rep rates larger than kpps) is the development of opening switches. Promising candidates for repetitive opening switches are e-beam or laser controlled diffuse discharges [1]. The schematic diagram of an electron-beam controlled opening switch as part of an inductive storage system is shown in Fig. 1. The switch chamber is filled with a gas of pressures of 1 atmosphere and above. The gas between the electrodes conducts and allows charging of the inductor, when an ionizing e-beam is injected (usually through one of the electrodes which might be a mesh or a foil). The switch voltage remains below the self breakdown voltage, so that avalanche ionization is negligible. Thus, the discharge is completely sustained by the e-beam. When the e-beam is turned off, electron attachment and recombination processes in the gas cause the conductivity to decrease and the switch opens. Consequently the current through the conductor is commutated into the load.

an evacuated ($p = 2 \cdot 10^{-7}$ Torr) Pyrex cylinder, between the two plates of a stripline. The anode consists of a grid of 250 μm molybdenum wires at a distance of 7 cm from the cathode. The anode grid covers the entrance of a 13 cm long drift tube which is terminated by a 25 μm titanium foil. The foil is supported by an array of titanium bars. The e-beam voltage is applied to the anode by a two-stage Marx generator. The generator (Physics International Co. FRP-250) can deliver a maximum voltage of 250 kV with a 10 ns rise time and with an exponential decay time constant of about 2.5 μs into a 300 Ω load.

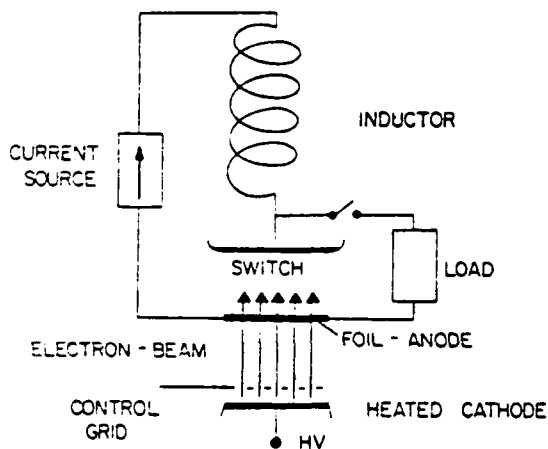


Fig. 1 Schematic of an E-Beam Controlled Diffuse Discharge Opening Switch.

Experimental Set-Up

For the investigation of e-beam controlled conductivity in a high pressure diffuse plasma a discharge system was constructed with an e-beam tetrode as the control element [2]. A schematic cross-section of the discharge chamber and e-beam tetrode is shown in Fig. 2. The e-beam cathode is located in

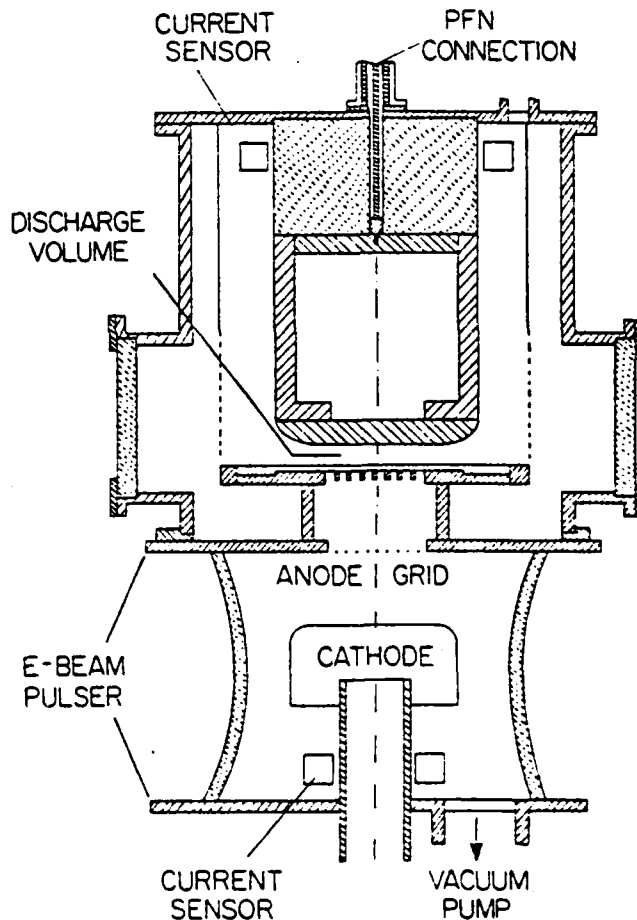


Fig. 2 Cross-Section of e-Beam Tetrode and Switch Chamber.

A cross-section of the cathode is shown in Fig. 3. The electron source is an electrically heated array of 375 μm diameter thoriated tungsten filaments. At a filament temperature of about 2100 K, the e-beam current density is about 4 A/cm² over the 100 cm²

*Supported by AFOSR and ARO

DISCUSSION

R. J. COMMISSO: How was E/N varied for N₂O?

K. SCHOENBACH: We varied the voltage across the switch down to 1 kV. No boundary effects were included.

E. E. KUNHARDT: You said you wanted the drift velocity to be low at high E/N and vice versa, while attachment should be low at low E/N and high at high E/N. Is this requirement on drift velocity necessary?

K. SCHOENBACH: It is desirable to have high mobility (not exactly drift velocity) and high electron density during conduction because conductivity is proportional to their product.

R. J. COMMISSO: You want the drift velocity to decrease at high E/N, but if attachment rate increases at high E/N the electron density will go down and resistivity can still go up.

L. G. CHRISTOPHOROU: SO₂ and N₂O both show pressure-dependent electron attachment processes at very low E/N, especially SO₂. Is that a problem?

K. SCHOENBACH: Our measurements showed increasing attachment rate with increasing E/N. We would like to see your data for SO₂ at very low E/N.

G. Schaefer et al.

It should be pointed out, that the set of processes considered in the Monte Carlo calculations and in the rate equation program are different. In the rate equation system, only those processes are considered which, according to the specific switching application, contribute to the electron density. Since the gas discharge is considered to stay relatively "cold" during one switch period, any *V. R. T-E* collisions (transfer of energy from vibrational, rotational, translational energy to electronic excitation) are neglected and transitions into rotational and vibrational states are considered only as loss mechanisms. On the other hand, in the Monte Carlo code a set of cross sections, as complete as possible, is employed. Such cross section sets, however, are only available for a few pure gases or rudimentary gas mixtures.

The calculations presented herein were performed for an e-beam sustained discharge in N_2 with admixtures of N_2O as the attachers. N_2 was used since a complete set of cross sections for inclusion in the Monte Carlo code was available (Phelps 1982), and the plasma chemistry in a mixture of N_2 and N_2O appears to be relatively simple. N_2O in an N_2 buffer gas exhibits an E/N -dependent electron decay rate, which increases more than a factor of 20 in the E/N -range from 3 Td to 15 Td (Lee *et al.* 1981; Gallagher *et al.* 1982). *It should be noted, however, that N_2 has an electron mobility which increases with E/N and therefore is not an optimum candidate for a buffer gas in diffuse discharge opening switch applications.*

In calculations by Morgan & Pitchford 1982, on the electron energy distribution function in weakly ionized plasmas, created by an electron beam in N_2 , it was demonstrated that the distribution function is different from just a superposition of the distribution function in a swarm and the distribution function of the electrons created in ionizing collisions of the fast electrons of the electron beam. Especially at low values of E/N , electrons produced at energies above the cross-sections for vibrational excitation create a side maximum in the distribution functions at E/N values where otherwise no electrons would be found. If admixtures of attachers are used with significant cross sections in this high energy range, a certain fraction of the created electrons will also be attached at low values of E/N . As a first approximation this effect could be considered when calculating the electron generation rate for a given electron beam, but according to the data available this effect will not change the electron density by more than a few percent.

Another objective was to investigate the feasibility of using photodetachment as an additional control mechanism. The N_2O undergoes dissociative attachment producing O^- . Photodetachment of O^- has already been proposed as a possible control mechanism for diffuse discharges (Schoenbach *et al.* 1982; Schaefer *et al.* 1983).

For switching, an e-beam sustained discharge has to work well below the self-breakdown limit. Electron generation should, therefore, during the closed phase (at low values of E/N), only depend on the direct ionization by the control e-beam electrons. The overall dynamic behavior, especially in the opening phase, however, may also depend on excitation and ionization processes through the discharge electrons. Thus, the E/N dependence of these processes must also be considered (Lowke & Davis 1977).

The following processes are considered in the set of rate equations. The required cross sections or rate constants were obtained from the literature.

- (1) Direct ionization (Rapp & Erlander-Golden; Lakshminarasihma *et al.* 1975).
- (2) Excitation of the metastable A-state of N_2 , direct or via other triplet states with subsequent optical transitions (Cartwright *et al.* 1977).
- (3) Ionization of N_2 from the metastable A-state (Kukulin *et al.* 1979).

Use of attachers in electron beam sustained discharge switches

- (4) N_2 metastable deactivation (Dreye & Perner 1973).
- (5) Electron-ion recombination (Douglas-Hamilton 1973).
- (6) Dissociative attachment of N_2O (Lee *et al.* 1981; Gallagher *et al.* 1982).
- (7) Collisional detachment of O^- (Tisone & Branscomb 1968).
- (8) Ion-ion recombination (Lorents 1981).
- (9) Photodetachment of O^- (Lee & Smith 1979).
- (10) Electron drift velocity (Christophorou 1971).

Experimentally derived rates as a function of E/N were used in the calculations, when available. If E/N dependent rates were not available, such as for processes (2), (3), and (7), or not known over the necessary E/N range, such as for (1), then the rate constants were calculated using the electron energy distribution function, evaluated through Monte Carlo calculations.

The electron energy distribution function, and subsequently the rate constants, change for a fixed value of E/N if the partial pressure of an attacher in a buffer gas is varied. This effect becomes very strong if a molecular attacher is added to an atomic buffer gas, since here the cross section of rotational and vibrational excitation and attachment are added in an energy range where the buffer gas does not have any appreciable inelastic cross section. Using N_2 as a buffer gas with an admixture of an attacher, only the attachment cross section of the attacher may cause a significant change of the electron energy distribution function (Pitchford & Phelps 1982). We, therefore, performed the Monte Carlo calculations with the cross sections of N_2 solely and for the cross sections of N_2 plus the attachment cross section of N_2O considering a 1% admixture of N_2O . As expected, the electron energy distribution function was lowered in the energy range above the attachment threshold and raised below this threshold energy. In the high energy range ($E > 6$ eV), at high values of E/N , this effect was not significant. All potential ionization processes (single and multi step) require a higher electron energy. The only process with a significant cross section in this range below 6 eV is collisional detachment of O^- . As will be seen later, the negative ion density will not reach values high enough to make collisional detachment a significant process if the discharge operation is optimized with respect to low losses.

For process (6), dissociative attachment of N_2O , two reported experimental data (Lee *et al.* 1981; Gallagher *et al.* 1982) and the calculated values differ only slightly. The calculated values, using the cross sections for $T = 300$ K (Chantry 1969), show a lower threshold at approximately 1.5 Td, while the experimental data (Lee *et al.* 1981) have a threshold at approximately 2.5 Td. For the calculations we used the experimental data (Lee *et al.* 1981) extended to high values of E/N according to our calculations (maximum rate constant of $1.1 \times 10^{-9} \text{ cm}^3 \text{ s}^{-1}$ at 30 Td and nearly constant above this value). Note that this attachment rate constant is only an *example* of a specific attachment characteristic that can be found among several attachers. Its important features are:

- (a) a low attachment rate for low values of E/N .
- (b) a threshold value of E/N with a strong increase of the attachment rate above this value.
- (c) an attachment rate that saturates at some higher value of E/N .

4. Discharge characteristics

The steady state characteristics were computed assuming a constant voltage, calculating the current for which $dj/dt = 0$. These calculations were performed for various sets

G. Schaefer et al.

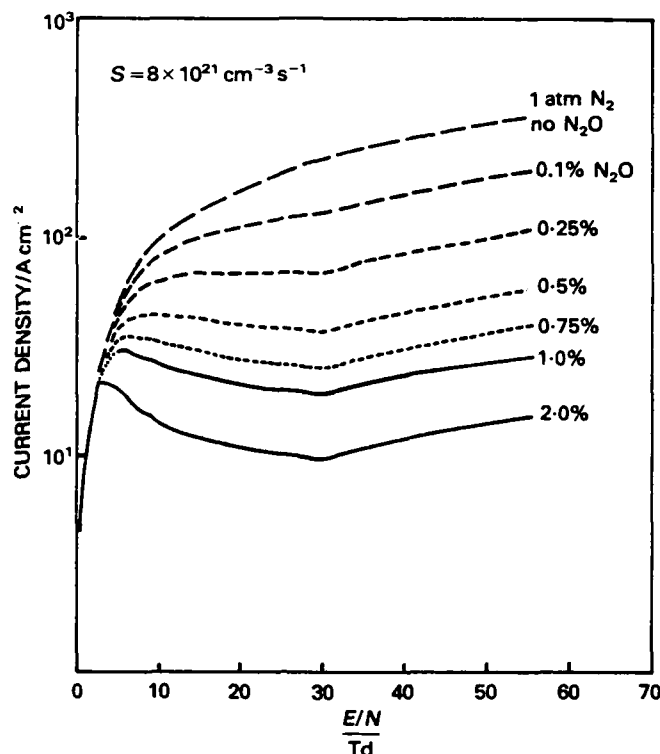


FIGURE 1. Calculated steady state E/N - j characteristics for an e-beam sustained discharge in N_2 with admixtures of N_2O . The electron generation rate is $8 \times 10^{21} \text{ cm}^{-3} \text{ s}^{-1}$. The variable parameter is the N_2O fraction in %.

of parameters. Figure 1 shows the steady state characteristics for different N_2O concentrations in an N_2 buffer gas. The total pressure is 1 atm and the e-beam electron generation rate is $8 \times 10^{21} \text{ cm}^{-3} \text{ s}^{-1}$. As expected, the steady state characteristics are not affected by the attachers in an E/N -range of 0 to 4 Td; while in the range of approximately 5 to 30 Td high attachers concentrations cause the current density to decrease if the field strength increases and, therefore, produces a current density maximum. The threshold value of E/N at which the current density no longer rises strongly with E/N is determined when attachment becomes the major loss mechanism. Thus the maximum of the current density shifts to higher E/N values when the attachers concentration decreases. It should be noted that attachers with a constant attachment rate coefficient result in steady state characteristics where the current density increases monotonically with E/N .

Figure 2 depicts the discharge characteristics for different values of the electron generation rate. (The attachers concentration is constant at 1%.) With increasing electron generation rates the electron density for a given value of E/N also increases. Since recombination depends quadratically on the electron density and only linearly on attachment, a higher value of E/N is required to cause attachment to become the major electron depletion mechanism. Therefore, the current density maximum shifts to higher values of E/N if the electron generation rate is increased. Figure 2 also demonstrates that the decrease of the current density with increasing E/N , caused by attachment, is more significant for lower electron generation rates.

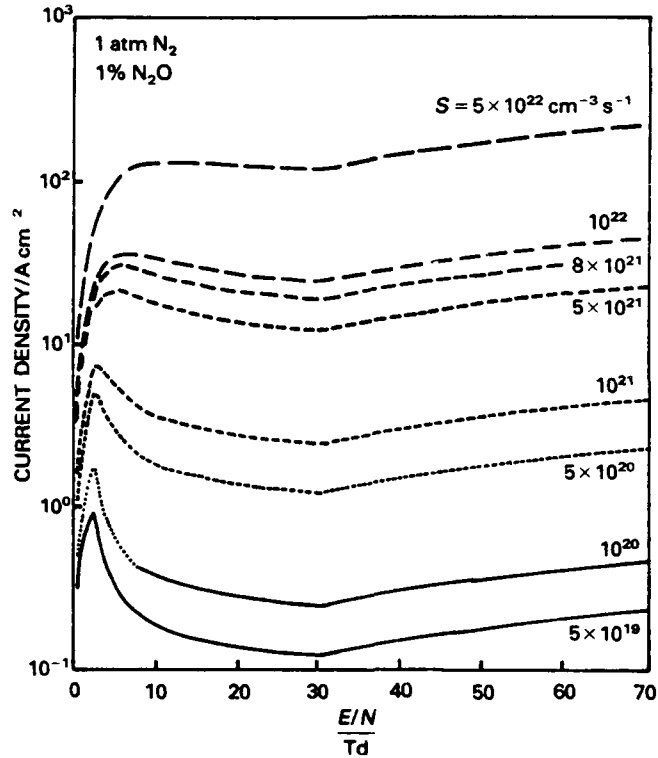


FIGURE 2. Calculated steady state E/N - j characteristics for an e-beam sustained discharge in N_2 with an N_2O fraction of 1%. The variable parameter is the electron generation rate.

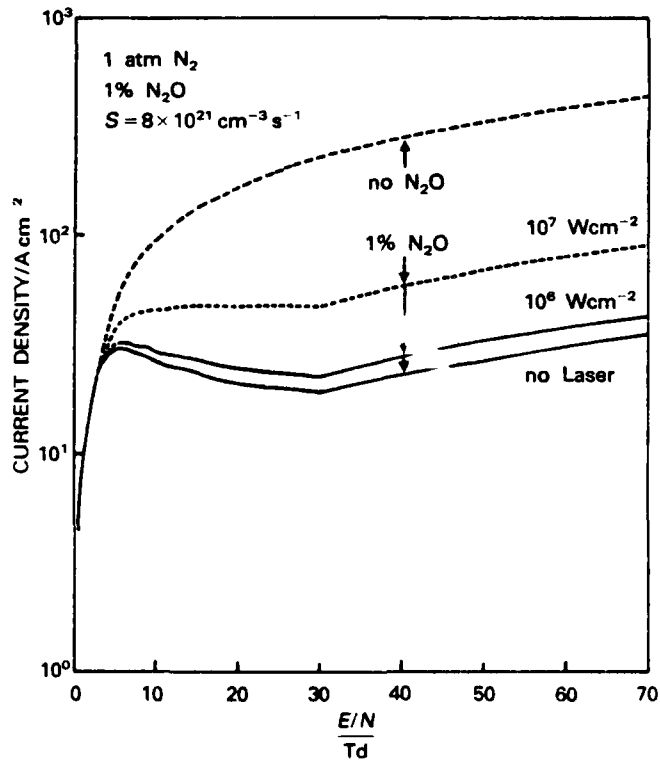


FIGURE 3. Calculated steady state E/N - j characteristics for an e-beam sustained discharge in N_2 with an N_2O fraction of 1%, including photodetachment of O . The electron generation rate is $8 \times 10^{21} \text{ cm}^{-3} \text{ s}^{-1}$. The variable parameter is the laser power density.

G. Schaefer et al.

These steady state characteristics give a strong hint as to which operating point or region would be ideal with diffuse discharges switches. In order to operate in the low loss region, which is not attachment dominated, the operating point should be on the left side of the current density maximum. In order to achieve fast opening, with no long delay, the operating point should be close to the maximum.

As mentioned before, the system $N_2 + N_2O$ has also been chosen to demonstrate the possibility of influencing the discharge properties by using photodetachment. If it is assumed that the dominant negative ion is O^- , then the dominant depletion mechanisms are O^- -ion recombination and/or photodetachment. Figure 3 shows the steady state characteristic for an N_2O fraction of 1% and an electron generation rate of $8 \times 10^{21} \text{ cm}^{-3} \text{ s}^{-1}$. The variable parameter is the power density of the illuminating laser operating in the photon energy range around 2 eV where the photodetachment cross section has a plateau. For comparison the steady state characteristics of a pure N_2 discharge are also shown. The calculation shows that photodetachment can compensate attachment in a significant E/N range, especially if a power density of 10^7 W/cm^2 or above is used.

5. Transient discharge behavior

As discussed in § 4, it should be possible to operate an e-beam sustained, low loss discharge which is not strongly affected by an attachment, provided the attachment rate constant has a clear threshold at a certain value of E/N , below which the attachment is not efficient. How fast such a steady state operation is approached when the e-beam is turned on and how fast the discharge opens if the e-beam is turned off, will depend strongly on the circuit as well. To examine the circuit influence, let us discuss two different applications. In both cases we will discuss an inductive energy storage system which has two separate loops, the charging loop and the discharge loop, having only the inductor in common (figure 4). In order to simplify our assessment let us assume that the load connected to the storage system is infinite during the inductor energizing phase, which can be achieved by an additional isolation spark gap in series with the load or if the load is a self-sustained gas discharge.

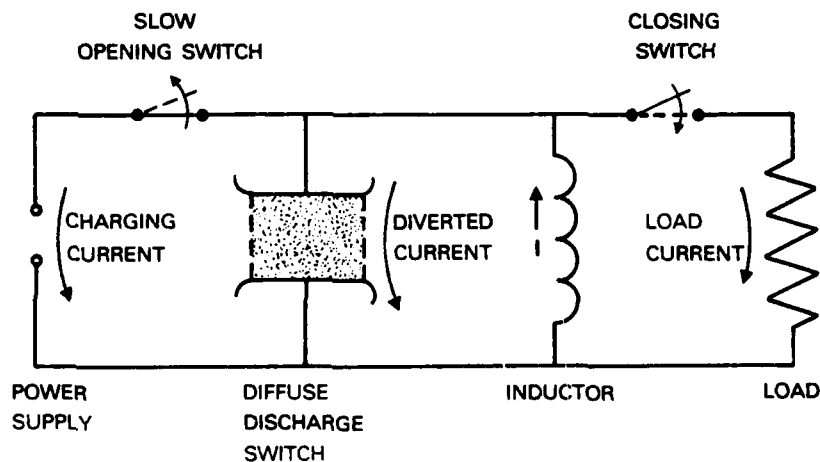


FIGURE 4. Schematic circuit for an e-beam sustained discharge switch in an inductive energy storage system.

Use of attachers in electron beam sustained discharge switches

5.1. Single pulse operation

In single pulse operation the switch has to close and open only once and it is thus possible to consider these two switching events in two different circuits. Let us assume that the discharge has to carry the total current after the inductor is already energized (figure 4). At this time the voltage drop across the inductor may be very small (i.e. $di/dt \sim 0$). If the electron beam is turned on at the same time the slow switch begins to open then the e-beam sustained discharge may reach the steady state starting from $j = 0$ and low E/N , without going through a range of high E/N values which would be in the attachment dominated range, i.e. high losses in the discharge. In addition, the slow switch does not experience a high voltage drop when it is opened. In this case, with appropriate circuit and discharge parameters, it can be shown, that the discharge approaches a steady state operation close to the maximum of the characteristics displayed in figure 2. It should be pointed out that in using a fuse as the slow opening switch the e-beam sustained discharge can not take over the current until the fuse has started to open, therefore the time dependent characteristics of the fuse have to be considered as well.

For the next phase (opening) let us consider the open circuit, i.e. infinite load, case. As discussed in § 2 the inductive energy storage system has to be considered as a transmission line with a high value of L' and a low value of C' , causing a very high impedance. The open circuit will produce the maximum value of E/N possible. Such a high impedance load line will definitely move the discharge into the range of high E/N values causing attachment to become most effective and affording fast opening times. At high values of E/N (>100 Td), however, ionization in the discharge becomes relevant. During switching operations, of course, the voltage drop across the discharge must stay well below that of a self-sustained discharge or self breakdown.

5.2. Burst operation

In a burst operation the inductor is charged once and the energy is then deposited into a load, in a burst of pulses, using an e-beam sustained discharge as a repetitive opening switch. In this case the final voltage drop across the load at the end of the pulse (which is the same as across the discharge cell), will define the initial E/N value for the closing process of the switch, i.e. when the e-beam is reintroduced. The closing process will thus go through a lossy state, slowing down the closing process. This effect will be greater the higher the E/N starting value is. As a result, we performed calculations on this transient behavior. The experimental arrangement shown in figure 5, will be used for validation of the general conclusions drawn from the model analysis.

It is obvious that a decreasing system impedance at a given impressed voltage will increase the current; the current density, however, can be kept constant if the discharge

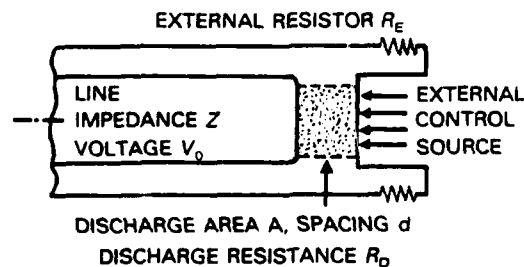


FIGURE 5. Schematic setup for an e-beam sustained discharge switch.

G. Schaefer et al.

area is increased by a corresponding factor. Thus the quantity $Z_t A$ acts as a similarity quantity, where $Z_t = Z + R_E$ is the total system impedance and A is the discharge area.

For all calculation in this section the following parameters were kept constant: ($A = 100 \text{ cm}^2$, $d = 1 \text{ cm}$, $p(\text{N}_2) = 1 \text{ atm}$, $V_0 = 50 \text{ kV}$, electron generation rate $R_e = 8 \times 10^{21} \text{ cm}^{-3} \text{ s}^{-1}$ for $0 \leq t \leq 100 \text{ ns}$). The values of the pressure p , voltage V_0 , and discharge length d correspond to a maximum value of $E/N = 185 \text{ Td}$. In an initial set of calculations, the total system impedance was kept constant at $Z_t = 20 \Omega$, giving a similarity quantity $Z_t A = 2 \times 10^3 \Omega \text{ cm}^2$. Figure 6 depicts the discharge characteristics for these parameters (see also figure 1) on a linear scale and, in addition, the load line for three system impedances, Z_t . The variable parameter is the percentage of N_2O . This graph indicates that, for $Z_t = 20 \Omega$, the system will approach the low range of E/N for N_2O concentrations of 0.75% and below, but not for an N_2O concentration as high as 1%. For 0.75% N_2O , the loadline ($Z_t = 20 \Omega$) comes very close to the steady state characteristics in an E/N range of $\sim 40 \text{ Td}$ and below. It can be seen that E/N and the current density would change very slowly for $E/N \leq 40 \text{ Td}$.

Figure 7 shows the time dependent E/N , current density j , and power loss per volume

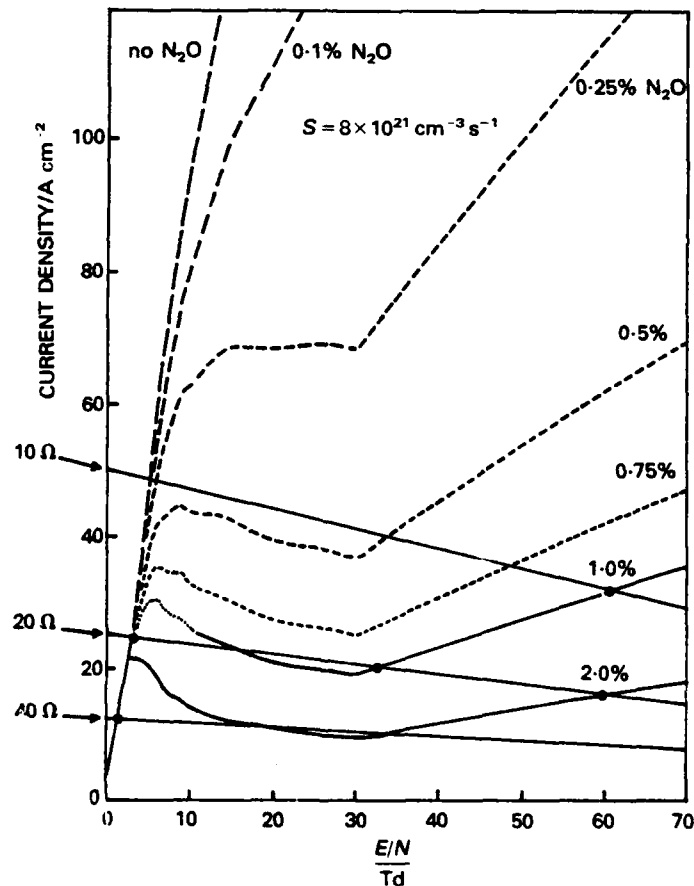


FIGURE 6. Calculated steady state E/N - j characteristics for an e-beam sustained discharge in atmospheric pressure N_2 with admixtures of N_2O . The electron generation rate is $8 \times 10^{21} \text{ cm}^{-3} \text{ s}^{-1}$. The parameters are the N_2O fraction in %. Also shown are three system load lines with the total system impedance, Z_t , as the variable parameter.

Use of attachers in electron beam sustained discharge switches

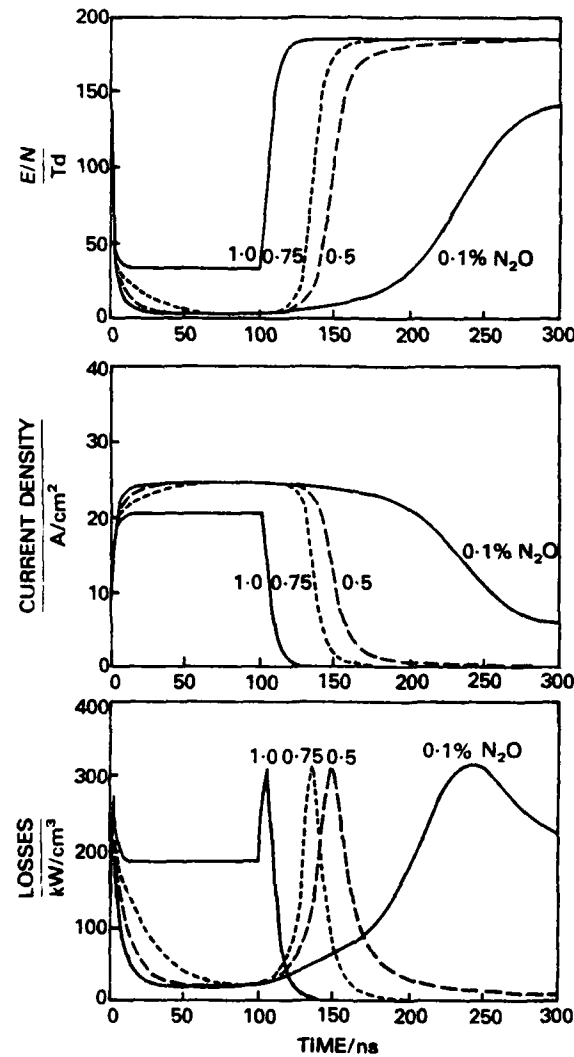


FIGURE 7 Time dependence of E/N (top), current density (middle), and power density loss (bottom) of an e-beam sustained discharge in 1 atm N_2 with admixtures of N_2O . The system impedance is $Z_1 = 20 \Omega$. The e-beam is on for $0 \leq t \leq 100$ ns. The variable parameter is the N_2O fraction in %.

behavior of the discharge. The curves for 0.1%, 0.5%, and 0.75% of N_2O approach the same steady state value for E/N and j in the conducting phase, demonstrating that under these conditions the discharge is not strongly influenced by attachment. Furthermore, after termination of the e-beam, the discharge properties change very slowly until an E/N -value is approached where attachment becomes effective. Such a time dependence has also been found by Chantry (1982). By contrast, for the case of 1% N_2O , the attachment is strong enough to prevent the discharge from ever reaching a low E/N -state and the steady state is therefore always attachment dominated. Thus, when the e-beam is turned off, the values for E/N and j change quite abruptly.

The power loss curve (figure 7, bottom) shows that, if the discharge is operating in a

G. Schaefer et al.

System impedance	N ₂ O-Concentration			
	0.1%	0.5%	0.75%	1.0%
10 Ω	92.9*	57.5	58.1	61.4
20 Ω	37.1*	15.8*	13.0*	22.0
40 Ω	12.4*	6.8*	4.4*	3.6*

TABLE 1. Energy density loss per switch cycle (300 ns) in mJ/cm³

For 0.1% N₂O and 0.5% N₂ the discharge was still on after 300 ns. At this time the power loss was still 70% of its maximum value for 0.1% N₂O and 3% for 0.5% N₂O, respectively.

* In these calculations the discharge reaches the low values of E/N .

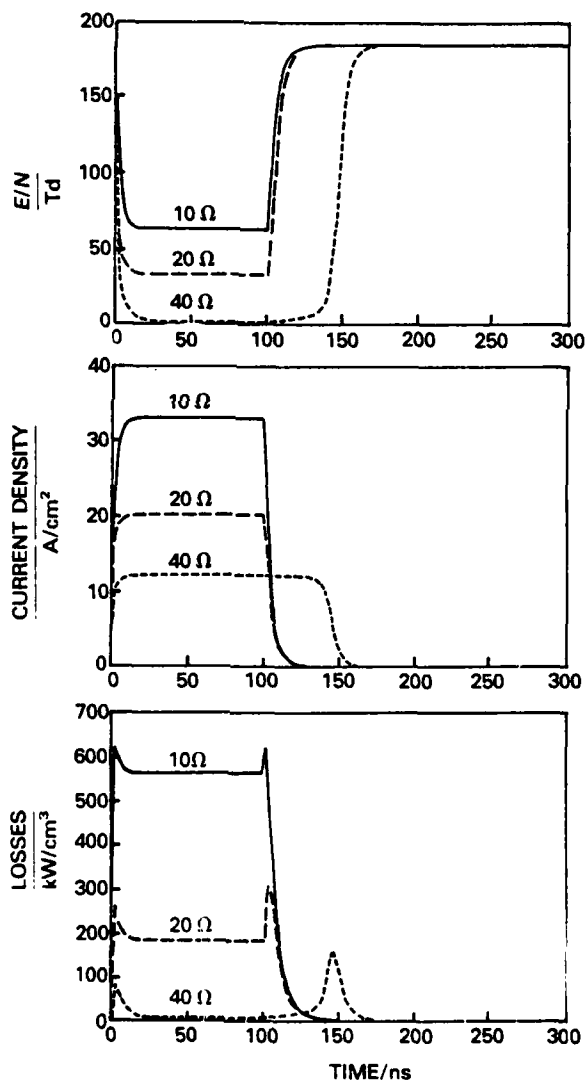


FIGURE 8. Time dependence of E/N (top), current density (middle), and power density loss (bottom) of an e-beam sustained discharge in 1 atm N₂ with an N₂O fraction of 1%. The e-beam is on for $0 \leq t \leq 100$ ns. The variable parameter is the system impedance, Z_i .

Use of attachers in electron beam sustained discharge switches

low E/N steady state, strong losses occur only in the transition region. The half width of the first loss peak (i.e. closing phase) increases as one increases the attacher concentration, while the half width of the second loss peak decreases. The values given in table 1 show the energy input per unit volume for one switching cycle, or for 300 ns if the discharge is still on at that time.

Another set of calculations was performed for a constant admixture of N_2O (1%) with the total impedance Z_t as the parameter. Figure 6 shows the steady state characteristics for a 1% N_2O admixture and three loadlines, allowing prediction of the steady state characteristics of such a diffuse discharge.

The time dependent behavior of the discharge for these parameters is shown in figure 8. At a value of 40Ω for the total impedance, the discharge reaches the low E/N region where attachment does not dominate. In this state the system impedance only, and not the switch discharge, limits the current. For lower impedances the discharge does not approach low E/N values and, therefore, remains essentially attachment dominated during the closing phase. The loss curves also make it evident that only for high system impedance can the losses be kept small.

Thus both the system impedance, Z_t , and the N_2O -concentration can determine whether or not the discharge reaches the low E/N region where attachment is not dominant, i.e. where the switch operates in the conduction phase at low losses. On the other hand, the opening phase ($t > 100$ ns) is controlled primarily by the attacher concentration. The specific dependence of the attachment rate will have an immediate effect if the E/N value is still high when the e-beam is turned off, and will become effective after some delay, if E/N is below 3 Td.

From figure 6 it would seem that the steady state operating point in the E/N - j diagram for some of the lower N_2O concentrations ($< 1\%$) can also offer possible operating points for N_2O levels as much as 1%. However, the circuit characteristics with a loadline which already crosses the steady state characteristics at a higher value of E/N , would prevent the transition of the system to the low E/N , steady-state operation. Lower E/N operation would have the advantage of low losses in the closed phase and fast opening time due to the higher attacher concentration.

There are several possibilities for combining these two features. One possibility for speeding up or enforcing this transition would be to use an e-beam current density with an additional peak at the beginning of the controlling pulse, i.e. tailor the shape of the external control input. Such an e-beam shaping was already discussed for electron beam sustained excimer laser discharges; in that case, however, to enhance stability (Brown & Nigham 1979). In figure 2 it was seen how the steady state current density moves to higher values if the electron generation rate is increased. Another possibility would be to use laser induced photodetachment to compensate for attachment during the transition from the open phase to the conduction phase. Figure 3 depicted how different laser power densities influence the steady state characteristics. Figure 9 exhibits the time dependent behavior of such a laser augmented discharge. The total impedance is 20Ω , the N_2O concentration is 1%, and the parameter is the laser power density. (The laser is on for the same duration as the e-beam.) With a laser power density of 10^6 W cm^{-2} the discharge can be switched into the low E/N region, however, it takes approximately 100 ns. With 10^7 W cm^{-2} the value of E/N drops very fast, and the total energy loss for one cycle is the lowest of all operating conditions for the same impedance (compare table 1 and table 2).

After a discharge has reached the low value of E/N , detachment will not strongly affect the electron balance and further laser irradiation to provide photodetachment is not warranted. Figure 10 depicts the time dependence of E/N for laser pulses of

G. Schaefer et al.

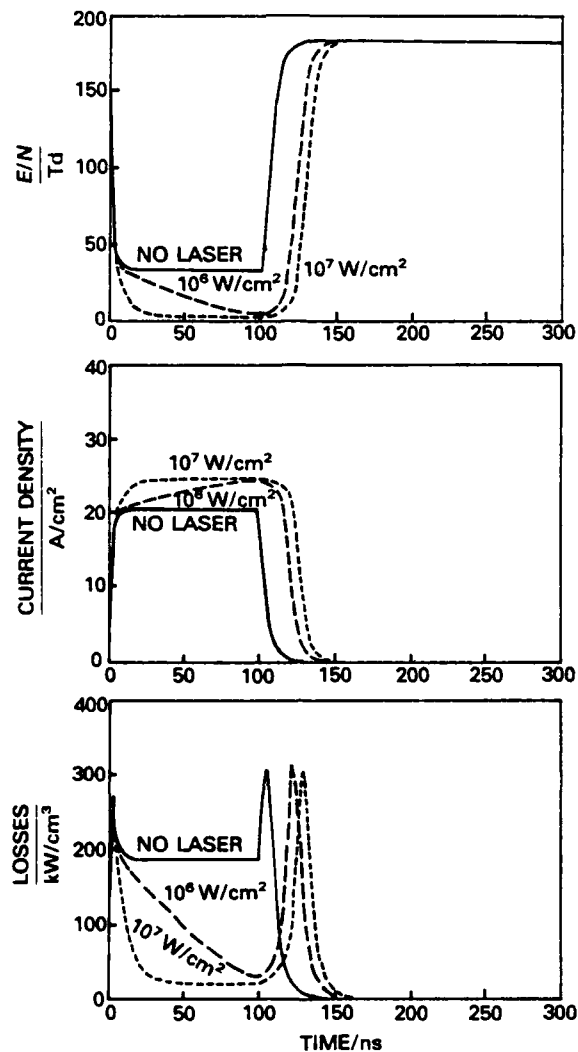


FIGURE 9. Time dependence of E/N (top), current density (middle), and power density loss (bottom) of an e-beam sustained, laser photodetachment assisted discharge in 1 atm N_2 with an N_2O fraction of 1%. The system impedance is $Z_r = 20 \Omega$. The e-beam and laser are on for $0 \leq t \leq 100$ ns. The variable parameter is the laser power density.

different length, t_L , starting simultaneously with the e-beam at $t = 0$ ns. The laser power density here is 10^7 W cm^{-2} . For short laser pulses ($t_L < 12.5$ ns) the discharge does not reach the region of low E/N values, while a laser pulse of $t_L = 20$ ns has nearly the same effect as a laser pulse covering the full e-beam period ($t_L = 100$ ns). The energy density loss for these calculations is listed in table 2.

The efficiency of using photodetachment depends on the density of negative ions. At $t = 0$ ns no negative ions have been produced, here laser irradiation in the first few ns is probably of little value. Figure 11 shows calculations of the time dependence of E/N for laser pulses of $t_L = 10$ ns length, but starting at different times. The power density again is 10^7 W cm^{-2} , so the beam fluence is 100 mJ cm^{-2} . For comparison, the curves

Use of attachers in electron beam sustained discharge switches

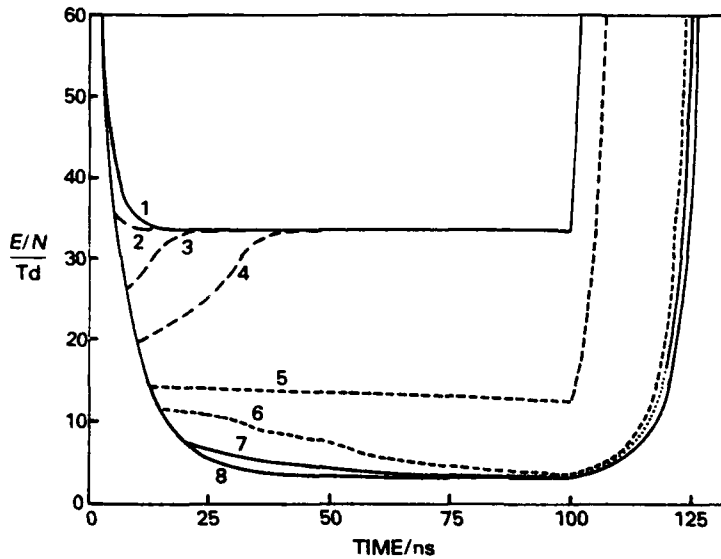


FIGURE 10. Time dependence of E/N for an e-beam sustained, photodetachment assisted discharge in 1 atm N_2 with an N_2O fraction of 1%. The system impedance is $Z_t = 20 \Omega$. The laser power density is 10^7 W cm^{-2} . The e-beam is on for $0 \leq t \leq 100 \text{ ns}$. The variable parameter is the laser pulse length (table 2).

without laser irradiation and for laser irradiation during the full e-beam period (0 to 100 ns) are also shown. The energy density loss for one switch cycle is listed in table 2. For the early pulses, as expected, the discharge does not proceed into the low E/N region. The lowest losses in the examples shown are achieved for a laser pulse starting after 7.5 ns. These calculations show that, on a high impedance load line, the transition from the high E/N , steady state operation to the low E/N , steady state operation can be induced with quite reasonable laser fluences.

6. Switch optimization

The calculations presented herein demonstrate the advantages of using e-beam controlled discharge switches with a gas mixture containing a buffer gas and admixtures of attachers with an attachment rate having a threshold at a given E/N value and then

# In figure 10	1	2	3	4	5	6	7	8
laser on								
from-to (in ns)	no laser	0-5	0-7.5	0-10	0-12.5	0-15	0-20	0-100
Energy density								
loss								
in mJ/cm^3	22.0	28.9	21.65	20.7	13.2	10.5	9.4	9.0
# In figure 11	1	2	3	4	5	6	7	
laser on								
from-to (in ns)	no laser	0-10	2.5-12.5	5-15	7.5-17.5	10-20	0-100	
Energy density								
loss								
in mJ/cm^3	22.0	20.7	13.2	10.8	10.0	10.1	9.0	

TABLE 2. Energy density loss per switch cycle for the curves shown in figure 10 and figure 11.

G. Schaefer et al.

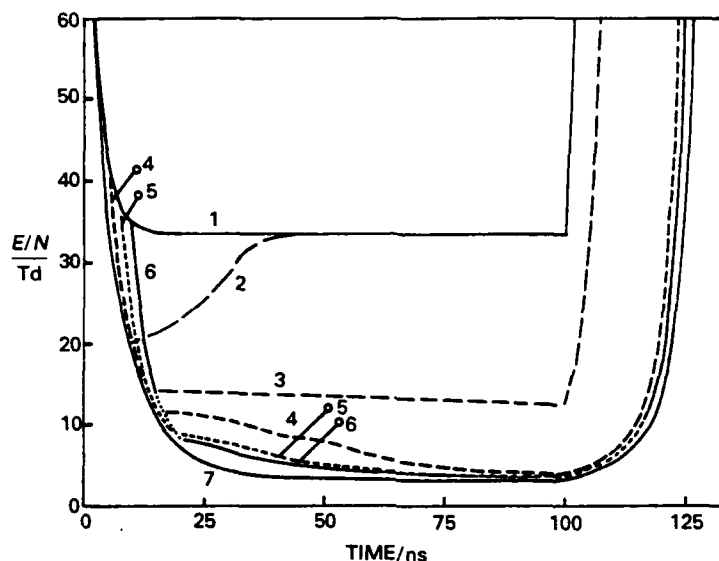


FIGURE 11. Time dependence of E/N for an e-beam sustained, photodetachment assisted discharge in 1 atm N_2 with an N_2O fraction of 1%. The system impedance is $Z_s = 20 \Omega$. The laser power density is 10^7 W cm^{-2} , and the pulse length is 10 ns. The e-beam is on for $0 \leq t \leq 100$ ns. The variable parameter is the delay of the laser pulse with respect to the e-beam (table 2).

increasing with E/N . Such a gas mixture enables the optimization of the discharge conditions in the steady state conduction phase and the opening phase, but adds difficulties in achieving fast closing. For an attachers in a molecular, or at least partly molecular buffer gas, an attachment rate having a threshold at a desired value of E/N can be realized if the attachment cross section has a threshold at some reasonable electron energy value, i.e. well above that of the dominating cross sections for vibrational excitation. Such properties will allow optimization of the discharge properties nearly independently in two E/N ranges.

In the E/N range below the threshold value for attachment, the discharge character is determined mainly by the buffer gas. The optimum operating point for the conduction phase can therefore be selected, considering the steady state characteristics for the pure buffer gas. For the selection of this steady state operating point, however, requirements which depend on the specific applications must be also considered, such as:

- (1) A practical consideration may be a limit on the size of the switch. If high total currents are required, one may be forced to operate at undesirably high current densities.
- (2) A high current density will limit the current gain. Kline (1982) shows that the current gain increases faster with decreasing e-beam current than the total current decreases, showing that the e-beam is used more efficiently at low current densities.
- (3) Stability requirements limit the total energy density dissipated in the discharge, and thus, for a given conduction time t_c , there are limits on the current density j .
- (4) Another consideration may be the necessity to optimize the ratio between the energy stored in the inductor, and the power dissipated in the switch. This is equivalent to a time constant T for the decrease of stored energy in the

Use of attachers in electron beam sustained discharge switches

conduction phase, with a disconnected power supply (figure 4). For a given system one obtains,

$$T = \frac{I^2 L}{IV} \propto \frac{I}{V} \quad \text{or} \quad T \propto \frac{j}{E/N}.$$

This means that straight lines in the E/N - j diagram: $j = \alpha T \times (E/N)$ where α is a system constant, are lines for the different constants, T . Considering a given conduction time t_c then the efficiency of the system would increase with increasing T . This would be achieved for an increasing e-beam current or electron generation rate (figure 2). A given electron generation rate will limit the current range as seen in figure 6. This approximation does not include the fractional power input of the electron beam, which of course increases with increasing beam current.

As can be appreciated, optimizing a steady state switch operation is difficult since the choice of the optimum steady state operating point is not obvious unless the application and its operating characteristics are clearly specified. The application affects the decision whether a system with low current density and high current gain or vice versa should be employed.

Once the steady state operating point has been determined the attacher and its concentration can be selected. For short delay switch opening the attachment threshold should be as close as possible to the steady state operating value of E/N . The maximum attachment rate, determined also by the attacher concentration, will then be responsible for the maximum value of (dj/dt) . It, of course, is also responsible for the time the switch needs to close again. Here a compromise has to be made, unless additional control means such as lasers are used.

For most applications, the switching times, both closing and opening, will be short, compared to the conduction phase. In these cases an additional control mechanism would only be required for a short time, compared to the steady state e-beam control. Additional control mechanisms to overcome attachment during closing, while still having an attachment dominated discharge during opening, would be to use a tailored e-beam with a stiffer beam current peak at the front of the pulse.

An additional control could be to use optical means, which were discussed in an earlier paper by Schoenbach *et al.* 1982. Relevant to an attachment dominated discharge is optically induced attachment, initiated in the opening phase when the e-beam is turned off, or, as discussed herein, photodetachment in the closing phase, during the beginning of the e-beam pulse.

It should be pointed out again that the gas mixtures used for these calculations are not optimum for all switching applications. For example, CH_4 as a buffer gas (Christophoru 1971), has a much higher drift velocity at low values of E/N , and N_2O as an attacher may not have the right threshold value of E/N for a desired steady state operating point. The calculations, however, show that the use of an attacher with a threshold E/N -value for attachment offers a unique combination of steady state and transient discharge properties, especially if additional control mechanisms are used.

Acknowledgment

Research sponsored by the Air Force Office of Scientific Research and the Army Research Office under Grant Number AFOSR F49620-79-C-0191. The U.S. Government is authorized to reproduce and distribute reprints for Governmental purposes notwithstanding any copyright notation thereon.

AD-A154 629

COORDINATED RESEARCH PROGRAM IN PULSED POWER PHYSICS
(U) TEXAS TECH UNIV LUBBOCK DEPT OF ELECTRICAL
ENGINEERING M KRISTIANSEN ET AL. 20 DEC 84

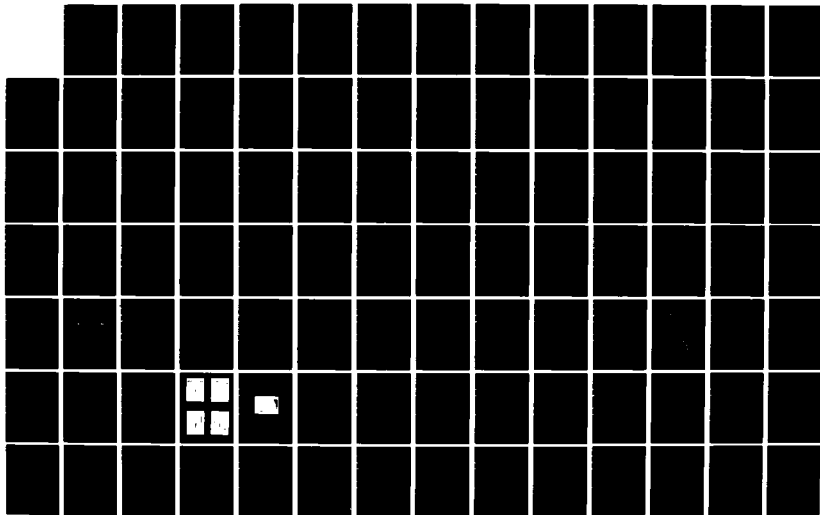
2/3

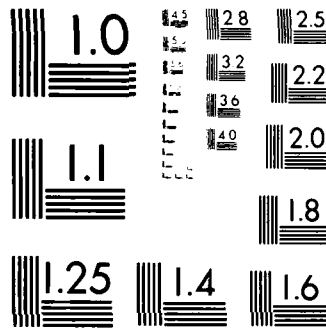
UNCLASSIFIED

AFOSR-TR-85-0457 AFOSR-84-0032

F/G 10/2

NL





MICROCOPY RESOLUTION TEST CHART
NATIONAL BUREAU OF STANDARDS-1963-A

G. Schaefer et al.

REFERENCES

- BLETZINGER, P. 1981 *Proc. 3rd IEEE Int. Pulsed Power Conf.*, Albuquerque, NM, 81.
- BLETZINGER, P. 1983 *Proc. 4th IEEE Pulsed Power Conf.*, Albuquerque, NM.
- BROWN, R. T. & NIGHAN, W. L. 1979 *Appl. Phys. Lett.* **35**, 142.
- CARTWRIGHT, D. C. CHUTJIAN, A. TRAJUAR, S. & WILLIAMS, W. 1977 *Phys. Rev. A*, **6**, 1041.
- CHANTRY, P. J. 1969 *J. Chem. Phys.* **51**, 3369.
- CHANTRY, P. J. 1982 *Workshop on Optical Control of Diffuse Discharges*, University of Oregon.
- CHRISTOPHOROU, L. G. 1971 *Atomic and Molecular Radiation Physics*, 247, Wiley-Interscience.
- CHRISTOPHOROU, L. G. HUNTER, S. R. CARTER, J. G. & MATHIS, R. A. 1982 *Appl. Phys. Lett.* **41**, 147.
- COMMISSO, R. J. FERNSLER, R. F. SCHERRER, V. E. & VITKOVITSKY, I. M. 1982 *IEEE Trans. Plasma Sci.*, **PS-10**, 241.
- COMMISSO, R. J., FERNSLER, R. F., SCHERRER, V. E. & VITKOVITSKY, I. M. 1983 *Proc. 4th IEEE Pulsed Power Conf.*, Albuquerque, NM.
- DOUGLAS-HAMILTON, D. H. 1973 *J. Chem. Phys.* **58**, 4820.
- DOUGLAS-HAMILTON, D. H. & MANI, S. A. 1974 *J. Appl. Phys.* **45**, 4406.
- DREYE, J. W. & PERNER, D. 1973 *J. Chem. Phys.* **58**, 1195.
- DZIMIANSKI, J. W. & KLINE, L. E. 1980 *Final Report*, Air Force Contract F33615-78-C-2010, Report AFWAL-TR-80-2041.
- FERNSLER, R. F., CONTE, D. & VITKOVITSKY, I. M. 1980 *IEEE Trans. Plasma Sci.*, **PS-8**, 176.
- GALLAGHER, J. W., BEATY, E. C., DUTTON, J., PITCHFORD, L. C. 1982 *JILA Info. Center Report* **22**, Boulder, CO.
- HALLADA, M. R., BLETZINGER, P. & BAILEY, W. F. 1982 *IEEE Trans. Plasma Sci.*, **PS-10**, 224.
- HARJES, H., SCHOENBACH, K., SCHAEFER, G., KROMPHOLZ, H., KRISTIANSEN, M., LEIKER, G. & HATFIELD, L. 1983 *Proc. 4th IEEE Pulsed Power Conf.*, Albuquerque, NM.
- HUNTER, R. O. 1976 *Proc. 1st IEEE Int. Pulsed Power Conf.*, Lubbock, TX, Paper IC8.
- KLINE, L. E. 1982 *IEEE Trans. Plasma Sci.*, **PS-10**, 224.
- KOVALCHUK, B. M., KREMNEV, V. V. & MESYATS, G. A. 1970 *Sov. Phys.-Dokl.*, **15**, 267.
- KOVALCHUK, B. M., KOROLEV, Yu. D., KREMNEV, V. V. & MESYATS, G. A. 1976a *Sov. Rad. Eng. Electron Phys.*, **21**, 112.
- KOVALCHUK, B. M. & MESYATS, G. A. 1976 *Proc. 1st IEEE Int. Pulsed Power Conf.*, Lubbock, TX, Paper IC7.
- KRISTIANSEN, M. 1981 *Proc. ARO Workshop on Repetitive Opening Switches*, Tamarron, CO.
- KRISTIANSEN, M. & SCHOENBACH, K. H. 1981 *Proc. ARO Workshop on Repetitive Opening Switches, Tamarron, CO*, Texas Tech University, Dept. Elec. Eng., Lubbock, TX 79409. DTIC No. AD-A110770.
- KRISTIANSEN, M. & SCHOENBACH, K. H. 1982 *Proc. ARO Workshop on Diffuse Discharge Opening Switches, Tamarron, CO*, Texas Tech University, Dept. Elec. Eng., Lubbock, TX 79409. DTIC No. AD-A115883.
- KROMPHOLZ, H., SCHAEFER, G. & SCHOENBACH, K. 1984 *to be published*.
- KUKULIN, V. I., OSIPOV, A. P. & CHUVILSKII, Yu. M. 1979 *Sov. Phys. Tech. Phys.* **24**, 883.
- LAKSHMINARASIMHA, C. S., LUCAS, J. & SNELSON, R. A. 1975 *Proc. Inst. Electr. Eng.* **122**, 1162.
- LEE, L. C. & SMITH, P. G. 1979 *J. Chem. Phys.* **70**, 1727.
- LEE, L. C., CHIANG, C. C., TANG, K. Y., HUESTIS, D. L. & LORENTS, D. C. 1981 *Second Annual Report on AFOSR sponsored Coordinated Research Program in Pulsed Power Physics*, Department of Electrical Engineering, Texas Tech University, Lubbock, TX. 189.
- LONG, W. H. 1979 *J. Appl. Phys.* **50**, 168.
- LORENTS, D. 1981 *private communication*.
- LOWKE, J. J. & DAVIS, D. K. 1977 *J. Appl. Phys.* **48**, 4991.
- LOWRY, J. F., KLINE, L. E. & HEBERLEIN, J. V. R. 1983 *Proc. 4th IEEE Pulsed Power Conf.*, Albuquerque, NM.
- MORGAN, W. L. & PITCHFORD, L. *Private communication—to be published*.
- PHELPS, A. V. 1982 *private communication*.

Use of attachers in electron beam sustained discharge switches

- PITCHFORD, L. C. & PHELPS, A. V. 1982 *35th Gaseous Electronics Conf.*, Dallas, TX.
- RAPP, D. & ERLANDER-GOLDEN, P. 1965 *J. Chem. Phys.* **43**, 1464.
- SCHAEFER, G., SCHOENBACH, K. H., TRAN, P., WANG, J.-S. & GUENTHER, A. H. 1983a *Proc. 4th IEEE Pulsed Power Conf.*, Albuquerque, NM.
- SCHAEFER, G., WILLIAMS, P. F., SCHOENBACH, K. H. & MOSLEY, J. 1983b *IEEE Trans. Plasma Sci.* **PS-11**
- SCHOENBACH, K. H., SCHAEFER, G., KRISTIANSEN, M., HATFIELD, L. L. & GUENTHER, A. H. 1982 *IEEE Trans. Plasma Sci.*, **PS-10**, 246.
- TISONE, G. C. & BRANSCOMB, L. M. 1968 *Phys. Rev.* **170**, 169.
- WATKINS, D. A. 1958 *Topics in Electromagnetic Theory*, Wiley & Sons, New York.

Transient Processes in the
Triggered Electrical Breakdown of Gases

(Final Report)

(S.K. Dhali, M.R. Wages, P.F. Williams, and G. Schaefer)

I. SUMMARY

Work during the contract period centered around two tasks: studying systematically streamer propagation and development and investigating experimentally the basic physical process occurring in trigatron-triggered electrical breakdown of gases. In collaboration with K. Schoenbach, work was also carried out investigating field distortion triggering, and photodetachment of electro-negative gases such as SF₆. The latter work is described elsewhere in this report. The work described here is the Final Report on this work element.

II. ACCOMPLISHMENTS

Work during the 1983-84 contract period involved primarily systematic studies of streamer propagation and development, and experimental investigations of trigatron-triggered breakdown. The streamer work is a continuation of work initiated the previous year and has been extremely fruitful. The trigatron work is a new area of study, and was just starting to yield results at the

end of the contract period. Work in this latter area is continuing at Texas Tech on a no-cost basis to the Air Force. The two areas of study are described separately in the following.

A. Streamer Calculations

Work in this area during the 1983-84 contract period centered around studying, in a systematic way, streamer propagation and development using numerical techniques developed previously. A large number of numerical calculations were performed to study the dependence of streamer properties on external parameters. In most calculations, the streamer was initiated by a small plasma hemispheroid placed as an initial condition on one electrode, and a tenuous, uniform preionization density throughout the gap was also assumed. Calculations were carried out to study the dependence of streamer properties on applied voltage (both magnitude and polarity), preionization density, and the density and size of the initial plasma spheroid. Calculations were also carried out to determine the effects of photoionization, and of the interaction between the laser and the propagating streamer tip as relevant to laser triggering of spark gaps. A technique for dynamic propagation analysis was developed which lends insight into the dynamics of streamer propagation, and which provides a stringent check on the accuracy with which the numerical algorithm solves the relevant transport and electric field equations. Each of these topics are described separately in the following sections.

The model and the numerical techniques used are discussed in detail in a previous annual report [1], and are therefore described only briefly here. The motion of the streamer is described by the coupled continuity equations for the electrons and positive ions, and Poisson's equation for the electric field.

$$\frac{\partial n_e}{\partial t} + \vec{\nabla} \cdot (v_e n_e) = \alpha n_e v_e + S \quad (1a)$$

$$\frac{\partial n_p}{\partial t} + \vec{\nabla} \cdot (v_p n_p) = \alpha n_e v_e + S \quad (1b)$$

$$\nabla^2 \phi = -q_e(n_p - n_e)/\epsilon_0 \quad (2)$$

where n_e and v_e , and n_p and v_p are the particle density and velocity for the electrons and positive ions, respectively, α is the Townsend ionization coefficient, ϕ the electric potential, and q_e is the (unsigned) electronic charge. The term S may describe effects of diffusion, or of any of several particle source or sink mechanisms, such as photoionization, attachment, or recombination. The transport equations are solved numerically using a flux-corrected transport technique, and the electric field is calculated using a novel algorithm based on Fourier transforming in the z -direction, and fitting the radial portion of the solution to a cubic spline.

For the results presented here we took the electron and ion drift velocities to be unique, empirically determined functions of E/P , and we included effects of diffusion, identifying both longitudinal and transverse components. We chose values appro-

priate for n_2 at 760 Torr. Specifically, for the pressure, P , in Torr and the electric field field, E , in kV/cm we used [2]

$$\alpha = 5.7 P e^{-260P/E} \quad (\text{cm}^{-1}).$$

For the fields of interest the electric field dependences of the electron and positive ion drift velocities are well approximated by a simple mobility model. We used [3]

$$\mu_e = 2.9 \times 10^5 / P \quad (\text{cm}^2 \text{volt}^{-1} \text{sec}^{-1})$$

and

$$\mu_p = 2.0 \times 10^3 / P \quad (\text{cm}^2 \text{volt}^{-1} \text{sec}^{-1})$$

The longitudinal and transverse diffusion coefficients, D_L and D_T , were (3)

$$D_L = 1800 \quad (\text{cm}^2 \text{sec}^{-1})$$

$$D_T = 2190 \quad (\text{cm}^2 \text{sec}^{-1})$$

We neglected positive ion diffusion.

Unless otherwise stated, the streamer was initiated with a plasma hemispheroid of density 10^{14} cm^{-3} and a minor axis diameter of .65 mm and a major axis diameter of .27 mm. The streamer propagated into a uniform, neutral preionization placed in the gap as an initial condition. For most calculations the initial density of the preionization was set as 10^8 cm^{-3} . The electrode spacing of the spark gap was 0.5 cm, and it was charged with a voltage source of 50 Ω output impedance.

1. Voltage Dependence

Calculations were carried out for applied fields of 36, 44, 52, and 60 kV/cm, corresponding to over-voltages of 103, 125, 148

and 170%, respectively, for both cathode and anode-directed streamers. Figures 1 through 3 show the results of these calculations for the on-axis z-dependence of the electron density and axial electric field component. The results shown for the cathode-directed streamer at 36 kV/cm extend only about half the distance across the gap because the density gradient became too large for the algorithm to handle, and numerical errors became large after this point. Also shown for selected fields are two dimensional contour plots of the electron density at fixed times. Several observations can be made from these results.

A quasi-steady state of streamer propagation is reached. After an initial period during which the shielding charges are building up on the plasma surface due to drift, the streamer starts to move across the gap, with its characteristics varying slowly. Much of the variation appears to be due to the build up of the preionization density due to avalanching in the applied field ahead of the streamer. Consistent with most experimental observations, the streamer velocity is in the range of 10^8 cm/s, increasing with increased applied field or preionization density ahead of the streamer. The velocity of a cathode-directed streamer is somewhat less than that of a corresponding anode-directed streamer.

For streamers of both polarities, we find that the electron density gradient at the streamer head increases with decreasing applied field, and that cathode-directed streamers have a steeper gradient than do anode-directed streamers. This effect is probably due to the need for increasing field enhancements as the

applied field is reduced. The maximum field enhancement ahead of the streamer is determined by the geometry of the streamer head. A planar head could give a maximum field enhancement of a factor of 2, a spherical head a factor of 3, and much higher enhancements are possible with sharper shapes. Thus at lower fields, a sharper head shape, coupled with a narrower plasma sheath region is required to produce the needed field enhancement.

As the streamer propagates across the gap, the velocity increases. This increase is caused by increases in the preionization density and in the range of the electric field enhancement ahead of the streamer. Partly offsetting this effect is a small decrease in the maximum field enhancement in most cases. Some increase with time of the radius of the streamer tip is observed.

The voltage dependences of the properties of cathode and anode-directed streamers are in some ways opposite. Streamers of both polarities propagate faster under high applied fields than under low fields, but the electron density in the body of the cathode-directed streamer increases with increasing applied field, whereas the density in the anode-directed streamer decreases. This behavior is expected, based on consideration of the relative direction of motion of the drifting electrons and the propagating streamer. In the anode-directed streamer case, the two directions are the same. In the limit of low field and therefore no impact ionization ahead of the streamer, the streamer reduces to a space-charge dominated swarm spreading out towards the anode, and the electron density inside the streamer body is reduced. For the cathode-directed streamer, the electron

drift direction is into the streamer body, and these drifting electrons must produce substantial ionization ahead of the streamer if it is to propagate toward the cathode. Thus, as the applied field is reduced, increased field enhancements are required to maintain the necessary level of impact ionization. These increased field enhancements are inconsistent with a decreasing free charge density inside the streamer and, in the light of the discussion below concerning the importance of the dielectric relaxation time to streamer propagation, may even require increased density.

These effects are seen directly in the electric field plots, especially in the results for lower fields. These plots show clearly that for anode-directed streamers the maximum field enhancement decreases with decreasing applied field, whereas the enhancement increases considerably for cathode-directed streamers. As discussed above, the maximum field enhancement and the range of this enhancement are related and are determined by the geometry of the streamer. This effect is clearly seen in the field plots for cathode-directed streamers at low applied field, where substantial field enhancements are observed, but with very limited range.

Also evident in the field is the fact that the field inside the propagating streamer is by no means reduced to zero by shielding. This observation implies that the dielectric relaxation time for the streamer plasma is not negligible, and, in fact, plays an important role in determining characteristics such as the propagation velocity and ionization density inside the

body of a streamer. This point does not seem to have been appreciated in the past. Assuming the ionization density in the streamer plasma to be 10^{14} cm^{-3} , we estimate the dielectric relaxation time to be $\tau_D = 14 \text{ ps}$, comparable to the time required for the streamer to travel a distance equal to the width of the front plasma sheath. The observation also calls into question theories, such as those of Lozanskii [4], in which a fully relaxed metallic model of the streamer interior is assumed.

2. Preionization Density Dependence

If we assume that the streamer at any moment after the initial formative period is propagating in a steady state configuration determined by, among other things, the preionization in front of it, then from the results shown here it is easy to obtain the dependence of streamer properties, such as propagation velocity on the preionization density ahead of the streamer. Plots of the propagation velocity as a function of electron density ahead of the streamer, obtained in this manner, are shown in Fig. 9. These plots imply that the velocity depends approximately logarithmically on this preionization density.

Unfortunately, more recent calculations have shown that a substantial portion of this velocity variation is due to changes in time of the shape of the streamer head. For example, Fig. 10 shows the propagation velocity as a function of electron density ahead of the streamer determined as above, for two cases, for both cathode and anode-directed streamers. The initial preionization densities in the two cases were 10^6 and 10^8 cm^{-3} ,

respectively. It is evident that the two calculations give significantly different results for the propagation velocity, implying that this quantity is not a simple function of the electron density ahead of the streamer, but depends on other quantities as well.

Figure 11 shows the z -dependence of the electron density and axial electric field for the 10^6 cm^{-3} calculation. Comparison with Fig. 1, which shows equivalent information for the 10^8 cm^{-3} calculation, shows that the shape of the streamer head, and particularly the range of the electric field enhancement is different in the two calculations for times which give the same preionization density ahead of the streamer. Thus it appears that the streamer propagation at each time has not reached an equilibrium configuration determined by the value of the preionization density ahead of it at that time.

3. Dependence on Initial Conditions

We have carried out a number of calculations designed to determine the dependence of the propagating streamer properties on the initiating plasma hemispheroid. We have made calculations with varying ionization densities inside the initial plasma, and with initial hemispheroids of differing radii. Briefly, we find that the properties of the streamer, once launched, do not depend on the initial plasma density, but that the radius of the initial hemispheroid determines the radius of the propagating streamer.

Figures 12 and 13 show results of calculations for conditions identical to those of Fig. 1, except that the density of

the initial plasma was 10^{13} and 10^{15} cm^{-3} , respectively. For comparison, Fig. 14 shows these results for streamers with three different initial densities on one plot. The primary difference we see between the streamers launched from initial plasma hemispheroids of differing density is that those launched from lower density plasmas take longer to develop. Otherwise, the properties of all three streamers are very similar. We conclude, therefore, that the ionization density inside a streamer is very much a natural property of the streamer, and that strong forces exist to drive this density back to the correct value in the event of some deviation.

Figures 15 through 18 show corresponding results for initial plasmas of density 10^{14} cm^{-3} , but differing radii of the plasma hemispheroid. Figures 15 and 17 show plots of the on-axis electron density and axial electric field, and Figs. 16 and 18 show contour plots of the electron density. Quasi steady-state propagation is observed in all cases, but the radius of the streamer depends on the radius of the initial hemispheroid. This observation demonstrates that the radius of the propagating streamer is only weakly determined by the environmental parameters, and that only weak forces exist to determine the natural streamer radius. Calculations such as the quasi-two-dimensional calculations of Davies et.al. [2], in which a streamer shape is arbitrarily imposed on the streamer, may, therefore, have more validity than might otherwise be supposed, but it must be recognized that the properties of the streamer will still be a strong function of the assumed shape.

pin. The length of the coaxial line corresponded to a pulse length of ~ 10 ns, and the line was charged through a large resistor connected to a D.C. power supply. The line was typically charged to a voltage around 8 kV, and the trigger system would produce a voltage pulse of amplitude 2-3 kV and 2-4 ns risetime at the trigger pin.

GaAs was chosen to allow D.C. charging of the coaxial line without suffering thermal run-away problems in the semiconductor. The material is a direct gap semiconductor, with short carrier lifetimes, and the gap is at about 830 nm, significantly bluer than the 1060 nm output of our laser. These two characteristics combined to make a rather inefficient switch. Even applying pulses with energy of the order of 100 mJ, the resistance of the switch in the on state appears to have been about 100 Ω . The delay in breakdown of the trigger gap was of the order of 10 ns, with a jitter of 1-2 ns.

Events occurring during the breakdown were investigated with streak photography, using a Hamamatsu C979 Temporal Dispenser, and associated control circuitry. Even through the streak camera was equipped with an electrical gate to turn the streak tube off at a set time, the emission from the spark phase was generally too intense to allow observation of the very weakly emitting events occurring during the initial breakdown phase. This problem was partly solved by using a very short, ~ 5 ns, charging cable for the main spark gap.

forming a region of enhanced field just outside the plasma boundary. With sufficient enhancement, substantial impact ionization occurs in this region, extending the boundary of the plasma, and forming a streamer. The streamer then propagates across the gap, forming a resistive connection between the main gap electrodes which is then rapidly heated ohmically to form the arc.

1. Experimental Apparatus

For experiments on trigatron breakdown, we modified the spark gap enclosure used for the laser-triggered breakdown work, and described in a previous annual report [1]. The upper electrode in the gap originally had a small hole drilled through the center and a lens and window to allow access for the laser beam. We replaced this electrode with another which contained a trigger pin electrically insulated from the electrode by a Macor ceramic sleeve. The tip of the trigger pin was filed to an asymmetric, knife edge shape in order to promote the occurrence of breakdown at only one position to simplify interpretation of streak photographs. The electrode assembly is shown schematically in Fig. 30.

An electrical schematic diagram of the trigatron system is shown in Fig. 31. Voltage pulses were applied to the trigger pin through the use of an optically controlled photoconductive switch. The switch consisted of a small wafer of high resistivity GaAs of dimensions $\sim 20 \times 5 \times 1$ mm, and was controlled by the fundamental output of our Nd:YAG laser at a wavelength of 1060 nm. Electrical contact was made at each end of the wafer by using conducting epoxy to attach fine copper wires. The switch connected a D.C. charged 50 Ω RG 58/U coaxial line to the trigger

Several processes for trigatron triggering have been proposed. The first, which we term the photoionization model, suggests that the spark from the breakdown of the trigger gap photoionizes the gas in the main spark gap, causing current flow. Ohmic heating of the fill gas molecules will occur, and if the initial current is large enough, this heating will result in additional free ionization and more heating, etc. Eventually, an arc channel will form, completing closure of the switch.

The second process we term the field distortion model, and was proposed by Shkuropat [10]. In this model, breakdown of the trigger gap is secondary to the triggering process. Applying a voltage pulse to the trigger pin causes field enhancement in the region around it. With sufficient field distortion, a streamer is initiated propagating towards the opposite electrode. After the streamer bridges the gap, a thin column of weak ionization connects the trigger pin to the opposite electrode, highly over-volting the gap between the trigger pin and the adjacent electrode. This gap then breaks down rapidly, completing the connection between the main gap electrodes. Finally, ohmic heating due to the current flowing in the resistive streamer channel occurs and rapidly forms the arc, completing switch closure.

The third process we call the streamer model. It is most similar to the process we found primarily responsible for laser triggering of spark gaps. In this case, the trigger gap breaks down first, forming a spark and a small volume of plasma. If the plasma is formed in a region where it is exposed to an applied field, the electrons drift to shield the plasma interior, thereby

B. Trigatron Triggering Experiments

Work in this area was suggested by the successful completion of a detailed experimental study of laser-triggering of spark gaps, carried out under AFOSR support [7]. In both types of triggering, the appearance of a small volume of plasma, due to either optical or electrical breakdown near one electrode, seems to be responsible for triggering breakdown. It seemed natural to make use of the experimental and analytical techniques developed for studying laser-triggered breakdown for study of breakdown in trigatrons. Work progressed more slowly than expected in this area, due primarily to the move of the Principal Investigator from Texas Tech University to the University of Nebraska, and work has been continuing at Texas Tech after the close of the contract period on a no-cost basis to the Air Force.

Briefly, a trigatron consists of a main spark gap with a trigger pin usually placed inside and on the axis of one electrode. The tip of the trigger pin is generally flush with or slightly recessed in the plane of the electrode. The main spark gap is D.C. charged to some fairly large fraction of the self-breakdown voltage (50-99%), and triggering is accomplished by applying a high voltage pulse to the trigger pin, overvolting the gap between the pin and the adjacent electrode. In most cases breakdown of the main gap follows breakdown of the trigger gap, although Shkuropat [10] reports breakdown of the main gap without breakdown of the trigger gap.

anode-directed streamer calculations depicted in Figs. 1 and 5. At all points ahead of the streamer the agreement is generally excellent, indicating that the numerical algorithm we used is performing well. Similar plots were obtained for the other calculations shown in Figs. 1-8, and with one exception, discussed below, the results were similar. In many cases, agreement was not good inside the streamer body, but this is to be expected since the slope of the electron density was very small here, and was in some cases negative. A negative slope leads to a sign ambiguity in the definition of phase velocity.

Figure 29 shows the "experimental" and "theoretical" phase velocities for the 18 kV, cathode-directed streamer calculation which became unstable. These phase velocities were determined at $t = 2.0$ ns, before the appearance of any obvious features in the numerical results which might indicate numerical difficulties. Two points are evident from the results in Fig. 29. First, there is substantial disagreement between the "experimental" and "theoretical" results, implying serious numerical errors, as became evident several nanoseconds later. Second, the figure shows "theoretical" phase velocities calculated with and without the diffusion term, and a significant difference is seen. Thus, it appears that in this case, the density gradient became sufficiently steep that diffusion was starting to become important. These are the only results we have obtained in which diffusion played a significant role.

Further insight into the evolution of the shape of the streamer head can be obtained by considering the positional dependence of the total phase velocity. As seen in Fig. 26, the phase velocity is slowly increasing ahead of the streamer, implying that the slope of the electron density curve ahead of the streamer is decreasing with time. As shown in Fig. 2, this effect is actually observed.

We can also obtain the phase velocity at each point at a given time directly from the numerical results, by simply noting how far a point of constant density moved during some short time interval. Comparison of the velocities obtained in this way, which we will term "experimental," with those obtained from Eq. (7), termed "theoretical," provides a sensitive check on the accuracy with which the FCT algorithm solves the transport equations. Since the flux-correction algorithm is highly non-linear, and therefore not easily amenable to error analysis, such a check is very useful in these calculations. We can also check on the Poisson solver at the same time by noting that if the Poisson solver is functioning properly,

$$\vec{\nabla} \cdot \vec{v}_e = \mu \vec{\nabla} \cdot \vec{E} = \frac{\mu \rho}{\epsilon_0} \quad (8)$$

where ρ is the net charge density. If we make this substitution in Eq. (7), the accuracy of the Poisson solver will be checked at the same time as the FCT algorithm.

Figures 27 and 28 show the "theoretical" and "experimental" phase velocities calculated in this way for the cathode and

In this expression, the first term on the right hand side corresponds to impact ionization, the second to dielectric relaxation, and the third to diffusion. Similar, but less general results have been obtained by several authors. It is difficult to obtain the quantities on the right hand side of Eq. (7) analytically, but they are known from our numerical calculations at any given time. The calculation of v_p from our numerical results is of interest because it provides insight into the reasons for changes in both the density gradient at the streamer head and the propagation velocity. Additionally, comparison of the phase velocity, as calculated from Eq. (7), with that determined directly from the numerical results provides a stringent test of the accuracy with which the numerical algorithm is solving the transport equations.

Figure 26 shows the on-axis phase velocity (3) as well as the separate contributions from the impact ionization (1) and dielectric relaxation (2) terms calculated using Eq. (7) for the cathode-directed streamer depicted in Fig. 2. For this case the diffusion term in Eq. (7) is negligible. Comparison of the curves allows the determination of the relative importance of the different sources of ionization. It is evident that the dielectric relaxation term dominates in the plasma sheath region just at the streamer tip, whereas the impact ionization term dominates elsewhere ahead of the streamer. This observation suggests a regional approximation approach to an analytic analysis of streamer propagation which has been used very recently with good success.

streamers with laser interaction than for those without. These observations are consistent with experimental comparisons in laser-triggered breakdown experiments between regions of laser-assisted and unassisted streamer propagation.

6. Dynamic Propagation Analysis

We can gain insight into the formation and propagation of streamers by using the electron continuity equation given in Eq. (1a) to determine the velocity of a point of constant density. In a true steady state propagation condition, this quantity is the velocity of propagation of the streamer. In a quasi-steady state condition, the variation of the quantity across the streamer head determines the change in shape of the streamer head. We will refer to this quantity as the phase velocity.

To define the phase velocity at the point r at time t_0 , we seek a path $\vec{P}(t)$, such that $\vec{P}(t_0) = \vec{r}$, and

$$\frac{d}{dt} n_e(\vec{P}(t), t) = 0 \quad (5)$$

$$\frac{\partial n_e(\vec{P}, t)}{\partial t} + \frac{d\vec{P}}{dt} \cdot \vec{\nabla} n_e(\vec{P}, t) = 0 \quad (6)$$

The quantity $\frac{d\vec{P}}{dt}$ is the desired phase velocity, \vec{v}_p . On axis we obtain from Eq. (1) and (6), including effects of diffusion but assuming $S = 0$ otherwise,

$$v_p = \frac{dP_z}{dt} = \frac{-\alpha |v_e| - \vec{\nabla} \cdot \vec{v}_e + \frac{1}{n_e} \frac{d^2 n_e}{dz^2}}{\frac{\partial n_e}{\partial z}} + v_{ez} \quad (7)$$

Since we were primarily interested in effects of interaction of the laser beam with the streamer head, we circumvented the problem by artificially increasing the power absorbed per electron by a factor of 10^6 over the value given by Eq. (4). The main effect of this approximation is to reduce the ionization density substantially in the body of the streamer. It should not have much direct effect on the streamer tip because the electron density is very tenuous ahead of the streamer, and very little optical power is absorbed until after the optical beam has entered the streamer body. There is probably an indirect effect on propagation, however, due to the more complete shielding expected with higher ionization density inside the streamer. As discussed in the previous section, more complete shielding inside generally leads to higher field enhancements outside the streamer. In any case, the results we show here are expected to underestimate the effects of laser interaction on streamer propagation.

The electron densities for several times are shown in Figs. 24 and 25 for cathode and anode-directed streamers, respectively. These results should be compared with Figs. 4 and 8 for corresponding streamers with slightly higher applied field, but without laser interaction. (The results of Figs. 4 and 8 also differ in that preionization but no photoionization was assumed, and the radius of the initial plasma hemispheroid was smaller.) The effects of laser interaction are very evident in these results. The speed of propagation is substantially faster, yet the ionization density in the body of the streamer is larger for the

keeping with conditions commonly encountered in laser-triggered breakdown experiments, we assumed an applied field of 34 kV/cm, and a nitrogen fill gas at 300 Torr. Photoionization was included in the calculation, and no initial preionization was assumed.

We encountered a numerical problem in these calculations. We accounted for absorption of the laser energy according to the formula given by Morgan [8],

$$P_{ab} = \frac{e^2 I}{m} \frac{1}{c \epsilon_0} \frac{v_m}{v_m^2 + \omega^2} \quad (4)$$

where P_{ab} is the power absorbed by a single electron, e and m are the electron charge and mass, c is the speed of light, ϵ_0 is the dielectric constant, and I is the intensity of the optical field. However, in passing through the head of the streamer, the absorption of optical power was negligible, so that the laser continually acted on the free electron density inside the streamer body, causing it to increase drastically, and eventually resulting in numerical difficulties. This interaction with ionization in the body of the streamer is actually observed in laser-triggered breakdown experiments as the formation of intensely radiating hot spots in the streamer channel [7]. As these hot spots form, the power absorbed from the laser is used with increasing efficiency to heat the fill gas molecules, instead of being used to create ionization. Our model does not take this heating into account, and this mechanism is therefore not available to dispose of the absorbed laser energy, causing steadily increasing ionization rates, and nonphysical results.

initial calculations of streamer propagation under conditions for which the streamer tip interacts with an intense optical electric field, such as a laser provides. The model of laser-streamer interaction we used was that described by Morgan [8], in which the interaction is treated by approximating the effects of the optical field to be the same as those of an effective, D.C. field given by

$$E = E_0 \sqrt{\frac{\nu_m^2}{\nu_m^2 + \omega^2}} \quad (3)$$

where E_0 is the RMS field of the laser beam, ν_m is the electron collision frequency for momentum transfer, and ω is the optical field frequency. As in most laser triggering experiments, the optical field was assumed to be perpendicular to the applied field, so the two were added in quadrature to obtain magnitude of the total effective field. This quantity at each point was then used to determine the local value of the Townsend ionization coefficient, α .

In our simulations, we assumed an initial plasma hemispheroid of peak density 10^{14} cm^{-3} , with axial and radial radii of 0.003 and 0.27 mm, respectively. The laser beam was assumed to be Gaussian and to be focussed on the starting electrode to a 100 μm spot size by a 10 cm focal length lens. The laser power was assumed to be 10 MW, giving a maximum RMS optical field of $6 \times 10^6 \text{ V/cm}$, the momentum transfer frequency was taken from Kroll and Watson [9] as $4 \times 10^{12} \text{ sec}^{-1}$, and the laser frequency was $2 \times 10^{15} \text{ sec}^{-1}$, all yielding a peak effective field of 120 kV. In

on the other hand, neither of these effects is present, and the density of "seed" electrons ahead of the streamer is determined primarily by the range of the photoionizing radiation. Figure 22 shows the relative strength of the two ionization source terms, impact ionization and photoionization, as a function of distance ahead of the streamer for a fixed time of 1.5 ns. The quantity plotted is the increase in ionization density during a 2 ps time period.

Similarly, when the initiating plasma hemispheroid was placed on the cathode a well defined anode-directed streamer was formed. The time evolution of the on-axis electron density and the axial field component for this case are shown in Fig. 23. The behavior of the anode-directed streamer with photoionization is similar to that of the cathode-directed streamer under corresponding conditions. Differences between the two are similar to differences observed for streamers without photoionization, but with preionization. Primarily, the anode-directed streamer propagates faster, has a lower field enhancement, and leaves behind a lower electron density than does a cathode-directed streamer. Additionally, the shielding inside the anode-directed streamer is not as complete.

5. Laser-Streamer Interaction

Bettis and Guentner [6], and Dougal and Williams [7] have shown that the laser-streamer interaction plays an important role in laser-triggered breakdown in the conventional, striking-the-electrode geometry. Accordingly, we have carried out several

resulting in better shielding inside the streamer body and in higher field enhancement just ahead of the streamer. Third, after the initial setup time, the shape of the streamer front stays nearly constant with time, although the propagation velocity increases. Similarly, the range of the field enhancement increases, but more slowly than in the case with preionization (see Fig. 1).

Insight into the reasons for this behavior can be obtained from Fig. 21 which shows the radial dependence of the electron density and axial field component at a fixed time, 1.5 ns, at a fixed distance from the anode, 1.95 mm, for the two cases. The increased field enhancement observed ahead of the streamer with photoionization can not be explained by simple shape effects at the streamer tip, since the widths of the streamers with and without photoionization are nearly the same. Instead, it appears that the increased field enhancement is due to the better shielding inside the streamer body. For a fixed potential drop across the spark gap, the lower the average field inside the streamer, the higher must be the field ahead of it.

The relatively constant shape of the streamer front is due primarily to the importance of photoionization well ahead of the streamer in determining streamer properties. With preionization, the shape of the front is constantly changing due to avalanching in the applied field of the preionization density far ahead of the streamer, and due to a steadily increasing range of the streamer foot due to enhanced avalanching in the weakly enhanced field in advance of the streamer head. With only photoionization,

4. Photoionization Effects

We have carried out initial calculations in which photoionization of the gas ahead of the propagating streamer by emission from the streamer head was explicitly included. In these calculations no initial preionization density was assumed. The model for the preionization process was based on the experimental results of Penny and Hummert [5] for technical grade nitrogen. Basically, these results provide a prescription for determining the photoionization rate at a point in the gas based on the current density at and distance to other points in the gas. In all calculations the streamer was initiated by a plasma hemispheroid of radius 0.27 mm in the z-direction and 0.065 mm in the radial direction. The applied field was 60 kV/cm, the fill gas was nitrogen at 760 Torr, and both anode and cathode-directed streamers were simulated.

When the initiating plasma hemispheroid was placed on the anode, a well defined cathode-directed streamer was formed. Figure 19 shows the on-axis electron density and axial field component, respectively, for this case and several different times. For comparison, Fig. 20 shows the electron density and axial field component for the two cases (photoionization without preionization, and preionization of 10^8 cm^{-3} without photoionization) at a fixed time of 1.5 ns. Several points are evident from these results. First, the drop in electron density ahead of the streamer is truly precipitous in the photoionization case in comparison to the case with preionization. Second, the electron density inside the body of the streamer is somewhat higher,

2. Experimental Results

Taking the potential of the electrode with the trigger pin in it to be zero, there are four possible polarity configurations for a trigatron gap; trigger pin positive or negative, and main gap polarity positive or negative. The voltage pulse on the trigger pin tends to decrease the field in the main gap in two cases, and to increase it in the other two. Voltage oscillograms showing the voltage on the trigger pin for the four cases are shown in Fig. 32. In these experiments a relatively long (800 ns) charging cable was used to supply current to the main gap. We found that the trigger gap always broke down before the main gap in all the experiments we conducted. This finding is opposite to that of Shkuropat, but is not necessarily contradictory because the voltages and dimensions involved in the two cases differed substantially.

A streak photograph of the early stages of trigatron breakdown is shown in Fig. 33. For streak photography, a very short charging cable (5 ns) was used to supply voltage to the main gap. In the case shown, the trigger pin was driven positive relative to the adjacent electrode, and the opposite main gap electrode was charged negative. The bright feature at the bottom of the photo is the trigger spark. A weak luminous front is clearly seen in this photo propagating from the trigger spark towards the cathode at a speed of 5×10^7 cm/s. We attribute this front to the passage of a cathode-directed streamer. Upon arrival of this front at the cathode, the heating phase sets in, and is characterized first by the very rapid propagation of a second luminous

front in the opposite direction from cathode to anode, followed by further heating and eventually intense optical emission. There is a weak, nearly vertical band in the upper left corner of the photo which is an artifact produced by scattering of electrons originating from the intense, but out-of-time-frame emission from the spark.

To the eye, the breakdown under these conditions seemed to consist of a narrow, constricted spark channel, perhaps surrounded by a weak, blue, diffuse glow. Under other conditions, not well established, no luminous front attributable to a streamer was seen in the streak photographs, and breakdown appeared to the eye to consist of the formation of a weak, blue or violet, diffuse glow of perhaps 1.0 cm diameter, extending across the gap. Although more work is needed, we believe these two conditions correspond to the streamer and photoionization mechanisms of trigatron breakdown discussed above. In the first case, conditions were appropriate to launch a streamer, either from the trigger spark plasma, or perhaps from the field distortion around the trigger pin. Photoionization may also have contributed to gap current, and may have acted to speed the propagation of the streamer, but the current due to photoionization was not sufficient to collapse the gap voltage before the streamer had traversed the gap. In the second case, either conditions were not appropriate for launching a streamer, or the streamer has not traveled a significant distance across the gap before the gap voltage started to collapse due to the current flow caused by the photoionization.

III. References

1. S.K. Dhali and P.F. Williams, "Excited State Spectroscopy of Electrically Excited Gases", Project No. 5, Final Report on AFOSR Contract No. 49620-79-C-0191, February 27, 1984.
2. A.J. Davies, C.S. Davies, and C.J. Evans, Proc. IEE 118, 816 (1971).
3. J. Dutton, J. Phys. Chem, Ref. Data 4 (1965).
4. E.D. Lozanskii and D.B. Pontekorvo, Zh. Tech. Fiz. 44, 2322 (1974); English translation in Sov. Phys. Tech. Phys. 19, 1432 (1975).
5. G.W. Penny and G.T. Hummert, J. Appl. Phys. 41, 572 (1970).
6. J.R. Bettis and A.H. Guenther, IEEE J. Quant. Elect. QE-6, 483 (1970).
7. R.A. Dougal and P.F. Williams, J. Phys. D: Appl. Phys. 17, 903 (1984).
8. C.G. Morgan, Rep. Prog. Phys. 38-2, 621, (1975).
9. N. Kroll and K. Watson, Phys. Rev. A 5, 1883, (1972).
10. P.I. Shkuropat, Zh. Tech. Fiz. 39 1256 (1969), English translation in Sov. Phys. Tech. Phys. 14, 943 (1970).

FIGURE CAPTIONS

1. Results for 60 kV/cm, cathode-directed streamer
 - a. On-axis electron density at 0.0, 0.5, 1.0, 1.5, 2.0, and 2.5 ns, respectively;
 - b. On-axis axial electric field component at same times;
 - c. Contour plot showing axial and radial dependence of electron density at $t = 1.5$ ns.
2. Results for 52 kV/cm, cathode-directed streamer
 - a. On-axis electron density at 0.0, 1.0, 2.0, 2.5, 3.0, and 3.5 ns, respectively;
 - b. On-axis axial electric field component at same times;
 - c. Contour plot showing axial and radial dependence of electron density at 2.5 ns.
3. Results for 44 kV/cm, cathode-directed streamer
 - a. On-axis electron density at 0.0, 1.0, 2.0, 3.0, 4.0, and 5.0 ns, respectively;
 - b. On-axis axial electric field component at same times;
 - c. Contour plot showing axial and radial dependence of electron density at 4.0 ns.
4. Results for 36 kV/cm, cathode-directed streamer. There is substantial numerical error in these results.
 - a. On-axis electron density at 0.0, 2.0, 4.0, and 6.0 ns, respectively;
 - b. On-axis axial electric field component at same times.
5. Results for 60 kV/cm, anode-directed streamer
 - a. On-axis electron density at 0.0, 0.5, 1.0, 1.5, and 2.0 ns, respectively;
 - b. On-axis axial electric field component at same times;
 - c. Contour plot showing axial and radial dependence of electron density at 1.5 ns.
6. Results for 52 kV/cm, anode-directed streamer
 - a. On-axis electron density at 0.0, 1.0, 2.0, 2.5, and 3.0 ns, respectively;
 - b. On-axis axial electric field component at same times;
 - c. Contour plot showing axial and radial dependence of electron density at 2.5 ns.
7. Results for 44 kV/cm, anode-directed streamer.
 - a. On-axis electron density at 0.0, 1.0, 2.0, 3.0, 4.0, and 5.0 ns, respectively;
 - b. On-axis axial electric field component at same times;
 - c. Contour plot showing axial and radial dependence of electron density at 4.0 ns.
8. Results for 36 kV/cm, anode-directed streamer.
 - a. On-axis electron density at 0.0, 2.0, 4.0, 6.0, and 8.0 ns, respectively;
 - b. On-axis axial electric field component at same times.

9. Phase velocity vs. preionization electron density ahead of the streamer for
 - a. cathode-directed streamers
 - b. anode-directed streamers.
10. Phase velocity vs preionization electron density ahead of the streamer for two different starting preionization densities.
 - a. cathode-directed streamer;
 - b. anode-directed streamer.
11. Results for 60 kV/cm, cathode directed streamer with initial preionization density 10^6 cm^{-3} .
 - a. On-axis electron density for 0.0, 0.5, 1.0, 1.5, 2.0, and 2.5 ns, respectively;
 - b. On-axis electron density for 0.0, 0.5, 1.0, 1.5, 2.0, and 2.5 ns, respectively
12. Results for 60 kV/cm, cathode-directed streamer initiated by plasma hemispheroid of density 10^{13} cm^{-3} .
 - a. On-axis electron density at 0.1, 1.0, 1.5, 2.0, 2.5, and 2.8 ns, respectively;
 - b. On-axis axial electric field component at same times.
13. Results for 60 kV/cm, cathode-directed streamer initiated by plasma hemispheroid of density 10^{15} cm^{-3} .
 - a. On-axis electron density at 0.05, 0.5, 1.0, 1.25, and 1.7 ns, respectively;
 - b. On-axis axial electric field component at same times.
14. Plots showing results for 60 kV/cm, cathode-directed streamers initiated by 10^{15} , 10^{14} , and 10^{13} cm^{-3} , respectively. Times were 1.0, 1.5, and 2.3 ns.
 - a. On-axis electron density;
 - b. On-axis axial electric field component.
15. Results for 52 kV/cm, cathode-directed streamer initiated by plasma hemispheroid with radial diameter of 0.068 mm.
 - a. On-axis electron density at 0.0, 1.0, 2.0, 2.5, 3.0, and 3.5 ns, respectively;
 - b. On-axis axial electric field component at same times.
16. Contour plots for streamer shown in Fig. 15 at
 - a. 1.5 ns
 - b. 2.0 ns
 - c. 2.5 ns
 - d. 3.0 ns
17. Results for 52 kV/cm, cathode-directed streamer initiated by plasma hemispheroid with radial diameter of 0.147 mm.
 - a. On-axis electron density at 0.0, 1.0, 2.0, 2.5, 3.0, and 3.3 ns, respectively;
 - b. On-axis axial electric field component at same times.

18. Contour plots for streamer shown in Fig. 17 at
 - a. 1.5 ns
 - b. 2.0 ns
 - c. 2.5 ns
 - d. 3.0 ns
19. Results for 60 kV/cm, cathode-directed streamer with photoionization, but with no preionization.
 - a. On-axis electron density at 0.0, 0.5, 1.0, 1.5, 2.0, and 2.5 ns, respectively;
 - b. On-axis axial electric field component at same times.
20. Comparison of results
 1. with photoionization but without preionization, and
 2. without photoionization but with 10^8 cm^{-3} preionization at fixed time of 1.5 ns
 - a. On-axis electron density;
 - b. On-axis axial electric field component.
21. Comparison similar to that in Fig. 20, except showing radial dependence at point 1.95 mm from cathode.
 - a. electron density;
 - b. axial electric field component.
22. Comparison of relative magnitudes of source terms due to
 1. electron impact ionization, and
 2. photoionization for same streamer depicted in Fig. 20.
23. Results for 60 kV/cm, anode-directed streamer with photoionization, but without preionization.
 - a. On-axis electron density at 0.0, 0.5, 1.0, 1.5, and 2.2 ns, respectively;
 - b. On-axis axial electric field component at same times.
24. Results for 34 kV/cm, cathode-directed streamer with laser interaction at 0.5, 1.0, 2.0, 3.0, and 3.5 ns, respectively. Photoionization was included, but there was no preionization.
25. Results for 34 kV/cm, anode-directed streamer with laser interaction at 0.5, 1.0, 2.0, 3.0, and 3.75 ns, respectively. Photoionization was included, but there was no preionization.
26. Phase velocities for 60 kV/cm, cathode-directed streamer.
 1. contribution due the $\nabla \cdot \nabla$ term,
 2. contribution due to impact ionization term, and
 3. total "theoretical" phase velocity. The x's are "experimental" points.
27. Comparison of "theoretical" and "experimental" phase velocities for streamer in Fig. 1.

28. Comparison of "theoretical" and "experimental" phase velocities for streamer in Fig. 5.
29. Phase velocities for 36 kV/cm, cathode-directed streamer showing onset of numerical difficulties.
 1. "theoretical" without diffusion term,
 2. "theoretical" with diffusion term. Circles are "experimental" values.
30. Diagram showing electrode assembly used in trigatron studies described here. The protrusion of the trigger pin past the surface of the main electrode can be adjusted.
31. Electrical schematic of the trigatron system. The photoconductive switch is controlled by the output pulse at 1.06 μm of a Nd:YAG laser.
32. Oscillograms showing trigger pin voltage. Voltage scale is 2 kV/cm; horizontal scale is 50 ns/cm, except d) 200 ns/cm. Polarities are (trigger pin opposite main gap electrode):
 - a. -, -
 - b. +, -
 - c. -, +
 - d. +, +
33. Streak photograph of trigatron breakdown showing a streamer traversing the gap. The trigger pin is in the lower electrode and it was pulsed positive.

CATHODE DIRECTED

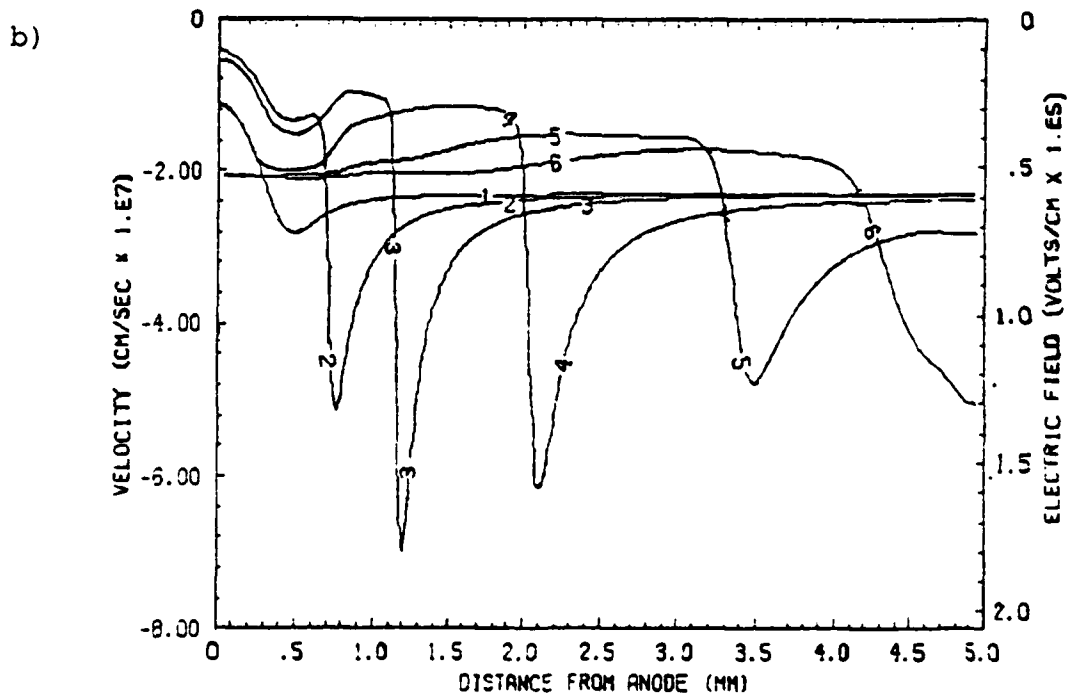
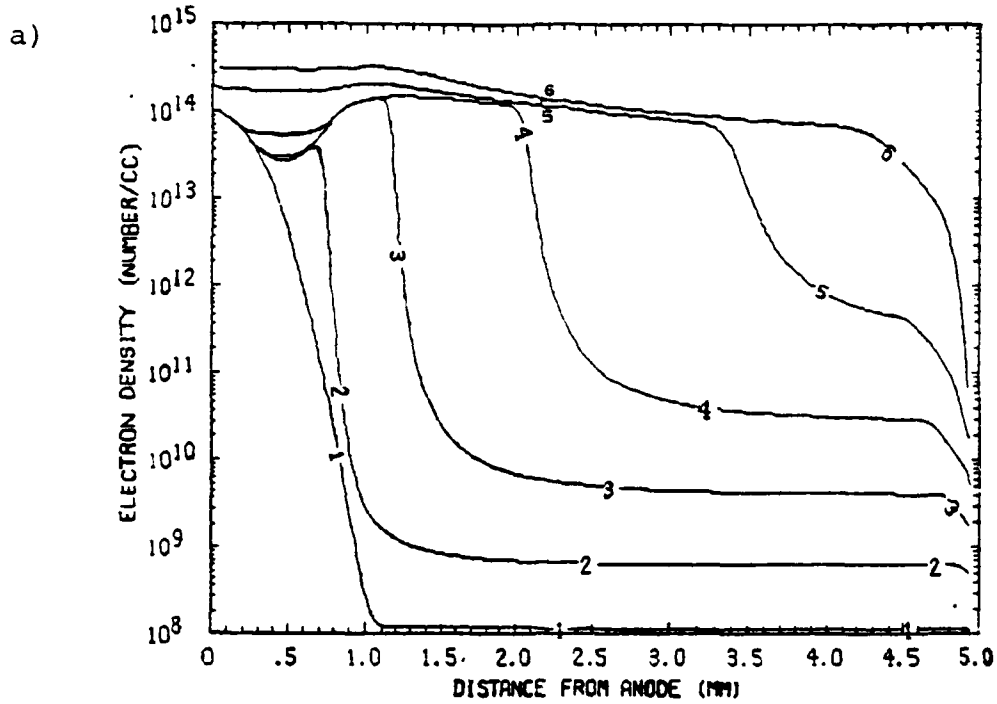
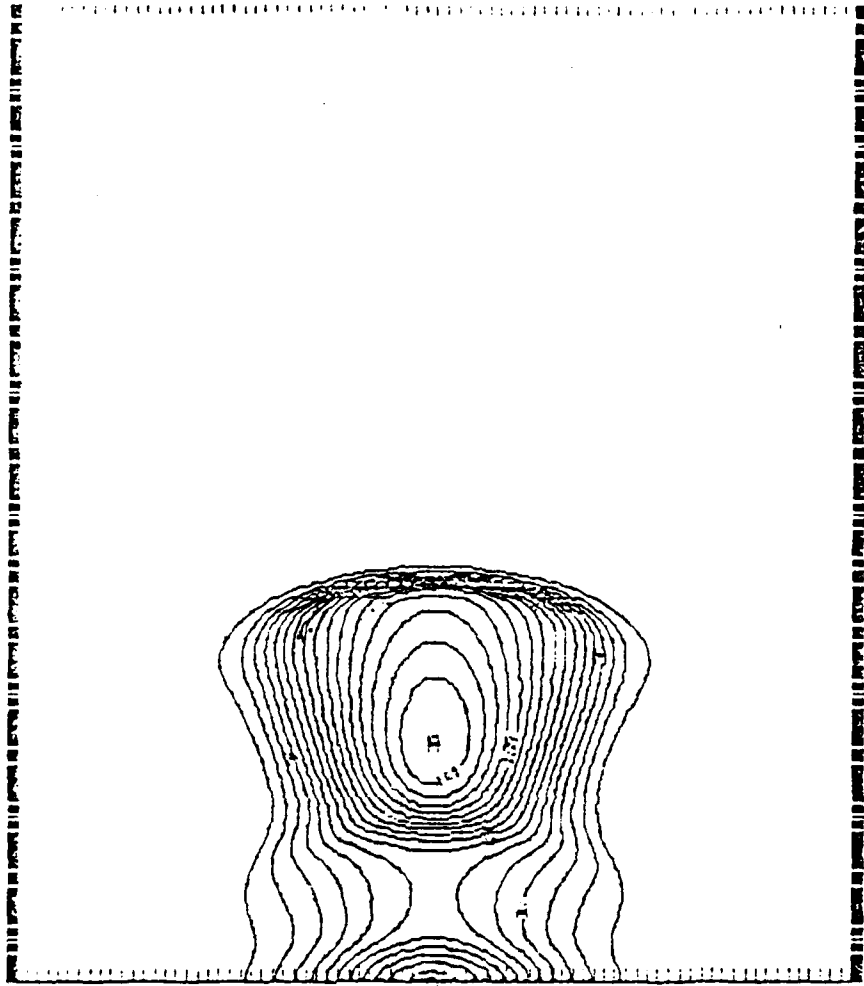


Figure 1

c)



105

Figure 1
(Continued)

CATHODE DIRECTED

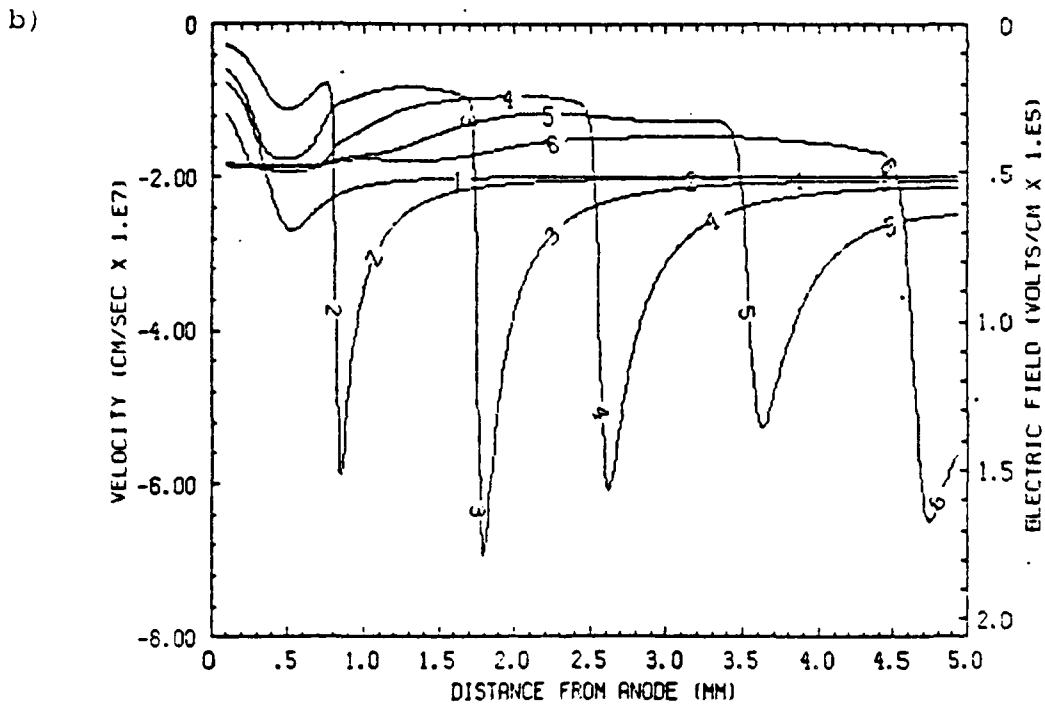
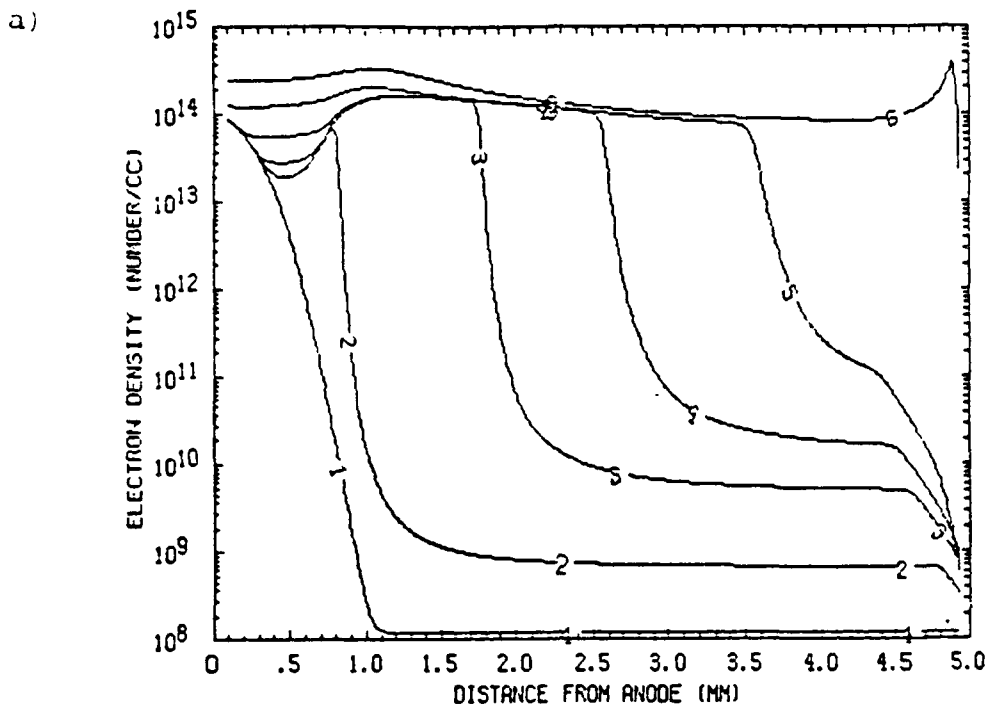
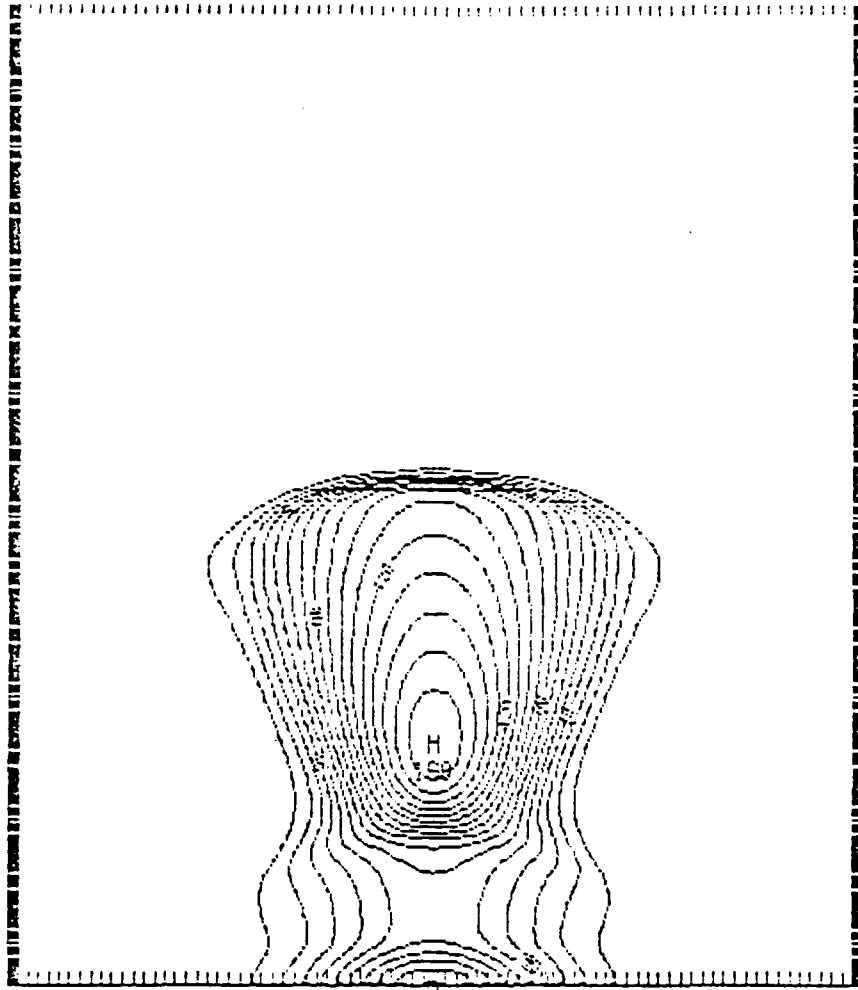


Figure 2

c)

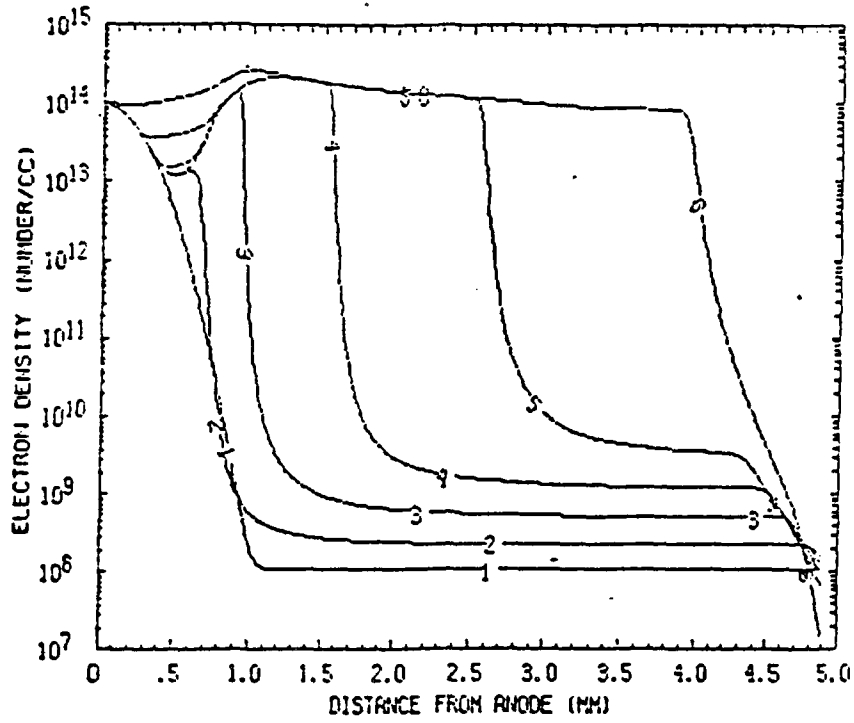


CONTOUR PLOT OF THE FUNCTION $f(x,y) = 100 - x^2 - y^2 + x^2y + xy^2$ WITH THE SADDLE POINT LOCUS SCALE BY 0.1000E-01

Figure 2
(Continued)

CATHODE DIRECTED

a)



b)

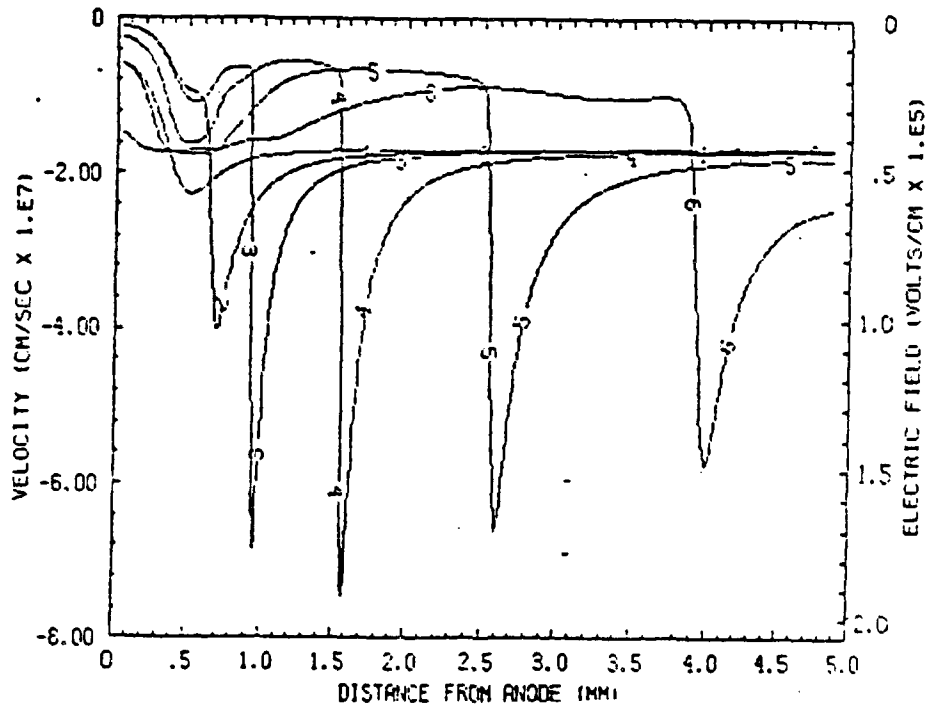
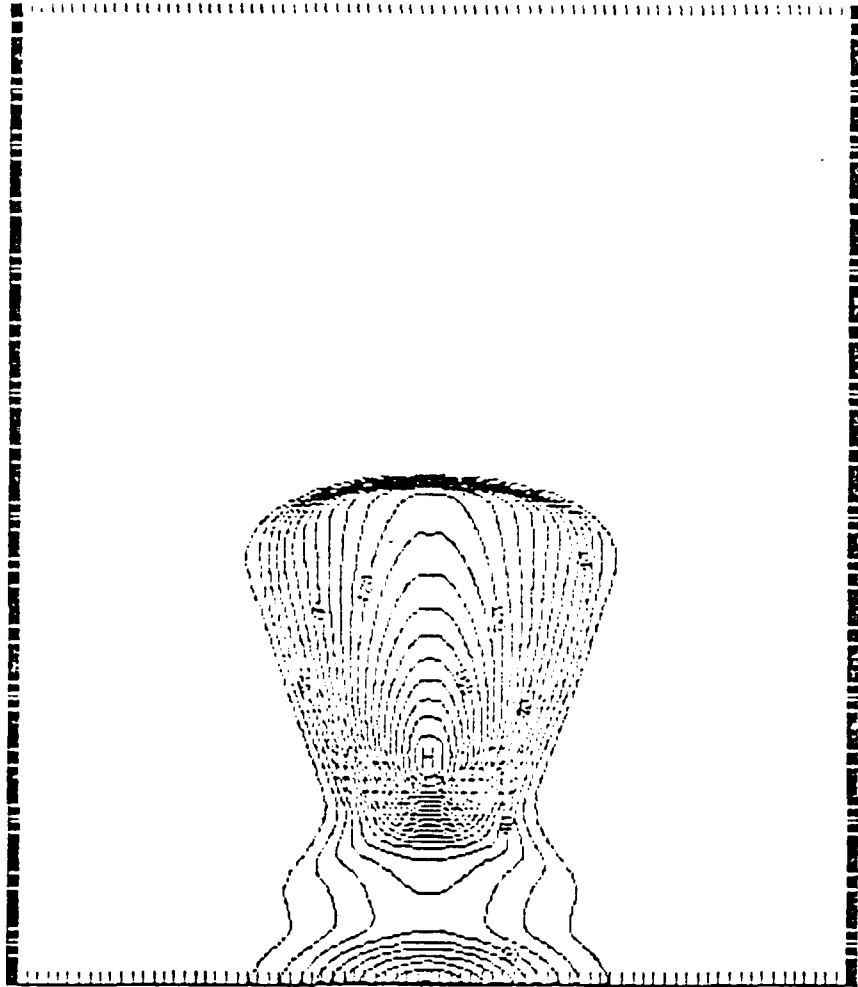


Figure 3

c)



99
0.00000E+00 TO 0.00000E+16 BY 0.00000E+01
0.00000E+00 TO 0.00000E+16 BY 0.00000E+01

Figure 3
(Continued)

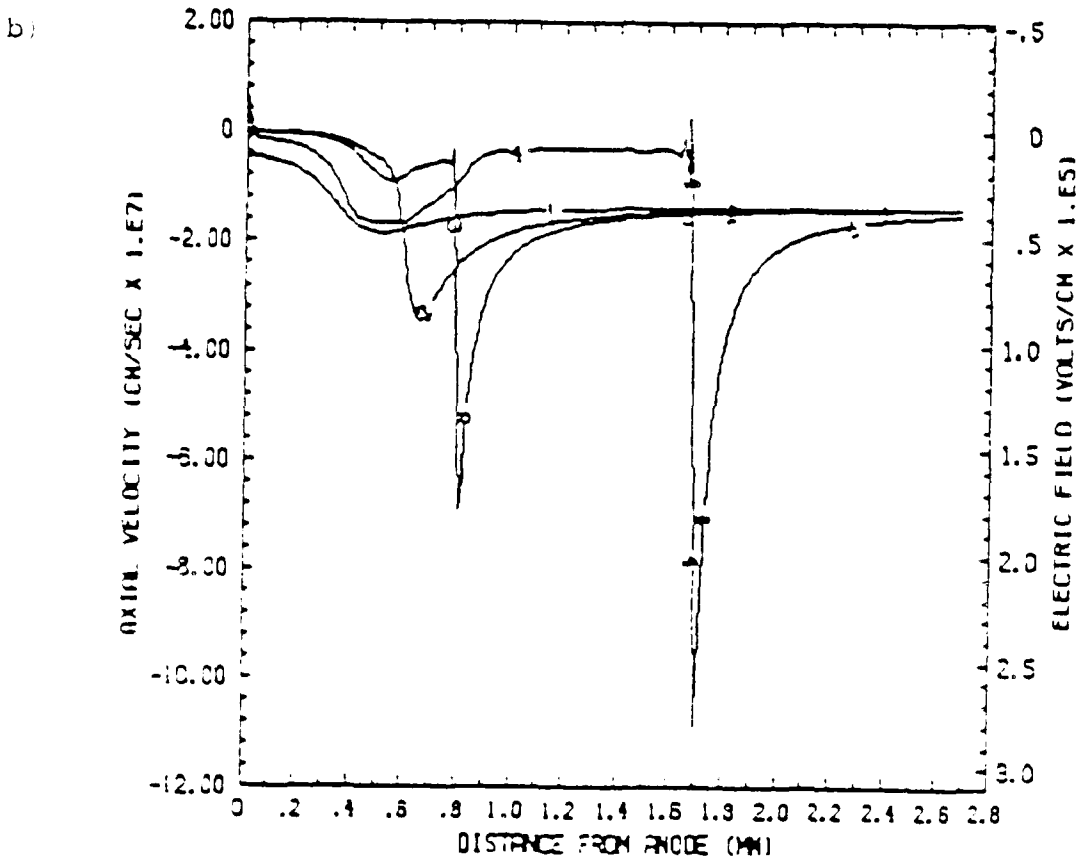
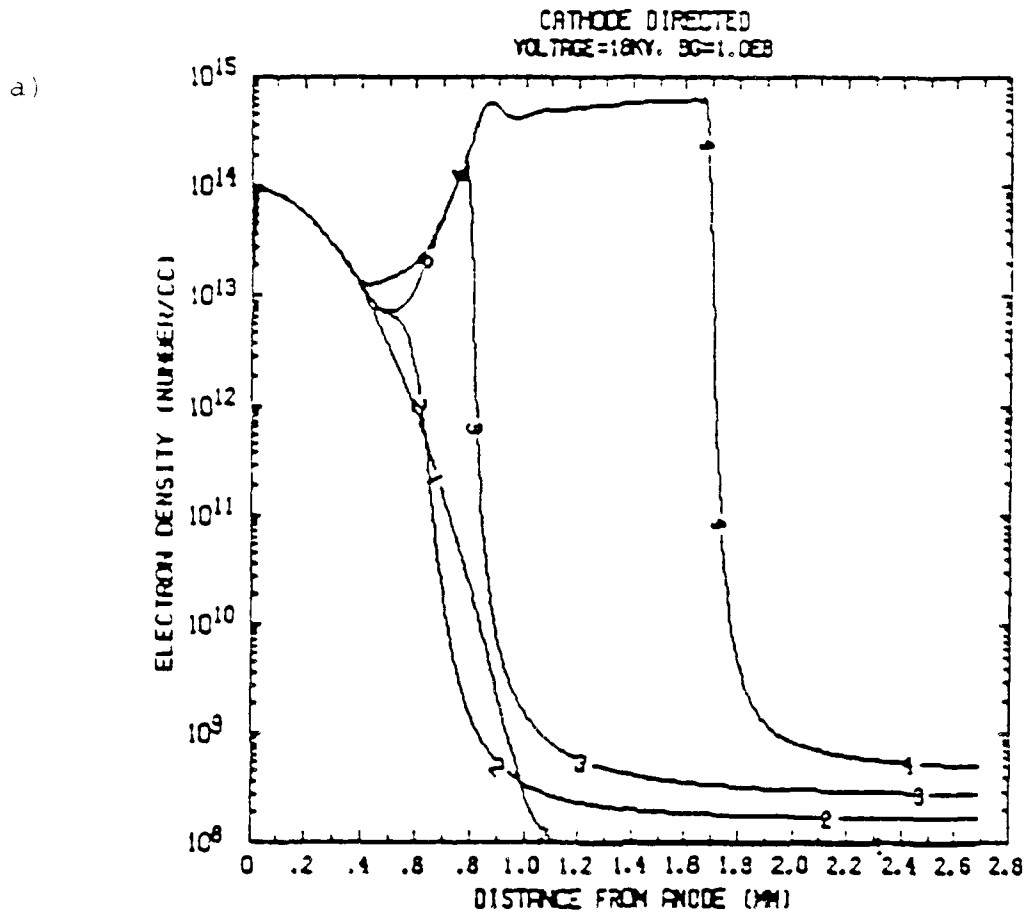
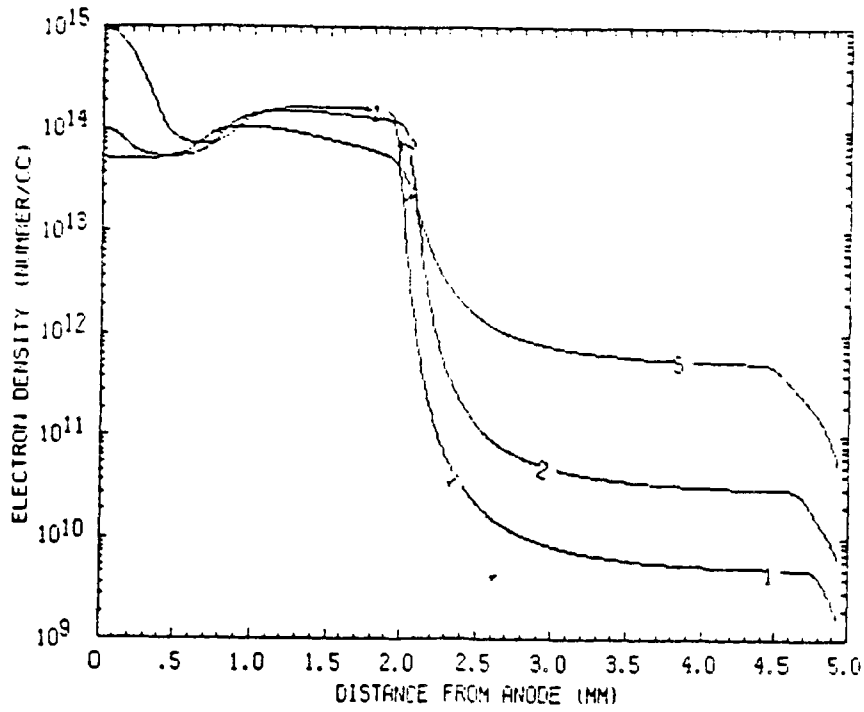


Figure 4

CATHODE DIRECTED

a)



b)

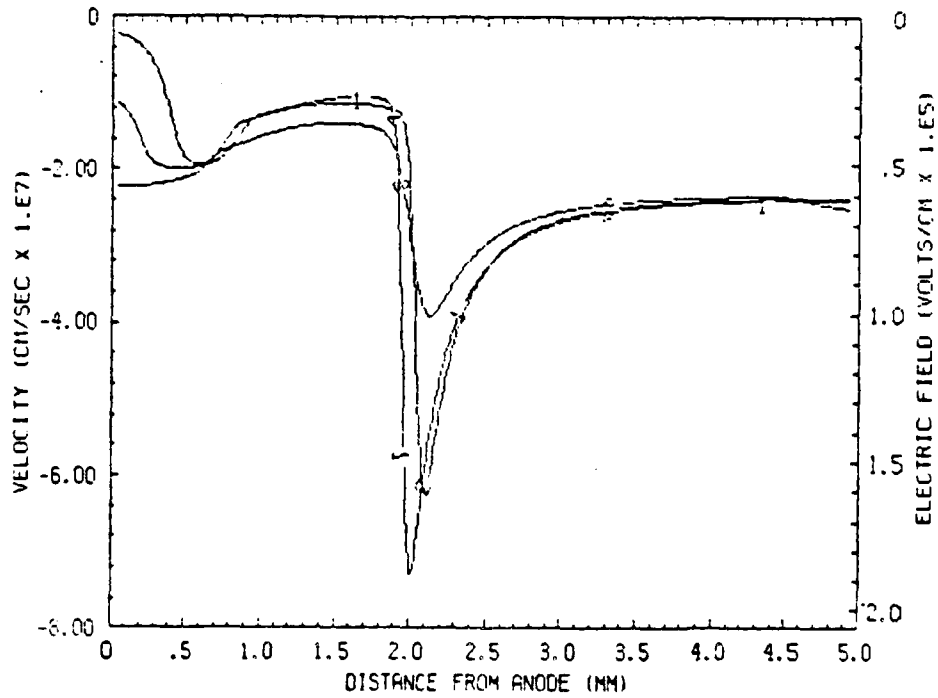


Figure 14

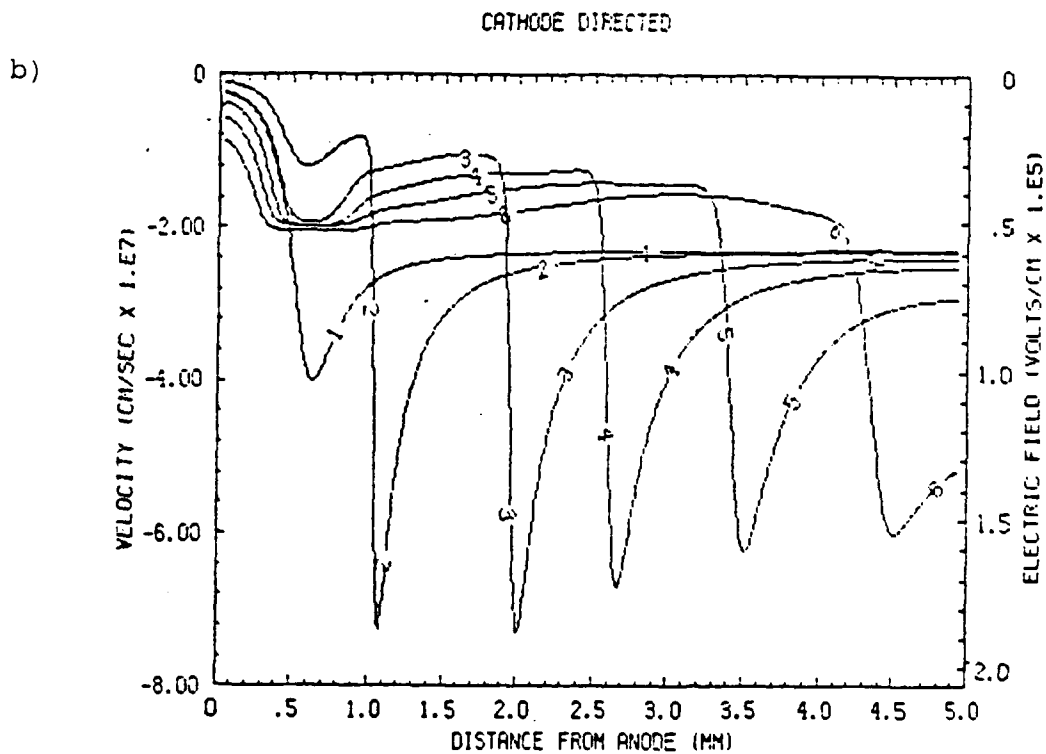
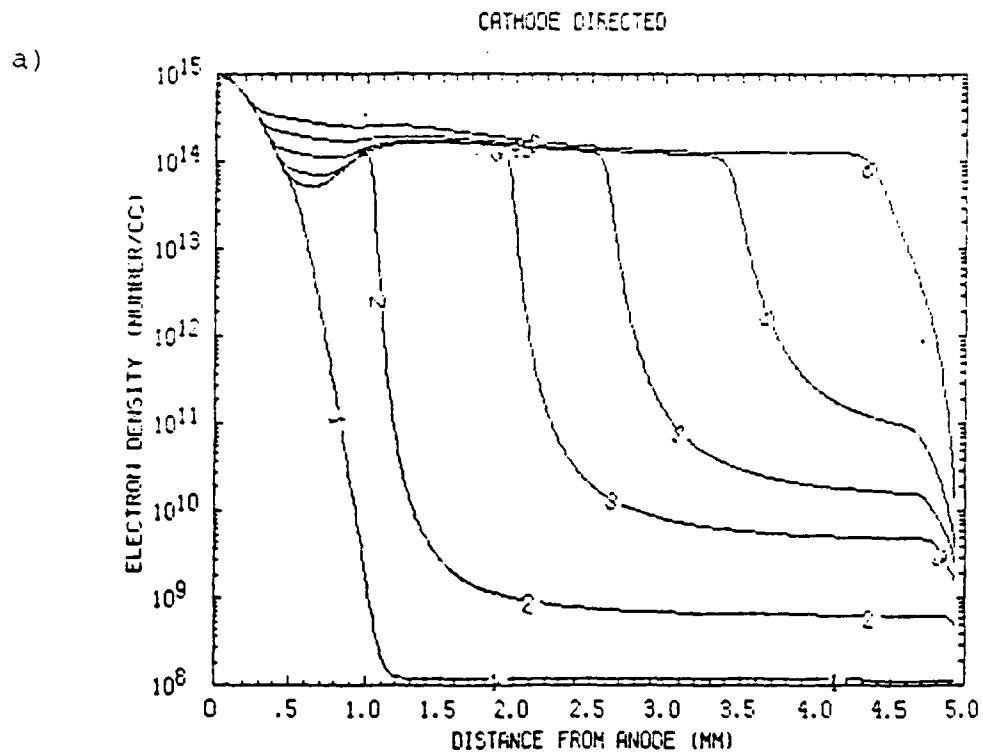
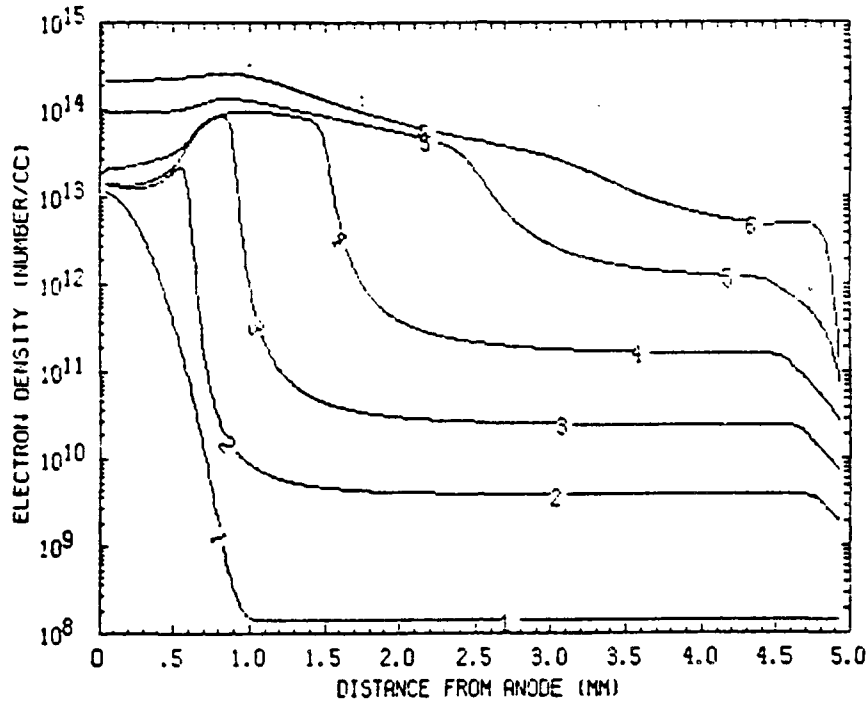


Figure 13

CATHODE DIRECTED

a)



b)

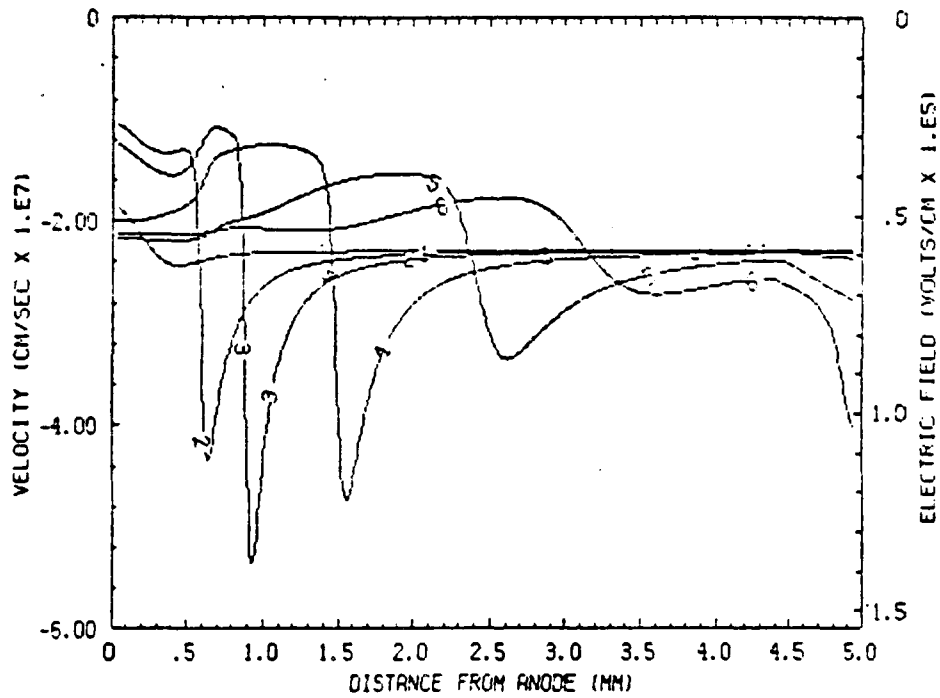
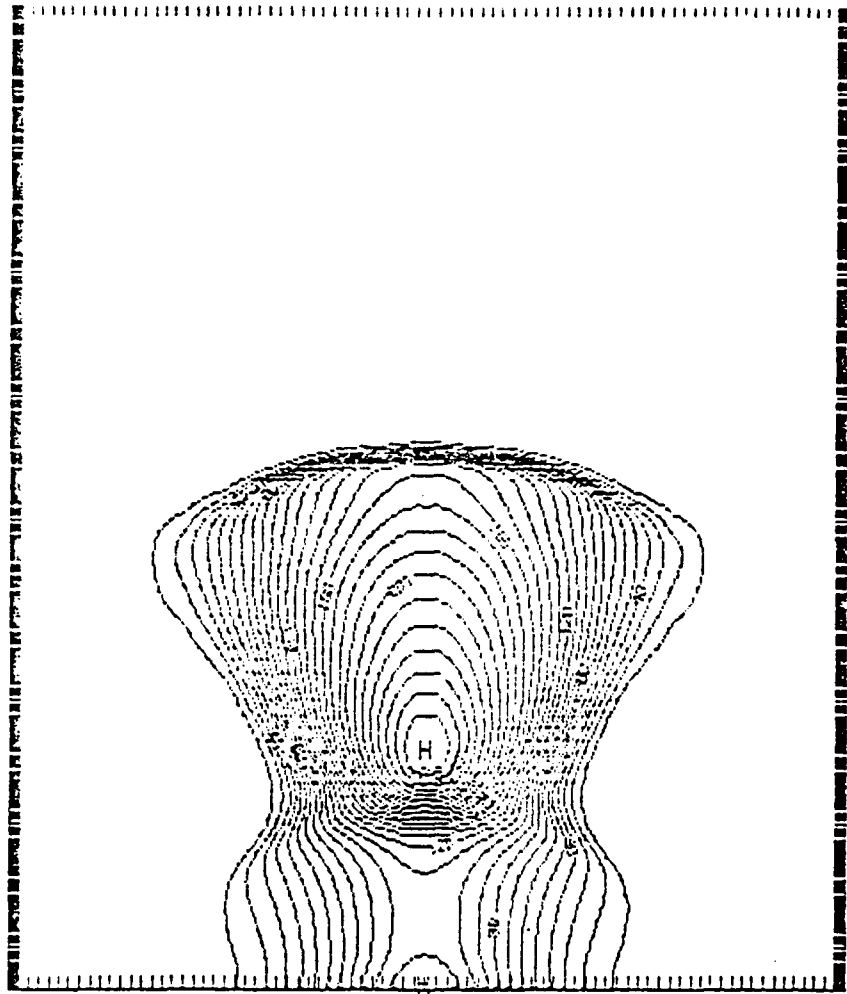


Figure 12

c)



120
CONT. OF FIG. 10. COORDINATE OF THE CENTER OF GRAVITY IN CM. OF THE POINTS OF THE FIGURE IS 1.0000E-14. THE COORDINATE OF THE CENTER OF GRAVITY IS 0.0000E+00. THE COORDINATE OF THE CENTER OF GRAVITY IS 0.0000E+00. THE COORDINATE OF THE CENTER OF GRAVITY IS 0.0000E+00.

Figure 11

(Continued)

CATHODE DIRECTED

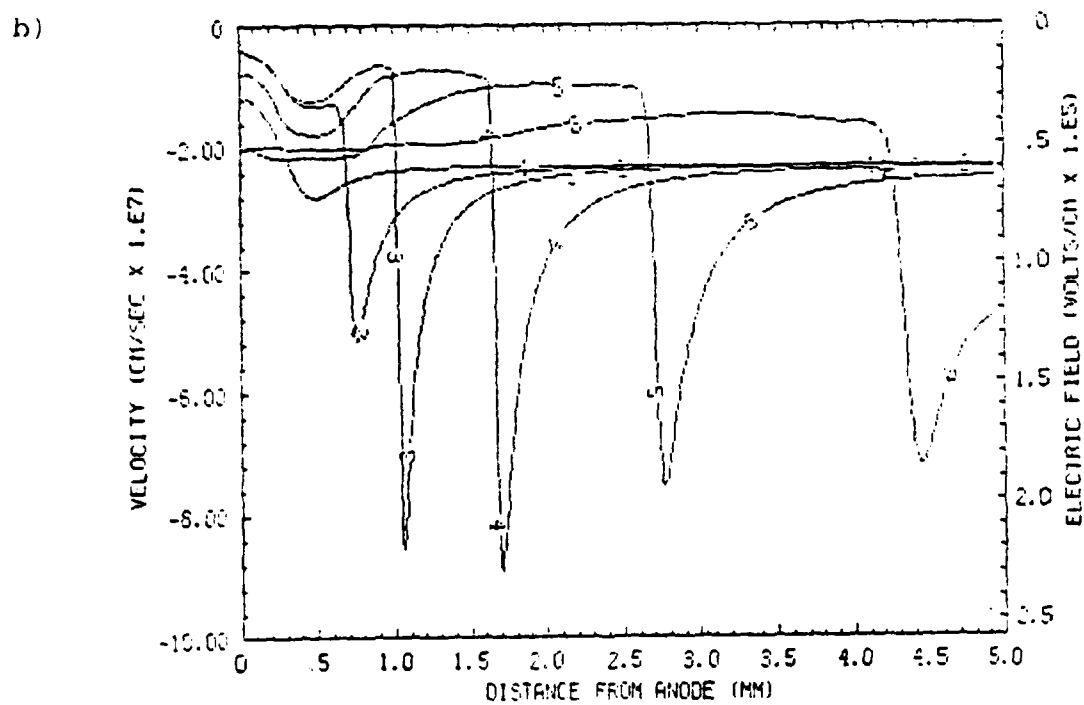
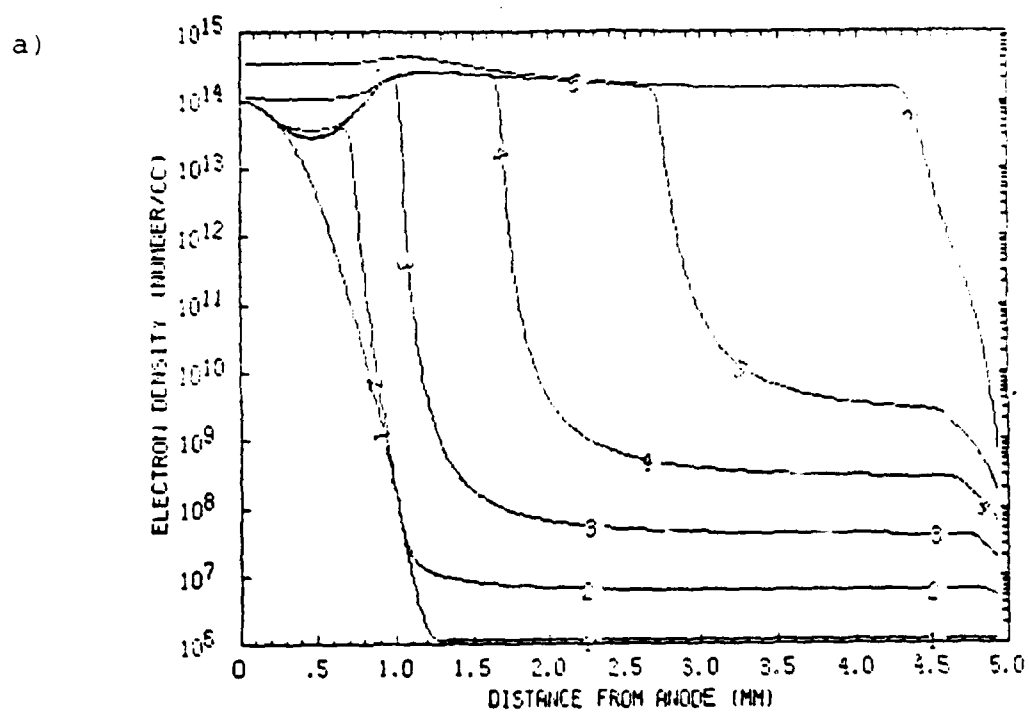


Figure 11

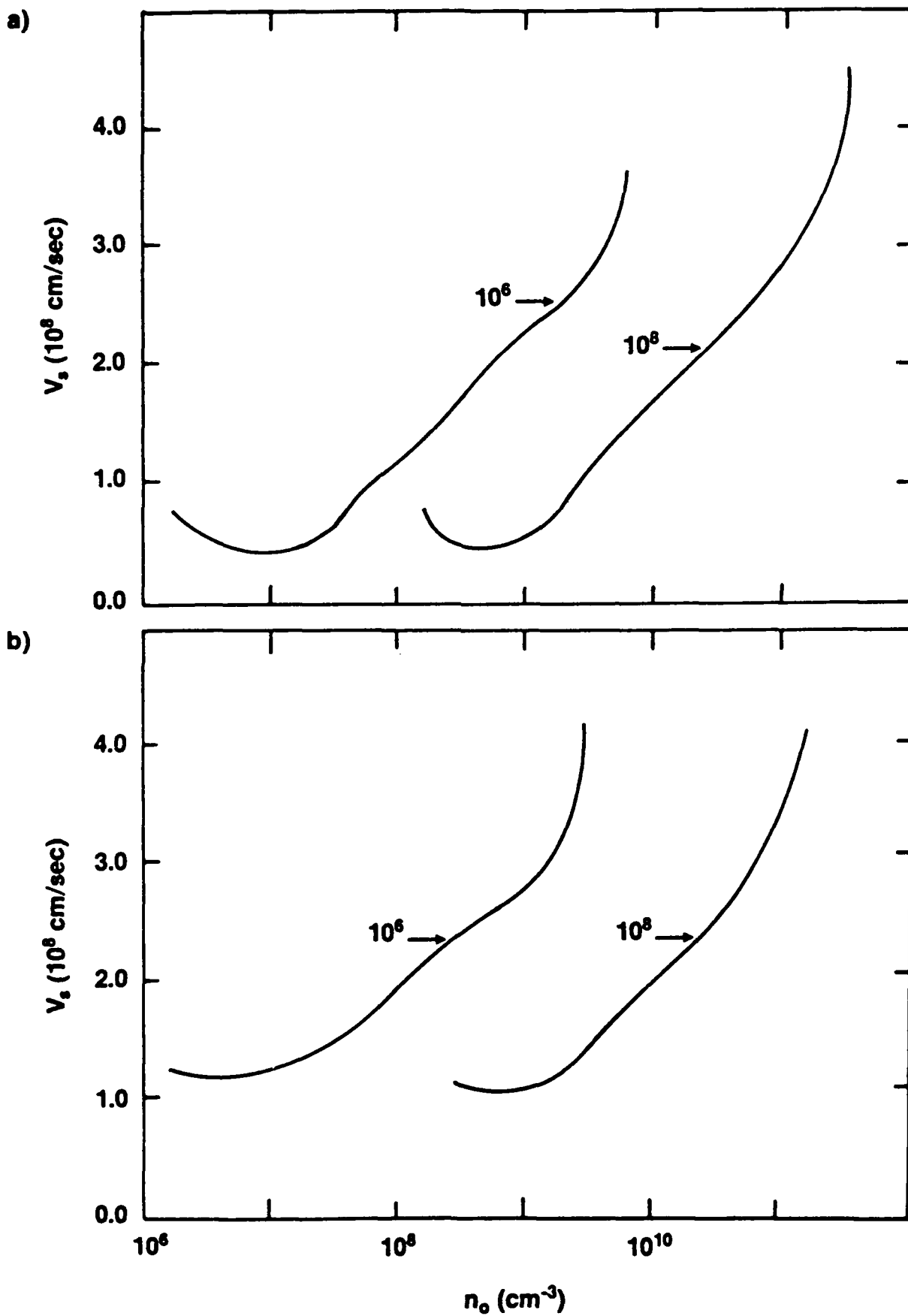
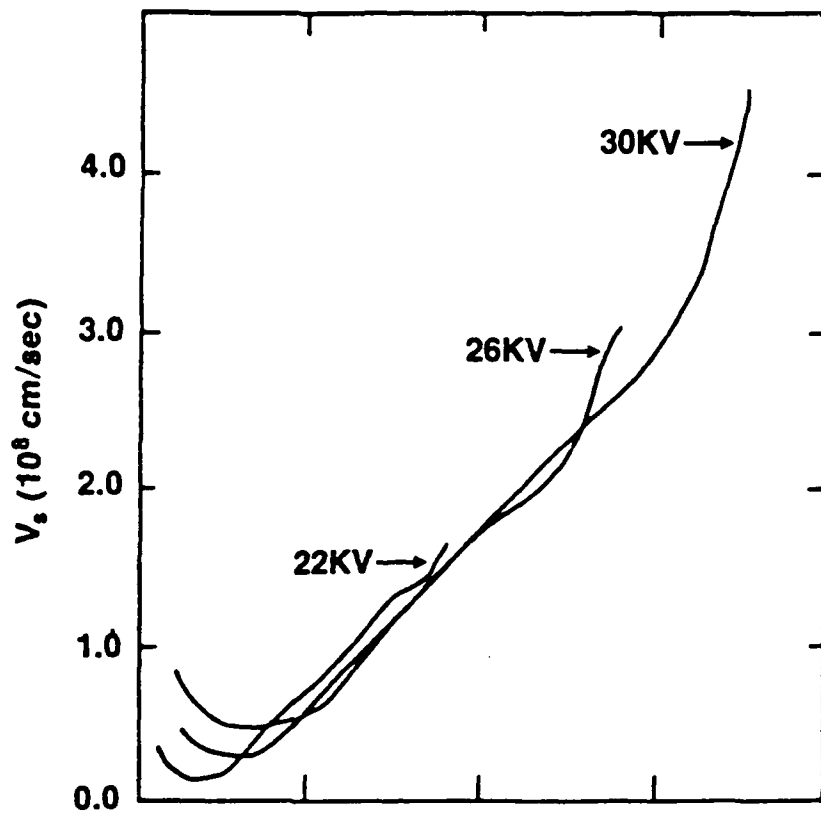


Figure 10

a)



b)

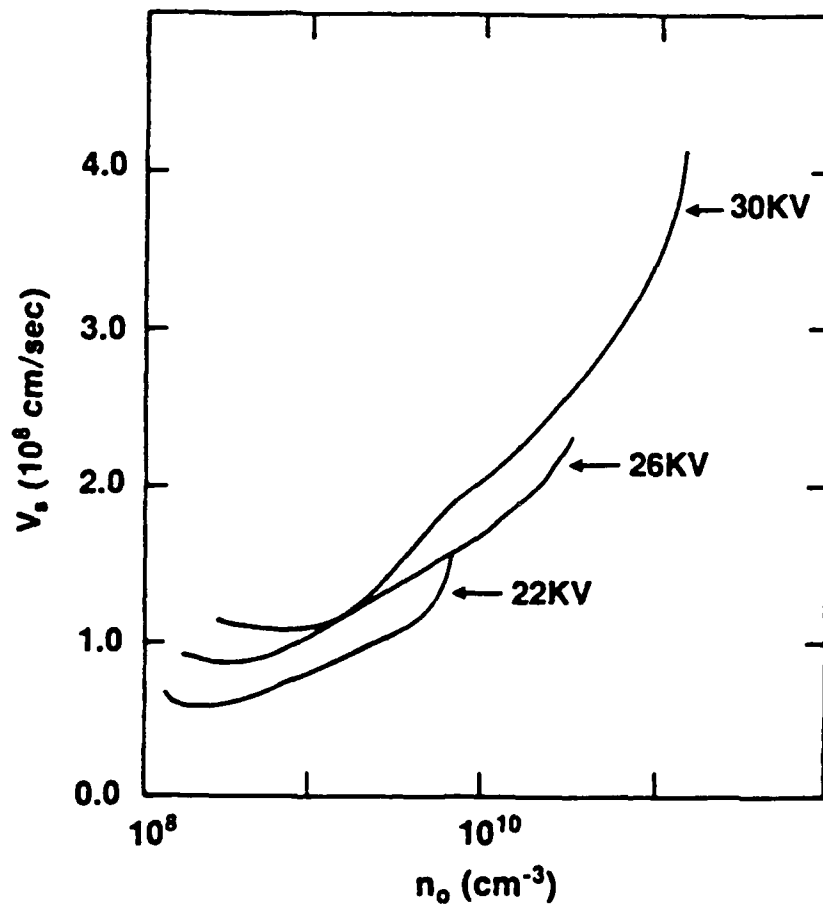


Figure 9

ANODE DIRECTED

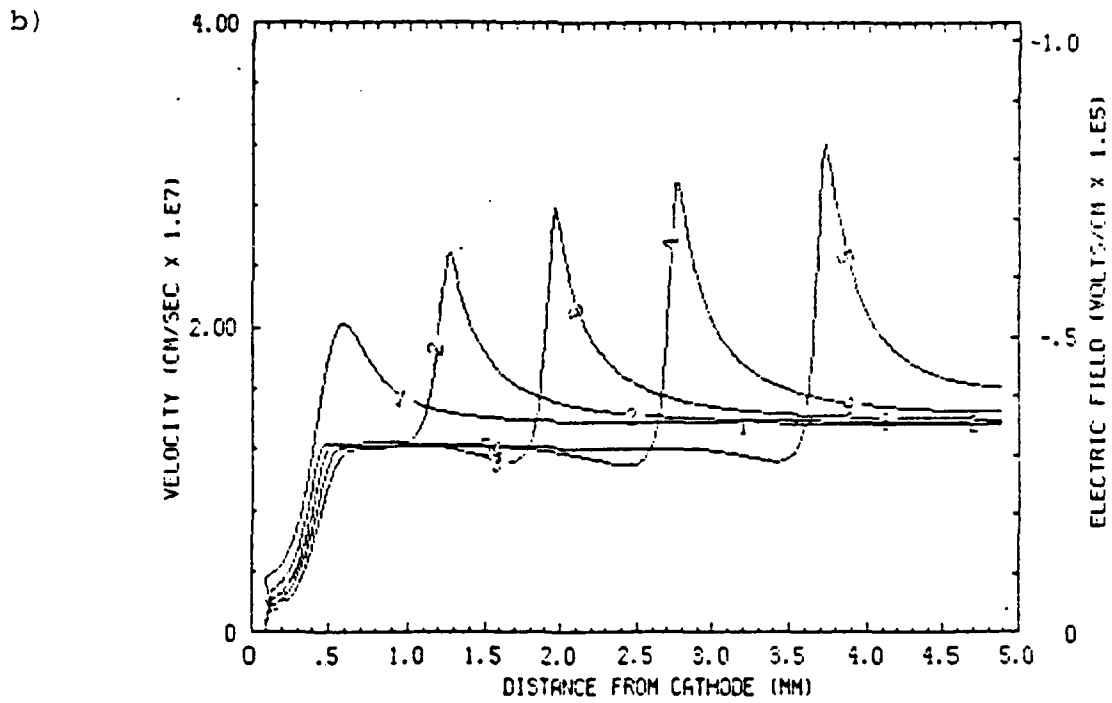
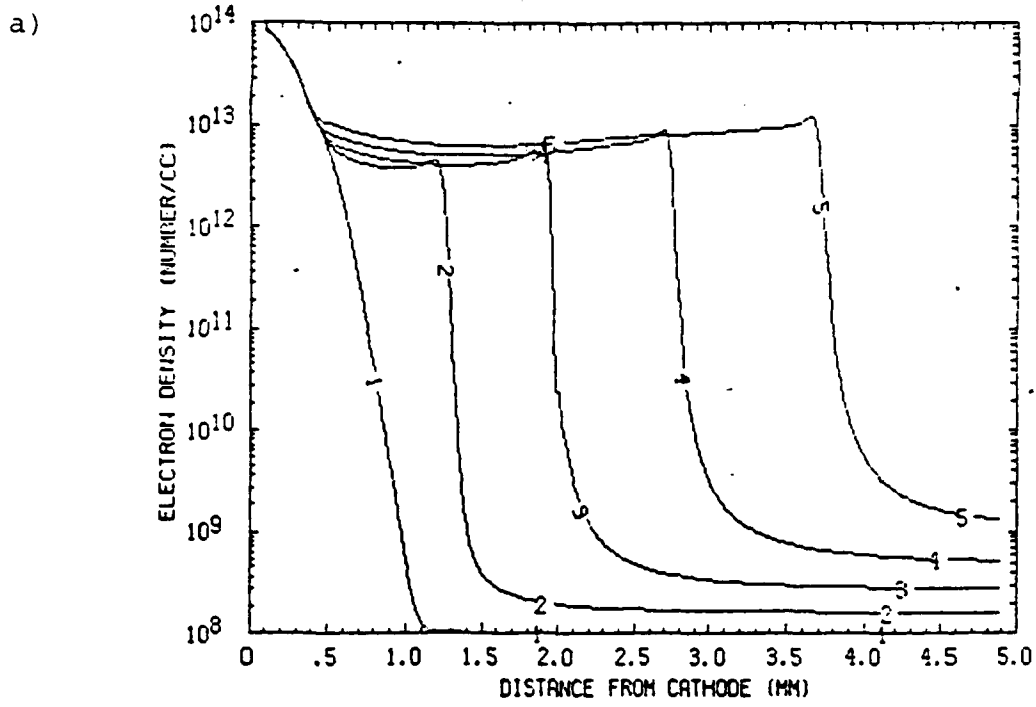


Figure 8

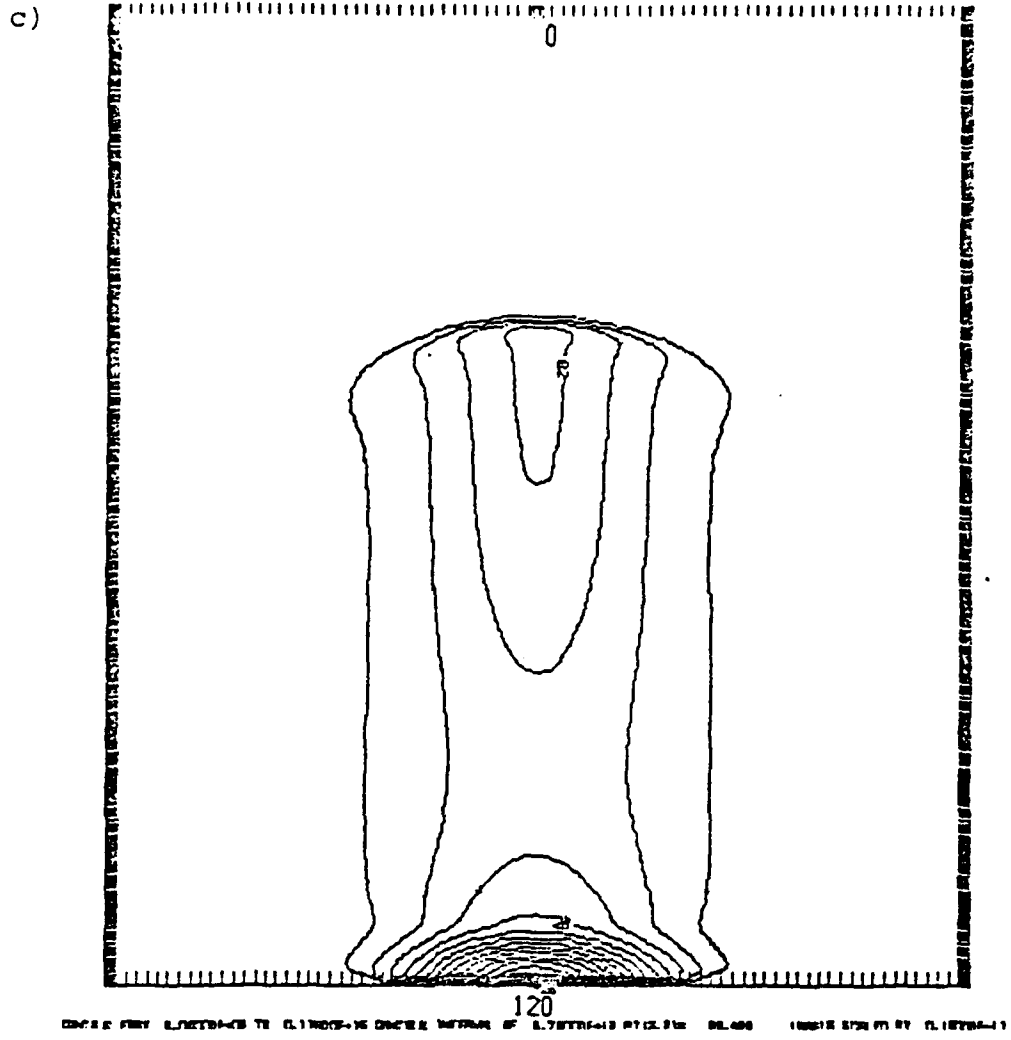


Figure 7
(Continued)

ANODE DIRECTED

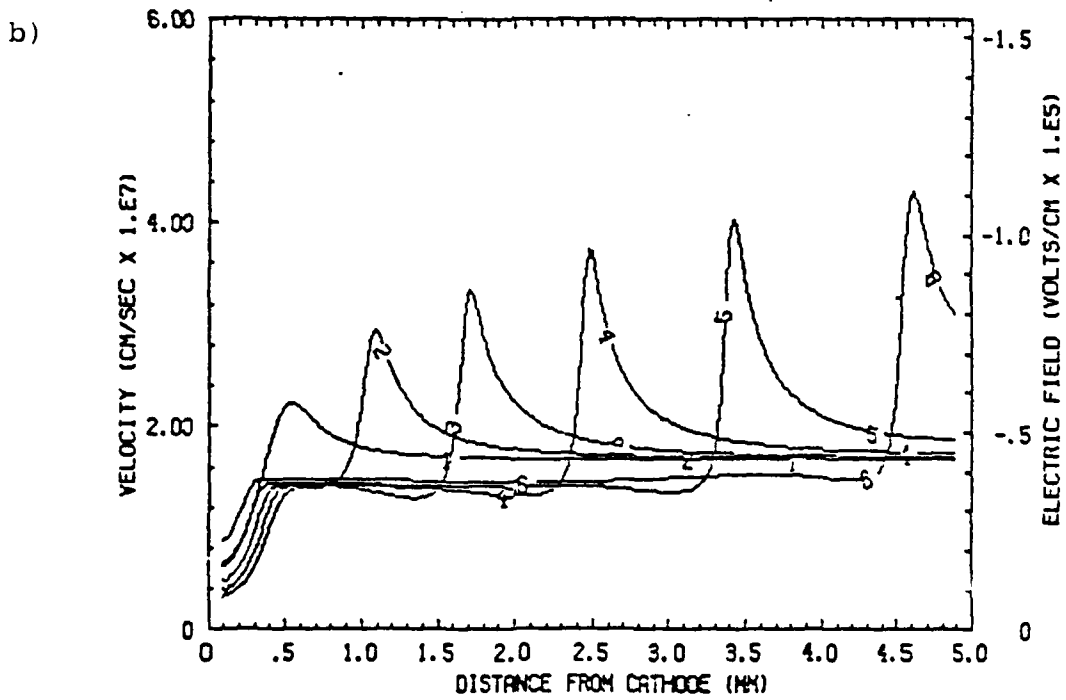
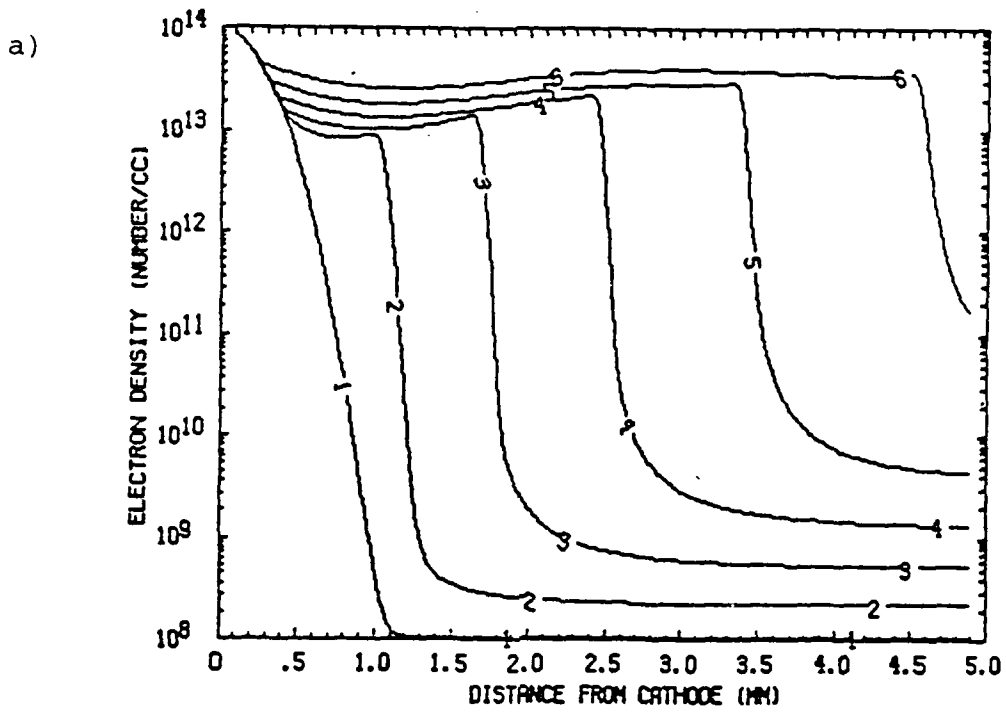
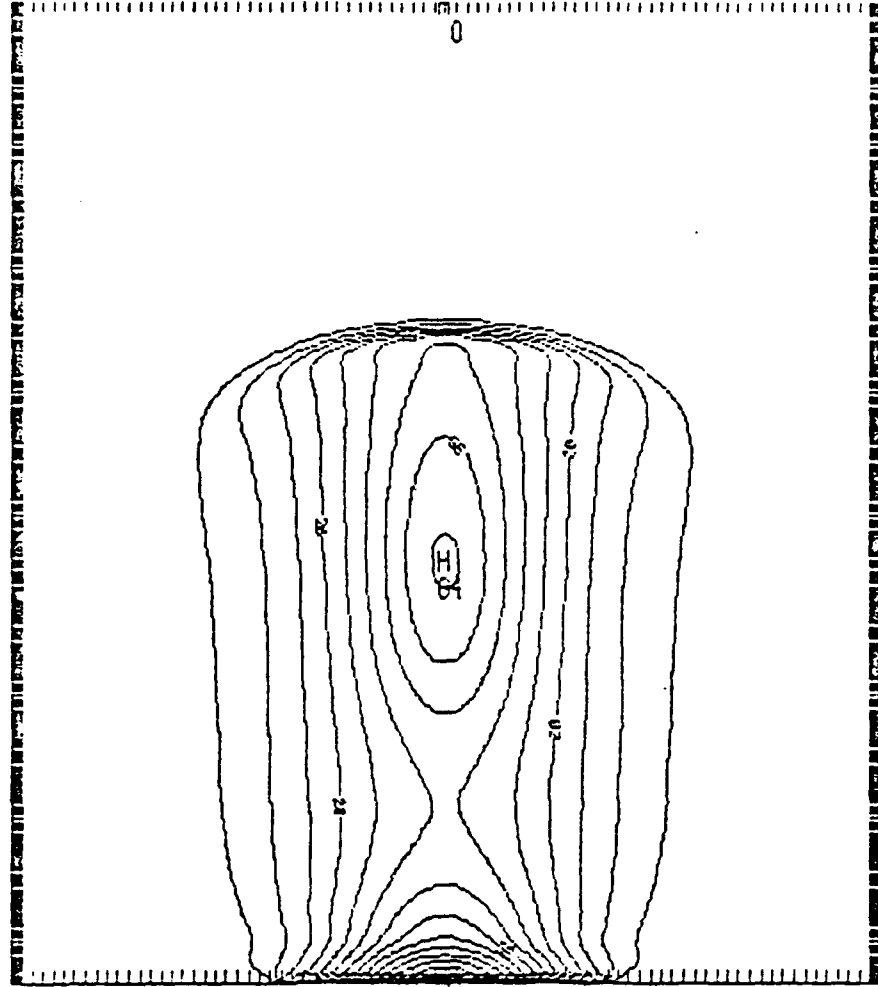


Figure 7

c)



122
DATA FROM 0.0000E+00 TO 0.1000E+16 CENTER INTERVAL OF 0.7000E+16 PT(10,21) 1981.2 LABELS SCALED BY 0.1000E+11

Figure 6
(Continued)

A NODE DIRECTED

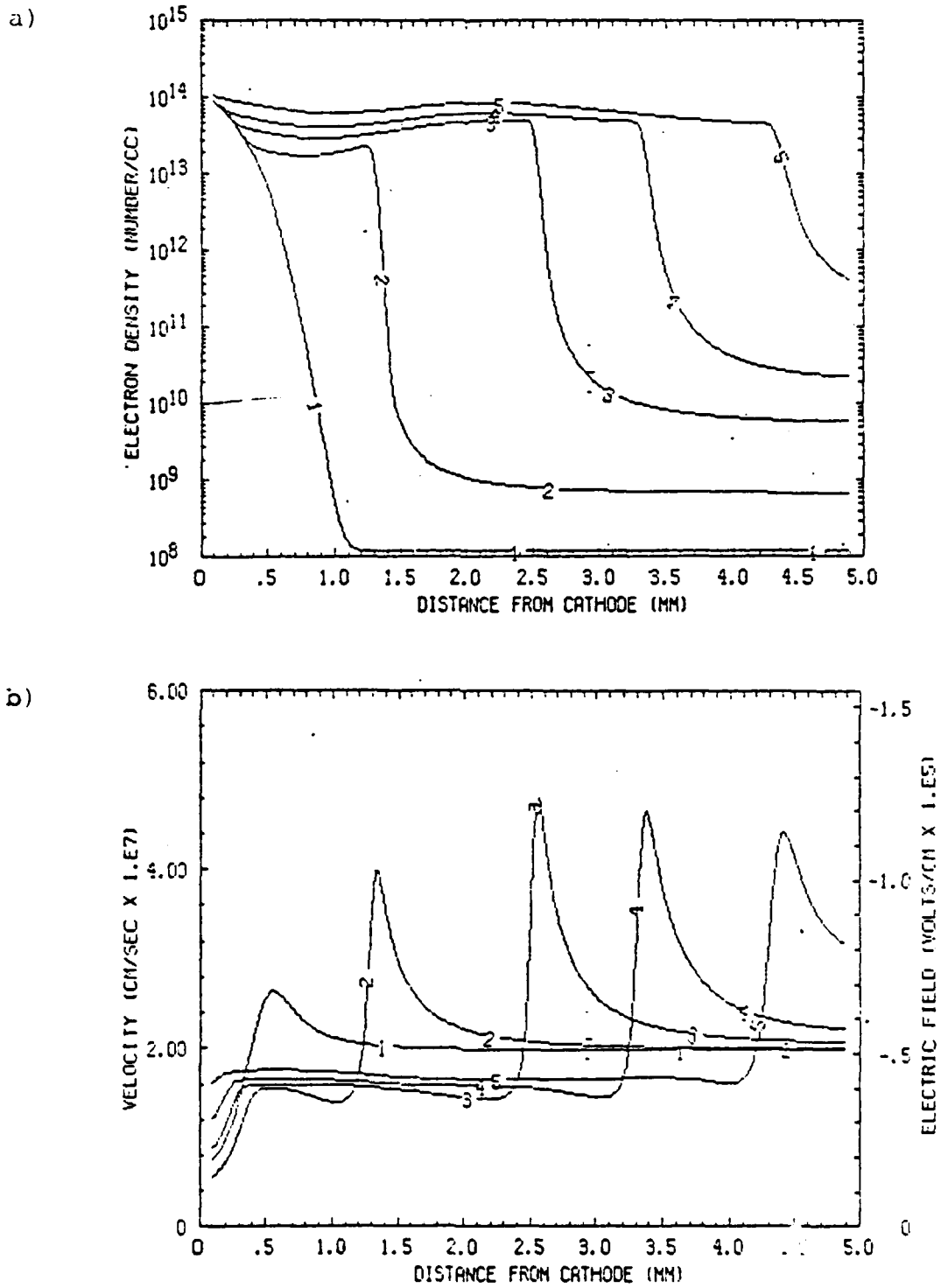


Figure 6

ANODE DIRECTED

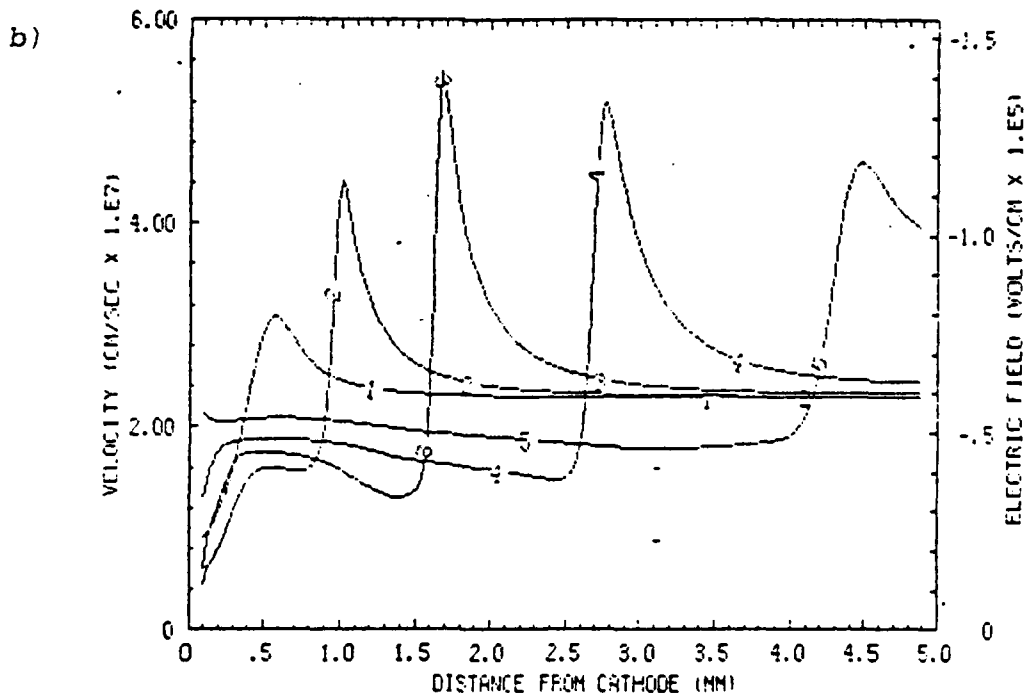
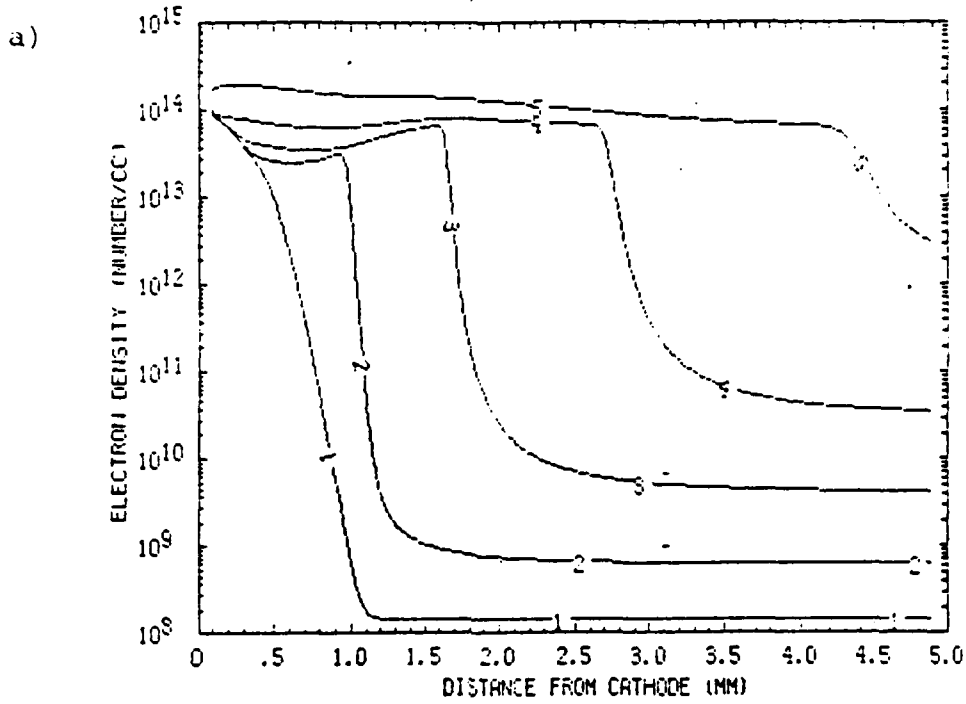
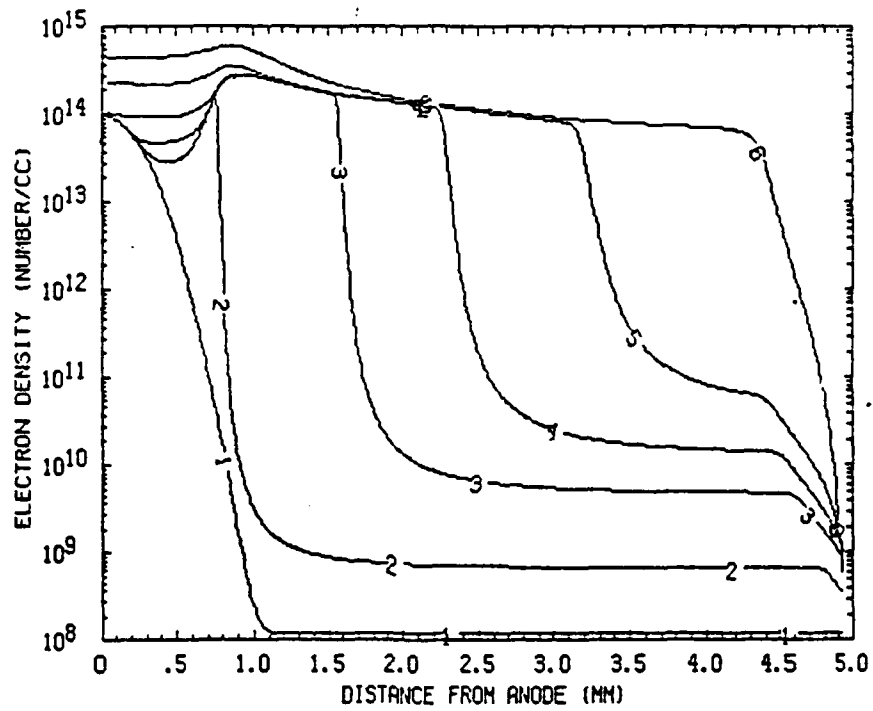


Figure 5

CATHODE DIRECTED

a)



b)

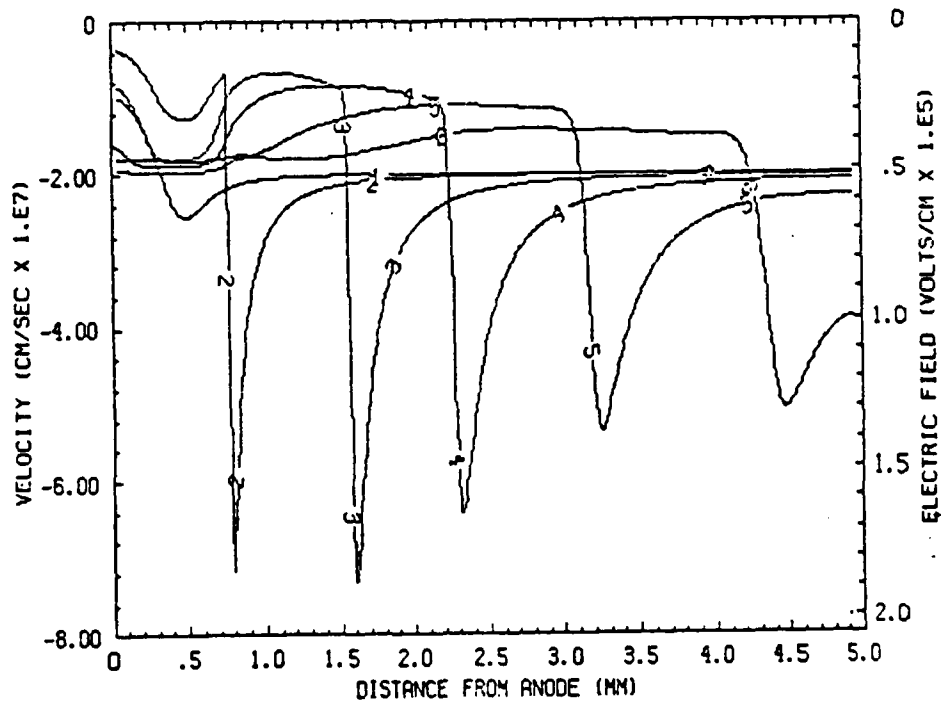


Figure 15

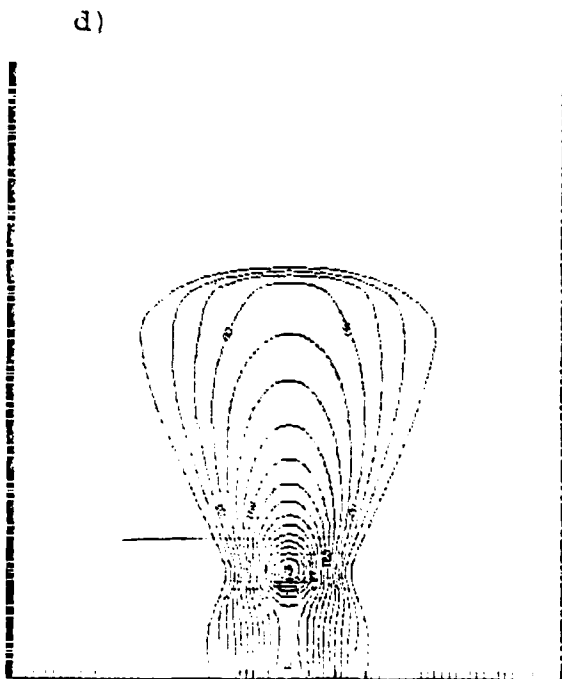
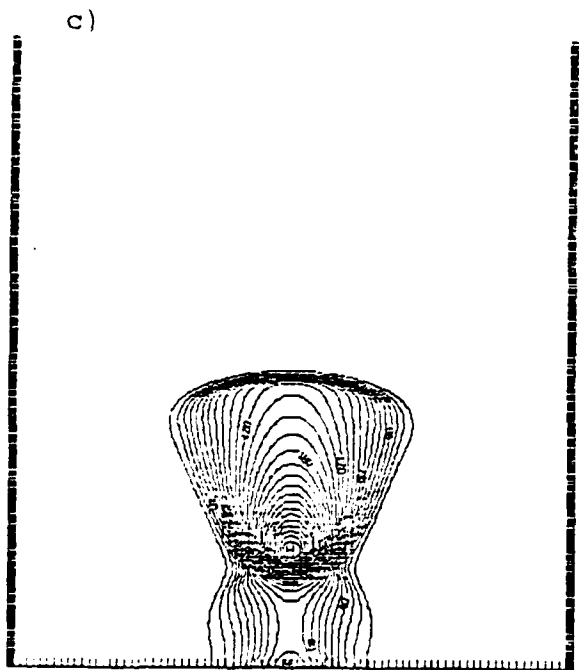
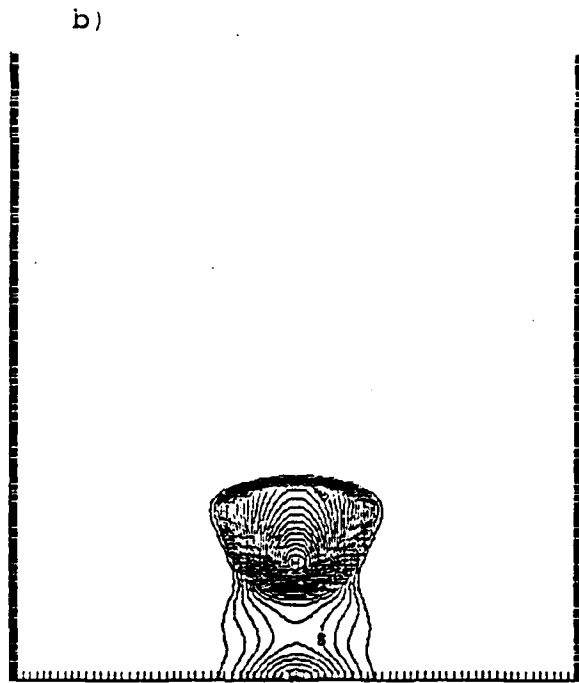
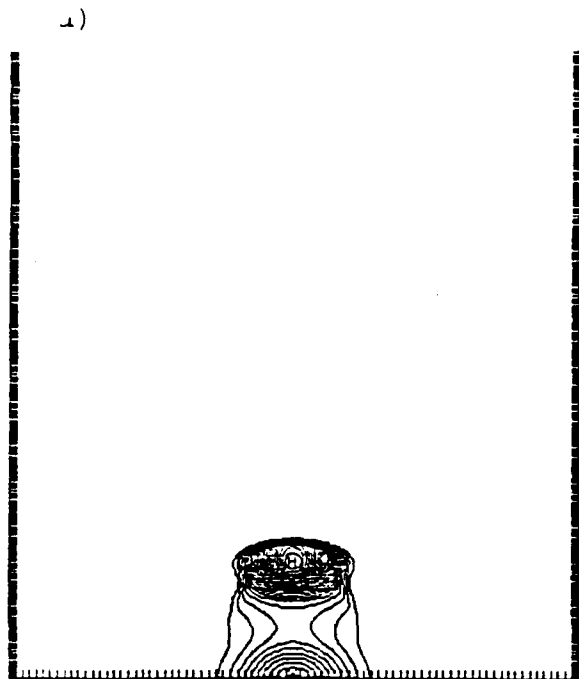
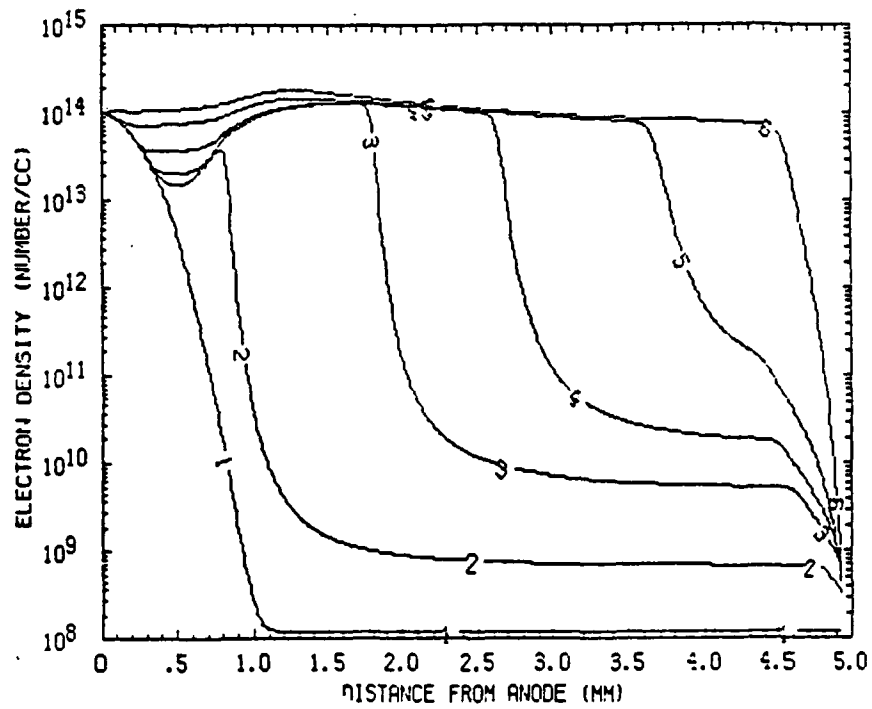


Figure 16

CATHODE DIRECTED

a)



b)

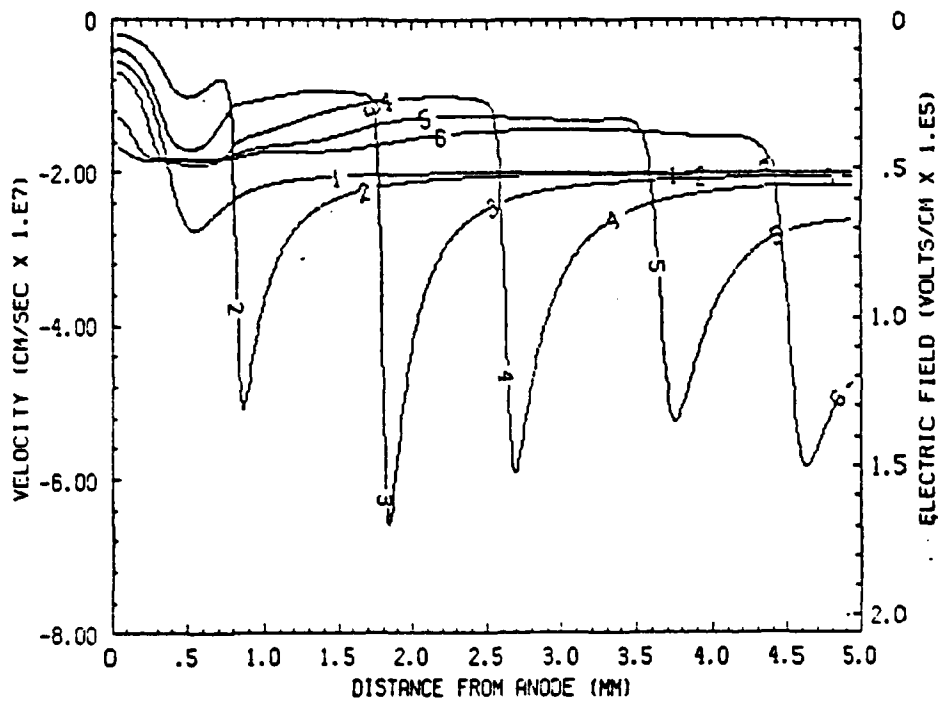
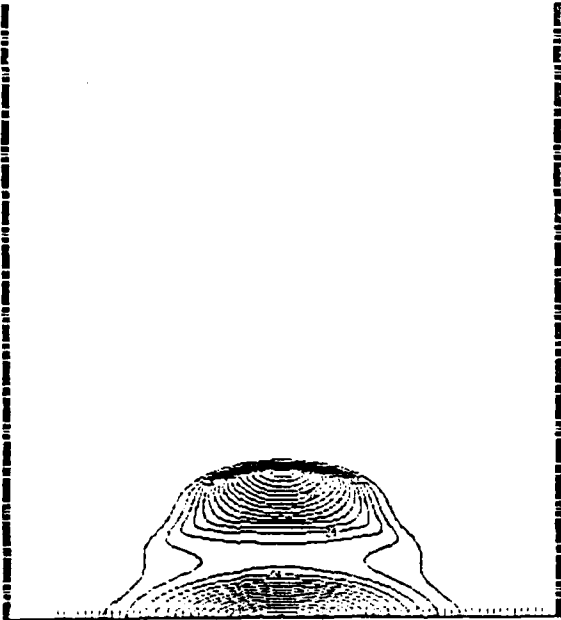
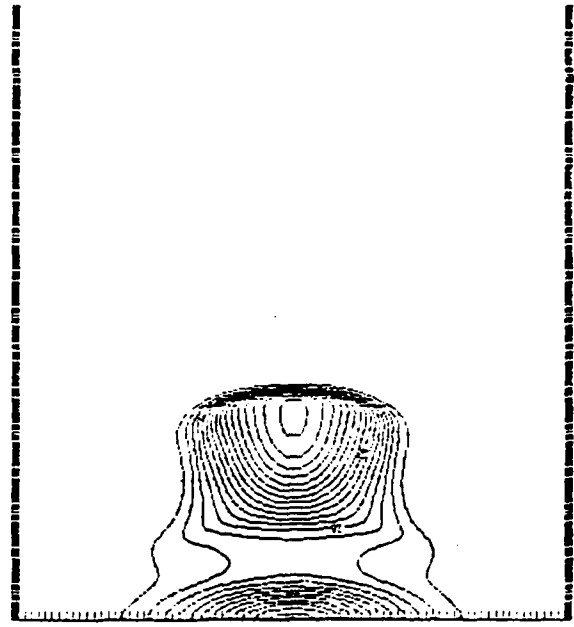


Figure 17

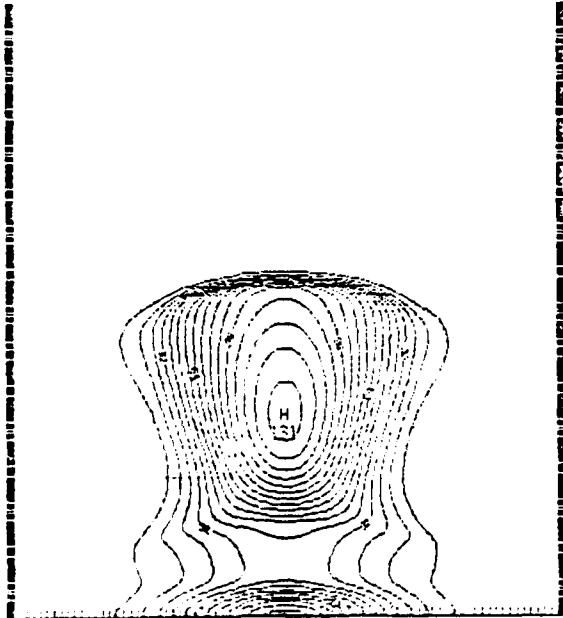
a)



b)



c)



d)

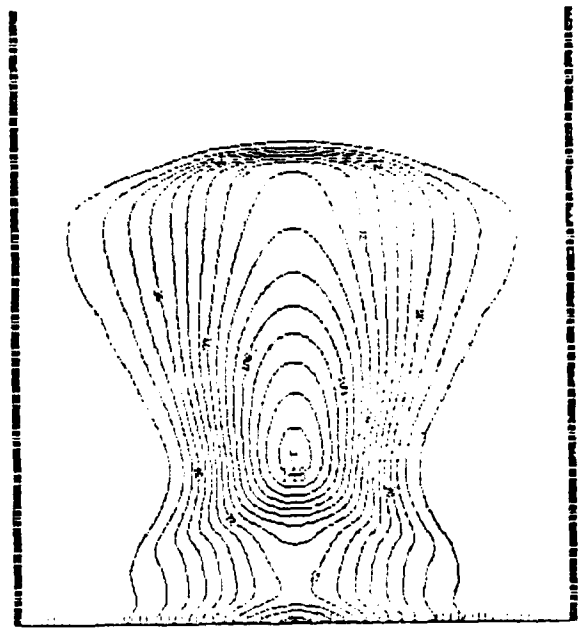


Figure 18

CATHODE DIRECTED
VOLTAGE = -30KV, PHOTOIONIZATION

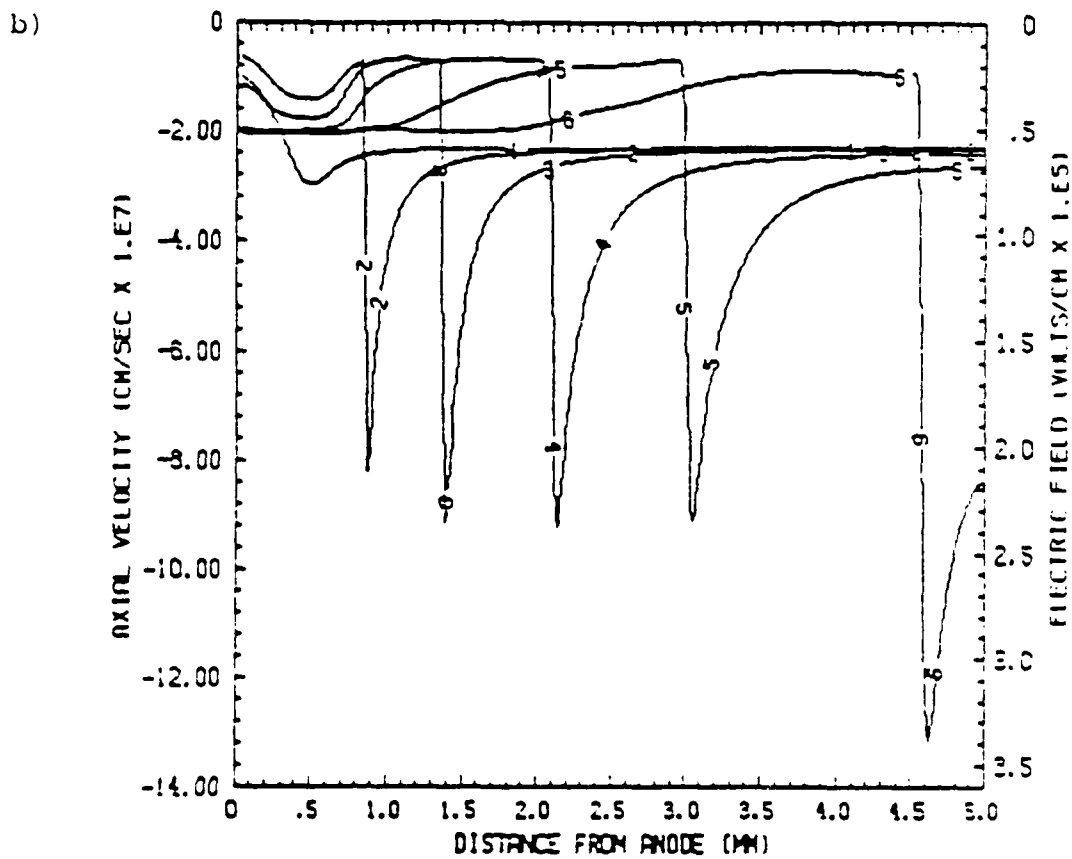
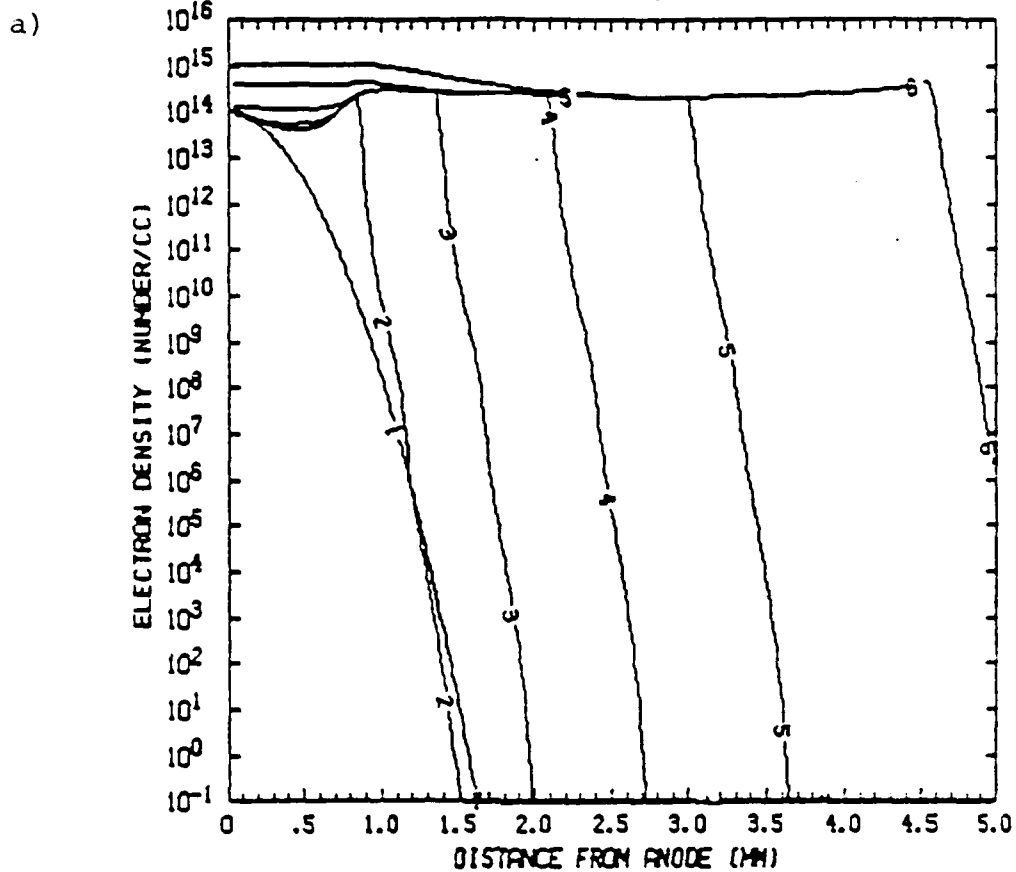
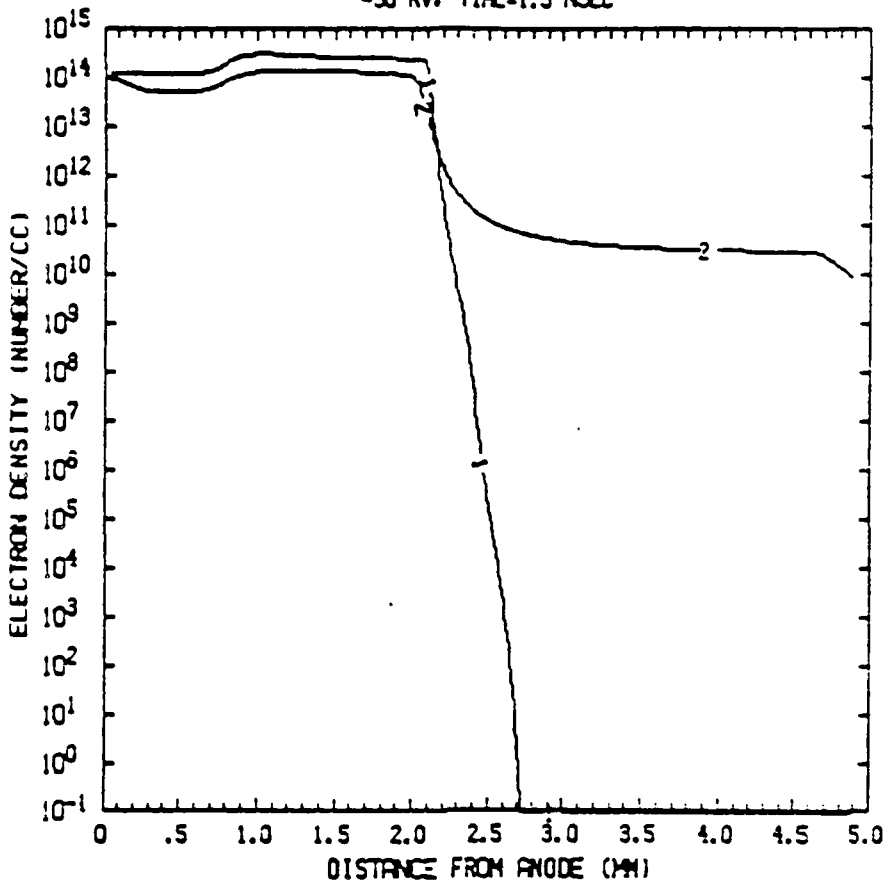


Figure 19

CATHODE DIRECTED
-30 KV. TIME=1.5 NSEC

a)



b)

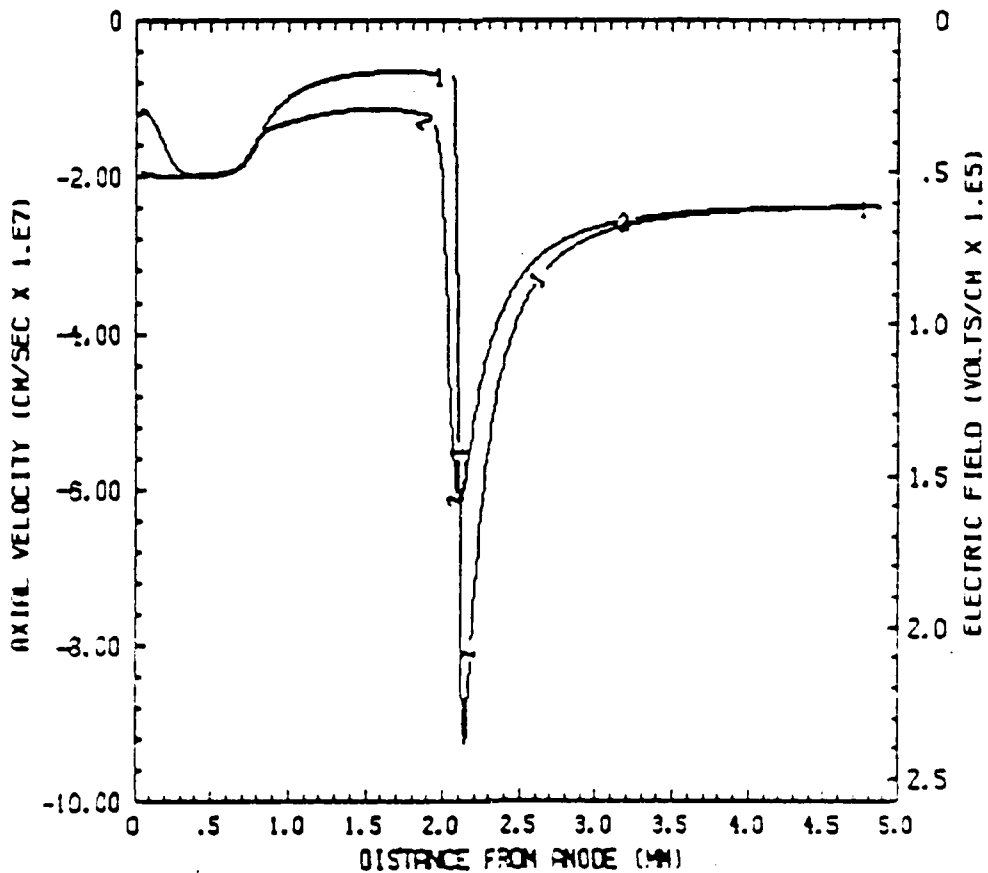
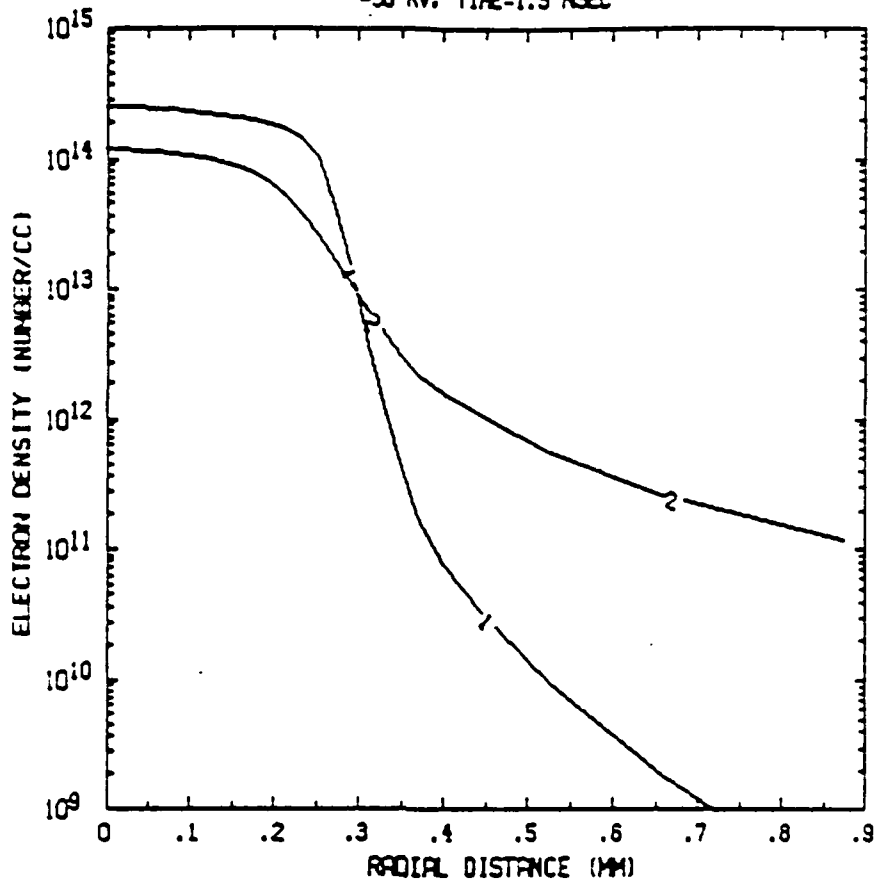


Figure 20

CATHODE DIRECTED
-30 KV. TIME=1.5 NSEC

a)



b)

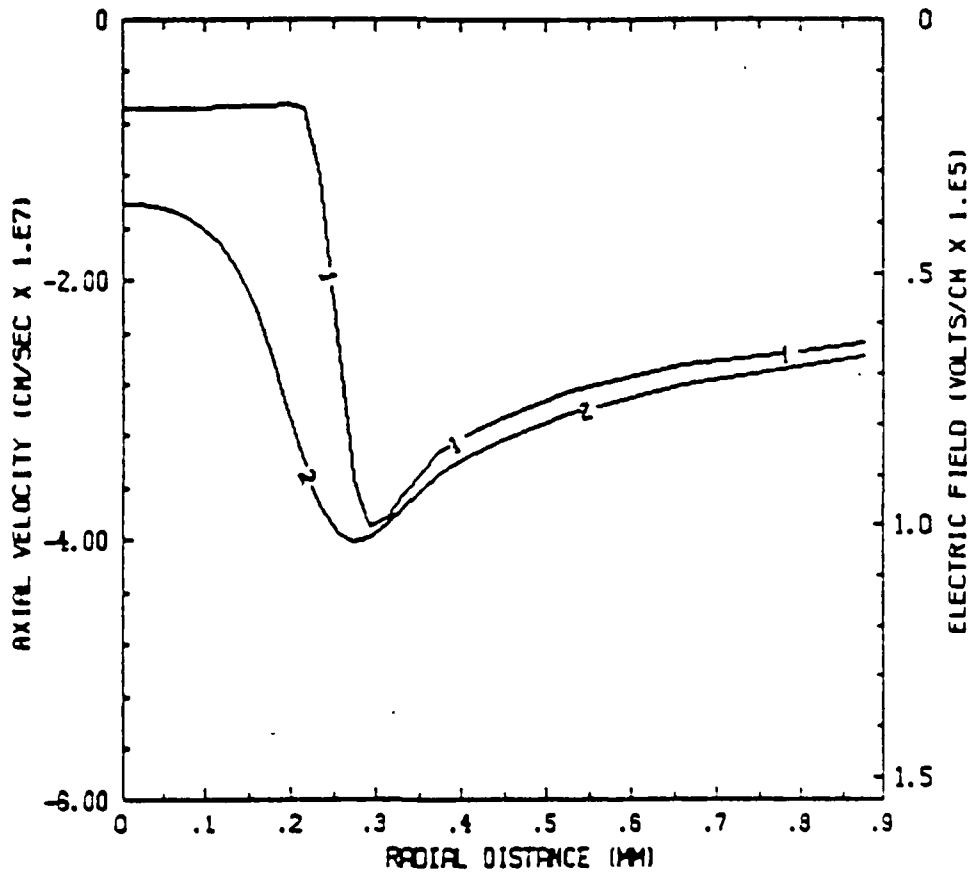


Figure 21

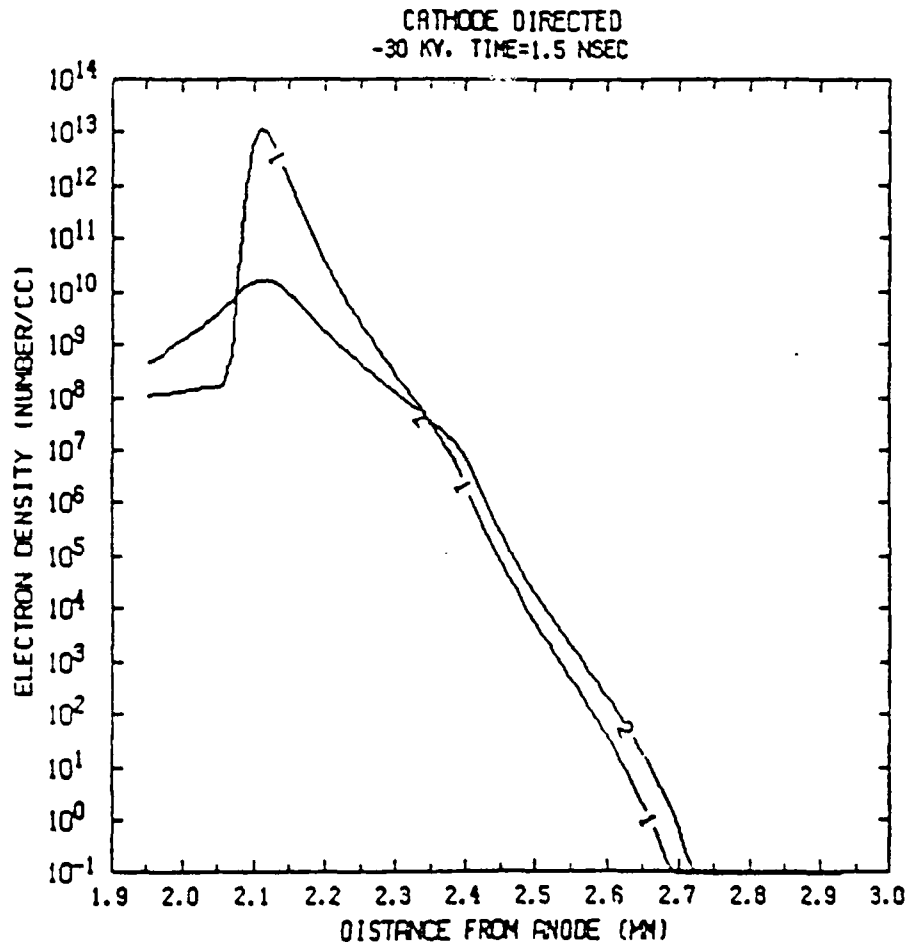


Figure 22

156
 ANODE DIRECTED
 VOLTAGE=30KV. PHOTOIONIZATION

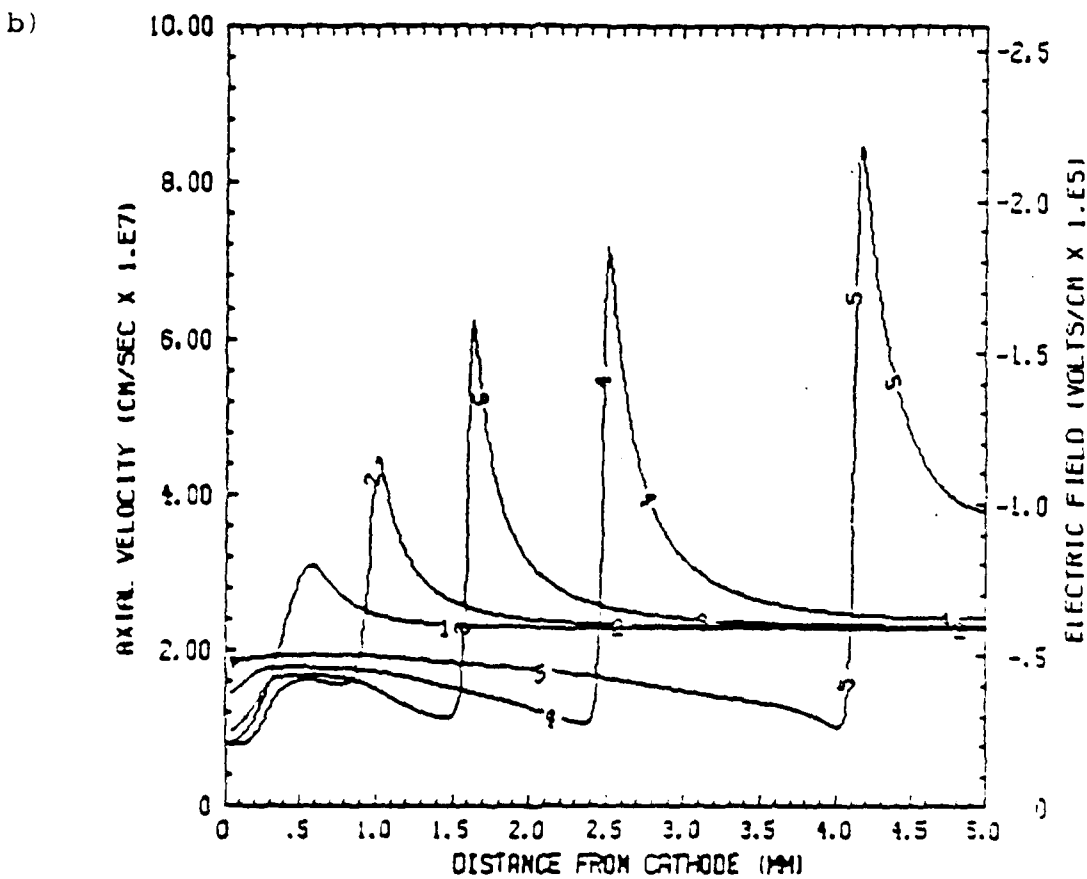
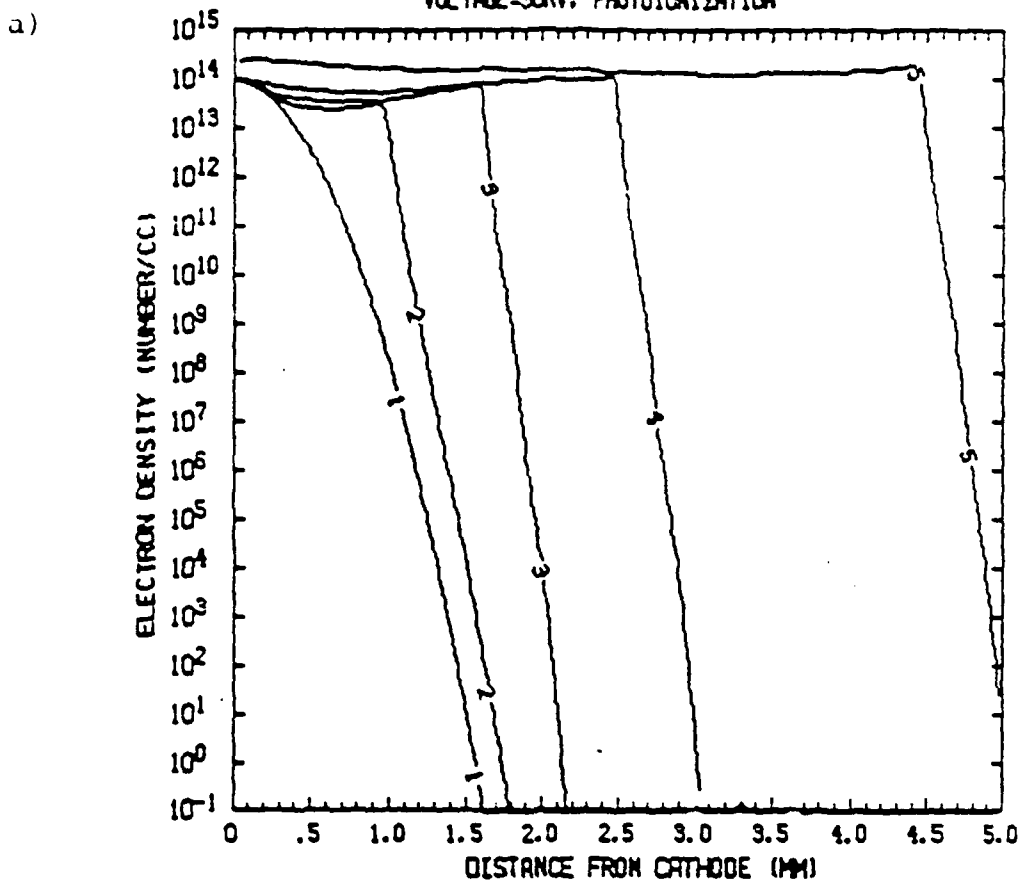


Figure 23

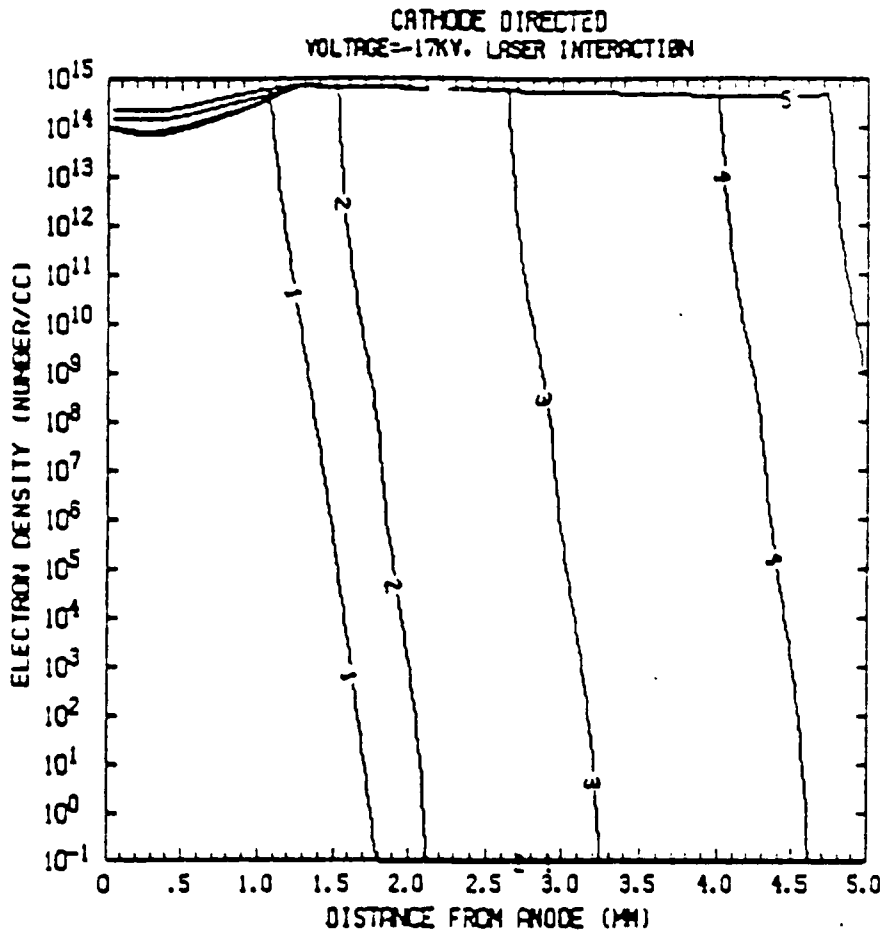


Figure 24

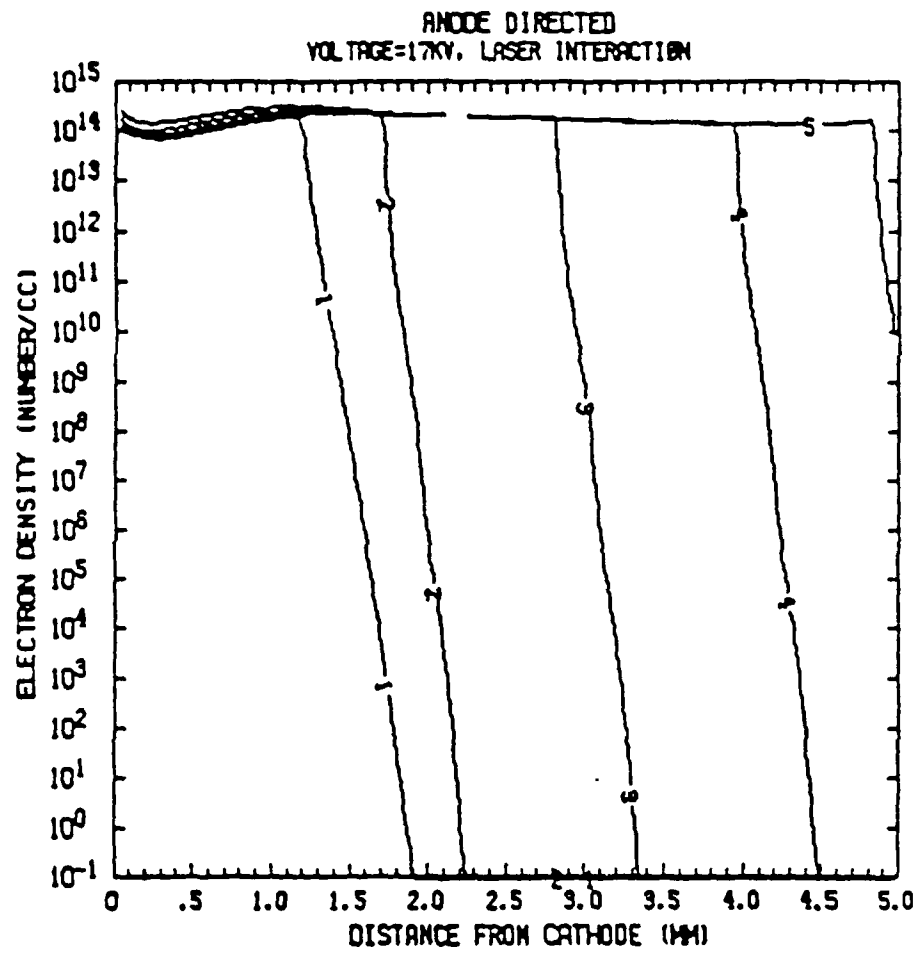


Figure 25

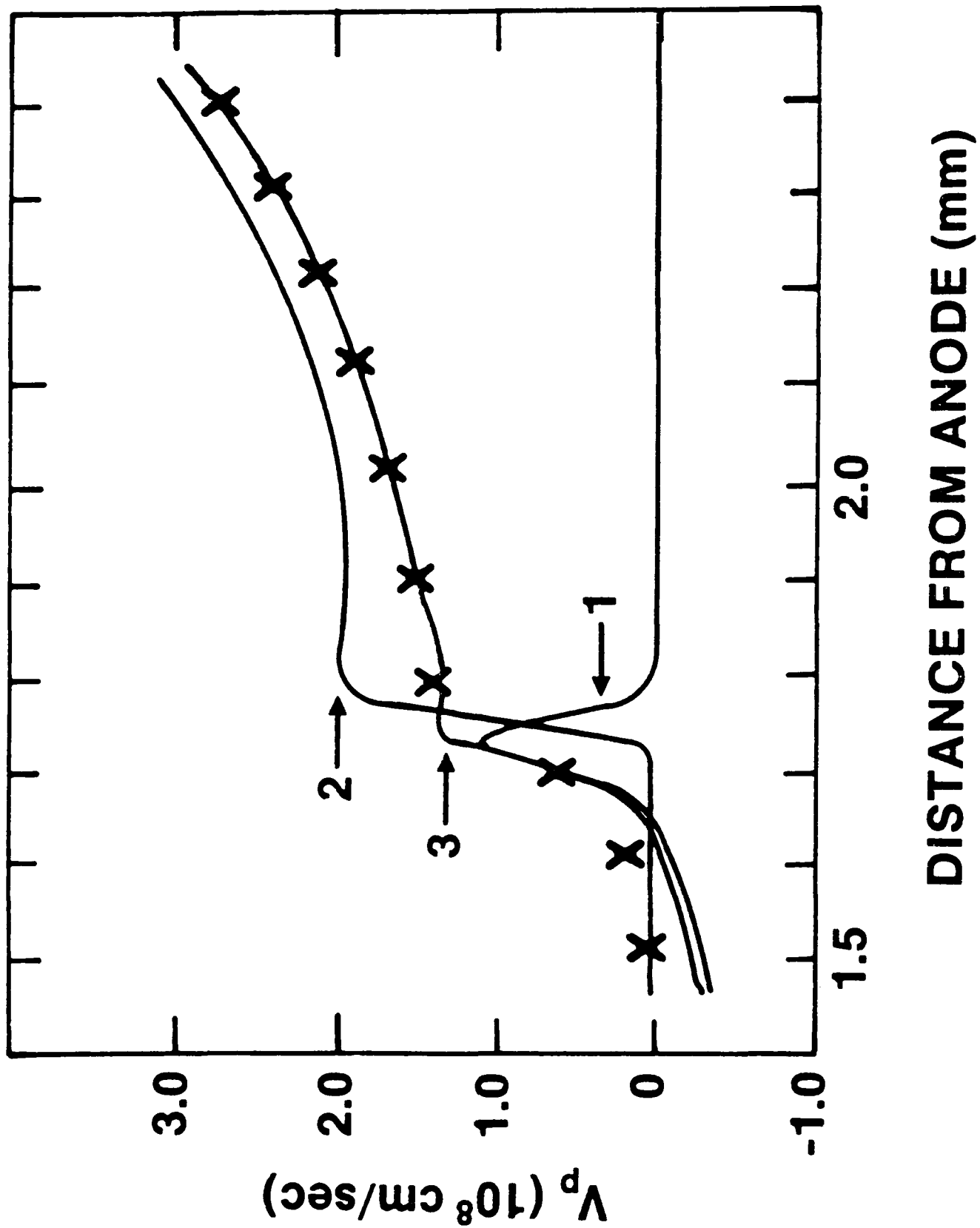


Figure 26

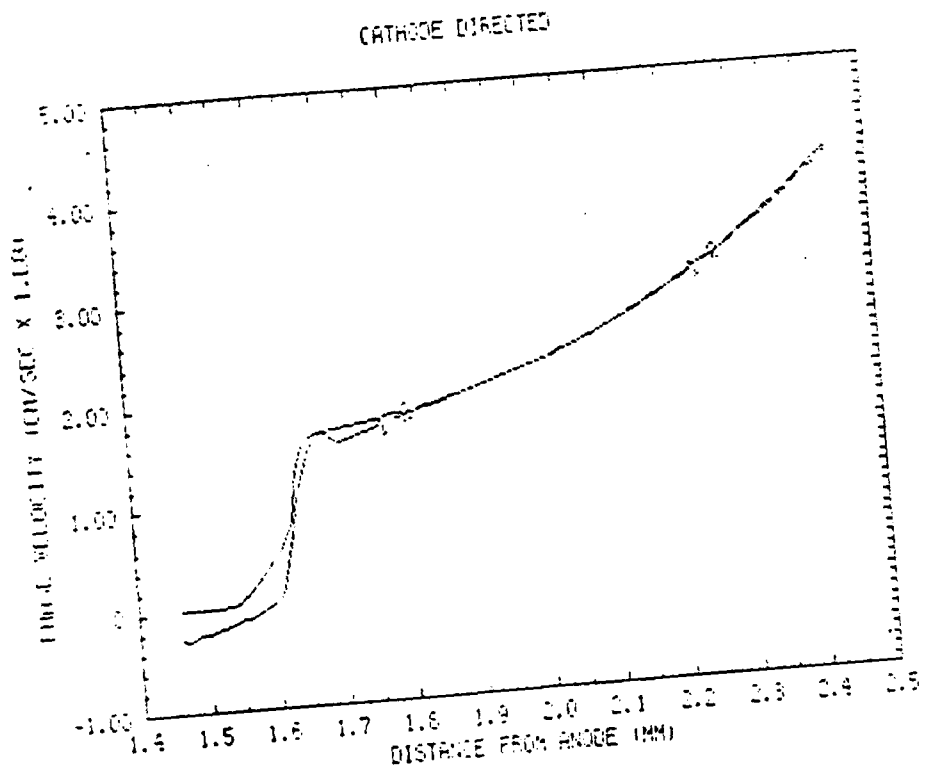


Figure 27

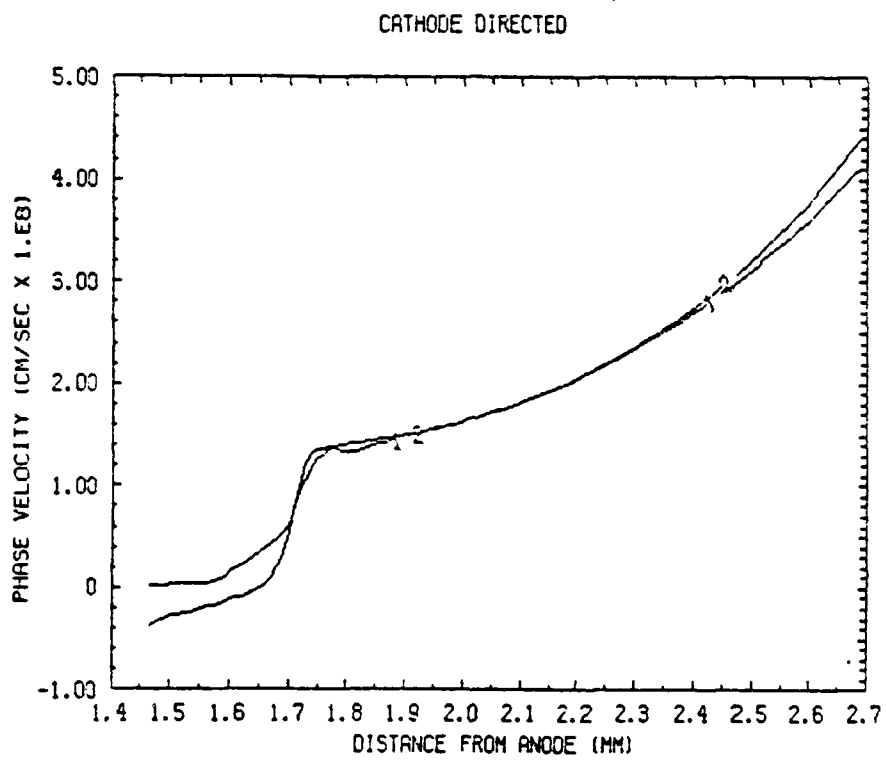


Figure 28

I. INTRODUCTION AND TRIGGER CONCEPT

Spark gaps using field distortion triggering are initially designed to provide hold-off voltage without trigger, and a trigger electrode shaped and located on an equipotential surface in the gap is then added. Triggering is accomplished by abruptly changing the potential of this electrode, thereby increasing the field between the trigger electrode and one of the gap electrodes. A typical example is the three electrode gap with a blade as a mid-plane trigger electrode located approximately half way between the main electrodes [1]. In the hold-off state the blade is in the plane of an equipotential and no field enhancement is generated at the edge of the blade. By changing the potential of the trigger electrode a very strong field enhancement at the edge can be produced. Since the maximum field enhancement occurs at the trigger electrode, however, the switch operates usually in a cascade mode in which the gap between one electrode and the trigger electrode is first closed initiated by the trigger pulse and then the second half of the gap is closed by the voltage across the switch.

To allow for geometrically enhanced field distortion and still to avoid cascade breakdown field enhancement at an edge of one of the main electrodes can be used. This edge, however, must also be shielded in the hold-off state of the gap [2]. A schematic diagram of a spark gap based on this concept is shown in Figure 1. In this device the trigger electrode is used to shape the electric field intensity in the gap in both the hold-off state and the triggering state. In the hold-off state the

A NEW DESIGN CONCEPT FOR FIELD DISTORTION TRIGGER SPARK GAPS

G. Schaefer, B. Pashaie, P.F. Williams*,

K.H. Schoenbach, and H. Krompholz,

Department of Electrical Engineering/Computer Science

Texas Tech University

Lubbock, Texas 179409

A common field distortion triggered spark gap utilizing geometric field enhancement at sharp edges usually operates in a cascade mode via the trigger electrode. A new trigger concept is proposed allowing strong field enhancement and direct breakdown between the two main electrodes. A test setup was designed to prove the feasibility of this concept. Experimental results on delay and jitter depending on percent breakdown voltage are presented. Best results achieved are a delay of 9 ns and a jitter of 2 ns at a selfbreakdown voltage of 15 kV.

* P.F. Williams is now with the University of Nebraska, Department of Electrical Engineering, Lincoln, Nebraska 68508

report. This included the Magnetically Controlled Switch and the Diffuse Discharge Electrode investigations.

A small effort was initiated to check some Soviet reports on an unusual discharge phenomenon. It was reported that if a modest voltage was applied, in air, to a carbon "fiber", then a "surface flashover" phenomenon would occur at very low electric fields ($E \approx 20$ kV/m). It is believed that the carbon fiber heats up, starts to emit thermionically, and that the flashover then occurs along the generated surface "sheath".

The basic phenomenon was verified. We achieved 1 m long discharges in Air, N_2 , and Ar at $V \approx 20$ kV. The energy source was 14 F capacitor. The fiber was actually fiber bundles with up to 12,000 fibers (7 m each) in a bundle. The best results were obtained with 3000-fiber bundles where the bundles lasted for 10's of shots (up to 100 shots) before breaking. If a more sophisticated electrode arrangement can be devised to make the discharge spread to the surrounding gas volume and not just be confined to the bundle surface region then this may have important applications for various intense light sources (flash-lamps). Even in the present arrangement, a multibundle (parallel) arrangement may be of interest if the bundles can be made to "fire" all at the same time. This work will be continued, using senior EE students, at no cost to the project, except for some consumable items (mainly fibers and gases).

To verify the proposed concept experimentally, a system has been constructed with the following parameters:

Z_0	(characteristic impedance)	50
l	(length)	1 m
N	(number of turns)	73
a	(inner radius)	2.85 cm
b/a	(ratio of radii, optimized)	1.65
ϵ_r	(rel. dielectr. const., water)	81
T	(Transit time, 1/2 pulse duration)	350 ns

In order to approximate the model calculations as close as possible, the inner conductor is formed using copper tape, 1/2" wide, and the outer conductor is slit in axial direction. The device performance is presently being measured.

VI. OTHER INVESTIGATIONS

(M. Kristiansen)

Funds from this program element have also been used to assist in various other investigations in our laboratory, such as the arc voltage measurements described in the Final Report on AFOSR Contract 84-0032, Spark Gap Electrode Erosion. The results are described in more detail in that report since the results are needed for the erosion mechanism investigations.

Assistance was also given to some of the small scale experiments described under the Opening Switch part of this

the hold-off state and direct breakdown between the main electrodes is initiated. An experimental set-up to prove this trigger concept has been designed and constructed. First experiments showed the feasibility of this concept. A paper describing these results has been accepted for publication in J. Appl. Phys [1]. A copy of this paper is attached as Appendix I.

1. G. Schaefer, B. Pashaie, P.F. Williams, K.H. Schoenbach, and H. Krompholz, "A New Design Concept for Field Distortion Triggered Spark Gaps", J. Appl. Phys., accepted for publication.

V. HELICAL WAVEGUIDE PULSE GENERATOR

(H. Krompholz)

The advantages of using a coaxial line with helical inner conductor as a pulse generator, compared to usual pulse forming networks (LC chains) or cable discharges, are

- rectangular output pulse without oscillations inherent to LC-chains
- small physical length as compared to ordinary coaxial lines designed to produce the same pulse duration.

Theoretical aspects with emphasis on the limiting factor for helical slow wave structures (dispersion) are summarized in Appendix II, where it was applied to a transmission line current sensor and unit step response, which is equivalent to a initially charged waveguide pulse generator.

introduced into a pressure chamber via a plexiglas window. The chamber contains the gas under study, and will be used at pressures up to 5 atm. Inside the chamber is a large rectangular electrode (12 cm long), separated by the gas from a series of twelve small collection electrodes. Each collection electrode is 8 mm long and 2 mm apart. When a potential is applied between the large electrode and the smaller ones, the electrons ionized by the x-rays will drift toward the collection electrodes. By monitoring the current extracted from these electrodes, the ionization density as a function of the distance travelled in the gas by x-rays can be obtained. This will be measured up to 12 cm from the source at increments of 1 cm, for various gases, mixtures, and pressures, and at different photon energies. If the results are favorable, a spark gap will be built with the tube mounted in one of the electrodes.

IV. FIELD DISTORTION TRIGGERING

(G. Schaefer, K.H. Schoenbach, and P.F. Williams)

A common gap using field distortion triggering is initially designed to provide optimum performance. A trigger electrode is then added, shaped and located on an equipotential surface. When a trigger pulse is applied, field enhancement occurs at an edge of this trigger electrode and in most cases cascade breakdown is initiated. Field enhancement at one of the main electrodes can be utilized if the trigger electrode shields this electrode in

(shattered), evidently from the shock forces. It appears that the best materials now are high temperature, relatively "soft" dielectrics, such as teflon or delrin. The voltage recovery of the switch also drops drastically after a few shots at a slow repetition rate (a few pulses per second) but blowing gas (air) onto the surface and the arc to help remove the heat improves the recovery rate significantly. It is expected that this investigation will be completed by June 1985.

III. X-RAY PREIONIZATION OF SPARK GAPS

(Mike Ingram, G. Schaefer, and M. Kristiansen)

X-rays have been successfully used to preionize various gas discharge lasers, providing a known preionized electron density and volume. This same method may also be used to preionize spark gaps, again providing known preionized electron densities and volumes. Before testing such a spark gap, however, a study has been undertaken to determine the effectiveness of x-ray preionization in typical spark gap gases and pressures (Air, N₂, SF₆, and mixtures).

We are currently investigating x-ray ionization of Air, N₂, and SF₆. The x-ray source is a cold cathode, flush, x-ray tube manufactured by ITT. It is driven by a fast (2 ns risetime) Marx bank at voltages up to 150 kV. Because of the large divergence of the tube, the x-rays are passed through a 2.5 mm diameter hole in a lead sheet to produce a narrow, conical beam, which is then

II. SURFACE DISCHARGE SWITCHING

(R. Curry, P. Ranon*, L. Hatfield, and M. Kristiansen)

The studies of triggered electric surface discharge switches described in earlier reports on AFOSR Contract #F49620-79-C-0191 has been completed and the results are being written up for publication. The optimum polarity and location of the trigger electrode was determined and a comparison was made of the trigger jitter and multichanneling for various electrode materials and ambient gases (all at 1 atm). Of the many combinations tried the best performance was obtained with G-10 (fiber-epoxy laminate) substrate material and air as the ambient gas.

A new effort involves checking the maximum possible, single channel, current in a surface discharge switch to see if it results in a significant arc lift-off, and hence increased switch inductance, and to see how the dielectric substrate damage mechanism changes from that at lower current levels. This project is only in its infancy but it is already clear from measurements done with a 140 kA peak current, ringing discharge that the damage mechanism is drastically changed and that the current lift-off is not as severe as expected. The dielectric surface damage can sometimes be quite dramatic. The G-10 surface which was among the best performers for multichanneling and low jitter triggering at lower current levels literally exploded

* USAF AECT student

Exploratory Concepts

(R. Curry, B. Maas, M. Ingram, P. Ranon, G. Schaefer,
L. Hatfield K. Schoenbach, H. Krompholz, and M. Kristiansen)

I. SUMMARY

Several small scale investigations were carried out and some of them show promise for further development and separate funding. In the past, several of these "mini-projects" have led to major, separately funded, efforts.

During the past year we have completed the studies of triggered surface discharge switches and started a new investigation of high current surface discharges. The investigations of arc resistance measurements were also completed. Significant results were obtained in investigations of geometrically enhanced field distortion triggering and an investigation of x-ray triggering of spark gaps was initiated. Surface discharges along current carrying, thermionically emitting, carbon fibers was investigated as a potential high efficiency, low voltage, pulsed light source.

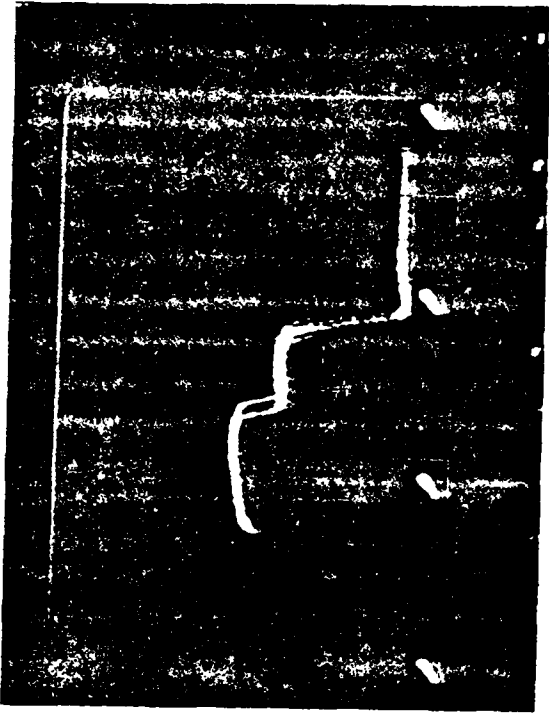


— —
— +

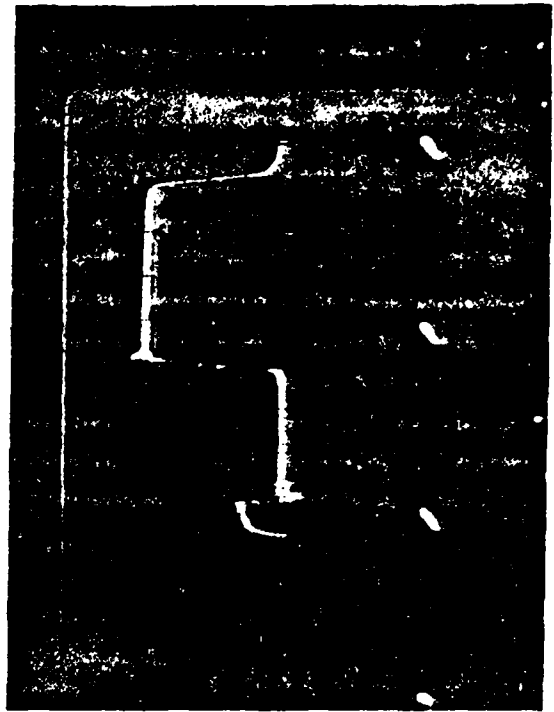
→|5 ns|←

Figure 33

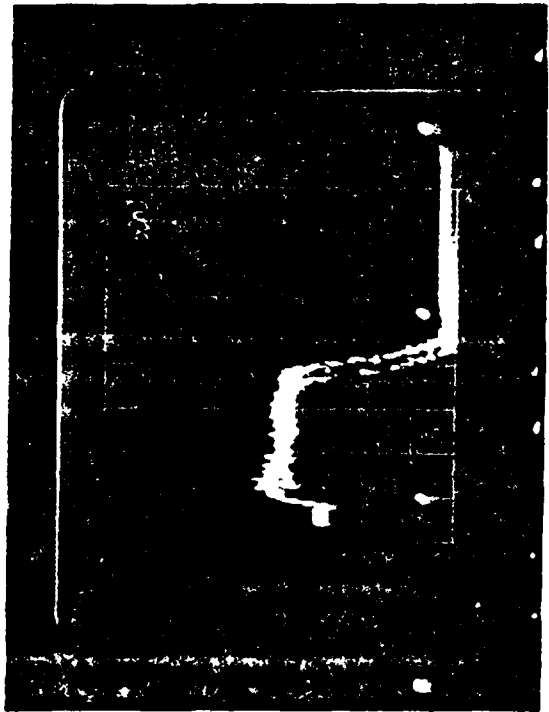
b)



d)



a)



c)

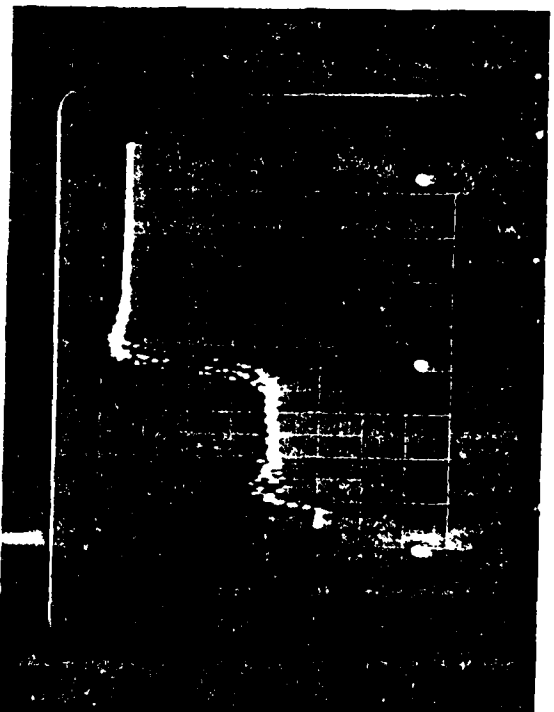


Figure 32

ELECTRICAL SCHEMATIC

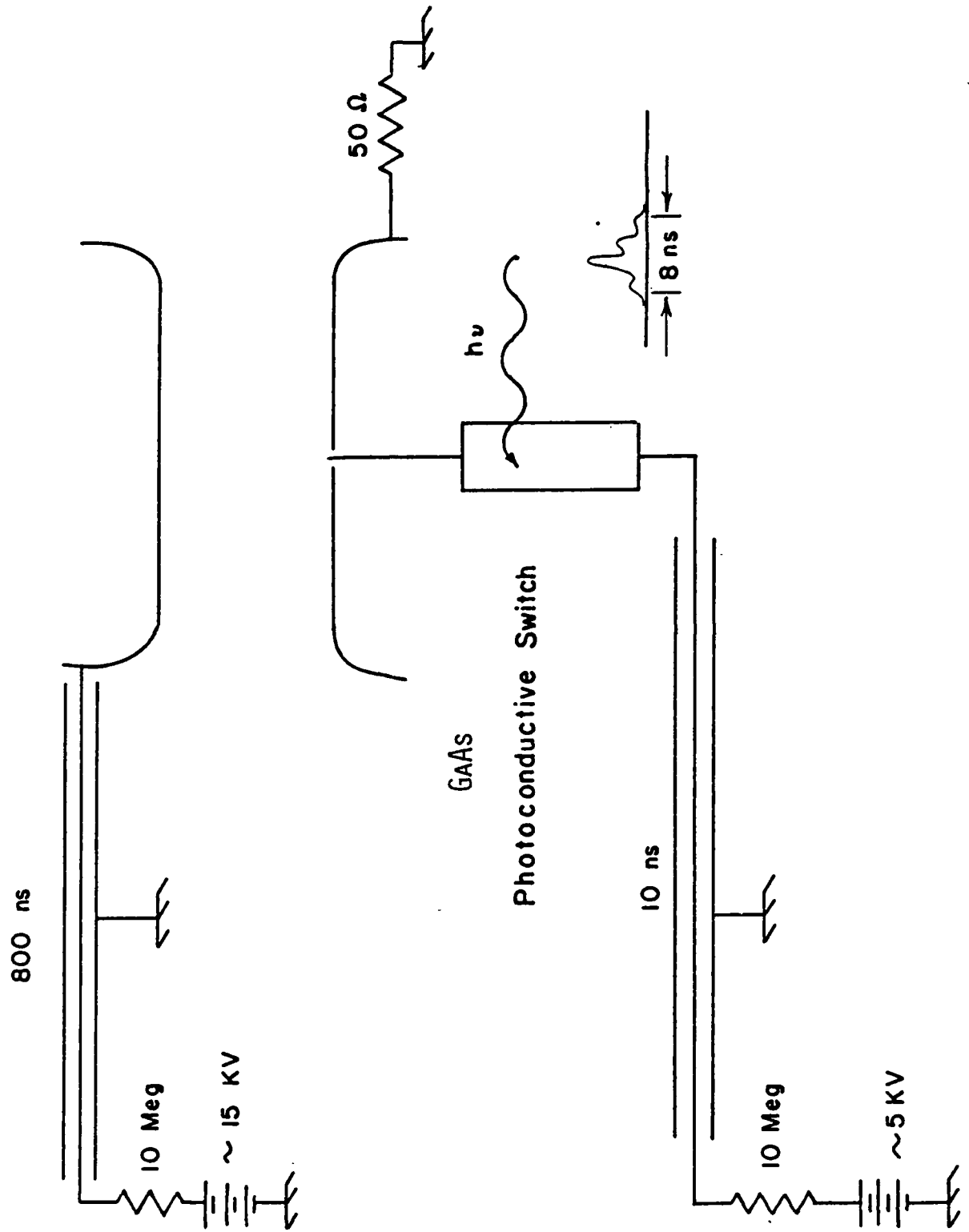


Figure 31

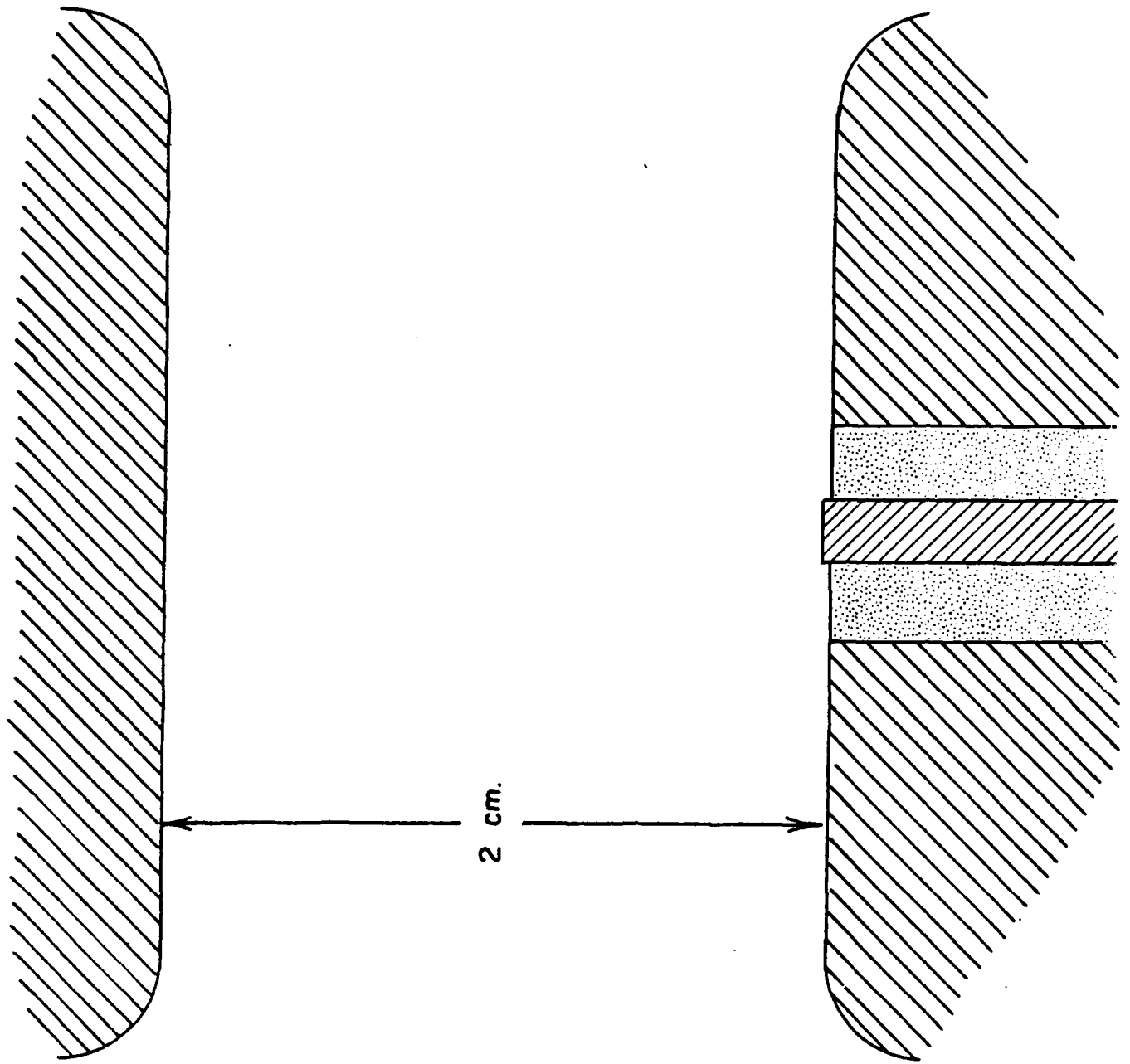


Figure 30

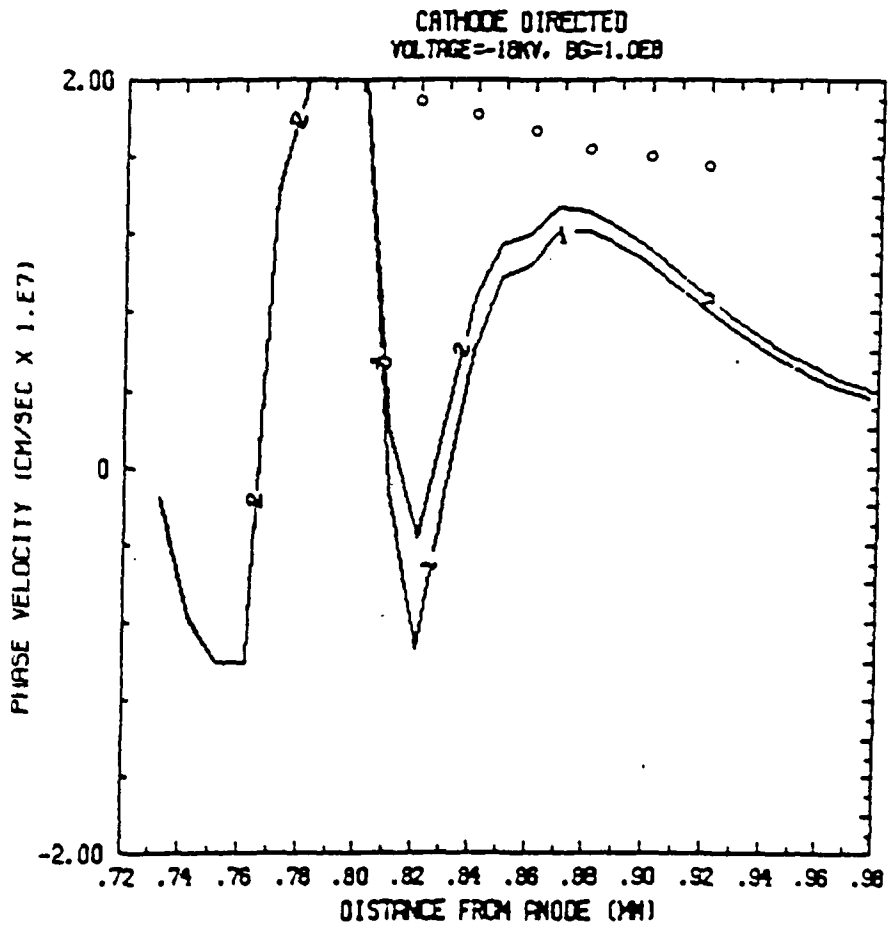


Figure 29

trigger electrode is kept at the same potential as electrode (1) and its surface towards the gap is shaped to minimize the geometric field enhancement effects at the main gap electrode, thereby maximizing the hold-off voltage. In the triggering state the potential of the trigger electrode is moved towards the potential of electrode (2). The trigger electrode subsequently serves to enhance the field, providing improved triggering, in two ways: moving the equipotential toward one gap electrode, and simultaneously turning on the geometric field enhancement. Such a trigger concept combines several advantages:

1. Geometrically enhanced field distortion can be utilized.
2. The strongest field enhancement occurs at one of the main electrodes and breakdown, without cascading via the trigger electrode, is possible.
3. Since the electrode can be shaped without changing the hold-off performance, the field enhancement at a main electrode can be much larger than in common field distortion triggering.
4. Shape and surface conditions of this main electrode do not determine the hold-off performance of the gap, making the gap more independent of erosion.

This concept would have to be applied to both main electrodes for protection of both.

II. TEST SET-UP

The experimental set-up used to test this trigger concept is shown in Figure 2. A parallel plane line was used as charging

and transmission line (total impedance $\sim 12.5 \Omega$). The switch consisted of 8 individual gaps. The upper conductor of the lines was divided into eight individual stripes to provide for transit time insulation of the individual gaps (impedance/stripe $\sim 100\Omega$). The time constant for the transit time insulation could be varied in the range of 0-5 ns by moving metal bars connecting the individual transmission and charging lines.

Two different electrode configurations were used as shown in Figure 3. The configuration (A) uses one triangular shaped main electrode (1) with a pair of two rods as trigger electrodes and one rounded main electrode (2), while the configuration (B) uses a symmetric configuration with two triangular main electrodes. The trigger electrodes in any case were pairs of rods triggering all eight individual gaps at the same time as demonstrated for the configuration (B) in Figure 4. Bare stainless steel bars as well as bars covered with a dielectric material (Glass tubes or epoxy) or with a resistive material (graphite-filled epoxy) have been used.

The trigger circuits are shown in Figure 5. The trigger pulse was provided by a secondary gap which was operated in the self breakdown mode and the breakdown voltage was adjusted through changing the secondary gap electrode separation. In the hold-off state the trigger electrodes are at the potential of the adjacent main electrode. When the secondary gap fires the potential of the trigger electrode is driven towards the potential of the opposite electrode.

For the circuits (A), (B), and (C) the full charging voltage of the line can be applied to the trigger electrode while for the circuit (D) both trigger electrodes potentials move towards the midplane potential of the gap.

III. EXPERIMENTAL RESULTS

The experiments performed concentrated on the spark gap performance with respect to delay and jitter depending on the applied voltage in percent of the breakdown voltage. The first experiments to determine the optimum type of trigger electrode and polarity were performed with an electrode geometry as shown in Figure 3(A) and a circuit as shown in Figure 5(A). Although the system could be triggered with either polarity, clearly better trigger results were obtained with the electrode (1) being at positive potential and the trigger electrode being driven towards a negative potential. Triggering was possible with all types of trigger electrodes used. Bare metal rods as trigger electrodes had the disadvantage that a very precise symmetric alignment was necessary to avoid arcs between the trigger electrode and the main electrode. The best results were obtained with electrodes covered with a dielectric layer (glass or epoxy). Since the system performance did not depend on repetition rate (10^{-2} - 1 Hz) surface charges on the surface of the dielectric seemed not to affect the performance of the trigger method at these low repetition rates. Surface charges could be eliminated with resistive layers instead of a dielectric, but arcing to the trigger electrode again required precise alignments

unless layers with high resistivity were used (thickness ~ 0.5 mm, resistivity ~ 10^5 cm).

The circuits in Figure 5 (B) and (C) are equivalent to circuit (A) since only one pair of trigger electrodes changes its potential. No significant differences in the performance of the spark gaps was realized for these circuits as long as the right polarity was used. The performance of the gap with the circuit shown in Figure 5 (D) was significantly worse with respect to delay and jitter.

The optimum position of the trigger electrodes was determined through measurements of the selfbreakdown voltage shown in Fig. 6 (A). In these experiments the pair of trigger electrodes was moved in the direction of the interelectrode spacing as shown in Fig. 6 (B). The results clearly show the shielding of the edged main electrode resulting in an increase of the selfbreakdown voltage of more than a factor of 2 compared to the gap without trigger electrodes. For optimum shielding no significant difference was observed for the two different types of trigger electrodes. The maximum selfbreakdown voltage observed is nearly the uniform field breakdown value.

The following measurements on the trigger performance were obtained with the circuit in Fig. 5 (A) and (D) and a positive charging voltage. All experiments are performed in atmospheric air. The rise time of the trigger pulse was of the order of 12 ns. Delay and jitter were determined by measuring the time between the voltage rise at the trigger electrode and at the main electrode. Figure 7 shows the delay depending on % self-

breakdown voltage ($\%V_{SB}$) for the two circuits. It should be pointed out that the maximum voltage of the trigger pulse always equals the charging voltage in the circuit used. So with a decreasing value of $\% V_{SB}$ the maximum voltage of the trigger pulse automatically decreased.

As demonstrated in Fig. 7, a minimum delay time of 9 ns was achieved with circuit Fig. 5 (A) for a selfbreakdown voltage of 15 kV. Above 90% V_{SB} selfbreakdown the delay does not significantly change with $\% V_{SB}$ as required for multichanneling or parallel triggering of several gaps.

Figure 8 shows the jitter depending on $\% V_{SB}$ for the same operation conditions as in Fig. 7. The jitter shown here is the maximum jitter in a series of 20 shots. Close to 100% V_{SB} a jitter of ~ 2 ns could be achieved.

These results were also proven through parallel operation of the eight gaps with one pair of trigger electrodes for all gaps as shown in Fig. 4. With a transit time insulation of 5 ns parallel triggering of all gaps was achieved if the charging voltage was kept above 95% V_{SB} . Fine adjustment of the self-breakdown voltage of each gap was difficult, however, and it is likely that some gaps were operated at significant lower values of $\% V_{SB}$.

IV. DISCUSSION

The exploratory experiments demonstrate the feasibility of the proposed field distortion trigger concept. Results on delay time and jitter indicate that this methods may be suitable for

multichanneling and the parallel operation of spark gaps. Field code calculations are required to optimize the geometry for a maximum hold-off voltage in the off-state and maximum field enhancement in the on-state. Further experiments are required with a test gap allowing operation in different gases with variable pressure and a trigger circuit allowing the independent variation of V_{GB} and trigger pulse parameters.

The physical mechanisms responsible for triggering are of interest. Referring to Fig. 1, in the triggered state with the trigger electrode connected electrically to electrode (2), a very high electric field exists in the vicinity of electrode (1), while a much reduced field is produced in the main gap region between the trigger electrode and electrode (2). Two mechanisms for triggered breakdown seem possible. In the first, a streamer is launched inside the high field region, and propagates past the trigger electrode into the low applied field region. Propagation continues because the streamer body forms a weakly conducting needle connected to electrode 1, thereby producing high electric fields in the vicinity of its tip. After the streamer has traversed the gap, ohmic heating occurs and converts the weakly conducting channel left by the streamer into an arc channel.

In the second case, initial breakdown occurs through a purely Townsend mechanism. In this case, the criterion for breakdown is that sufficient electron avalanche multiplication occur so that one electron leaving the cathode may reproduce itself at the cathode through the avalanching and other appropriate secondary processes. Here, the relevant quantity is the electron ampli-

cation due to impact ionization, $A = \int_0^d \alpha(E) dx$, where $E = E(x)$ is the applied field, assuming no space-charge distortion. E is subject to the constraint $\int_0^d E(x) dx = V$, where V is the gap voltage. Since the impact ionization coefficient, α , is a strongly increasing function of field for fields around the breakdown field, the amplification factor, A , will be much larger for the highly non-uniform field produced in the triggering state than for the uniform field produced when the triggering electrode is connected to electrode (1). Thus, according to the Townsend criterion, the gap may be strongly overvolted in the triggered configuration, while remaining undervolted in the normal configuration.

The experimental data on delay suggest that both mechanisms occur. For applied voltages near the static breakdown voltage, the delay is found to be approximately 10 ns. Considering the substantially reduced field in the region between the triggering electrode and electrode 2, electrons emitted from the cathode (electrode 2) would require ~ 50 ns to traverse the gap. Thus, it seems difficult to explain delay times less than about 100 ns with the Townsend mechanism. At the opposite extreme, delays approaching 1 μ s are observed for low applied voltages. Even considering the dielectric relaxation time required for a streamer to produce the high field enhancements needed in this regime, a streamer transit time exceeding 100 ns seems unlikely. Additional time is required, of course, to convert this streamer channel into an arc channel but this time should not be a strong function of the applied voltage, and considering the 10 ns delay

observed at 95% V_{SB} , should not exceed several tens of ns at 50% V_{SB} . Thus the low voltage data suggest that a Townsend mechanism is at work. The two mechanisms, streamer and Townsend, are not incompatible, and it is likely that there is continuous transition from one to the other as the gap voltage is reduced.

V. PERSPECTIVES

The proposed trigger concept is well suited to combine field distortion with other trigger concepts to improve the switch performance. The important feature of this concept here again is that the field enhancement occurs close to the surface of one main electrodes and that this main electrode is partially shielded from the field in the hold-off state.

For trigatrons, it is well known that delay and jitter are drastically improved by overvolting the gap. Subsequently the combination of a trigatron trigger in the main electrode and a field enhancement generated by a field distortion in volume close to this trigatron electrode could provide for the same condition without the need to overvolt the total gap. The same considerations also hold for those laser triggered gaps where the laser spark is produced at or close to the surface of one main electrodes. The combination of the proposed field distortion concept with one of these trigger methods would therefore provide significantly improved performance in an undervolted main gap.

ACKNOWLEDGMENT

This work was supported jointly by the Air Force Office of Scientific Research and the Army Research Office.

References

- [1] A.E. Bishop and G.d. Edmonds, Proc. IEE 113, 1549 (1966).
- [2] J.K. Hepworth, R.C. Klewe, and B.A. Tozer, Proc. IEE, 119, 1751 (1972).

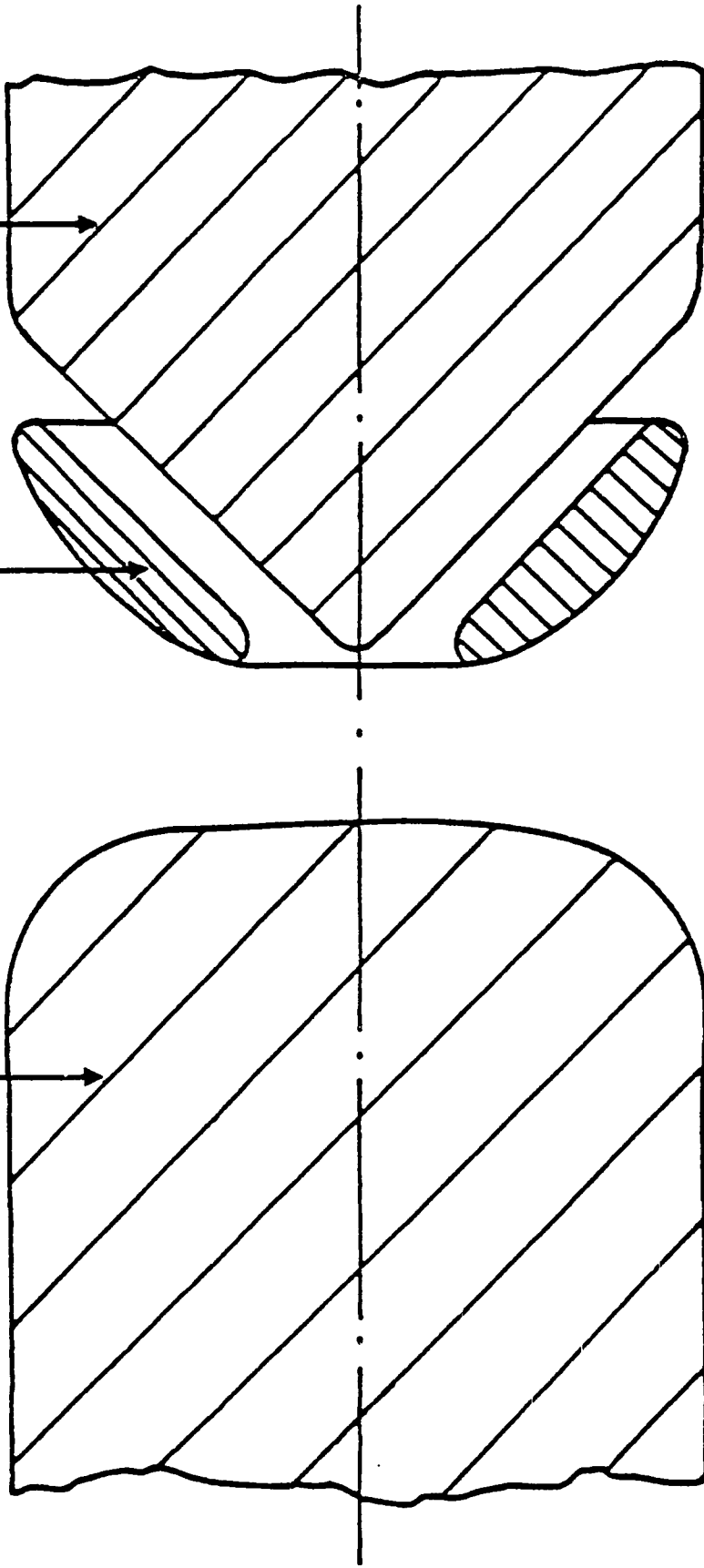
Figure Captions

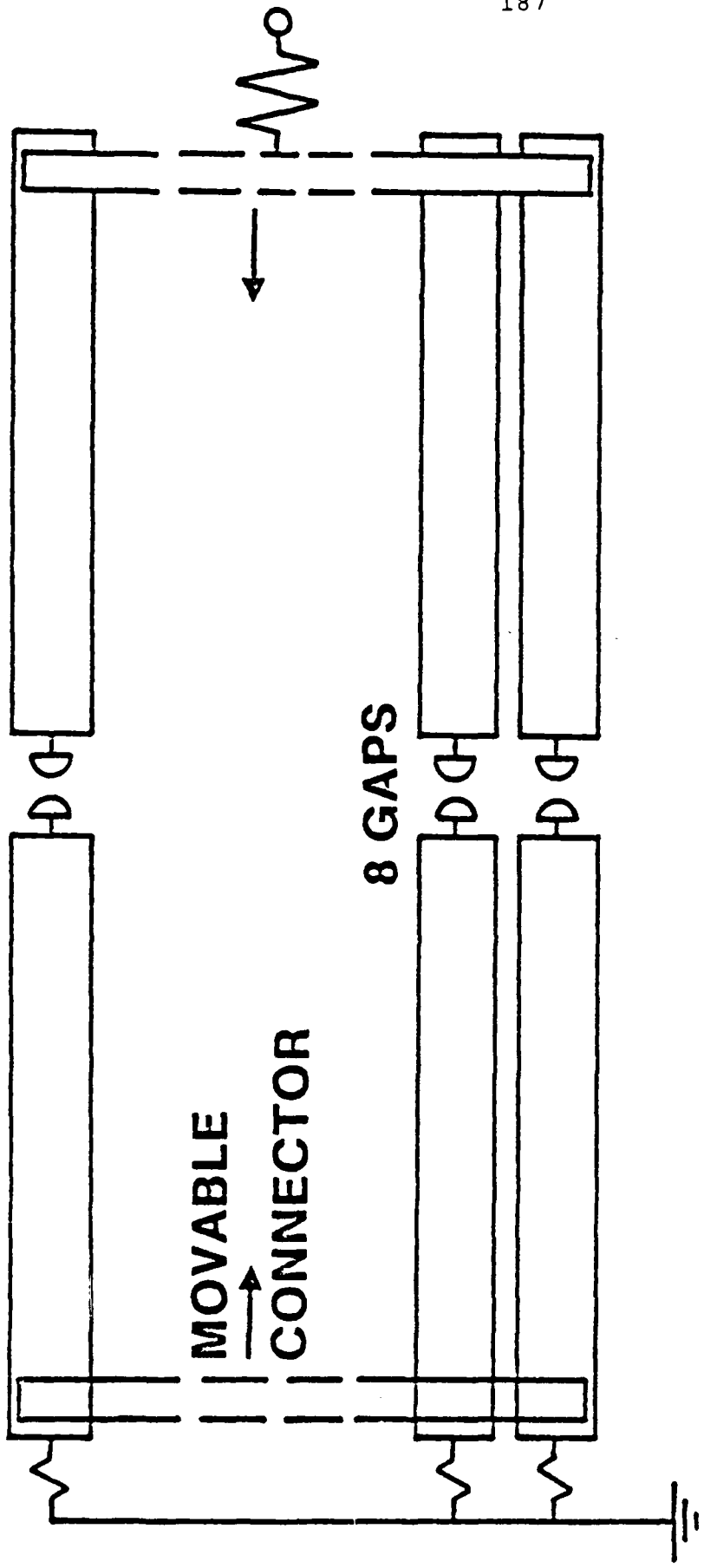
1. Schematic diagram of a spark gap with geometrically enhanced field distortion at the main electrode
2. Experimental setup
3. Electrode geometrics
4. Trigger electrode arrangement
5. Trigger circuits
6. Selfbreakdown voltage as a function of trigger electrode position (A) and electrode geometry (B)
7. Delay versus % selfbreakdown voltage for two trigger circuits ($V_{SB} = 15$ kV)
8. Jitter versus % selfbreakdown voltage for two trigger circuits ($V_{SB} = 15$ kV)

ELECTRODE (1)

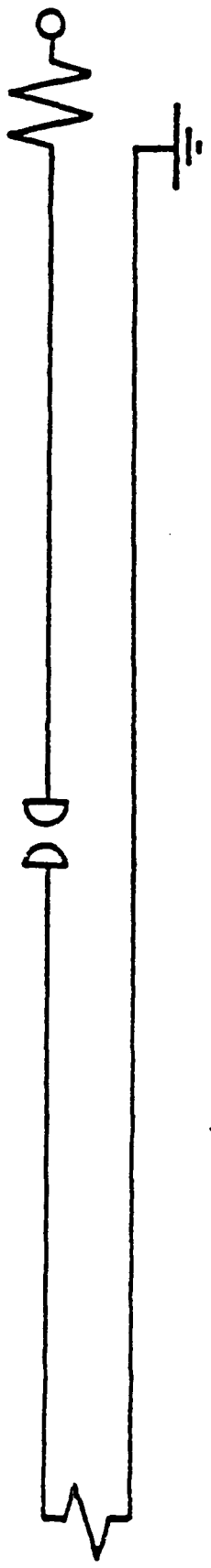
TRIGGER
ELECTRODE

ELECTRODE (2)





**MATCHING TRANSMISSION
RESISTORS** **CHARGING
LINE**



TRIGGER ELECTRODE

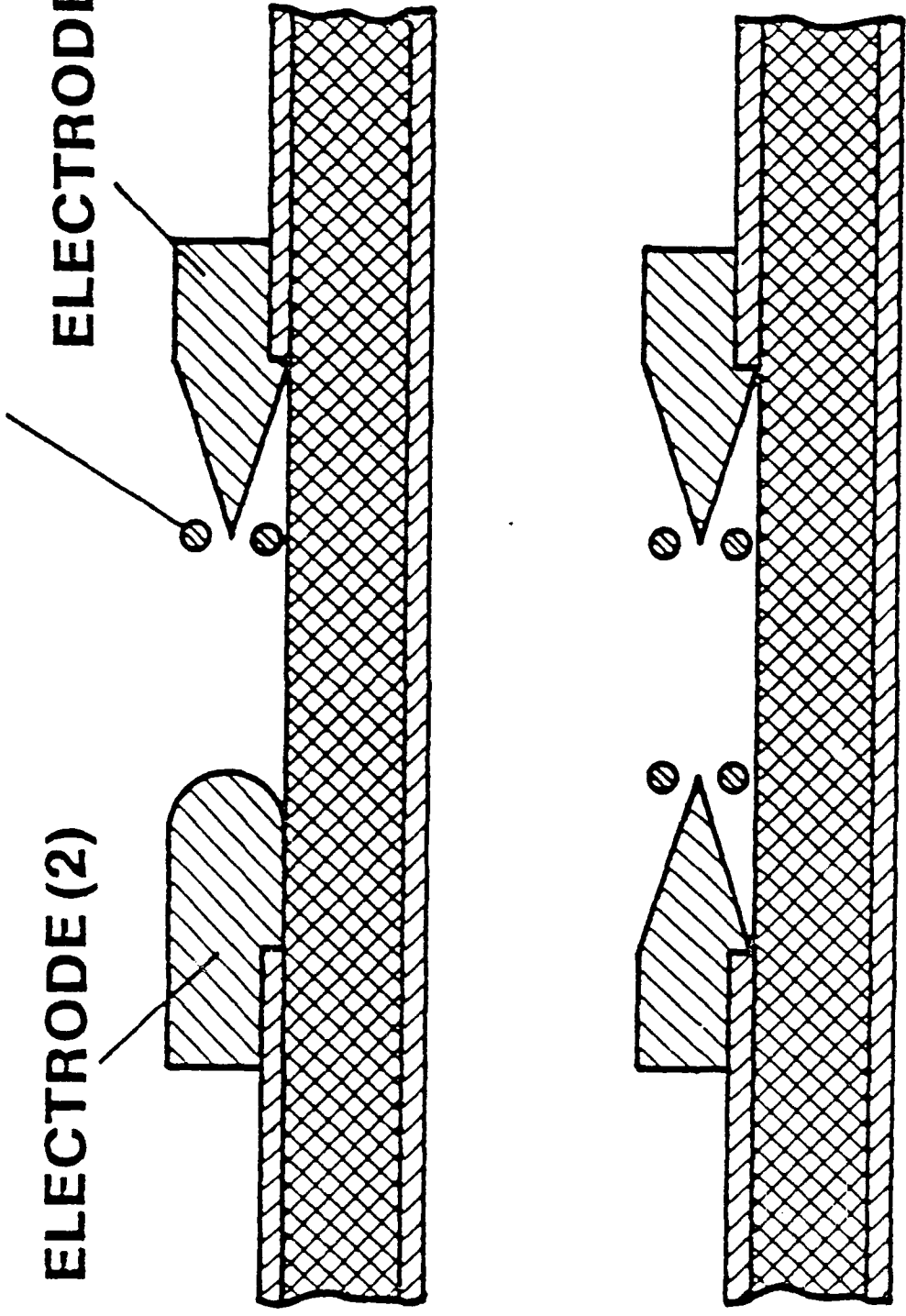
ELECTRODE (2)

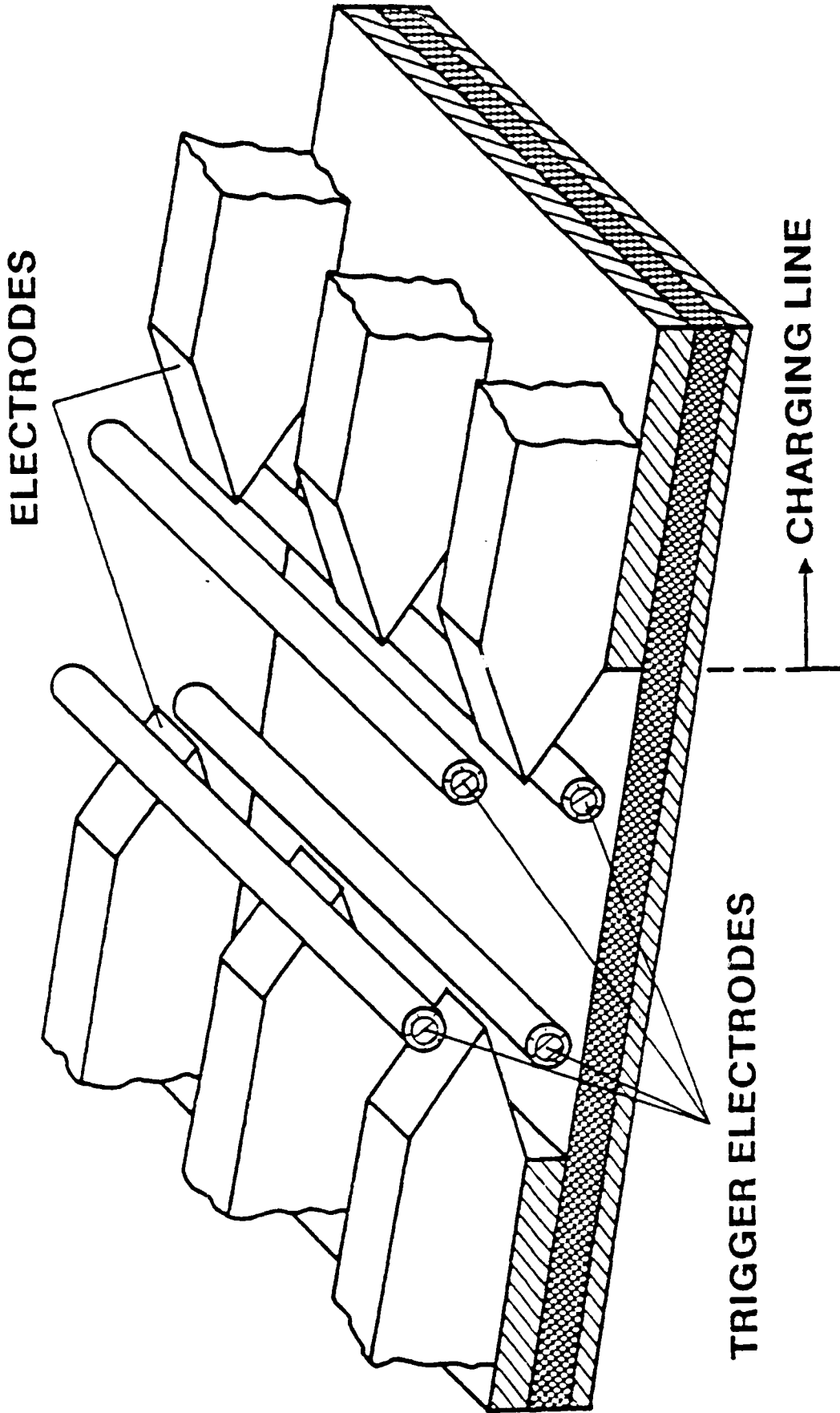
ELECTRODE (1)

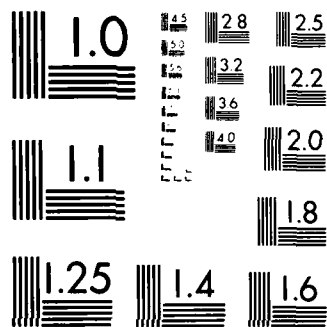
LINE

(A)

(B)

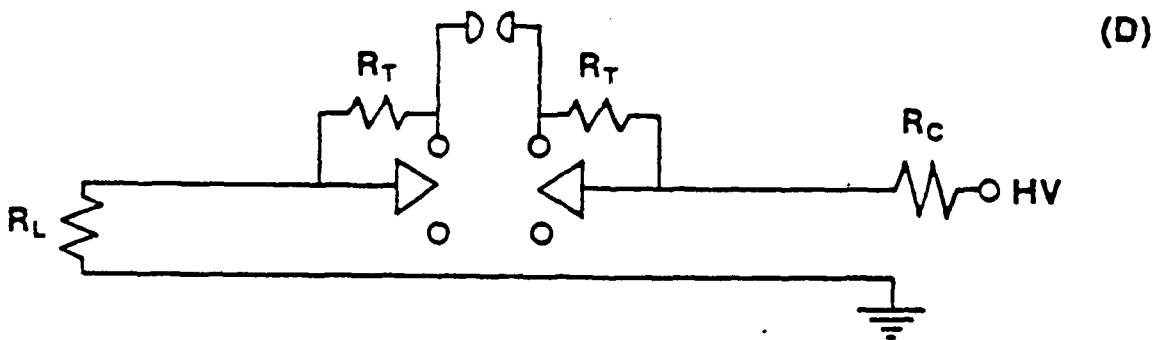
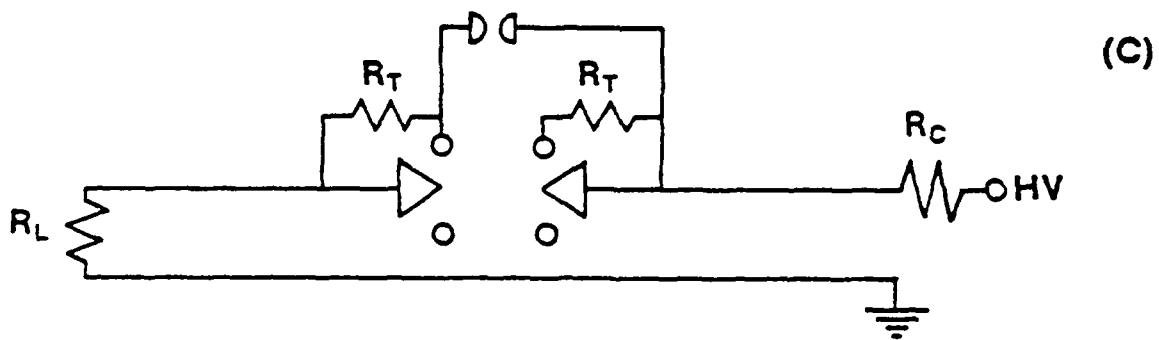
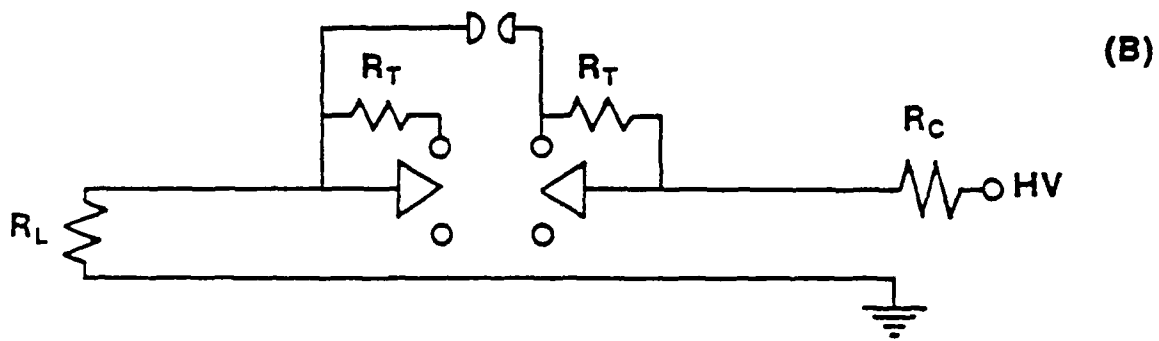
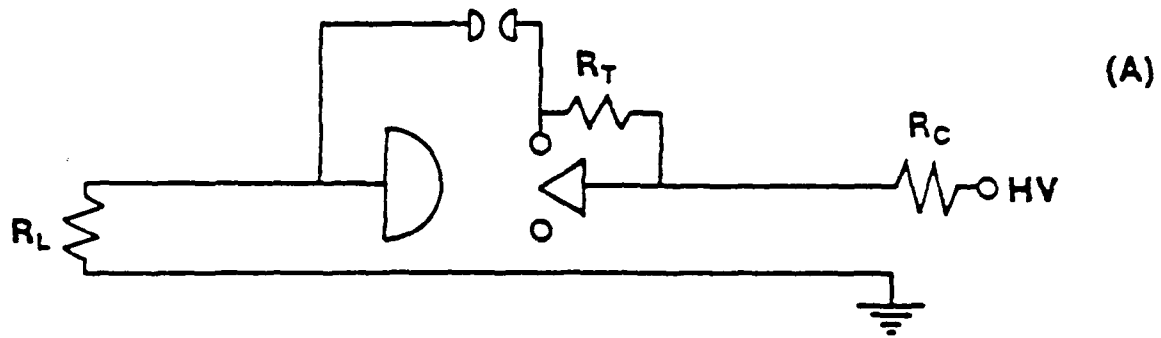


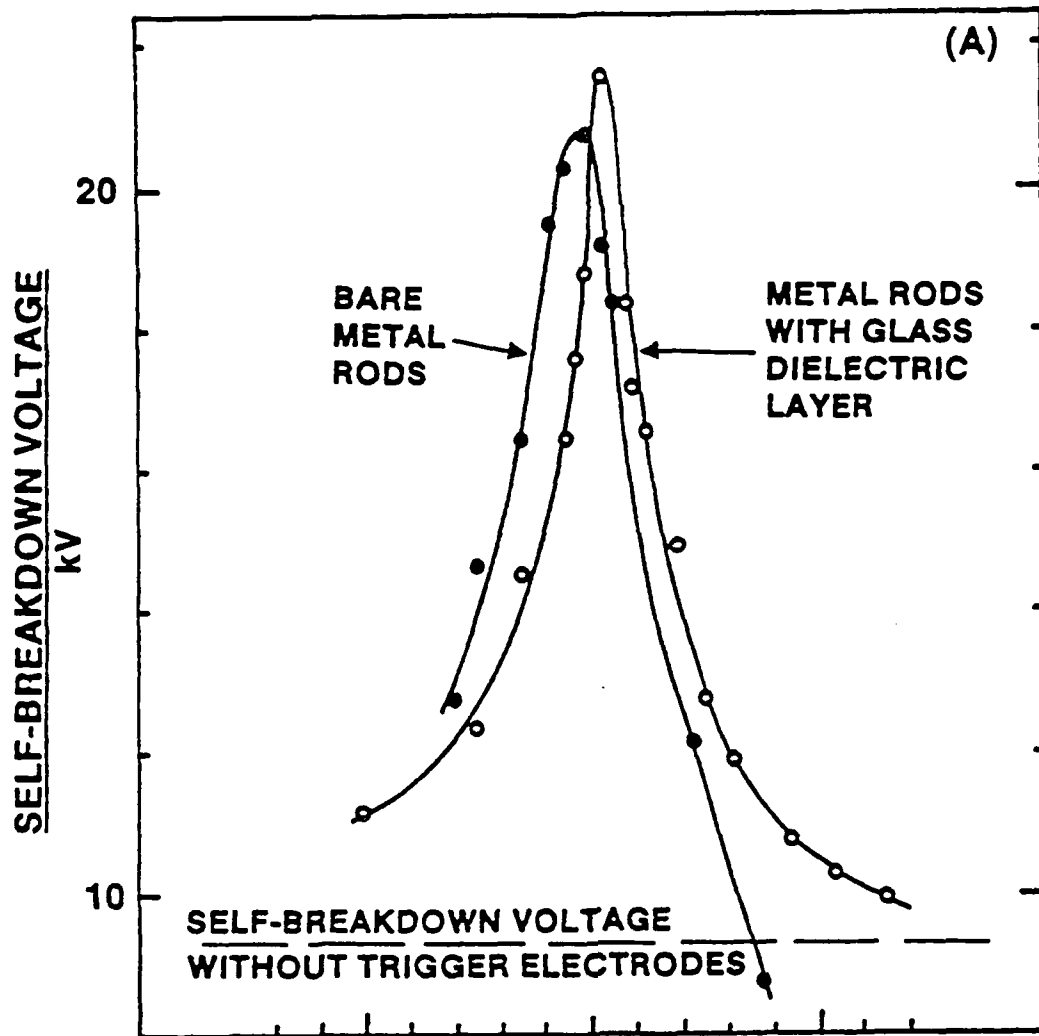




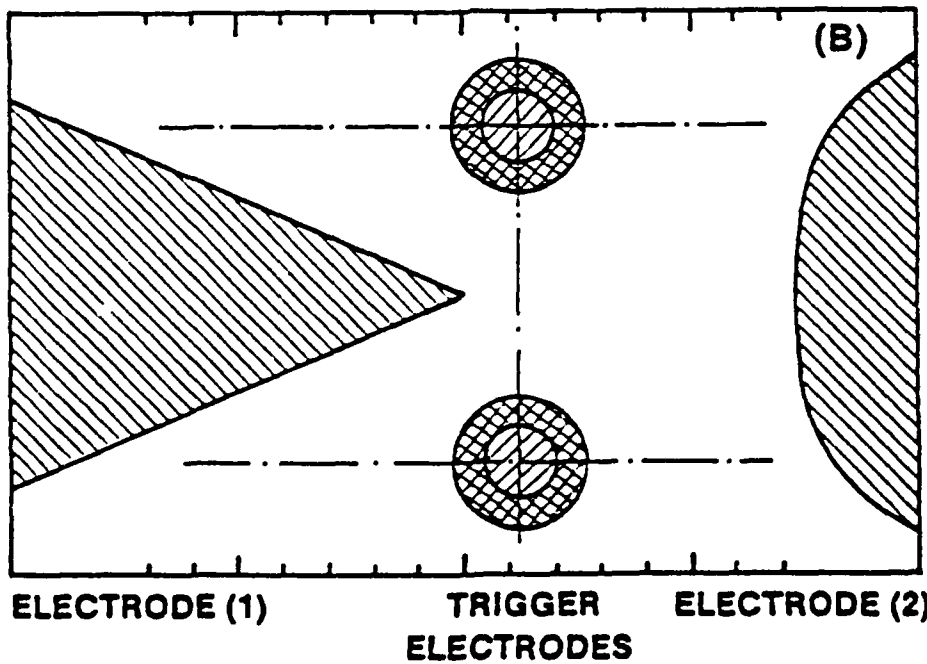
MICROCOPY RESOLUTION TEST CHART
NATIONAL BUREAU OF STANDARDS-1963-A

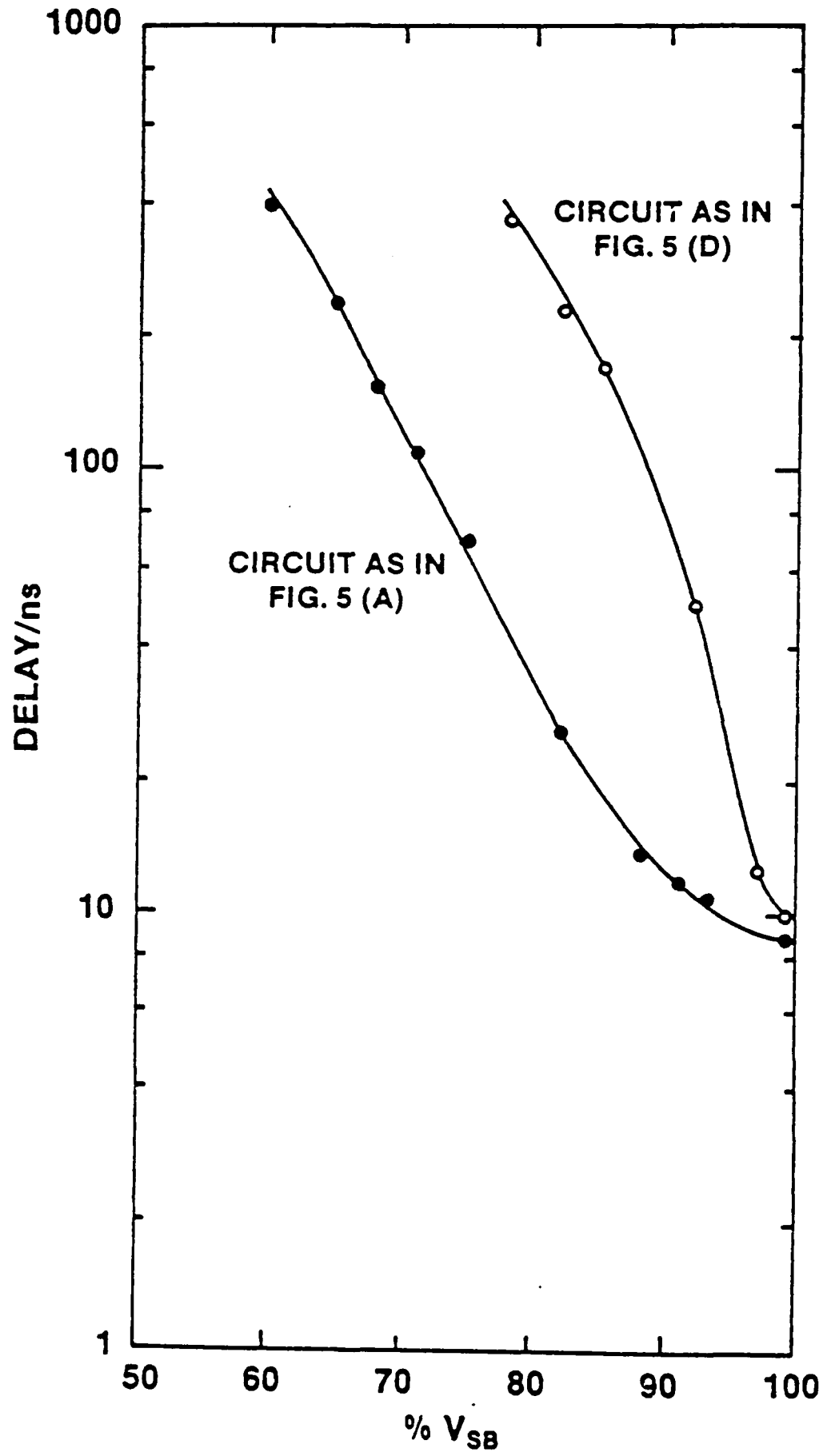
SECONDARY GAP

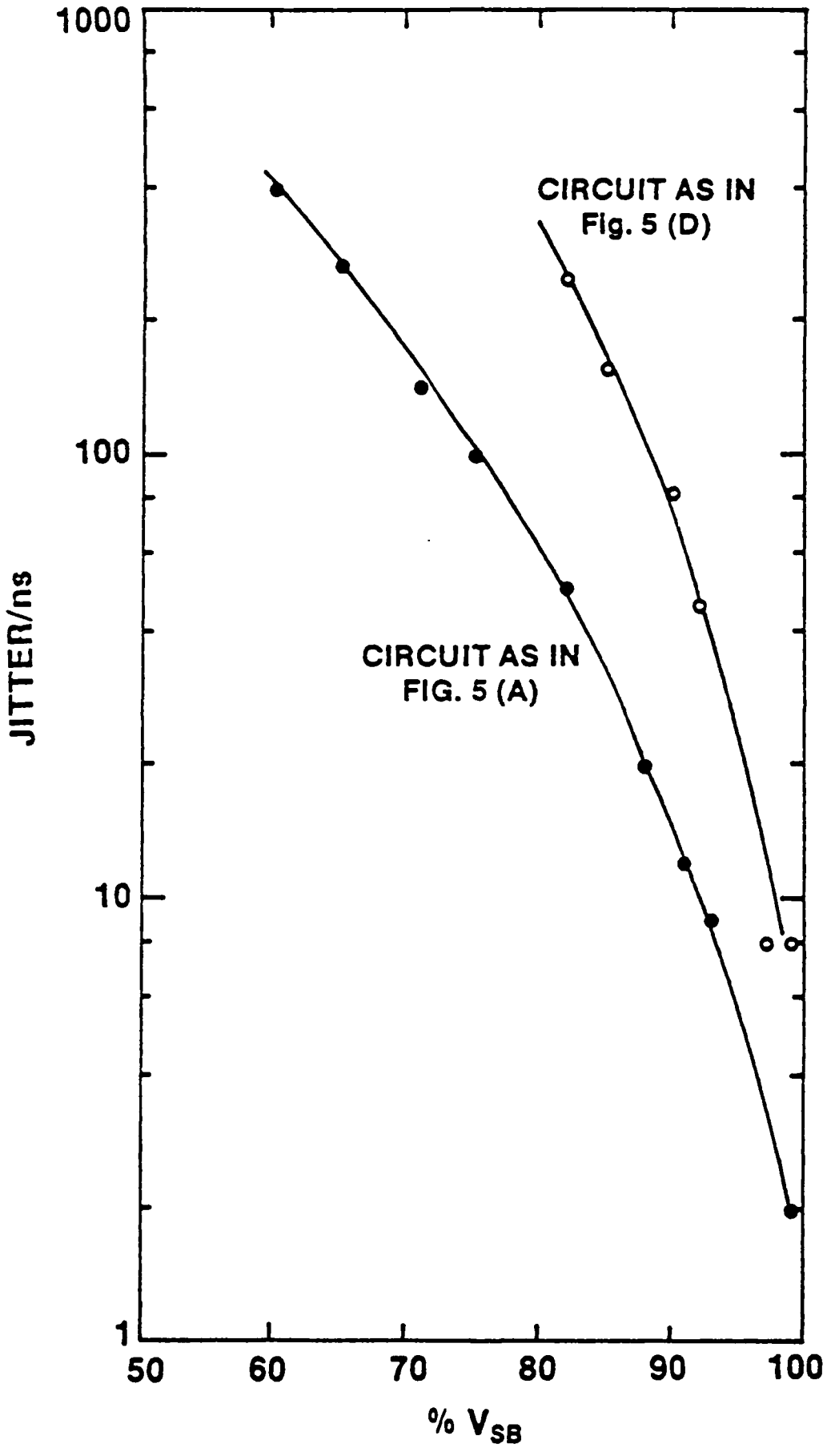




TRIGGER ELECTRODE POSITION (1mm/div)







Paper Accepted for Presentation at the
IEEE Instrumentation Measurement Technology
Conference, Tampa, FL, March 21-22, 1985

APPENDIX II

Transmission Line Current Sensor

H. Krompholz, K. Schoenbach, and G. Schaefer

Department of Electrical Engineering
Texas Tech University
Lubbock, Texas 79409

Abstract

A matched slow wave transmission line is used as a current probe. It provides a linear response, fast risetime (< 2 ns) and high sensitivity (≈ 1 V/A) for current pulses up to microsecond duration. The duration of a distortion-free monitored current pulse is limited by dispersion in the slow wave transmission line.

1. Inductive Current Sensors

Rogowski coils are commonly used as current sensors in pulsed power experiments. They consist of a helical coil placed around the current to be measured with an induced voltage related to this primary current. In the usual mode of operation, the coil is terminated with a small resistance R . The output signal, i.e. the voltage measured across this resistor is

$$V(t) = -\frac{R}{N} \int \frac{dI}{dt}(t') \exp\left(-\frac{R}{L}(t'-t)\right) dt' \quad (1)$$

where N = number of turns
 L = coil inductance
 dI/dt = time derivative of the current to be measured.

The risetime of these devices is usually in the order of 1 ns with a sensitivity [1] R/N in the order of 10^{-2} V/A. For high current experiments this sensitivity is sufficient, for currents less than 100 A, however, characteristic output signals are in the millivolt range and therefore susceptible to noise.

2. Transmission line current sensor

A more detailed consideration of this current transformer - especially for temporal variations of the primary current in the nanosecond regime - has to take transit time effects into account [2]. In this approximation the distributed capacitance between coil and surroundings (e.g. an electrostatic shield) enters as additional parameter. The equivalent

circuit of the transformer can be described as a transmission line (Fig. 1) with distributed induced voltage sources

$$V_{IND} dz = -\frac{N \mu_0}{(2\pi a)^2} S \frac{dI}{dt} dz \quad (2)$$

where a is the major diameter, S is the cross-sectional area of the coil. The probe current i is then described by the inhomogeneous wave equation

$$\frac{\partial^2 i}{\partial t^2} - \frac{1}{L'c'} \frac{\partial^2 i}{\partial z^2} = -\frac{1}{N} \frac{d^2 I}{dt^2} \quad (3)$$

and the boundary conditions: shorted at one end, terminated with the resistor R at the other end.

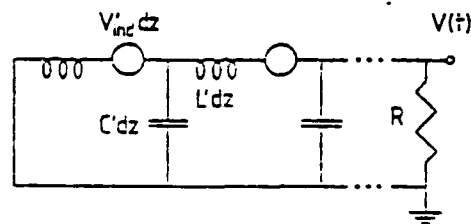


Fig. 1 Equivalent Circuit

In order to illustrate the response of such a transmission line current sensor, an input current $I(t)$ as a unit step function is assumed producing output signals as sketched in Fig. 2. Using the lumped parameter description for $R \ll \sqrt{L' C'}$, an exponentially decaying output signal is produced, whereas the transmission line properties generate a stepwise decreasing function due to reflections at both ends of the line. If the terminating resistance is large compared to the line impedance, the output is oscillatory with a periodicity of four times the transit time.

For the matching terminating resistor ($R = \sqrt{L/C}$) the output voltage is exactly proportional to the primary current for times smaller than twice the transit time

$$T = \sqrt{LC} \quad (4)$$

resulting in the response on the general input $I(t)$

$$V(t) = \frac{R}{2N} \{I(t) - I(t-2T)\} \quad (5)$$

From equations (4) and (5) it is obvious, that for a transmission line transformer the sensitivity and characteristic time of the system can be adjusted independently from each other, whereas in common Rogowski coils there is always a trade-off between sensitivity and decay time.

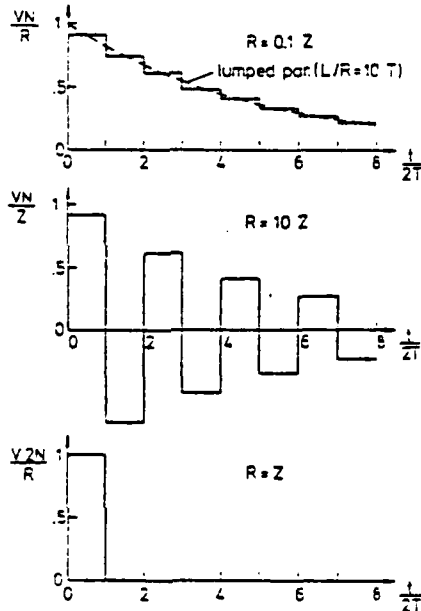


Fig. 2 Unit Step Response for Different Load Resistances

For the transmission line probe, two modes of operation and evaluation depending on the ratio of pulse duration and twice the transit time are possible. If the duration of the primary current is larger than $2T$, a simple discrete time shift deconvolution (inversion of equation (5)) allows reconstruction of the primary current from the measured voltage. If, on the other hand, the transit time is increased to values larger than the

duration of the primary current pulse, the probe acts as an ideal current transformer (output voltage exactly proportional to input current). High sensitivities in the order of 1 V/A are possible, and the transit time T can be increased by either high values of the distributed inductance or the distributed capacitance.

3. Experimental device

In order to utilize the concept of a waveguide current probe with high transit time, a matched device has been constructed which consists of a helix in a slotted metallic torus with high capacitance between helix and torus [3] (Fig. 3, Data are given in Table 1).

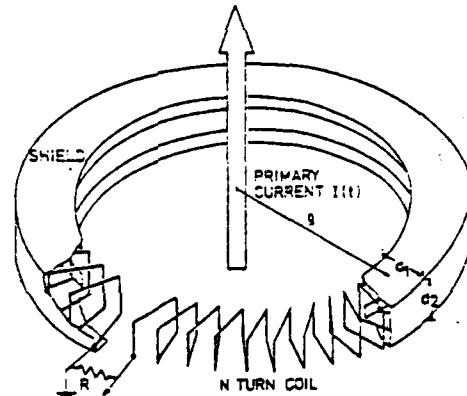


Fig. 3 Experimental Current Probe

Table 1

l	(number of turns)	:400
ρ	(major radius)	:8.7 cm
$d_1=d_2$	(sides of cross section)	:1.06 cm
L'	(inductance per unit length)	:1.518 H/cm
C'	(capacitance per unit length)	:19.2 pF/cm
z	(characteristic impedance)	:260
v	(propagation velocity)	: 1.9×10^8 cm/s
T	(transit time)	:290 ns
R_w	(wire resistance)	:1.8
$S = \frac{R}{2N}$	(sensitivity)	:0.35 V/A

The probe has been tested in a coaxial 50-Ohm cavity with rectangular input current pulses of variable duration. Examples for input current pulses and responses are depicted in Fig. 4. Figure 4a shows the risetime in the order of 2 ns. For input current duration < 200 ns the output is proportional to the input, for higher input current durations increasing oscillations are observed indicating deviations from the simple transmission line model (Fig. 4b, 4c).

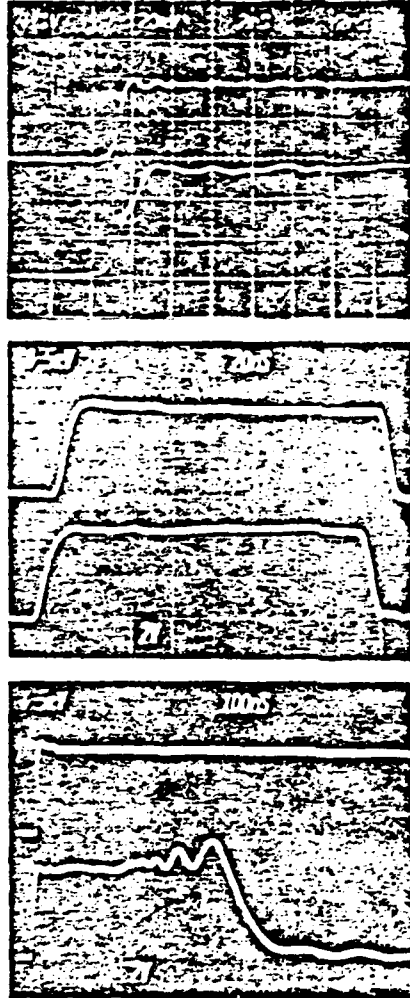


Fig. 4 Measured Probe Responses
 a) risetime
 b) input pulse duration 160 ns
 c) step function input

4. Limitations due to dispersion

In order to describe the oscillation effects quantitatively, an analysis of the system using field theory has been performed. The helical inner conductor was modeled as "sheet-helix", i.e. an anisotropic conductor with infinite conductivity in the direction of the helix and zero conductivity in all other

directions. The slit in the outer conductor which allows the penetration of the primary current magnetic field into the probe prevents azimuthal current flow. This structure allows modelling of the outer conductor with currents only in axial direction.

Maxwell's Equations for this system have been solved resulting in the dispersion relation for waves travelling in axial direction [4]

$$\frac{k^2}{c^2 v^2} \cot^2 \psi = - \frac{I_0'(ta)}{I_1'(ta)K_1'(ta)I_0'(tb)} \cdot [I_0'(ta)K_0'(tb) - I_0'(tb)K_0'(ta)] \quad (6)$$

where $v^2 = c^2 - \frac{\omega^2}{k^2}$

ψ is the angle between helical and azimuthal direction
 I_0, I_1, K_0, K_1 modified Bessel functions
 a, b radii of inner and outer conductor

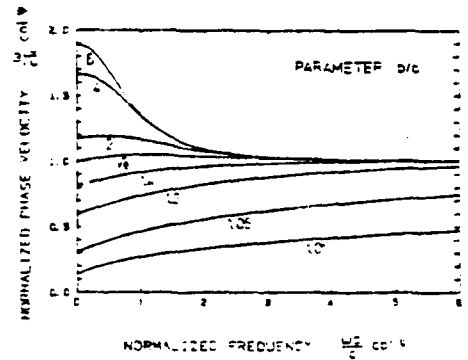


Fig. 5 Dispersion relation

The phase velocity, v/k as a function of frequency ω is plotted in normalized units in Fig. 5. The previously discussed transmission line behavior with neglected dispersion is given by the limit $\omega \rightarrow 0$. Minimum dispersion is achieved for the ratio of radii, b/a of $\sqrt{2}$. Using the equivalent data of the experimental device in Table 1, Fourier transform has been used to calculate its unit step response. The result is plotted in Fig. 6. Here an

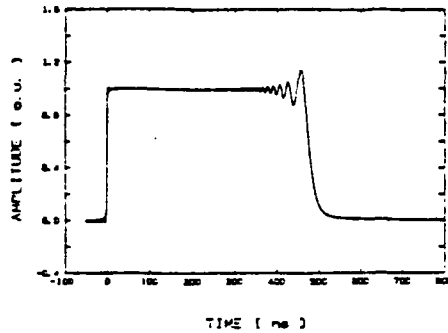


Fig. 6 Calculated unit step response

additional damping factor proportional to the frequency has been assumed. This factor describes dielectric losses in the system. The agreement between measured and calculated behavior is good considering the simplifying model assumptions.

To minimize dispersion, the concept of increasing the transit time by increasing the capacitance has to be abandoned, since the ratio of radii is fixed to the value of $\sqrt{\epsilon}$. Only the inductance (number of turns per unit length) remains as a variable determining the transit time. Results of pulse response calculations for an optimized coil are plotted in Fig. 7.

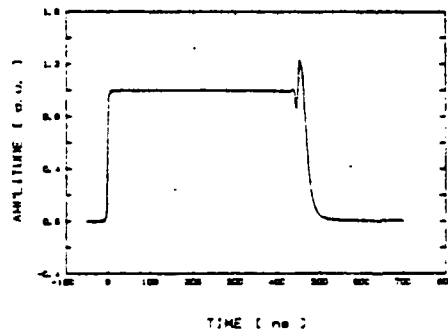


Fig. 7. Calculated unit step response of optimized probe (input pulse risetime 2 ns)

4. Discussion

Consideration of current sensors as transmission lines including dispersion show the feasibility for construction of distortion-free current sensors with a large transit time of up to the micro-

second range and a sensitivity in the order of 1 V/A. This sensitivity is high enough to measure current amplitudes in the order of milliamperes with standard oscilloscopes.

Further applications of the discussed helical slow wave structures are in the field of compact pulse generators for rectangular pulses with a duration of several microseconds and rise and fall times in the nanosecond regime [5].

Limitations are imposed by dispersive effects, however, through careful design it is possible to minimize these effects for applications in electrical diagnostics as well as for pulse forming networks.

References

1. M. DiCapua in "Measurements of Electrical Quantities in Pulse Power Systems", edited by R.M. McKnight and R.E. Hebner (NBS, Colorado 1982) p. 175.
2. W. Stygar and G. Gerdin, IEEE Trans. Plasma Science, PS-10, p. 40 (1982).
3. B. Krompholz, J. Doggett, K. Schoenbach, J. Ganl, C. Harjes, G. Schaefer, and M. Kristiansen, Rev. Sci. Instrum., 55, 127 (1984).
4. D.A. Watkins, "Topics in Electromagnetic Theory", Wiley, p. 62 (1958).
5. B. Krompholz, K. Schoenbach, G. Schaefer, "Pulse Forming Network Using a Helical Delay Line", to be published.

This work was supported by the Air Force Office of Scientific Research (AFOSR) and the Army Research Office (ARO).

Journal Papers and Conference Proceeding Papers

Published with AFOSR Support

1. H. Krompholz, J. Doggett, K.H. Schoenbach, J. Gahl, C. Harjes, G. Schaefer, and M. Kristiansen, "Nanosecond Current Probe for High Voltage Experiments", Rev. Sci. Instr., 55, 127 (1984).
2. G. Schaefer, K.H. Schoenbach, H. Krompholz, M. Kristiansen, and A.H. Guenther, "The Use of Attachers in Electron Beam Sustained Discharge Switches - Theoretical Consideration", Laser and Particle Beams, 2 part 3, 273 (1984).
3. K.H. Schoenbach, M. Kristiansen, and G. Schaefer, "A Review of Opening Switch Technology for Inductive Energy Storage", Proc. IEEE, 72, 1019 (1984).
4. G. Schaefer, P. Husoy, K.H. Schoenbach, H. Krompholz, "Pulsed Hollow-Cathode Discharge with Nanosecond Risetime", IEEE Trans. Plasma Sci., PS-12, 271 (1984).
5. C.H. Harjes, K.H. Schoenbach, G. Schaefer, M. Kristiansen, H. Krompholz, and D. Skaggs, "An Electron Beam Tetrode for Multiple, Submicrosecond Pulse Operation", Rev. Sci. Instr., 55, 1684 (1984).
6. K.H. Schoenbach, G. Schaefer, M. Kristiansen, H. Krompholz, H. Harjes, and D. Skaggs, "Investigations of E-Beam Controlled Diffuse Discharges", Gaseous Dielectrics IV, ed., L. Christophorou, Pergamon Press, p. 246 (1984).

7. G. Schaefer, B. Pashaie, P.F. Williams, K.H. Schoenbach, and H. Krompholz, "A New Design Concept for Field Distortion Trigger Spark Gaps", J. Appl. Phys., accepted for publication in J. Appl. Phys.
8. K.H. Schoenbach, G. Schaefer, M. Kristiansen, H. Krompholz, H.C. Harjes, and D. Skaggs, "An Electron-Beam Controlled Diffuse Discharge Switch", J. Appl. Phys, accepted for publication.
9. K. Schoenbach, G. Schaefer, M. Kristiansen, H. Krompholz, H.C. Harjes, and D. Skaggs, "A Rep-Rated E-Beam Controlled Diffuse Discharge Switch", 16th Modulator Symposium, Arlington, VA, June 1984.
10. M. Kristiansen, K. Schoenbach, and G. Schaefer, "Opening Switches", Proc. 3rd All-Union Conf. on Engineering Problems of Fusion Research, Leningrad, USSR, June 1984. (Invited)
11. S.K. Dahli and P.F. Williams, "Numerical Simulation of Streamer Propagation in Nitrogen at Atmospheric Pressure", Submitted to Phys. Rev. A.
12. G. Jackson, L. Hatfield, M. Kristiansen, M. Hagler, J. Marx, A. Donaldson, G. Leiker, R. Curry, R. Ness, L. Gordon, and D. Johnson, "Surface Studies of Dielectric Materials Used in Spark Gaps", J. Appl. Phys., 55, 262 (1984).
13. R.A. Dougal and P.F. Williams, "Fundamental Processes in Laser-Triggered Electrical Breakdown of Gases", J. Phys. D, 17, 903 (1984).

14. E. Kunhardt and P.F. Williams, "Fast Algorithm for Numerically Integrating Poisson's Equation in Cylindrically Symmetric Geometries", to appear in J. Comp. Phys. 1985).
15. S.K. Dhali and P.F. Williams, "Numerical Simulation of Streamer Propagation in Nitrogen at Atmospheric Pressure", to appear in Phys. Rev. A, Feb (1985).

Interactions

1983-84

a) Papers Presented

During the last contract period (October 1, 1983 - October 31, 1984), the following papers were presented:

1. K. Schoenbach, G. Schaefer, M. Kristiansen, H. Krompholz, H.C. Harjes, and D. Skaggs, "Investigations of E-Beam Controlled Diffuse Discharges", IEEE International Conference on Plasma Science, St.Louis, MO, 1984.
2. J.R. Cooper, K.H. Schoenbach, G. Schaefer, J.M. Proud, and W.W. Byszewski, "Magnetic Control of Low Pressure Glow Discharges", 37th Gaseous Electronics Conference, Boulder, CO, Oct 1984.
3. M.R. Wages, P.F. Williams, G. Schaefer, and K.H. Schoenbach, "Streak Photographic Studies of Trigatron Triggered Breakdown", 37th Gaseous Electronics Conference, Boulder, CO, Oct. 1984.
4. S.K. Dhali and P.F. Williams, "Two Dimensional Numerical Simulation of Space-Charge-Controlled Transport at High Charge Densities", 36th Annual Gaseous Electronics Conference, Albany, NY, Oct. 1983.
5. R.A. Dougal and P.F. Williams, "Fundamental Processes in Laser-Triggered Electrical Breakdown", 36th Annual Gaseous Electronics Conference, Albany, NY, Oct. 1983.

6. G.Z. Hutcheson, L.E. Thurmond, G. Schaefer, K.H. Schoenbach, and P.F. Williams, "Optical Control of the Breakdown of a Diffuse Discharge Using Photodetachment", 37th Annual Gaseous Electronics Conference, Boulder, CO, Oct. 1984.
7. S.K. Dhali and P.F. Williams, "2-D Numerical Simulations of Streamers in Atmosphere N₂", 37th Annual Gaseous Electronics Conference, Boulder, CO, Oct. 1984.
8. M. Kristiansen, K. Schoenbach, and G. Schaefer, "Opening Switches", (Invited Paper), 3rd All Union Conference on Engineering Aspects of Fusion Research, Leningrad, USSR, June 1984.
9. R. Curry, M. Kristiansen, L. Hatfield, V. Agarwal and G. Jackson, "Surface Charging of Insulators in Surface Discharge Switches", Conf. on Electrical Insulation and Dielectric Phenomena, Buckhill Falls, PA, Oct 1983.

b. Consultative and Advisory Functions

During the 1983-84 contract period, the following functions were undertaken:

1. Dr. M. Kristiansen served on the USAF Scientific Advisory Board (SAB).
2. Dr. Kristiansen served on the Air Force SAB committee to study Basic Research in the Air Force.
3. Dr. M. Kristiansen served on the Air Force SAB Ad Hoc committee on Effects of High Altitude EMP on Military C³.

4. Dr. Kristiansen served as the Co-organizer (with Dr. A. Hyder of Auburn University) of the DoD workshop on "Foreign Switch Technology".
5. Dr. Kristiansen served as a Visiting Staff Member (Collaborator) at Los Alamos National Laboratory and supervised a completed Ph.D research project by one of their Staff Members.
6. Dr. Kristiansen directed the Foreign Applied Science Assessment Centers Study of Soviet Macroelectronics (Pulsed Power).
7. Prof. G. Schaefer taught a graduate course on Gaseous Electronics at ERADCOM, Ft. Monmouth, NJ in August 1984.
8. Prof. P.F. Williams visited Alan Garscadden's group at AFWAL, gave a talk entitled "Streamers and Space-Charge Dominated Transport in Discharges", Nov. 17, 1983.
9. Prof. P.F. Williams visited the Pulsed Power Group at NSWC in Dahlgren, VA, August 22, 1984.
10. M. Kristiansen gave a series of invited lectures on pulsed power techniques and high power switching and inertial confinement fusion at the Nuclear Research Center in Taiwan, and at Keio University, Kyoto University, City of Hakodate, and Hakone Conference Center during the period July 3-23, 1984.
11. M. Kristiansen gave a seminar entitled "Pulsed Power Research at Texas Tech University" at the University of Oslo, Norway, September 17, 1984.

Interactions - c) Other interactions

Numerous interactions with other universities, industry and government laboratories were carried out during the contract period. Our group effectively served as a coordination point for much of the ongoing work in high power gas discharges for switching applications in the U.S.

1. Prof. G. Schaefer and F. Williams attended the 36th Gaseous Electronics Conference in Albany, NY, in October 1983.
2. Prof's. G. Schaefer and K.H. Schoenbach, L. Hatfield, and M. Kristiansen attended the ARO Workshop on Foreign Switch Technology in Santa Fe, NM in March 1984.
3. Prof. G. Schaefer attended the Conference on Laser and Electrooptics in Anaheim, CA in June 1984.
4. Prof. G. Schaefer visited the Department of Electrical Engineering at USC (Prof's. M. Gundersen and C. Wittig) in Los Angeles, CA in June 1984.
5. Prof. G. Schaefer visited Jet Propulsion Laboratory (Dr.'s A. Chutjian and S. Srivastava) in Pasadena, CA in June 1984.
6. Prof's. G. Schaefer and K.H. Schoenbach attended the 4th Int. Symposium on Gaseous Dielectrics in Knoxville, TN in April 1984.
7. Prof's. K.H. Schoenbach and H. Krompholz attended the 16th Power Modulator Symposium, Arlington, VA, June 1984.

8. Prof. Schoenbach visited GTE Laboratories in Waltham, MA (Dr's. J. Proud, L. Pitchford, W. Byszewski) in June 1984 and gave a seminar on Low Pressure Diffuse Discharge Switches.
9. Prof's. H. Krompholz and M. Kristiansen attended the IEEE International Conference on Plasma Science, St. Louis, MO, May 1984.
10. Prof. F. Williams attended the 37th Gaseous Electronics Conference in Denver, CO in Oct. 1984.
11. Prof. M. Kristiansen visited SNL (Mr. T. Martin) and AFWL (Dr. A.H. Guenther) in Albuquerque, NM in August, 1984.
12. Prof. M. Kristiansen visited LLNL (Dr. diCapua) in September 1984.
13. Prof. M. Kristiansen visited AFWL (Dr. A.H. Guenther), SNL (Mr. T. Martin), and Tetra Corp (Mr. W. Moeny) in Albuquerque, NM in September 1984.
14. Prof. M. Kristiansen visited AFOSR (Maj. H. Pugh) in November 1984.

ADVANCED DEGREES AWARDED

(1983-84)

1. Shirshak Komer Dhali, Ph.D., "Breakdown Processes in Laser Triggered Switching ", May, 1984.
2. Emanuel M. Honig, Ph.D., "Repetitive Energy Transfers from an Inductive Energy Store", August 1984.
3. Gary R. Leiker, M.S., "Design and Construction of a High Power Electron Gun", May 1984.

SEMINARS
1983-84

Charles R. Kost	"A History of Solid State Airborne Radar" November 17, 1983 Texas Instruments Lewisville, TX
William Moeny	"Computational Solutions of Electric Fields in Discharges" November 21, 1983 Tetra Corporation Albuquerque, NM
John Barber	"A Perspective on Pulsed Power and Electromagnetic Guns" February 1, 1984 IAP Research, Inc. Dayton, Ohio
Lloyd B. Gordon	"Pulsed Power at LLNL" February 10, 1984 Lawrence Livermore National Laboratory Livermore, CA
John Owens	"Status of Magnetostatic Wave Devices" February 28, 1984 University of Texas at Arlington Austin, TX
Allen R. Stubberud	"Quality Engineering Education - Does Anyone 'Out There' Really Care" March 1, 1984 Chief Scientist, U.S. Air Force Washington, DC
Ronald B. Standler	"Protection of Electronics from Lightning and EMP" March 19, 1984 Rochester Institute of Technology Rochester, NY
Kenneth A. Buckle	"A Numerical Stability Analysis Method for Confined Plasmas" March 25, 1984 University of Wisconsin Madison, WI

Don W. Reid

"High Power Microwaves; A Resurging
Technology"
March 28, 1984
Los Alamos National Laboratory
Los Alamos, NM

Rogal A. Dougal

"The Recovery of a Vacuum Switch"
June 28, 1984
University of South Carolina
Columbia, NC

G.R. Govinda Raju

"Electron Energy Distributions in Gases
in Crossed Electric and Magnetic
Fields"
August 24, 1984
University, of Windsor
Windsor, Canada

Wayne W. Hofer

"High Power Microwave Research"
October 3, 1984
Lawrence Livermore National
Laboratories
Livermore, CA

Guests of Plasma and Switching Laboratory
 October 1, 1983 - October 31, 1984

October 15, 1984

William Streifer	Xerox PARC, Palo Alto, CA
Paul K. Predecki	Univer. of Denver, Denver, CO
Rex E. Phillips	Westinghouse Electrical Corp., Dallas, TX
Billy C. Brock	Sandia National Laboratory
John W. Welch	IBM Corp, Austin, TX
W.C. Nunnally	Los Alamos National Laboratory
Merle Whatley	Texas Instruments, Dallas, TX
H. Ray Kerby	IBM, Corp., San Jose, CA
John Ragland	Hicks & Ragland, Lubbock, TX
Dick Brooks	Central Power & Light, Corpus Christi, TX

November 29, 1983

William M. Moeny	Tetra Corp, Albuquerque, NM
John D. Jukes	Culham Laboratory, United Kingdom
Trevor James	Culham Laboratory, United Kingdom

December 16, 1983

Anthony K. Hyder	Auburn University, Auburn, AL
Tomoo Fujioka	Keio University, Yokohama, Japan

January 18, 1984

A.H. Guenther	AFWL, Albuquerque, NM
---------------	-----------------------

January 19, 1984

George Jackson	BDM Corporation, Huntsville, AL
----------------	---------------------------------

February 1, 1984

Don Johnson	IAP Research, Inc, Dayton, OH
Reuben Hackam	University of Windsor, Windsor Canada

February 27, 1984

A.H. Guenther	AFWL, Albuquerque, NM
John Dimmock	ONR, Washington, DC
Bob Gregory	SNL, Albuquerque, NM

February 28, 1984

J.M. Owens

University of Texas, Arlington, TX

March 1, 1984James M. Walton
Tony Sobol
Mike Mottern
Allen StubberudAFWL, Kirtland AFB, NM
AFWL, Kirtland AFB, NM
AF Chief Scientist's Office, Washington, DC
Hdq USAF, Washington, DCMarch 28, 1984

Don W. Reid

LANL, Los Alamos, NM

April 10-11, 1984Henry Pugh
Randy Jones
Clifford E. Rhoades
Peter Bletzinger
Richard Gullickson
Tom Martin
Bobby Junker
Douglas J. Klein
James C. Aller
Frank Rose
A.H. GuentherAFOSR, Bolling AFB, Washington, DC
ARO, Research Triangle Park, NC
AFOSR, Bolling AFB, Washington, DC
AFWAL, Wright-Patterson AFB, OH
DARPA, Arlington, VA
SNL, Albuquerque, NM
ONR, Arlington, VA
ONR, Arlington, VA
NSF, Washington, DC
NSWC, Dahlgren, VA
AFWL, Kirtland AFB, NMMay 21, 1984Manny Honig
Long Chi LeeLANL, Los Alamos, NM
San Diego State Univ., San Diego, CAJune 28, 1984

Rodney Cross

University of Sydney, Sydney, Australia

July 11, 1984

Rolf Girus

German Ministry of Defense, Bohnn, Germany

August 23, 1984

G.R. Govinda Rafi

University of Windsor, Windsor, Canada

Annual Report
on
COORDINATED RESEARCH PROGRAM
IN
PULSED POWER PHYSICS

AFOSR Grant #84-0032

December 20, 1984

Program Director: M. Kristiansen

Principal Investigators: M. Kristiansen
H. Krompholz
G. Schaefer
K. Schoenbach
F. Williams

Associate Investigator: L. Hatfield
L. Michel

Technician III: K. Zinsmeyer

Secretary III: M. Byrd
J. Davis

Graduate Students: G. Hutcheson R. Cooper
H. Harjes S. Dahli
R. Curry E. Strickland
R. Ness D. Skaggs
L. Thurmond C. Yeh*

* Paid by the Republic of China (Taiwan)

END

FILMED

7-85

DTIC